VOL 11
ISSUE 1
JAN 2026

eMetN METEOR JOURNAL

eJournal for meteor observers www.emetn.net

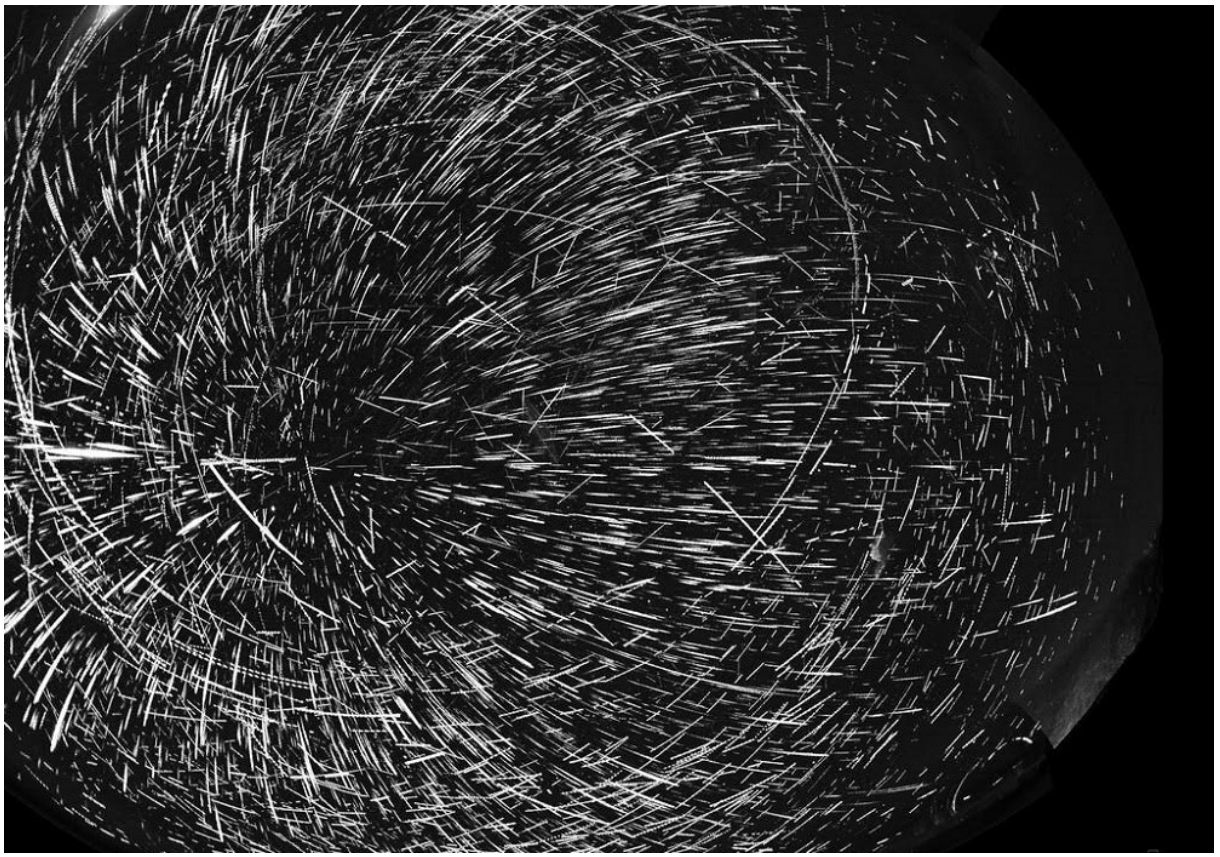

Track-stack mosaic created from approximately 12000 individual archived frames, recording around 11000 meteors during the Geminid maximum in 2025 by six cameras of the Global Meteor Network with 4 mm lenses at the Tićan Observatory, Croatia. Author: Aleksandar Merlak.

ISSN 3041 - 4261

Contents

October epsilon-Carinids (OEC#1172)

Paul Roggemans[1], **Denis Vida**[2,3], **Damir Šegon**[4,5], **James M. Scott**[6], **Jeff Wood**[7]

[1] **Pijnboomstraat 25, 2800 Mechelen, Belgium**

[2] **Department of Physics and Astronomy, University of Western Ontario, Richmond Street, London, N6A 3K7, Ontario, Canada**

[3] **Institute for Earth and Space Exploration, University of Western Ontario, Perth Drive, London, N6A 5B8, Ontario, Canada**
denis.vida@gmail.com

[4] **Astronomical Society Istra Pula, Park Monte Zaro 2, 52100 Pula, Croatia**

[5] **Višnjan Observatory, Istarska 5, 52463 Višnjan, Croatia**

[6] **Department of Geoscience, Aarhus University, Høegh-Guldbergs Gade 2. DK-8000 Aarhus C, Denmark**
jscott@geo.au.dk

[7] **PO Box 162, Willetton, Western Australia 6955, Australia**

Enhanced activity has been recorded during October 14 – 15, 2025 from the October epsilon-Carinids (OEC#1172) by the Global Meteor Network. 201 meteors belonging to this meteor shower were observed between $197.0° < \lambda_{\odot} < 204.0°$ during the period 2023 to 2025 from a radiant at R.A. = 110.7° and Decl.= –60.4°, with a geocentric velocity of 28.9 km/s. This case study confirms the existence of this meteor shower, and the most likely parent body is Asteroid 2010 HY_{22}.

1 Introduction

On 15 October 2025 some unusually strong activity was spotted near the South Pole (*Figure 1*). The radiant source was identified as the October epsilon-Carinids (OEC#1172), first reported in 2022 by Jenniskens (2023) from CAMS southern hemisphere low-light video observations in 2019–2021 with a total of 84 meteors identified as OEC#1172[1].

In 2025, Global Meteor Network detected 118 meteors identified as October epsilon-Carinids. Another 43 shower members were found in 2024 and 40 in 2023. The shower's enhanced activity in 2025 and the significant statistical sample with 201 October epsilon-Carinids recorded in 2023–2025 justified a case study to improve the IAU-MDC working list of meteor showers for this poorly known activity source.

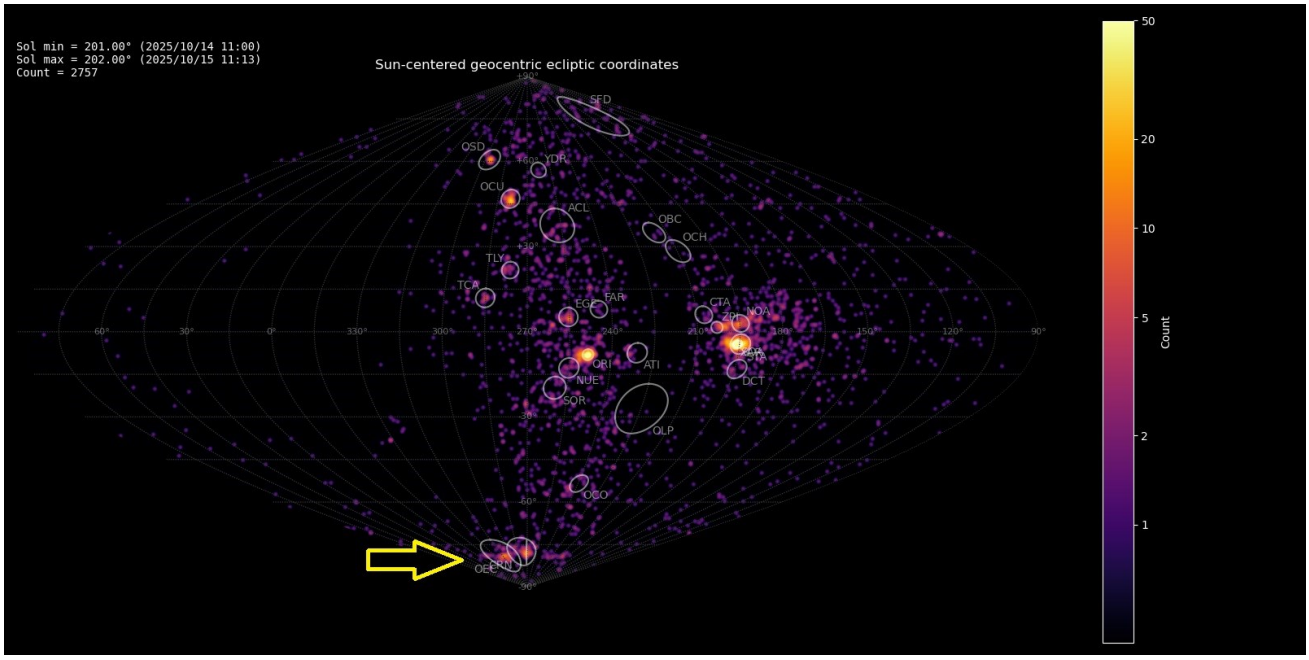

Figure 1 – Radiant density map with 2757 radiants obtained by the Global Meteor Network during 14–15 October, 2025. The position of the October epsilon-Carinids in Sun-centered geocentric ecliptic coordinates is marked with a yellow arrow.

[1] https://www.ta3.sk/IAUC22DB/MDC2022/Roje/pojedynczy_obiekt.php?lporz=02122&kodstrumienia=01172

2 Shower classification based on radiants

The GMN shower association criteria assume that meteors within 1° in solar longitude, within 5.1° in radiant in this case, and within 10% in geocentric velocity of a shower reference location are members of that shower. Further details about the shower association are explained in Moorhead et al. (2020). Using these meteor shower selection criteria, 201 orbits have been identified as October epsilon-Carinids.

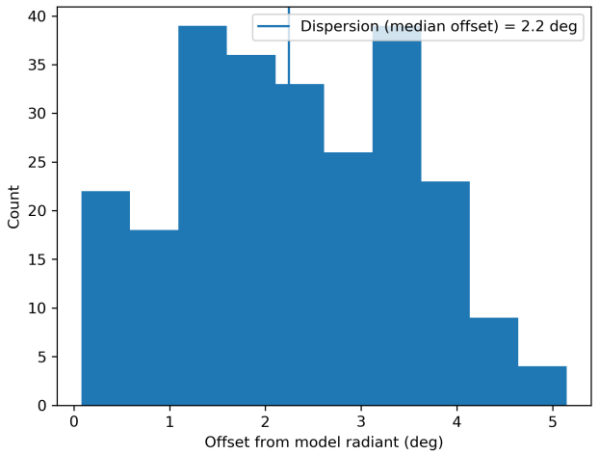

Figure 2 – Dispersion median offset on the radiant position.

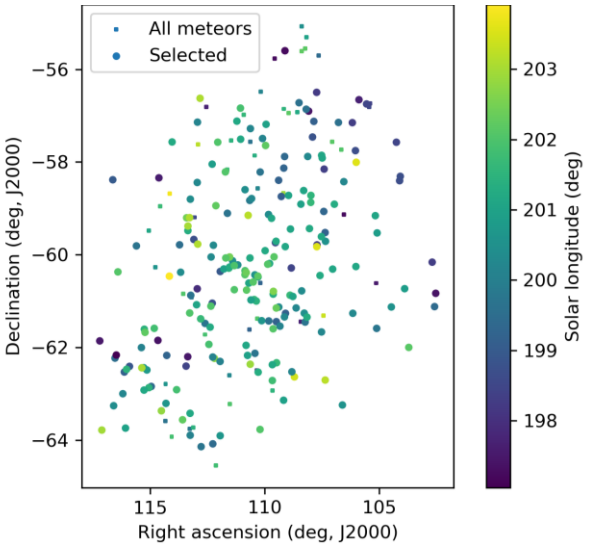

Figure 3 – The radiant distribution during the solar-longitude interval 197° – 204° in equatorial coordinates.

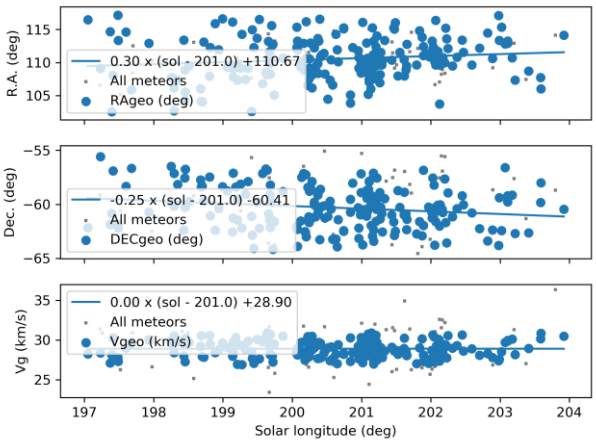

Figure 4 – The radiant drift.

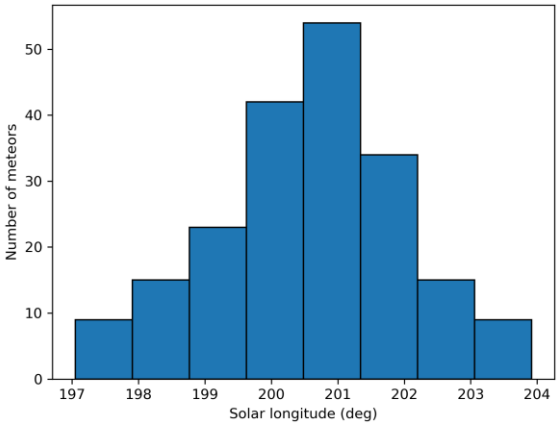

Figure 5 – The uncorrected number of shower meteors recorded per degree in solar longitude.

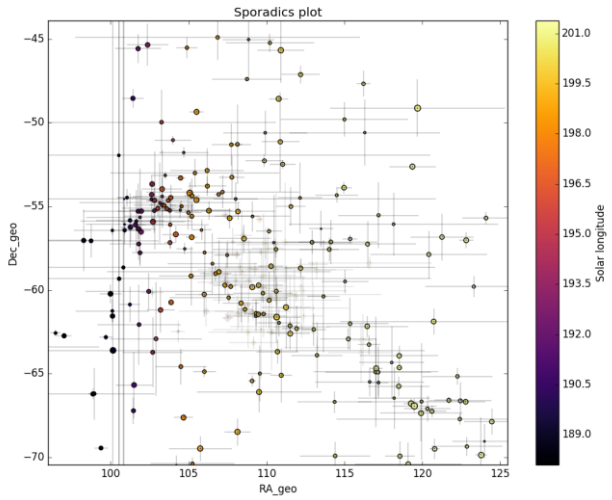

Figure 6 – All non-shower meteor radiants in geocentric equatorial coordinates during the shower activity. The pale diamonds represent the shower radiants plots, error bars represent two sigma values in both coordinates.

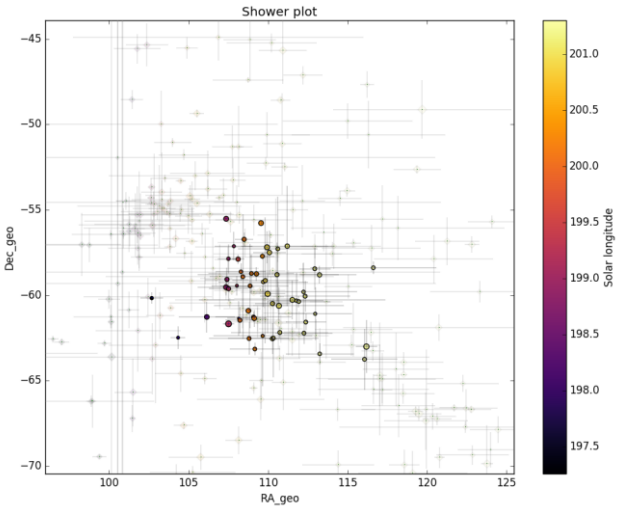

Figure 7 – The reverse of *Figure 6*, now the shower meteors are shown as circles and the non shower meteors as grayed out diamonds.

The shower was independently observed by 212 cameras in five countries (Australia, Brazil, Malaysia, New Zealand and South Africa). The shower had a median geocentric radiant with coordinates R.A. = 110.7°, Decl. = –60.4°, within a circle with a standard deviation of ±2.2° (equinox J2000.0). The radiant drift in R.A. is +0.30° on the sky per

degree of solar longitude and –0.25° in Dec., both referenced to $\lambda_\odot = 201.0°$ (*Figures 3 and 4*). The plot with uncorrected raw numbers of shower meteors per degree in solar longitude indicates that most OEC-meteors were recorded around $\lambda_\odot = 201.0°$ (*Figure 5*). *Figures 6 and 7* show that the October epsilon-Carinids appeared on top of the sporadic background noise. The median Sun-centered ecliptic coordinates were $\lambda - \lambda_\odot = 315.1°$, $\beta = -78.9°$ (*Figure 8*). The geocentric velocity was 28.9 ± 0.1 km/s. The shower parameters as obtained by the GMN method are listed in *Table 1*.

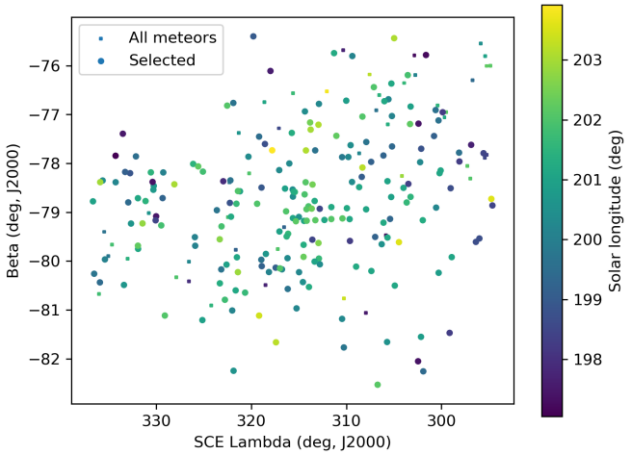

Figure 8 – The radiant distribution during the solar-longitude interval 197° – 204° in Sun centered geocentric ecliptic coordinates.

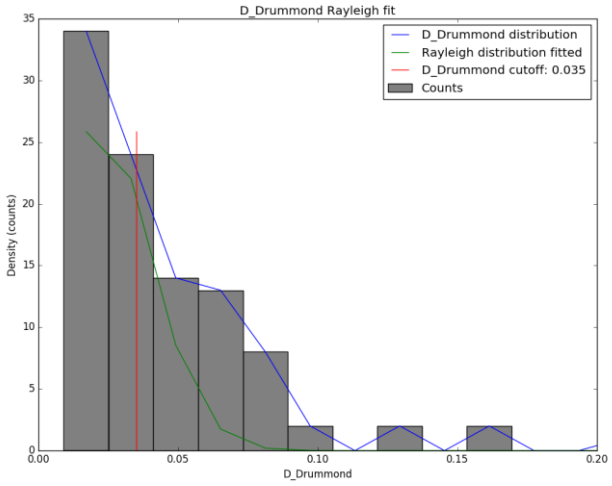

Figure 9 – Rayleigh distribution fit and Drummond D_D criterion cutoff.

3 Shower classification based on orbits

Meteor shower identification strongly depends upon the methodology used to select candidate shower members. The sporadic background is almost everywhere present and risks contamination of selections of shower candidates. In order to double check GMN meteor shower detections, another method based on orbit similarity criteria is used. This approach serves to make sure that no spurious radiant concentrations are mistaken as meteor showers.

A reference orbit is required to start an iterative procedure to approach a mean orbit, which is the most representative orbit for the meteor shower as a whole, removing outliers and sporadic orbits (Roggemans et al., 2019). Three different discrimination criteria are combined in order to have only those orbits which fit the different criteria thresholds. The D-criteria that we use are these of Southworth and Hawkins (1963), Drummond (1981) and Jopek (1993) combined. Instead of using a cutoff value for the thresholds of the D-criteria, these values are considered in different classes with different thresholds of similarity. Depending on the dispersion and the type of orbits, the most appropriate threshold of similarity is selected to locate the best fitting mean orbit as the result of an iterative procedure.

The Rayleigh distribution fit indicates that a very small cut-off value is required with $D_D < 0.035$ (*Figure 9*). The use of D-criteria requires caution as the threshold values differ for different types of orbits. Because of the very small cutoff for the threshold values of the D-criteria, only three classes were plotted:

- Medium: $D_{SH} < 0.1$ & $D_D < 0.04$ & $D_J < 0.1$;
- High: $D_{SH} < 0.075$ & $D_D < 0.03$ & $D_J < 0.075$.
- Very high: $D_{SH} < 0.05$ & $D_D < 0.02$ & $D_J < 0.05$.

This method resulted in a mean orbit with 98 related orbits that fit within the similarity threshold with $D_{SH} < 0.075$, $D_D < 0.03$ and $D_J < 0.075$ between October 10 and 17 in the period 2023 to 2025. The plot of the radiant positions in equatorial coordinates, color-coded for different D-criteria thresholds, has its radiant at 110.4° in Right Ascension and –60.9° in declination (*Figure 10*). A slightly more tolerant threshold of the D-criteria with $D_{SH} < 0.10$, $D_D < 0.04$ and $D_J < 0.1$ results in 173 orbits that fit these threshold values, but with a risk of including contamination with sporadics. Both solutions are mentioned in *Table 1*.

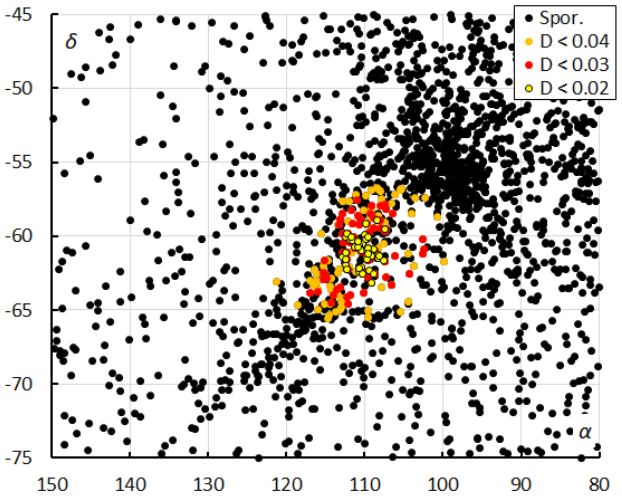

Figure 10 – The radiant distribution during the solar-longitude interval 196° – 207° in equatorial coordinates, color-coded for different threshold values of the D_D orbit similarity criterion.

The dense concentration top right from the OEC radiant are the A Carinids (CRN#842), an episodic shower that displayed an outburst in 2025. Most likely both meteoroid streams are components with a common origin. Looking at the Sun-centered geocentric ecliptic coordinates, the radiant appears stretched in Sun centered longitude because of its

position close to the ecliptic South Pole. The dense concentration just right from the OEC radiant is again the CRN radiant. A case study about the A Carinids[2] has been published in another report (Roggemans et al., 2026).

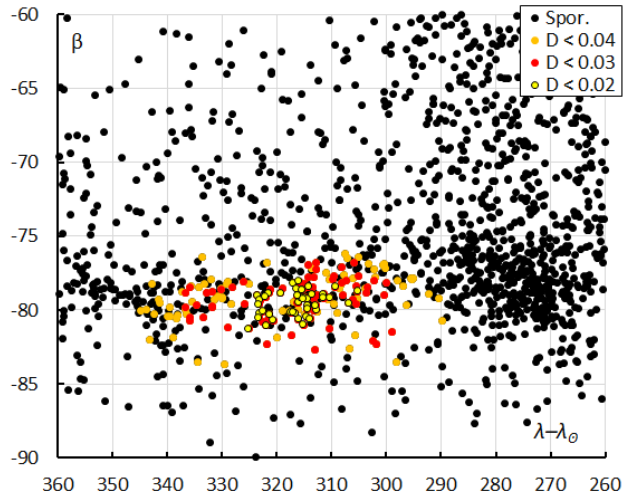

Figure 11 – The radiant distribution during the solar-longitude interval 196° – 207° in Sun-centered geocentric ecliptic coordinates, color-coded for different threshold values of the D_D orbit similarity criterion.

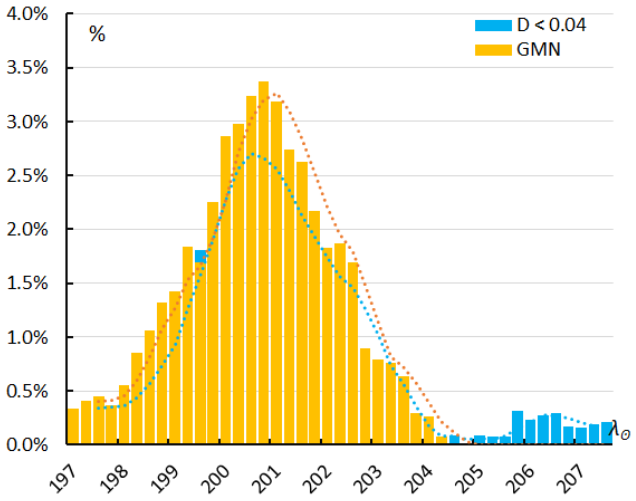

Figure 12 – The percentage of OEC meteors relative to the total number of meteors recorded by cameras at the Southern Hemisphere. Orange is the result for the GMN shower classification, blue for the orbit D-criteria method.

If we look at the ratio OEC-meteors to non-OEC-meteors recorded by GMN at the Southern Hemisphere (*Figure 12*) in 1.0°-time bins in solar longitude in steps of 0.25°, the best rates occurred around $\lambda_\odot = 201.0°$. The orbit-based shower identification found some orbits after $\lambda_\odot = 204.0°$ but the main activity period is situated between solar longitude 197° and 204°. The bias caused by the fact that most GMN cameras at the Southern Hemisphere are installed in Australia and New Zealand, and with less coverage of other longitudes has been solved by combining data collected during three years (2023, 2024 and 2025) to cover the entire time span in solar longitude.

The results obtained from both shower association methods are in good agreement, although both methods had only 95 meteors in common. 106 OEC-meteors were identified by the radiant method but not selected by the orbit method with $D_{SH} < 0.075$ & $D_D < 0.03$ & $D_J < 0.075$. Only three orbits were identified as OEC-orbits but not identified by the radiant based method.

4 Orbit and parent body

Looking at the diagram of inclination versus longitude of perihelion, we can see a dense concentration (*Figure 13*). The concentration right next to the OEC-points are the A Carinids and the concentration near the upper-left are the October 6-Draconids (OSD#745)[3], which were active 10 days later than listed in the MDC working list of meteor showers.

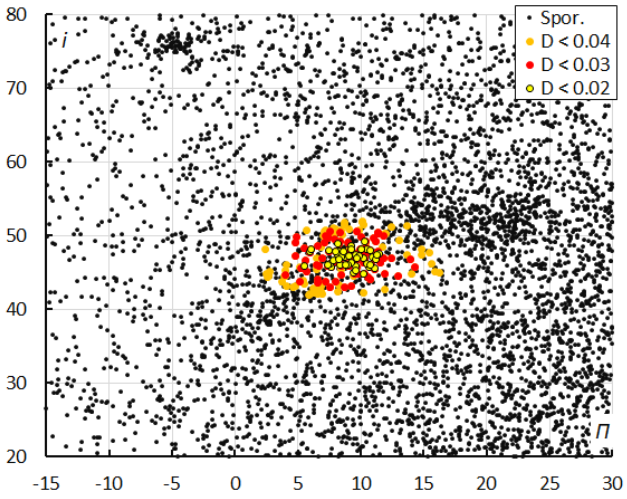

Figure 13 – The diagram of the inclination *i* against the longitude of perihelion Π color-coded for different classes of D criterion threshold, for $\lambda_\odot$ between 196° and 207°.

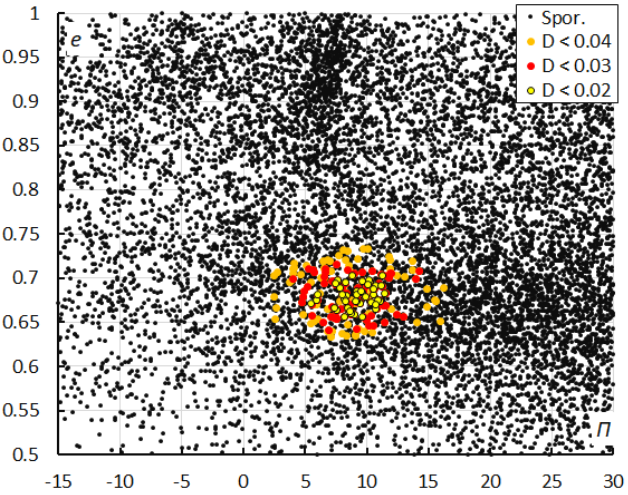

Figure 14 – The diagram of the eccentricity *e* against the longitude of perihelion Π color-coded for different classes of D criterion threshold, for $\lambda_\odot$ between 196° and 207°.

The diagram in *Figure 14* shows the concentration in longitude of perihelion and eccentricity. The concentration

[2] https://www.ta3.sk/IAUC22DB/MDC2022/Roje/pojedynczy_obiekt.php?lporz=01772&kodstrumienia=00842

[3] https://www.ta3.sk/IAUC22DB/MDC2022/Roje/pojedynczy_obiekt.php?lporz=01636&kodstrumienia=00745

at right from the OEC-meteors are the A Carinids, the concentration above the OEC-meteors represents mainly the October Ursae Majorids (OCU#333)[4] and some 31-Lyncids (TLY#613)[5].

Figure 15 shows the concentration in eccentricity and inclination. The cloud around the OEC-meteors are meteors identified by the radiant method as OEC, CRN and some weaker activity sources. The small concentration in the bottom left corner is caused by 62-Andromedids (San#924)[6].

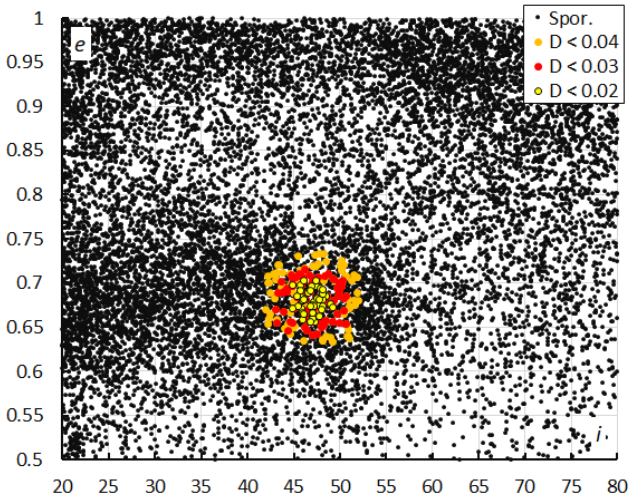

Figure 15 – The diagram of the eccentricity e against the inclination i color-coded for different classes of D criterion threshold, for $\lambda_\odot$ between 196° and 207°.

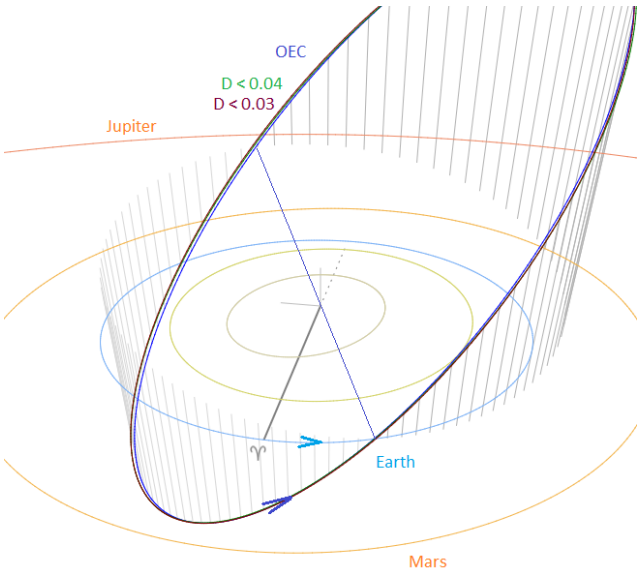

Figure 16 – Comparing the mean orbits for the solutions for the October epsilon-Carinids based on the shower identification according to two methods, blue is for the GMN-method, green for the orbit method with $D_D < 0.04$ and maroon for $D_D < 0.03$ in *Table 1*, close-up at the inner Solar System. (Plotted with the Orbit visualization app provided by Pető Zsolt).

Table 1 – Comparing solutions derived by two different methods, GMN-method based on radiant positions and orbit association for $D_D < 0.04$ and $D_D < 0.03$.

	GMN	$D_D < 0.04$	$D_D < 0.03$
$\lambda_\odot$ (°)	201.0	200.7	201.1
$\lambda_{\odot b}$ (°)	197.0	196.5	197.3
$\lambda_{\odot e}$ (°)	204.0	207.2	204.3
α_g (°)	110.7	110.6	110.4
δ_g (°)	–60.4	–61.1	–60.9
$\Delta\alpha_g$ (°)	+0.30	+0.68	+0.94
$\Delta\delta_g$ (°)	–0.25	–0.69	–0.48
v_g (km/s)	28.9	28.6	28.6
H_b (km)	91.1	90.4	89.9
H_e (km)	82.3	81.2	81.3
H_p (km)	87.0	86.0	86.0
Mag_{Ap}	+0.3	+0.2	+0.3
λ_g (°)	156.12	156.8	156.7
$\lambda_g - \lambda_\odot$ (°)	315.12	315.6	315.4
β_g (°)	–78.87	–79.1	–79.1
a (A.U.)	3.055	3.11	3.09
q (A.U.)	0.986	0.986	0.987
e	0.677	0.683	0.681
i (°)	47.5	46.9	47.0
ω (°)	347.6	347.8	347.8
Ω (°)	20.6	20.8	21.1
Π (°)	8.2	8.6	8.9
T_j	2.47	2.45	2.45
N	201	173	99

Table 2 – Top ten matches of a search for possible parent bodies with $D_D < 0.15$

Name	D_D
2010 HY_{22}	0.046
2020 VM_1	0.081
2010 LG_{64}	0.092
2018 VG_1	0.105
2019 WF_1	0.114
2019 UQ_7	0.119
2016 XP_{23}	0.122
2017 UZ_{42}	0.131
(523820) 2011 GN_{44}	0.139
2017 XC	0.147

The Tisserand's parameter relative to Jupiter, T_j (= 2.47) identifies the orbit as of a Jupiter Family Comet type orbit. *Figure 16* shows that the plotted orbits are almost identical for all three solutions. The OEC meteoroid stream intersects

[4] https://www.ta3.sk/IAUC22DB/MDC2022/Roje/pojedynczy_obiekt.php?lporz=00846&kodstrumienia=00333
[5] https://www.ta3.sk/IAUC22DB/MDC2022/Roje/pojedynczy_obiekt.php?lporz=01458&kodstrumienia=00613
[6] https://www.ta3.sk/IAUC22DB/MDC2022/Roje/pojedynczy_obiekt.php?lporz=01868&kodstrumienia=00924

the Earth orbit at its ascending node, hitting the planet from deep south of the ecliptic. The position of the descending node in the ecliptic plane is relatively close to the orbit of Jupiter.

A parent-body search top 10 resulted in candidates with a threshold for the Drummond D_D criterion value lower than 0.15 (*Table 2*). Asteroid 2010 HY_{22} with $D_D < 0.046$ looks a plausible candidate but orbit integrations are required to assess if there is a relationship. The A Carinids, which occur at the same time, also appear to derive from this parent body (Roggemans et al., 2026)

5 Past years' activity

The only video meteor observations known for this shower are CAMS observations from 2019–2021 published by Jenniskens (2023). A search through historic visual meteor observations confirms that this shower has been observed in the past as a single source that included the A Carinids (CRN#842). The two radiants couldn't be distinguished by visual observers in the past. A more detailed summary of visual observations has been given in a separate case study on the A Carinids which produced an outburst in 2025 (Roggemans et al., 2026).

6 Conclusion

Global Meteor Network observations confirm the existence of the minor meteor shower known as the October epsilon-Carinids (OEC#1172). The orbit parameters obtained by GMN are in good agreement with those derived by Jenniskens (2023) based on CAMS low-light video cameras, except for the eccentricity and the Sun-centered ecliptic longitude.

Acknowledgments

This report is based on the data of the Global Meteor Network (Vida et al., 2020a; 2020b; 2021) which is released under the CC BY 4.0 license[7]. We thank all 825 participants in the Global Meteor Network project for their contribution and perseverance. A list with the names of the volunteers who contribute to GMN has been published in the 2024 annual report (Roggemans et al., 2025). The following 212 cameras recorded October epsilon-Carinids that have been used in this study:

AU0002, AU0003, AU000A, AU000B, AU000C, AU000D, AU000E, AU000F, AU000G, AU000Q, AU000R, AU000S, AU000T, AU000U, AU000V, AU000W, AU000X, AU000Y, AU000Z, AU001A, AU001B, AU001C, AU001D, AU001E, AU001F, AU001L, AU001P, AU001Q, AU001R, AU001S, AU001U, AU001V, AU001W, AU001X, AU001Z, AU0028, AU0029, AU002A, AU002B, AU002C, AU002D, AU002F, AU0030, AU003E, AU003G, AU003J, AU0041, AU0042, AU0046, AU0047, AU0048, AU004J, AU004K, AU004L, AU004Q, BR000M, BR000Y, BR001M, BR002C, MY0001, MY0002, NZ0001, NZ0002, NZ0003, NZ0007, NZ0008, NZ0009, NZ000A, NZ000B, NZ000C, NZ000D, NZ000F, NZ000G, NZ000H, NZ000J, NZ000K, NZ000L, NZ000M, NZ000N, NZ000P, NZ000Q, NZ000R, NZ000S, NZ000T, NZ000U, NZ000V, NZ000W, NZ000X, NZ000Z, NZ0010, NZ0011, NZ0012, NZ0014, NZ0015, NZ0016, NZ0018, NZ0019, NZ001A, NZ001C, NZ001E, NZ001G, NZ001N, NZ001P, NZ001R, NZ001S, NZ001V, NZ001X, NZ001Y, NZ001Z, NZ0020, NZ0021, NZ0022, NZ0023, NZ0024, NZ0025, NZ0026, NZ0027, NZ0028, NZ0029, NZ002B, NZ002C, NZ002E, NZ002F, NZ002G, NZ002H, NZ002K, NZ002L, NZ002N, NZ002P, NZ002Q, NZ002R, NZ002S, NZ002T, NZ002U, NZ002V, NZ002W, NZ002X, NZ002Y, NZ002Z, NZ0030, NZ0033, NZ0034, NZ0035, NZ0036, NZ0037, NZ0038, NZ0039, NZ003A, NZ003B, NZ003C, NZ003E, NZ003G, NZ003H, NZ003K, NZ003N, NZ003Q, NZ003R, NZ003S, NZ003T, NZ003U, NZ003V, NZ003W, NZ003Y, NZ003Z, NZ0040, NZ0041, NZ0042, NZ0044, NZ0045, NZ0046, NZ0049, NZ004A, NZ004B, NZ004C, NZ004D, NZ004E, NZ004H, NZ004J, NZ004L, NZ004M, NZ004N, NZ004R, NZ004S, NZ004T, NZ004U, NZ004V, NZ004X, NZ004Y, NZ0051, NZ0059, NZ005A, NZ005B, NZ005C, NZ005D, NZ005E, NZ005G, NZ005K, NZ005M, NZ005N, NZ005Z, NZ0061, NZ0063, NZ0065, NZ0066, NZ0067, NZ0068, NZ0069, ZA0002, ZA0006, ZA0007, ZA0008, ZA000C.

References

Drummond J. D. (1981). "A test of comet and meteor shower associations". *Icarus*, **45**, 545–553.

Jenniskens P. (2023). Atlas of Earth's meteor showers. Elsevier, Cambridge, United states. ISBN 978-0-443-23577-1. Page 791.

Jopek T. J. (1993). "Remarks on the meteor orbital similarity D-criterion". *Icarus*, **106**, 603–607.

Jopek T. J., Rudawska R. and Pretka-Ziomek H. (2006). "Calculation of the mean orbit of a meteoroid stream". *Monthly Notices of the Royal Astronomical Society*, **371**, 1367–1372.

Moorhead A. V., Clements T. D., Vida D. (2020). "Realistic gravitational focusing of meteoroid streams". *Monthly Notices of the Royal Astronomical Society*, **494**, 2982–2994.

Roggemans P., Johannink C. and Campbell-Burns P. (2019). "October Ursae Majorids (OCU#333)". *eMetN Meteor Journal*, **4**, 55–64.

Roggemans P., Campbell-Burns P., Kalina M., McIntyre M., Scott J. M., Šegon D., Vida D. (2025). "Global Meteor Network report 2024". *eMetN Meteor Journal*, **10**, 67–101.

[7] https://creativecommons.org/licenses/by/4.0/

Roggemans P., Vida D., Šegon D., Scott J., Wood J. (2026). "A Carinids (CRN#842) outburst in 2025". *eMetN Meteor Journal*, **11**, 8–15.

Southworth R. B. and Hawkins G. S. (1963). "Statistics of meteor streams". *Smithsonian Contributions to Astrophysics*, **7**, 261–285.

Vida D., Gural P., Brown P., Campbell-Brown M., Wiegert P. (2020a). "Estimating trajectories of meteors: an observational Monte Carlo approach - I. Theory". *Monthly Notices of the Royal Astronomical Society*, **491**, 2688–2705.

Vida D., Gural P., Brown P., Campbell-Brown M., Wiegert P. (2020b). "Estimating trajectories of meteors: an observational Monte Carlo approach - II. Results". *Monthly Notices of the Royal Astronomical Society*, **491**, 3996–4011.

Vida D., Šegon D., Gural P. S., Brown P. G., McIntyre M. J. M., Dijkema T. J., Pavletić L., Kukić P., Mazur M. J., Eschman P., Roggemans P., Merlak A., Zubrović D. (2021). "The Global Meteor Network – Methodology and first results". *Monthly Notices of the Royal Astronomical Society*, **506**, 5046–5074.

A Carinids (842#CRN) outburst in 2025

Paul Roggemans[1], **Denis Vida**[2,3], **Damir Šegon**[4,5], **James M. Scott**[6], **Jeff Wood**[7]

[1] **Pijnboomstraat 25, 2800 Mechelen, Belgium**

[2] **Department of Physics and Astronomy, University of Western Ontario, Richmond Street, London, N6A 3K7, Ontario, Canada**

[3] **Institute for Earth and Space Exploration, University of Western Ontario, Perth Drive, London, N6A 5B8, Ontario, Canada**
denis.vida@gmail.com

[4] **Astronomical Society Istra Pula, Park Monte Zaro 2, 52100 Pula, Croatia**

[5] **Višnjan Observatory, Istarska 5, 52463 Višnjan, Croatia**

[6] **Department of Geoscience, Aarhus University, Høegh-Guldbergs Gade 2. DK-8000 Aarhus C, Denmark**
jscott@geo.au.dk

[7] **PO Box 162, Willetton, Western Australia 6955, Australia**

The Global Meteor Network recorded an outburst from the A Carinids (842#CRN) during October 13 – 14, 2025. In total, 171 meteors belonging to this meteor shower were observed between 196.0° < λ_O < 204.0° from a radiant at R.A. = 100.9° and Decl.= –55.4°, with a geocentric velocity of 31.5 km/s. In 2023 and 2024, only 15 and 29 possible CRN-meteors were recorded. This case study confirms the existence of this meteor shower with a new solution added to the IAU-MDC working list of meteor showers.

1 Introduction

On 13–14 October 2025 some unusually strong activity was spotted near the South Pole (*Figure 1*). The radiant source was identified as the A Carinids (842#CRN)[8], first reported by Jenniskens (2018) from CAMS southern hemisphere low-light video observations. The night of October 13 on 14, 2020 displayed an outburst (Jenniskens, 2020). Because of enhanced activity observed in 2014 and 2019–2020, with weak activity in between, the shower has been listed as an episodic shower (Jenniskens, 2023). The 2025 outburst confirms this periodic nature. *Figure 1* shows the position of the A Carinids radiant which is close to the South Pole and close to the October epsilon-Carinids (OEC#1172).

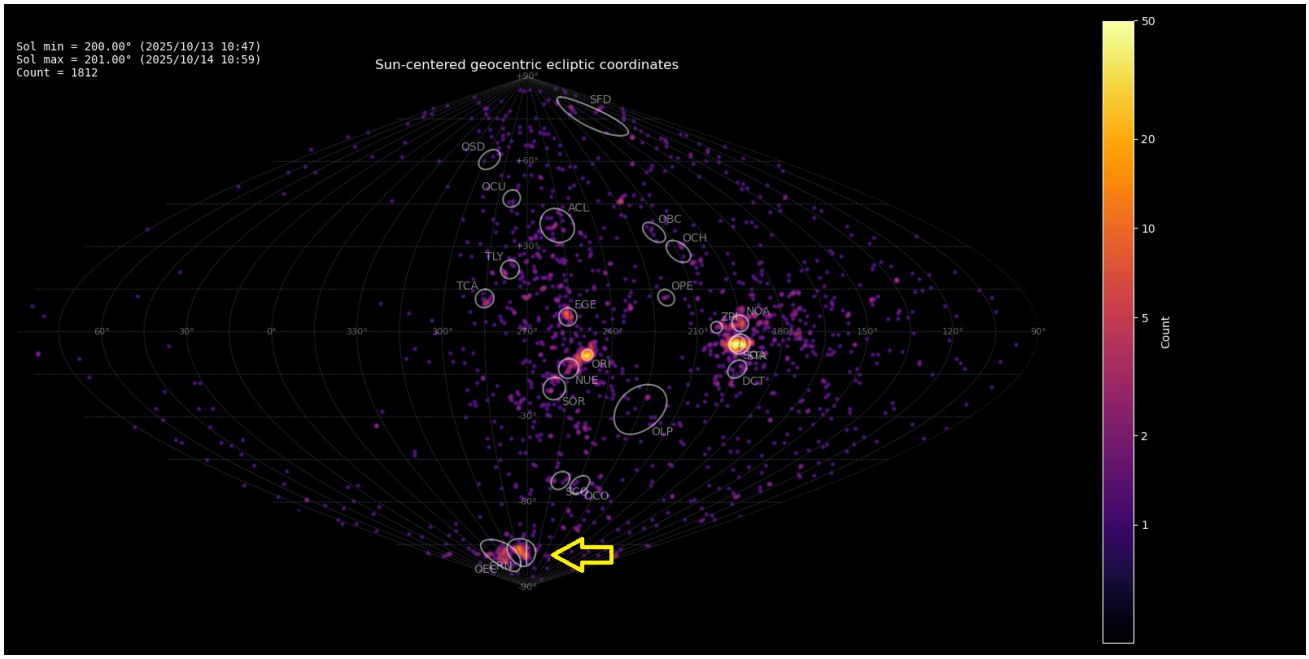

Figure 1 – Radiant density map (sinusoidal projection) with 1812 radiants obtained by the Global Meteor Network during 13–14 October, 2025. The position of the A Carinids in Sun-centered geocentric ecliptic coordinates is marked with a yellow arrow.

[8] https://www.ta3.sk/IAUC22DB/MDC2022/Roje/pojedynczy_objekt.php?lporz=01772&kodstrumienia=00842

2 Shower classification based on radiants

The GMN shower association criteria assume that meteors within 1° in solar longitude, within 4.9° in radiant in this case, and within 10% in geocentric velocity of a shower reference location are members of that shower. Further details about the shower association are explained in Moorhead et al. (2020). Using these meteor shower selection criteria, 171 orbits have been identified as A Carinids.

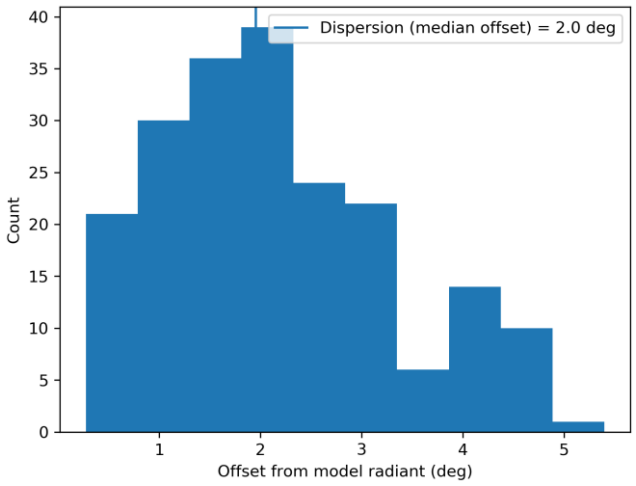

Figure 2 – Dispersion median offset on the radiant position.

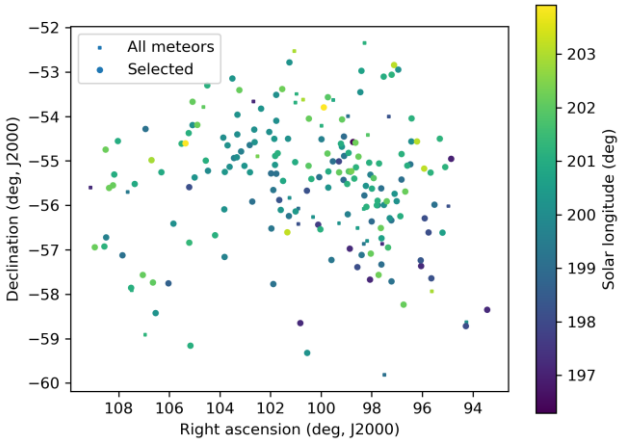

Figure 3 – The radiant distribution during the solar-longitude interval 196° – 204° in equatorial coordinates.

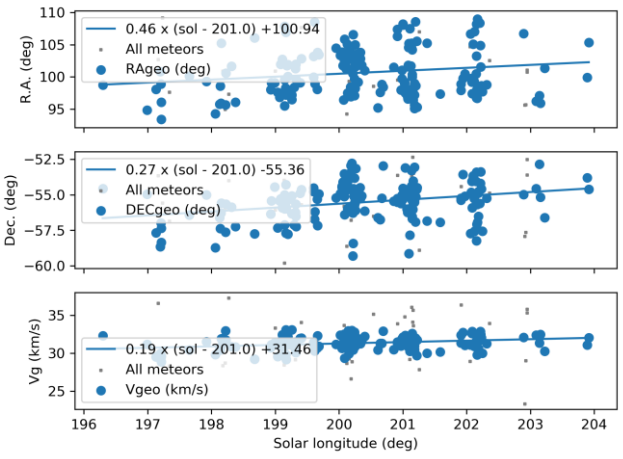

Figure 4 – The radiant drift.

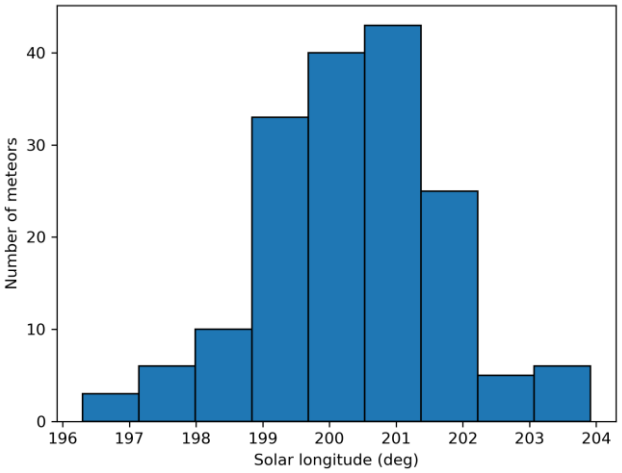

Figure 5 – The uncorrected number of shower meteors recorded per degree in solar longitude.

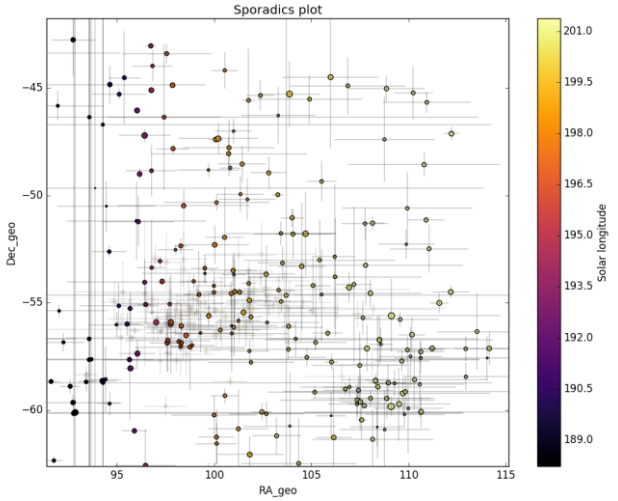

Figure 6 – All non-shower meteor radiants in geocentric equatorial coordinates during the shower activity. The pale diamonds represent the shower radiants plots, error bars represent two sigma values in both coordinates.

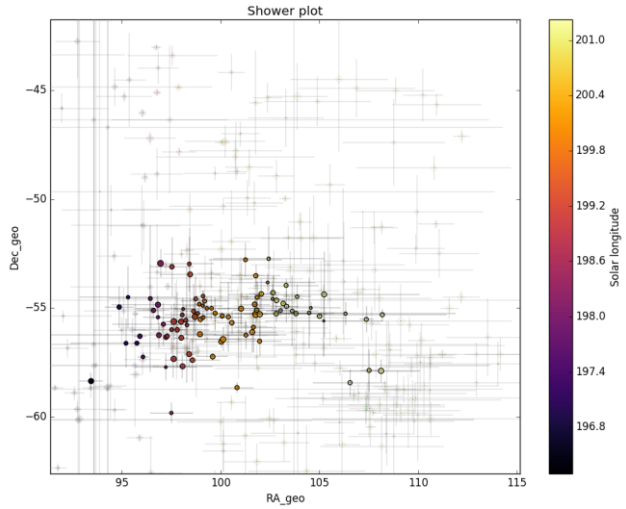

Figure 7 – The reverse of *Figure 6*, now the shower meteors are shown as circles and the non shower meteors as grayed out diamonds.

The shower was independently observed in 2025 by 186 cameras in Australia, Brazil, Chile, New Zealand and South Africa. The shower had a median geocentric radiant with coordinates R.A. = 100.9°, Decl. = –55.4°, within a circle

with a standard deviation of ±2.0° (equinox J2000.0). The radiant drift in R.A. is +0.46° on the sky per degree of solar longitude and +0.27° in Dec., both referenced to $\lambda_\odot = 201.0°$ (*Figures 3 and 4*). The uncorrected raw numbers of shower meteors per degree in solar longitude indicate that most CRN-meteors were recorded around $\lambda_\odot = 201.0°$ (*Figure 5*). *Figures 6 and 7* show that the A Carinids appeared on top of the sporadic background noise. The median Sun-centered ecliptic coordinates were $\lambda - \lambda_\odot = 279.0°$, $\beta = -77.5°$ (*Figure 8*). The geocentric velocity was 31.5 ± 0.1 km/s. The shower parameters as obtained by the GMN method are listed in *Table 1*.

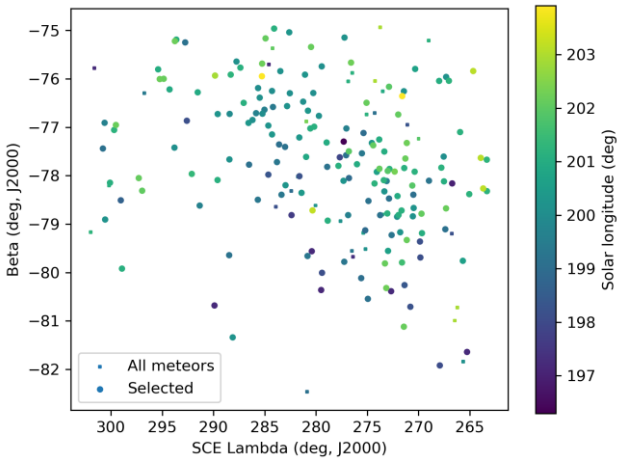

Figure 8 – The radiant distribution during the solar-longitude interval 196° – 204° in Sun centered geocentric ecliptic coordinates.

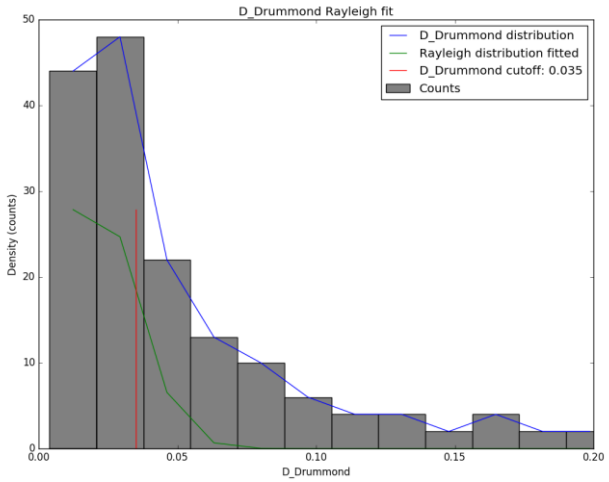

Figure 9 – Rayleigh distribution fit and Drummond D_D criterion cutoff.

3 Shower classification based on orbits

Meteor shower identification strongly depends upon the methodology used to select candidate shower members. The sporadic background is almost everywhere present and risks contamination of selections of shower candidates. In order to double check GMN meteor shower detections, another method based on orbit similarity criteria is used. This procedure serves to make sure that no spurious radiant concentrations are mistaken as meteor showers.

A reference orbit is required to start an iterative procedure to approach a mean orbit, which is the most representative orbit for the meteor shower as a whole, removing outliers and sporadic orbits (Roggemans et al., 2019). Three different discrimination criteria are combined in order to have only those orbits which fit the different criteria thresholds. The D-criteria that we use are these of Southworth and Hawkins (1963), Drummond (1981) and Jopek (1993) combined. Instead of using a single cutoff value for the threshold of the D-criteria, these values are considered in different classes with different thresholds of similarity. Depending upon the dispersion and the type of orbits, the most appropriate threshold of similarity is selected to locate the best fitting mean orbit as the result of an iterative procedure.

The Rayleigh distribution fit indicates that a very small cutoff value is required with $D_D < 0.035$ (*Figure 9*). The use of D-criteria requires caution as the threshold values differ for different types of orbits. Because of the very small cutoff of the threshold values of the D-criteria, only three classes were plotted:

- Medium: $D_{SH} < 0.1$ & $D_D < 0.04$ & $D_J < 0.1$;
- High: $D_{SH} < 0.075$ & $D_D < 0.03$ & $D_J < 0.075$.
- Very high: $D_{SH} < 0.05$ & $D_D < 0.02$ & $D_J < 0.05$.

This method resulted in a mean orbit with 101 related orbits that fit within the similarity thresholds with $D_{SH} < 0.075$, $D_D < 0.03$ and $D_J < 0.075$, recorded October 10 – 18, 2025. The plot of the radiant positions in equatorial coordinates, color-coded for different D-criteria thresholds, has its radiant at 99.7° in Right Ascension and –55.1° in declination (*Figure 10*). A slightly more tolerant threshold of the D-criteria with $D_{SH} < 0.10$, $D_D < 0.04$ and $D_J < 0.1$ results in 126 orbits that fit these threshold values, but with a risk of including contamination with sporadics. Both solutions are mentioned in *Table 1*.

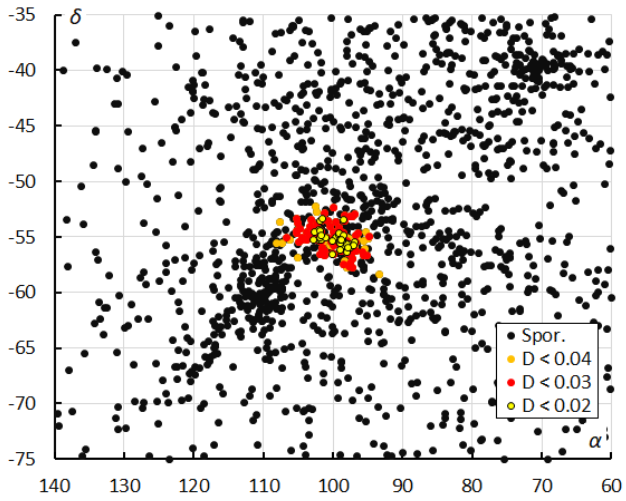

Figure 10 – The radiant distribution during the solar-longitude interval 196° – 207° in equatorial coordinates in 2025, color-coded for different threshold values of the D_D orbit similarity criterion.

The dense concentration just left below from the CRN radiants are the October epsilon-Carinids (OEC#1172), an annual shower. Most likely both meteoroid streams are components with a common origin. Near the upper-right

corner another concentration of radiants is visible. These are the Caelids (CAE#837)[9].

Looking at the Sun-centered geocentric ecliptic coordinates (*Figure 11*), the radiant appears stretched in Sun centered longitude because of its position close to the ecliptic South Pole. The dense concentration just left from the CRN radiant is again the OEC radiant. A case study about the October epsilon-Carinids[10] has been published in another report (Roggemans et al., 2026).

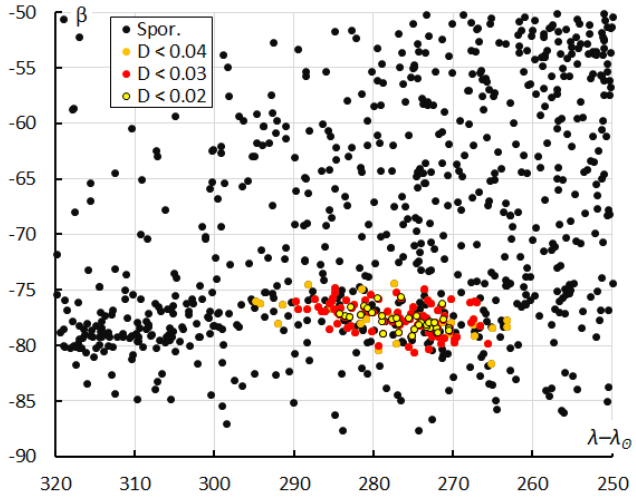

Figure 11 – The radiant distribution during the solar-longitude interval 196° – 207° in Sun-centered geocentric ecliptic coordinates, color-coded for different threshold values of the D_D orbit similarity criterion.

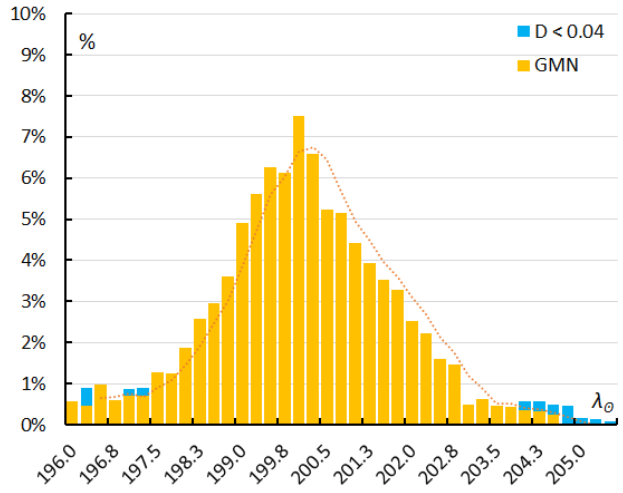

Figure 12 – The percentage of OEC meteors relative to the total number of meteors recorded by cameras at the Southern Hemisphere. Orange is the result for the GMN shower classification, blue for the D-criteria threshold method.

If we look at the ratio CRN-meteors to non-CRN-meteors recorded by GMN at the Southern Hemisphere (*Figure 12*) in 1.5°-time bins in solar longitude in steps of 0.25°, the moving average (dotted line), indicates that best rates occurred around $\lambda_\odot = 200.0$. However, the best rates may have occurred later and missed by the fact that most GMN cameras at the Southern Hemisphere are installed in Australia and New Zealand with rather little or no coverage at other longitudes. A short duration peak like observed in 2020 at $\lambda_\odot = 200.9°$ (Jenniskens, 2020) has not been recorded in 2025.

The results obtained from both shower association methods are in good agreement although both methods identified 116 meteors in common with different additional meteors in each sample. 55 CRN-meteors were identified based on the radiant method but not selected by the orbit method with $D_{SH} < 0.1$ & $D_D < 0.04$ & $D_J < 0.1$. Only ten orbits were identified as CRN-orbits but not identified by the radiant based method, six of these were recorded after $\lambda_\odot = 204.0°$.

The radiant classification method has searched only the 2025 GMN data as no significant activity was found in previous years. The orbit classification method applied on previous years found only 17 orbits in 2023 and 29 orbits in 2024 that fit the thresholds $D_{SH} < 0.075$, $D_D < 0.03$ and $D_J < 0.075$. This shows that there is a modest annual activity. The much higher activity recorded in 2025 cannot be explained by the expansion of the GMN camera network and definitely concerns an outburst.

4 Orbit and parent body

Looking at the diagram of inclination versus longitude of perihelion, we can see a dense concentration (*Figure 13*). The concentration on the lefthand side of the CRN-points are the October epsilon-Carinids and the concentration near the upper-left are the October 6-Draconids (OSD#745)[11], which were active 10 days later than listed in the MDC working list of meteor showers.

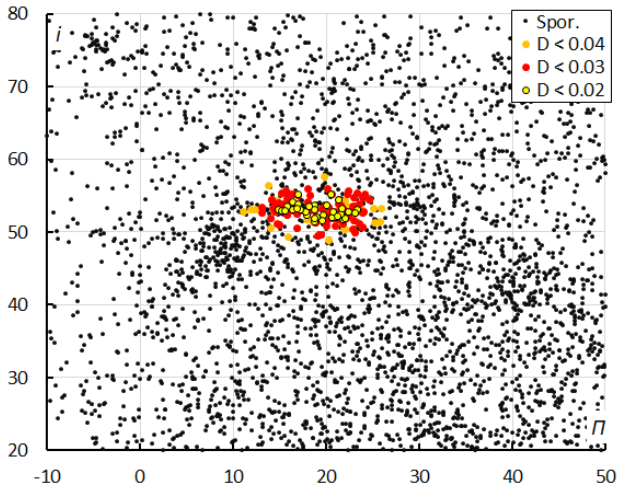

Figure 13 – The diagram of the inclination *i* versus the longitude of perihelion *Π* color-coded for different classes of D criteria thresholds, for $\lambda_\odot$ between 196° and 207°.

[9] https://www.ta3.sk/IAUC22DB/MDC2022/Roje/pojedynczy_obiekt.php?lporz=01766&kodstrumienia=00837
[10] https://www.ta3.sk/IAUC22DB/MDC2022/Roje/pojedynczy_obiekt.php?lporz=02122&kodstrumienia=01172
[11] https://www.ta3.sk/IAUC22DB/MDC2022/Roje/pojedynczy_obiekt.php?lporz=01636&kodstrumienia=00745

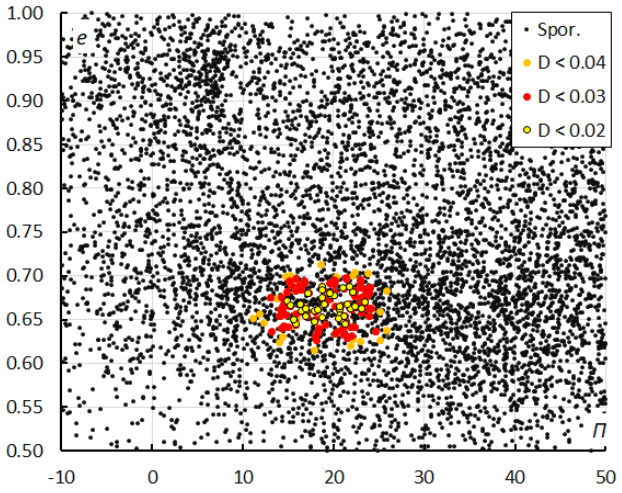

Figure 14 – The diagram of the eccentricity e versus the longitude of perihelion Π color-coded for different classes of D criteria thresholds, for $\lambda_\odot$ between 196° and 207°.

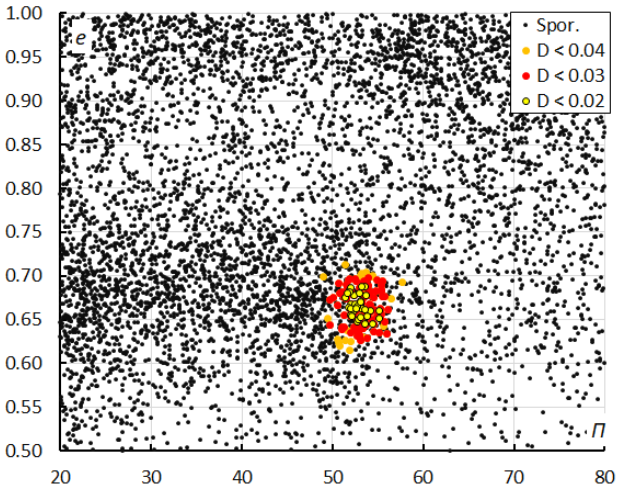

Figure 15 – The diagram of the eccentricity e versus the inclination i color-coded for different classes of D criteria thresholds, for $\lambda_\odot$ between 196° and 207°.

The diagram in *Figure 14* shows the distribution in longitude of perihelion and eccentricity. The concentration to the left from the CRN-meteors are the October epsilon-Carinids, and the concentration in the upper left consists mainly of the October Ursae Majorids (OCU#333).

Figure 15 shows the concentration in eccentricity and inclination. The cloud left of the CRN-meteors are meteors identified by the radiant method as OEC and some weaker activity sources.

Table 1 – Comparing solutions derived by two different methods, GMN-method based on radiant positions and the orbit association method for $D_D < 0.04$ and $D_D < 0.03$ in 2025, 2023–2024 and 2023–2025.

	2025			2023–2024		2023–2025	
	GMN	$D_D < 0.04$	$D_D < 0.03$	$D_D < 0.04$	$D_D < 0.03$	$D_D < 0.04$	$D_D < 0.03$
$\lambda_\odot$ (°)	201.0	200.4	200.3	198.4	198.2	200.1	200.1
$\lambda_{\odot b}$ (°)	196.0	196.2	197.0	196.2	196.2	196.2	196.2
$\lambda_{\odot e}$ (°)	204.0	205.3	205.2	204.7	201.8	205.7	204.8
α_g (°)	100.9	99.7	99.7	98.0	97.9	99.0	98.7
δ_g (°)	–55.4	–55.1	–55.1	–57.1	–57.2	–55.5	–55.5
$\Delta\alpha_g$ (°)	+0.46	+0.59	+0.49	+0.15	–0.20	+0.48	+0.44
$\Delta\delta_g$ (°)	+0.27	+0.21	+0.19	+0.09	+0.08	+0.30	+0.22
v_g (km/s)	31.5	31.4	31.4	30.5	30.4	31.1	31.2
H_b (km)	97.2	99.0	99.4	98.6	99.3	99.1	99.3
H_e (km)	83.1	83.2	83.2	81.8	81.4	83.2	83.0
H_p (km)	89.3	90.9	92.8	89.6	91.1	91.1	91.4
Mag_{Ap}	0.0	0.0	–0.2	–0.4	–0.4	–0.1	–0.1
λ_g (°)	120.03	116.6	116.5	114.1	113.7	115.0	114.7
$\lambda_g - \lambda_\odot$ (°)	279.03	276.7	275.6	275.9	274.8	275.4	274.7
β_g (°)	–77.53	–77.6	–77.5	–79.6	–79.8	–78.2	–78.2
a (A.U.)	3.018	2.96	2.97	3.14	3.18	3.00	3.01
q (A.U.)	0.996	0.996	0.996	0.997	0.997	0.996	0.996
e	0.670	0.664	0.665	0.682	0.686	0.669	0.669
i (°)	52.6	53.0	53.1	50.8	50.7	52.2	52.3
ω (°)	357.7	358.5	358.6	359.0	359.1	359.1	359.4
Ω (°)	20.4	20.6	20.6	18.6	18.5	20.1	20.0
Π (°)	18.12	19.1	19.2	17.6	17.6	19.1	19.4
T_j	2.41	2.44	2.43	2.38	2.36	2.43	2.42
N	171	126	101	78	47	210	132

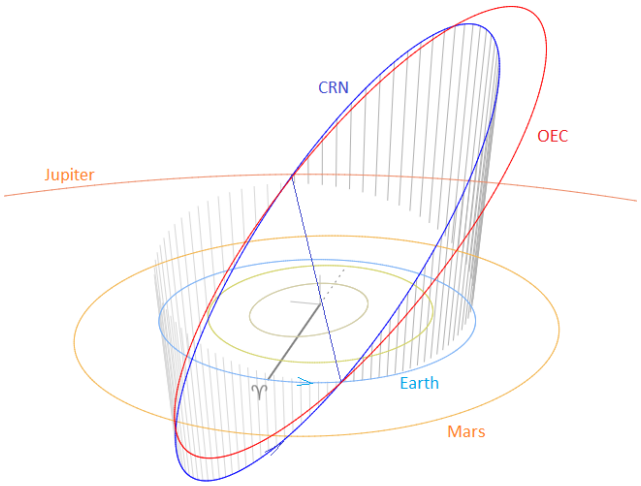

Figure 16 – Comparing the mean orbits for the solutions for the A Carinids (blue) and the October epsilon-Carinids (red) based on the radiant identification, close-up at the inner Solar System. (Plotted with the Orbit visualization app provided by Pető Zsolt).

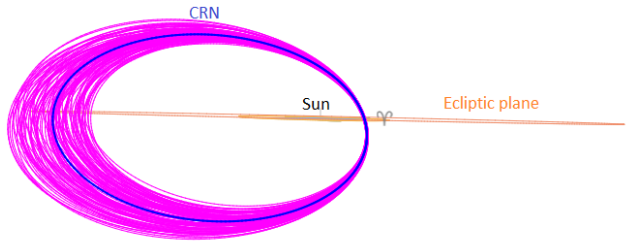

Figure 17 – 101 A Carinid orbits and their mean orbit as seen in the ecliptic plane. (Plotted with the Orbit visualization app provided by Pető Zsolt).

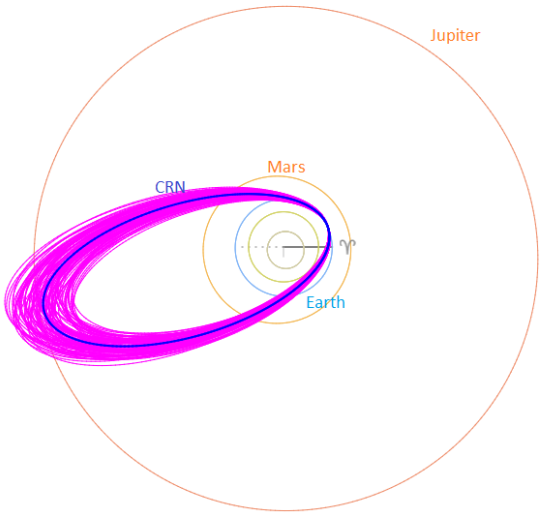

Figure 18 – 101 A Carinid orbits and their mean orbit as seen on top of the ecliptic plane. (Plotted with the Orbit visualization app provided by Pető Zsolt).

The Tisserand's parameter relative to Jupiter, T_j (= 2.41) identifies the orbit as of a Jupiter Family Comet type orbit. *Figure 16* compares the orbits of the A Carinids with the October epsilon-Carinids. The CRN meteoroid stream intersects the Earth orbit at its ascending node, hitting the planet from deep south of the ecliptic. The position of the descending node in the ecliptic plane is relatively close to the orbit of Jupiter. The CRN orbit is higher inclined to the ecliptic than the OEC orbit. Apart from the inclination, both streams differ mainly in longitude of perihelion with about 10°.

All 101 CRN-orbits recorded in 2025 that fit within $D_{SH} < 0.075$, $D_D < 0.03$ and $D_J < 0.075$ have been plotted in *Figure 17* as seen in the ecliptic plane and in *Figure 18* projected on the ecliptic plane. Despite the very strict D criteria cutoff values, the slightest uncertainty at the encounter with the Earth results in a large dispersion at the aphelia. In reality, the meteoroid stream will be more compact at its aphelion. The plotted dispersion is mainly due to measurement uncertainties.

A parent-body search of the top 10 results in candidates with a threshold for the Drummond D_D criterion value lower than 0.16 (*Table 2*). Asteroid 2010 HY22 with $D_D < 0.086$ looks like the most plausible candidate but orbit integrations are required to assess if there is a relationship. Jenniskens (2023) mentions 2009 SG18 as a possible, but uncertain, source, although this object does not appear in the top ten candidates found by GMN.

Table 2 – Top ten matches of a search for possible parent bodies with $D_D < 0.16$

Name	D_D
2010 HY22	0.086
2010 LG64	0.107
2020 VM1	0.108
2022 RX3	0.119
2017 UZ42	0.13
2018 VG1	0.139
2019 WF1	0.14
(89830) 2002 CE	0.15
2019 UQ7	0.156
2016 XP23	0.158

5 Past years' activity

The only video meteor observations known for the A Carinids are CAMS observations from 2019–2021 published by Jenniskens (2023). A search through historic visual meteor observations indicates that this shower has been observed in the past, but that it was not distinguished from the October epsilon-Carinids. The oldest records were by Cuno Hoffmeister (1948) with his observations in 1937 in Namibia, when some radiants were established from solar longitude 200.1° to 203.6° at R.A. 95°– 99° and decl. –53° to –55°. None of the later meteor observers in Australia, New Zealand, South Africa or South American observers from Bolivia, Brazil, Argentina, Columbia and Chile report any activity from this source. In Australia it was not detected by Maurice Clark's group (WA), V. Williams (Parramatta NSW, 1880s) and R. Shinkfield (Adelaide SA, 1920s to 1970s) either. Michael Buhagiar

and his group recorded it on several occasions during the period 1971 to 1977. In Buhagiar's shower list he records a weak shower at an average radiant at R.A. 91° and Decl. –64°. This was identified from six plotted radiants. Buhagiar describes the shower as active from 14 until 21 October with a maximum on 15 October. Further observations were recorded by Darryl Skelsey in 1972 and 1973 at Colo NSW. The radiant on 16 October 1972 was at RA 108° and Decl. –58° and on 12 October 1973 at RA 97° and Decl. –56°. The shower has been observed on several occasions by WAMS/NAPOMS over the period 1981 – 1997 with a total of 9 plotted radiants providing a mean radiant position of RA 97° and Decl. –52° The shower was listed as the alpha-Carinids #222 in the Southern Hemisphere Meteor Stream List (Wood, 1990). This gives an activity period from 7 to 18 October with a maximum ZHR of 3–4 meteors per hour on 13 October.

6 Conclusion

The Global Meteor Network observations confirm the existence of the minor meteor shower known as the A Carinids (CRN#842), which displayed an outburst in 2025. The orbit parameters obtained by GMN are in good agreement with those derived by Jenniskens (2023) based on CAMS low-light video cameras, except for the eccentricity and the Sun-centered ecliptic longitude. The shower has been noticed by visual meteor observers as a weak activity source in the 20th century.

Acknowledgments

This report is based on the data of the Global Meteor Network (Vida et al., 2020a; 2020b; 2021) which is released under the CC BY 4.0 license[12]. We thank all 825 participants in the Global Meteor Network project for their contribution and perseverance. A list with the names of the volunteers who contribute to GMN has been published in the 2024 annual report (Roggemans et al., 2025). The following 229 cameras recorded A Carinids that made this study possible: AU0001, AU0002, AU0003, AU000A, AU000B, AU000C, AU000D, AU000E, AU000F, AU000G, AU000L, AU000Q, AU000R, AU000S, AU000T, AU000U, AU000V, AU000W, AU000X, AU000Y, AU000Z, AU0010, AU001A, AU001B, AU001D, AU001E, AU001F, AU001K, AU001P, AU001Q, AU001R, AU001S, AU001U, AU001V, AU001W, AU001X, AU001Y, AU001Z, AU0021, AU0028, AU0029, AU002B, AU002C, AU002D, AU0030, AU003E, AU003G, AU003J, AU0042, AU0043, AU0046, AU0047, AU0048, AU004J, AU004K, AU004L, AU004Q, BR000M, BR000Q, BR000T, BR000Y, BR001M, BR001T, BR001U, BR002A, BR002C, CL0002, CL0003, NZ0001, NZ0002, NZ0003, NZ0004, NZ0007, NZ0008, NZ000A, NZ000B, NZ000C, NZ000D, NZ000F, NZ000G, NZ000H, NZ000K, NZ000L, NZ000M, NZ000N, NZ000P, NZ000Q, NZ000R, NZ000S, NZ000T, NZ000U, NZ000V, NZ000W, NZ000X, NZ000Y, NZ000Z, NZ0010, NZ0011, NZ0012, NZ0013, NZ0014, NZ0015, NZ0016, NZ0017, NZ0018, NZ0019, NZ001A, NZ001C, NZ001E, NZ001G, NZ001H, NZ001L, NZ001N, NZ001P, NZ001Q, NZ001R, NZ001S, NZ001V, NZ001Y, NZ001Z, NZ0020, NZ0021, NZ0022, NZ0023, NZ0024, NZ0025, NZ0026, NZ0027, NZ0029, NZ002B, NZ002C, NZ002D, NZ002E, NZ002F, NZ002G, NZ002H, NZ002J, NZ002K, NZ002L, NZ002N, NZ002P, NZ002Q, NZ002R, NZ002S, NZ002T, NZ002U, NZ002V, NZ002W, NZ002X, NZ002Y, NZ002Z, NZ0030, NZ0032, NZ0033, NZ0034, NZ0035, NZ0036, NZ0037, NZ0038, NZ0039, NZ003A, NZ003B, NZ003C, NZ003E, NZ003G, NZ003H, NZ003K, NZ003N, NZ003Q, NZ003R, NZ003S, NZ003T, NZ003V, NZ003W, NZ003Y, NZ003Z, NZ0040, NZ0041, NZ0042, NZ0044, NZ0045, NZ0046, NZ0049, NZ004A, NZ004B, NZ004C, NZ004D, NZ004E, NZ004H, NZ004J, NZ004L, NZ004M, NZ004N, NZ004R, NZ004S, NZ004T, NZ004U, NZ004V, NZ004W, NZ004X, NZ004Y, NZ004Z, NZ0051, NZ0059, NZ005A, NZ005B, NZ005C, NZ005D, NZ005E, NZ005F, NZ005G, NZ005J, NZ005K, NZ005L, NZ005M, NZ005N, NZ005Z, NZ0061, NZ0063, NZ0065, NZ0066, NZ0067, NZ0068, NZ0069, ZA0002, ZA0006, ZA0007, ZA0008, ZA000C.

References

Drummond J. D. (1981). "A test of comet and meteor shower associations". *Icarus*, **45**, 545–553.

Hoffmeister C. (1948). "Meteorströme". Leipzig, J.A. Barth, 1948.

Jenniskens P., Baggaley J., Crumpton I., Aldous P., Pokorny P., Janches D., Gural P. S., Samuels D., Albers J., Howell A., Johannink C., Breukers M., Odeh M., Moskovitz N., Collison J. and Ganjuag S. (2018). "A survey of southern hemisphere meteor showers". *Planetary Space Science*, **154**, 21–29.

Jenniskens P. (2020). "A Carinids (CRN#842) outburst 2020". *eMetN Meteor Journal*, **6**, 369.

Jenniskens P. (2023). Atlas of Earth's meteor showers. Elsevier, Cambridge, United states. ISBN 978-0-443-23577-1. Page 791.

Jopek T. J. (1993). "Remarks on the meteor orbital similarity D-criterion". *Icarus*, **106**, 603–607.

Jopek T. J., Rudawska R. and Pretka-Ziomek H. (2006). "Calculation of the mean orbit of a meteoroid stream". *Monthly Notices of the Royal Astronomical Society*, **371**, 1367–1372.

Moorhead A. V., Clements T. D., Vida D. (2020). "Realistic gravitational focusing of meteoroid streams". *Monthly Notices of the Royal Astronomical Society*, **494**, 2982–2994.

Roggemans P., Johannink C. and Campbell-Burns P. (2019). "October Ursae Majorids (OCU#333)". *eMetN Meteor Journal*, **4**, 55–64.

[12] https://creativecommons.org/licenses/by/4.0/

Roggemans P., Campbell-Burns P., Kalina M., McIntyre M., Scott J. M., Šegon D., Vida D. (2025). “Global Meteor Network report 2024”. *eMetN Meteor Journal*, **10**, 67–101.

Roggemans P., Vida D., Šegon D., Scott J., Wood J. (2026). “October epsilon Carinids (OEC#1172)”. *eMetN Meteor Journal*, **11**, 1–7.

Southworth R. B. and Hawkins G. S. (1963). “Statistics of meteor streams”. *Smithsonian Contributions to Astrophysics*, **7**, 261–285.

Vida D., Gural P., Brown P., Campbell-Brown M., Wiegert P. (2020a). “Estimating trajectories of meteors: an observational Monte Carlo approach - I. Theory”. *Monthly Notices of the Royal Astronomical Society*, **491**, 2688–2705.

Vida D., Gural P., Brown P., Campbell-Brown M., Wiegert P. (2020b). “Estimating trajectories of meteors: an observational Monte Carlo approach - II. Results”. *Monthly Notices of the Royal Astronomical Society*, **491**, 3996–4011.

Vida D., Šegon D., Gural P. S., Brown P. G., McIntyre M. J. M., Dijkema T. J., Pavletić L., Kukić P., Mazur M. J., Eschman P., Roggemans P., Merlak A., Zubrović D. (2021). “The Global Meteor Network – Methodology and first results”. *Monthly Notices of the Royal Astronomical Society*, **506**, 5046–5074.

Wood J. (1990). “Southern Hemisphere Meteor Stream List”. NAPOMS Bulletin 237.

New meteor shower in Pegasus (M2025-U1)

Damir Šegon[1,2], Denis Vida[3,4], Paul Roggemans[5], James M. Scott[6], Jeff Wood[7]

[1] **Astronomical Society Istra Pula, Park Monte Zaro 2, 52100 Pula, Croatia**

[2] **Višnjan Observatory, Istarska 5, 52463 Višnjan, Croatia**

[3] **Department of Physics and Astronomy, University of Western Ontario, Richmond Street, London, N6A 3K7, Ontario, Canada**

[4] **Institute for Earth and Space Exploration, University of Western Ontario, Perth Drive, London, N6A 5B8, Ontario, Canada**
denis.vida@gmail.com

[5] **Pijnboomstraat 25, 2800 Mechelen, Belgium**

[6] **Department of Geoscience, Aarhus University, Høegh-Guldbergs Gade 2. DK-8000 Aarhus C, Denmark**
jscott@geo.au.dk

[7] **PO Box 162, Willetton, Western Australia 6955, Australia**

A new meteor shower from a Jupiter Family Comet type orbit (T_J = 2.87) was detected during October 19 – 27, 2025 by the Global Meteor Network. 124 meteors belonging to the new shower were observed between 206° < $\lambda_\odot$ < 214° from a radiant at R.A. = 359.7° and Decl.= +12.2° in the constellation of Pegasus, with a geocentric velocity of 14.0 km/s. The new meteor shower has been listed in the IAU MDC Working List of Meteor Showers under the temporary name-designation: M2025-U1.

1 Introduction

The GMN radiant maps for October 19 – 27, 2025, showed a clear concentration of related radiants in the constellation of Pegasus. The activity lasted one week with an almost constant level of activity with the radiant well visible on the radiant density maps see *Figures 1 and 2*. When the activity had completely ceased, 124 meteors of this new meteor shower had been registered by the Global Meteor Network[13] low-light video cameras. The shower was independently observed by 348 cameras in Australia, Bosnia and Herzegovina, Belgium, Bulgaria, Brazil, Canada, Chile, Croatia, Czechia, Denmark, Germany, Greece, France, Hungary, the Netherlands, New Zealand, Poland, Portugal, Romania, Russia, Slovakia, South Korea, Spain, Switzerland, Ukraine, United Kingdom and the United States.

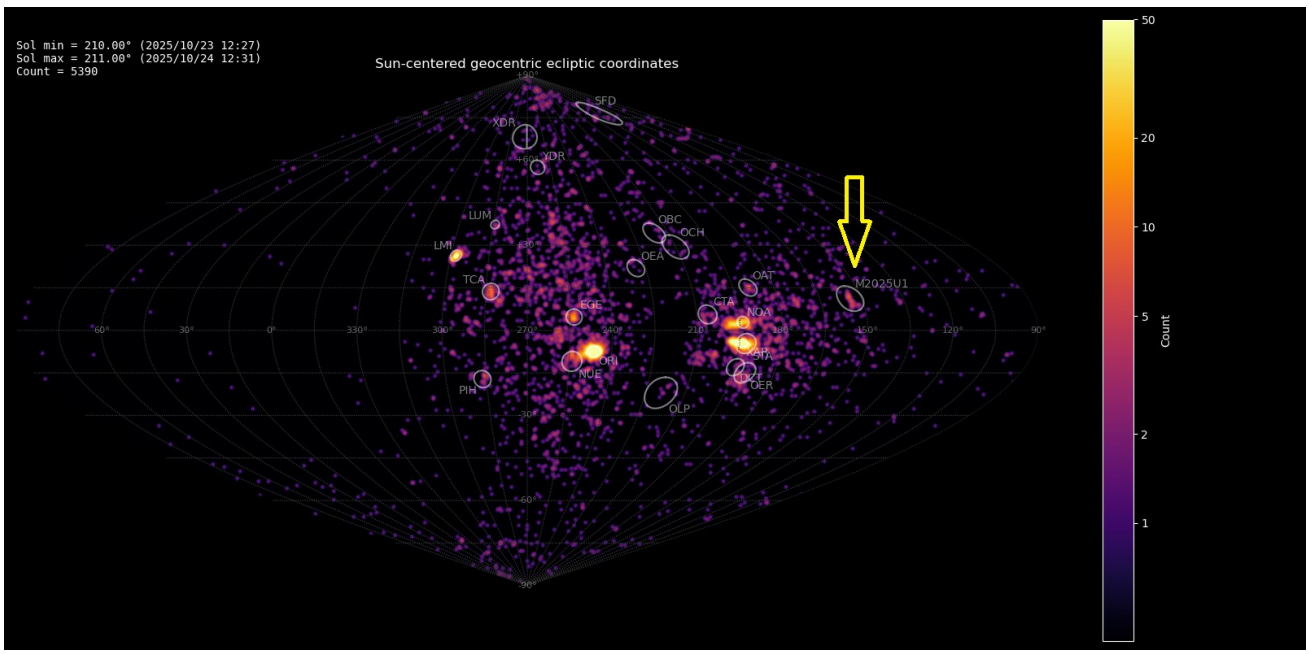

Figure 1 – Radiant density map in sinusoidal projection with 5390 radiants obtained by the Global Meteor Network during October 23 – 24, 2025. A distinct concentration is visible in Sun-centered geocentric ecliptic coordinates which was identified as a new meteor shower with the temporary identification M2025-U1. Activity from this new source was detected during an entire week.

[13] https://globalmeteornetwork.org/data/

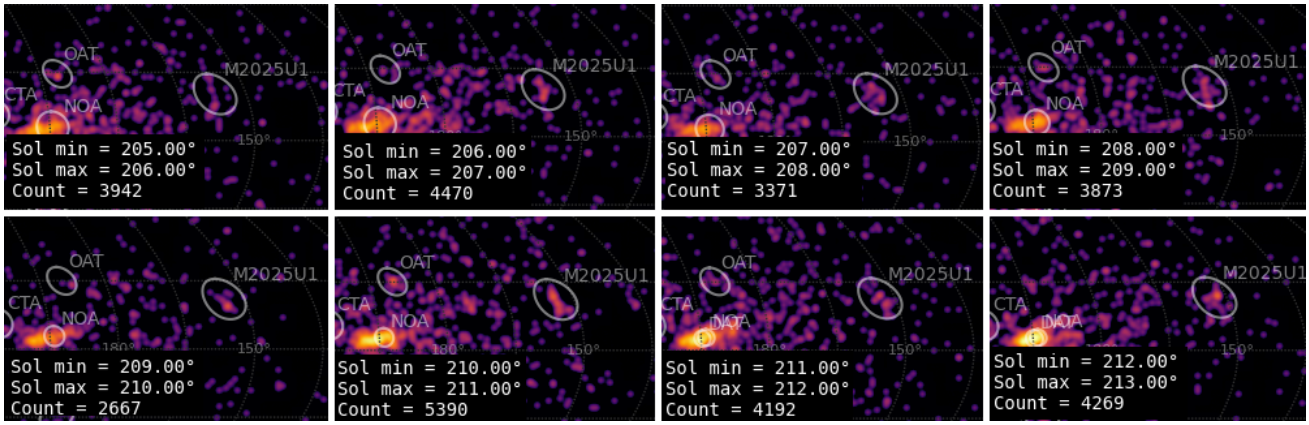

Figure 2 – The appearance of the M2025-U1 radiant during the activity period.

2 Shower classification based on radiants

The GMN shower association criteria assume that meteors within 1° in solar longitude, within 4.2° in radiant in this case, and within 10% in geocentric velocity of a shower reference location are members of that shower. Further details about the shower association are explained in Moorhead et al. (2020).

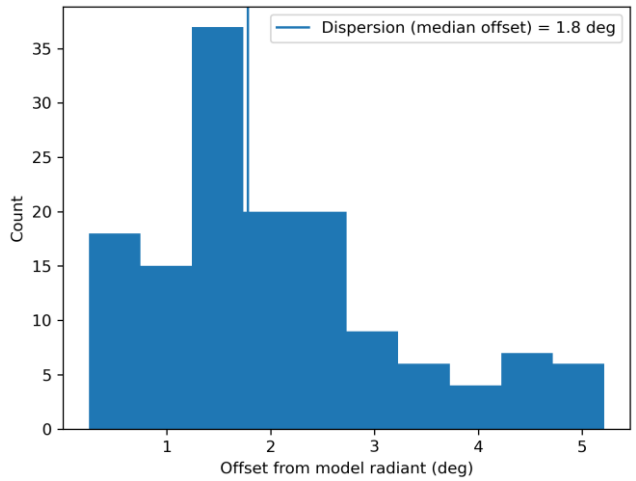

Figure 3 – Dispersion median offset on the radiant position.

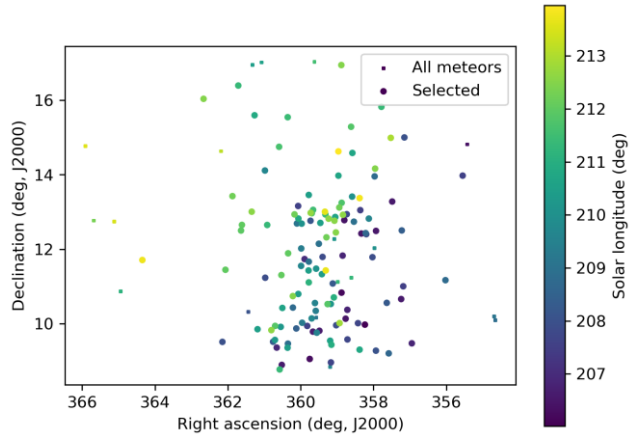

Figure 4 – The radiant distribution during the solar-longitude interval 206° – 214° in equatorial coordinates.

The shower had a median geocentric radiant with coordinates R.A. = 359.7°, Decl. = +12.2°, within a circle with a standard deviation of ±1.7° (equinox J2000.0). The radiant drift in R.A. is +0.22° on the sky per degree of solar longitude and +0.34° in Dec., both referenced to $\lambda_\odot = 211.0°$ (*Figures 4 and 5*). The uncorrected raw numbers of shower meteors per degree in solar longitude show a constant activity level (*Figure 6*). *Figures 7 and 8* show that the new activity source appeared on top of the sporadic background noise. The median Sun-centered ecliptic coordinates were $\lambda - \lambda_\odot = 153.6°$, $\beta = +11.3°$ (*Figure 9*). The geocentric velocity was 14.0 ± 0.1 km/s. The shower parameters as obtained by the GMN method are listed in *Table 1*.

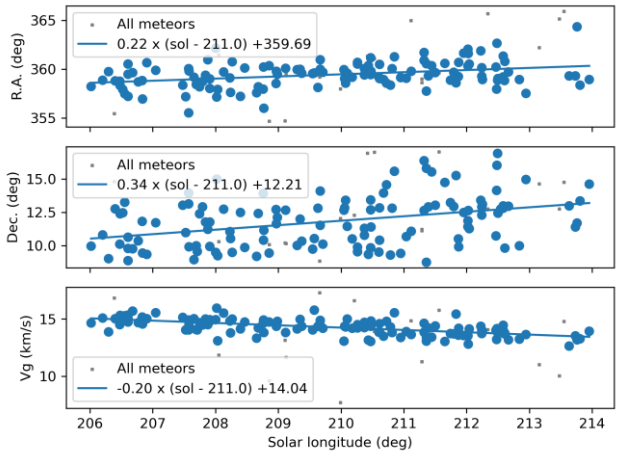

Figure 5 – The radiant drift.

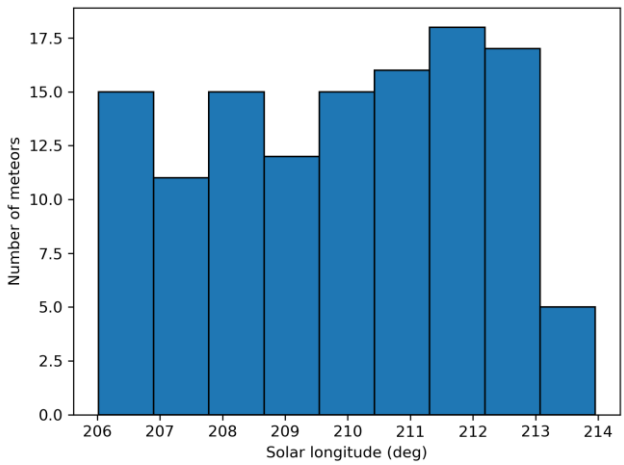

Figure 6 – The uncorrected number of shower meteors recorded per degree in solar longitude.

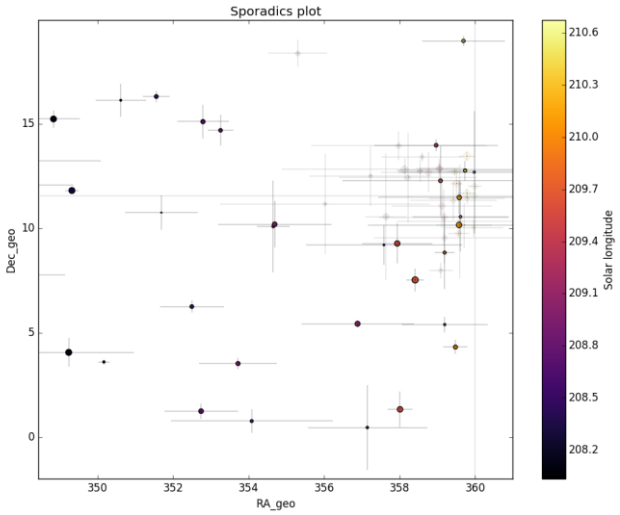

Figure 7 – All non-shower meteor radiants in geocentric equatorial coordinates during the shower activity. The pale diamonds represent the shower radiants plots, error bars represent two sigma values in both coordinates.

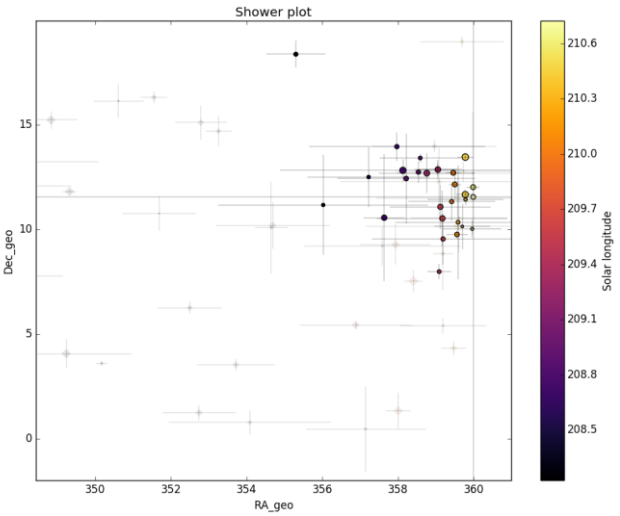

Figure 8 – The reverse of *Figure 7*, now the shower meteors are shown as circles and the non shower meteors as grayed out diamonds.

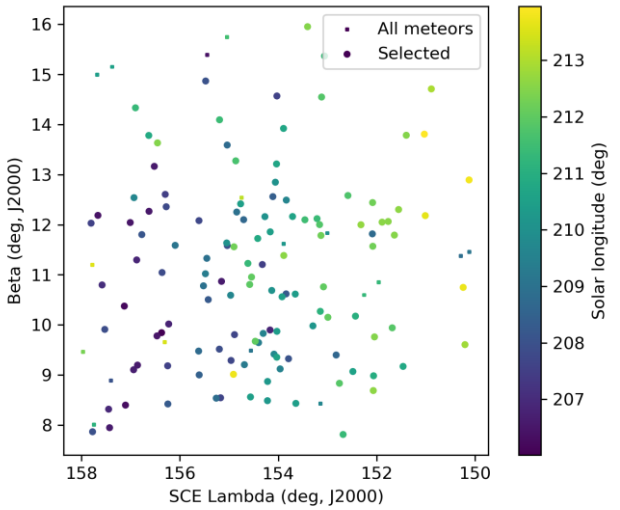

Figure 9 – The radiant distribution during the solar-longitude interval 206° – 214° in Sun centered geocentric ecliptic coordinates.

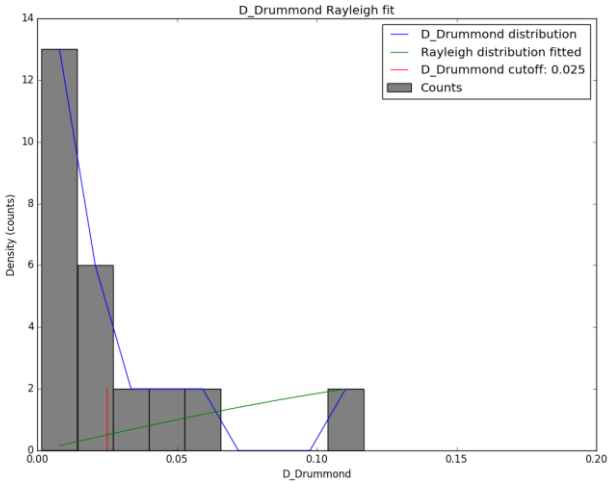

Figure 10 – Rayleigh distribution fit and Drummond D_D criterion cutoff.

3 Shower classification based on orbits

Meteor shower identification strongly depends upon the methodology used to select candidate shower members. The sporadic background is everywhere present and risks contamination of the selections of shower candidates. In order to double check GMN meteor shower detections, another method based on orbit similarity criteria is used. This approach serves to make sure that no spurious radiant concentrations are mistaken as new meteor showers.

A reference orbit is required to start an iterative procedure to approach a mean orbit, which is the most representative orbit for the meteor shower as a whole because it removes outliers and sporadic orbits (Roggemans et al., 2019). Three different discrimination criteria are combined in order to have only those orbits that fit the different criteria thresholds. The D-criteria that we use are these of Southworth and Hawkins (1963), Drummond (1981) and Jopek (1993) combined. Instead of using a cutoff value for the thresholds of the D-criteria, these values are considered in different classes with different thresholds of similarity. Depending on the dispersion and the type of orbits, the most appropriate threshold of similarity is selected to locate the best fitting mean orbit as the result of an iterative procedure.

The Rayleigh distribution fit indicates that a very small cut-off value is required with $D_D < 0.025$ (*Figure 10*). The use of D-criteria requires caution as the threshold values differ for different types of orbits. Because of the very small cutoff for the threshold values of the D-criteria, only three classes were plotted:

- Medium high: $D_{SH} < 0.075$ & $D_D < 0.03$ & $D_J < 0.075$.
- High: $D_{SH} < 0.05$ & $D_D < 0.02$ & $D_J < 0.05$.
- Very high: $D_{SH} < 0.025$ & $D_D < 0.01$ & $D_J < 0.025$;

This method resulted in a mean orbit with 89 related orbits that fit within the similarity threshold with $D_{SH} < 0.05$, $D_D < 0.02$ and $D_J < 0.05$, recorded between October 18 and 29, 2025. The plot of the radiant positions in equatorial coordinates, color-coded for different D-criteria thresholds, has its radiant at 358.4° in Right Ascension and +11.6° in declination (*Figure 10*). A slightly more tolerant threshold

of the D-criteria with $D_{SH} < 0.075$, $D_D < 0.03$ and $D_J < 0.075$ results in 125 orbits that fit these threshold values, but with a risk of including contamination with sporadics. Both solutions are mentioned in *Table 1*.

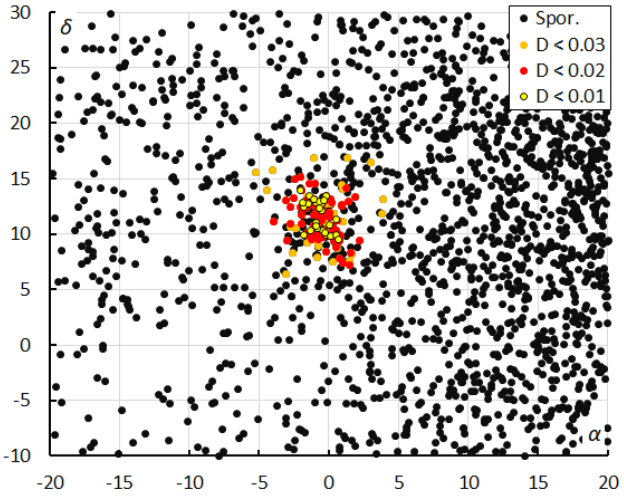

Figure 11 – The radiant distribution during the solar-longitude interval 204° – 216° in equatorial coordinates, color-coded for different threshold values of the D_D orbit similarity criterion.

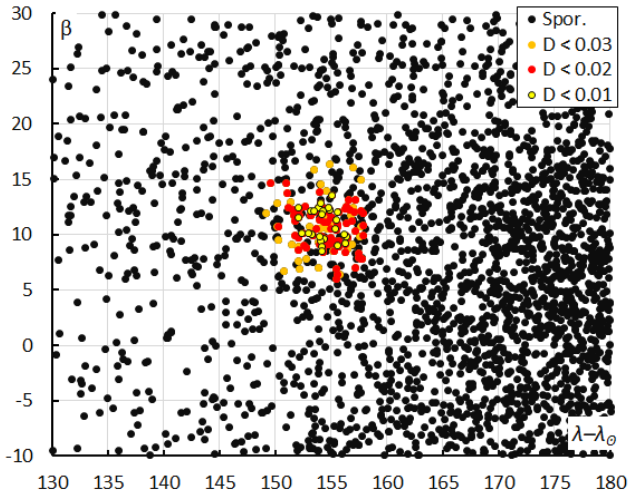

Figure 12 – The radiant distribution during the solar-longitude interval 204° – 216° in Sun-centered geocentric ecliptic coordinates, color-coded for different threshold values of the D_D orbit similarity criterion.

If we look at the ratio shower meteors to non-shower meteors recorded by GMN (*Figure 13*) in 1.5°-time bins in solar longitude in steps of 0.25°, we see an almost constant activity level from $\lambda_\odot = 207.0°$ to $\lambda_\odot = 212.8°$. The orbit-based shower identification found some orbits before $\lambda_\odot = 206.0°$ and after $\lambda_\odot = 214.0°$ but the main activity period is situated between solar longitude 206° and 214°.

The results obtained from both shower association methods are in good agreement although both methods identified 99 meteors in common with a number of different meteors in each selection. 25 meteors were identified based on the radiant but not selected by the orbit method with $D_{SH} < 0.075$ & $D_D < 0.03$ & $D_J < 0.075$. 26 orbits were identified as shower members but not identified by the radiant based method, 16 of these before or after the activity period determined by the radiant method.

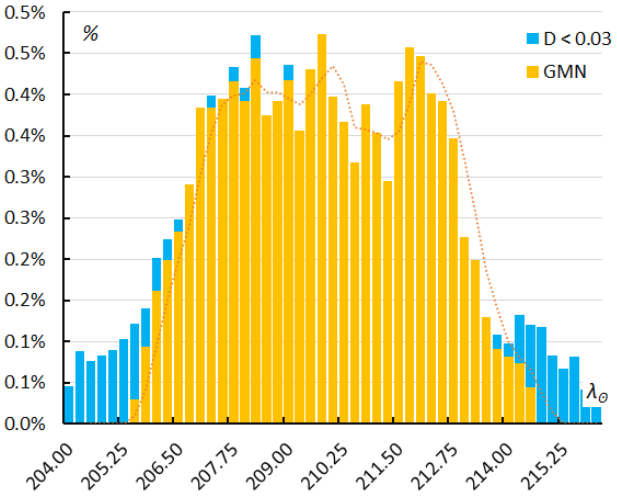

Figure 13 – The percentage of shower meteors relative to the total number of meteors recorded by GMN. Orange is the result for the GMN shower classification, blue for the orbit D-criteria method.

4 Orbit and parent body

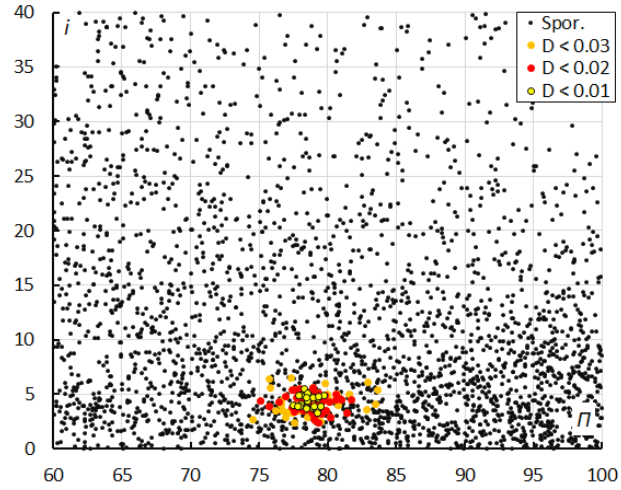

Figure 14 – The diagram of the inclination i against the longitude of perihelion Π color-coded for different classes of D criterion threshold, for $\lambda_\odot$ between 204° and 216°.

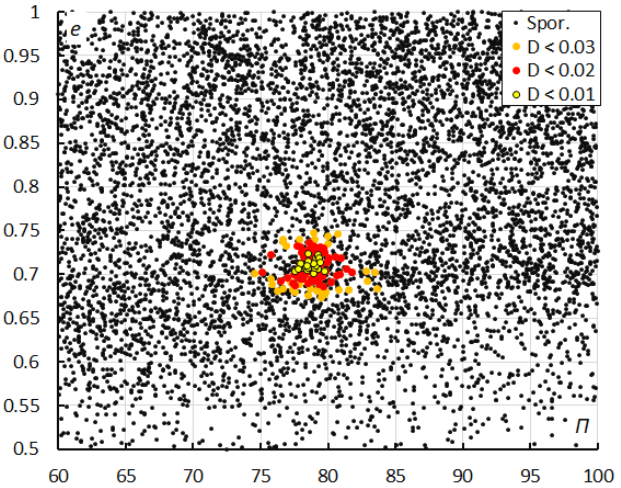

Figure 15 – The diagram of the eccentricity e against the longitude of perihelion Π color-coded for different classes of D criterion threshold, for $\lambda_\odot$ between 204° and 216°.

Looking at the diagrams of inclination versus longitude of perihelion (*Figure 14*) and eccentricity versus longitude of

perihelion (*Figure 15*), the concentration of shower points appears very distinct. *Figure 16* shows the dense population of low inclination meteor orbits in which this new meteor shower is situated.

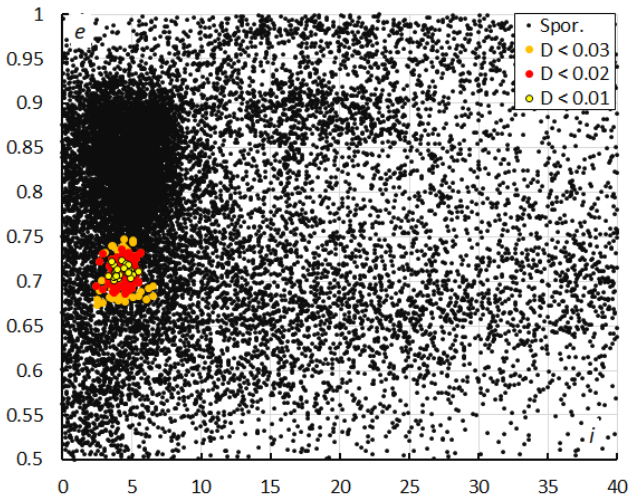

Figure 16 – The diagram of the eccentricity e against the inclination i color-coded for different classes of D criterion threshold, for $\lambda_\odot$ between 204° and 216°.

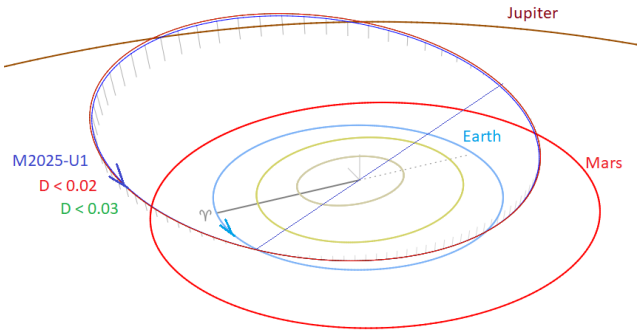

Figure 17 – Comparing the mean orbits for the three solutions obtained by two methods, close-up at the inner Solar System. (Plotted with the Orbit visualization app provided by Pető Zsolt).

The Tisserand's parameter relative to Jupiter, T_j (= 2.87) identifies the orbit as of a Jupiter Family Comet type orbit. *Figure 17* compares the three solutions as listed in *Table 1* obtained by two different methods. The different solutions almost coincide in the plotted version. The M2025-U1 meteoroid stream encounters the Earth at its descending node, with a low inclination (~4°). The aphelion relatively close to Jupiter and low inclination means that the dust will suffer significant gravitational perturbation during each passage of Jupiter.

A top 10 parent-body search resulted in candidates with a threshold for the Drummond D_D criterion value lower than 0.05 (*Table 2*). Asteroids 2017 UP and 2010 UM7 look plausible candidate parent bodies. However, Greaves (2025) warned that these two asteroids had very few observations spread over only a day or three days, respectively, so the orbits for them are poor and not worth considering at all.

Table 1 – Comparing solutions derived by two different methods, GMN-method based on radiant positions and orbit association for $D_D < 0.03$ and $D_D < 0.02$.

	GMN	$D_D < 0.03$	$D_D < 0.02$
$\lambda_\odot$ (°)	211.0	209.7	209.3
$\lambda_{\odot b}$ (°)	206.0	204.5	204.7
$\lambda_{\odot e}$ (°)	214.0	215.8	215.8
α_g (°)	359.7	359.4	359.3
δ_g (°)	+12.2	+11.6	+11.6=
$\Delta\alpha_g$ (°)	0.22	0.25	0.15
$\Delta\delta_g$ (°)	0.34	0.27	0.31
v_g (km/s)	14.0	14.4	14.4
H_b (km)	92.3	92.5	92.9
H_e (km)	80.9	80.9	80.9
H_p (km)	85.5	85.5	85.5
Mag_{Ap}	+0.6	+0.4	+0.3
λ_g (°)	4.6	4.1	4.1
$\lambda_g - \lambda_\odot$ (°)	153.6	154.3	154.7
β_g (°)	+11.3	+10.8	+11.0
a (A.U.)	2.868	2.95	2.95
q (A.U.)	0.853	0.851	0.851
e	0.702	0.711	0.711
i (°)	4.4	4.3	4.3
ω (°)	229.0	229.2	229.2
Ω (°)	209.8	209.5	209.5
Π (°)	78.9	78.7	78.7
T_j	2.87	2.82	2.82
N	124	125	89

Table 2 – Top ten matches of a search for possible parent bodies with $D_D < 0.05$.

Name	D_D
2017 UP	0.013
2010 UM7	0.024
2018 SP3	0.034
2020 TM7	0.034
2021 CY	0.039
2011 SE97	0.04
2020 BJ14	0.042
2019 SV7	0.043
2022 CG2	0.043
2004 TN1	0.043

5 Past years' activity

No relevant activity could be found in past years' meteor orbit data. In 2024, we had 33 orbits with $D_D < 0.03$ and less than half of this number per year in 2021 to 2023. In 2020 and 2019 respectively 20 and 11 orbits were recorded with $D_D < 0.03$. It seems that the activity remained far below the threshold of detectability since the GMN had less cameras than in 2025. Further searches in other meteor orbit datasets revealed only two orbits in 2020 and two orbits in 2014 among the SonotaCo meteor orbit dataset with $D_D < 0.02$. Edmond had only two orbits in 2014 with $D_D < 0.02$. CAMS had five in 2013 and three in 2014 with $D_D < 0.02$. The discovery of this meteor shower was possible thanks to the capacity of the GMN to detect weak activity sources. Future observations may reveal if there is any periodicity.

Greaves (2025) draw our attention at the coincidence with a removed shower in the MDC working list which had 2010 UM7 as a possible parent body. The November gamma-Pegasids (NGP#482) reported by Rudawska and Jenniskens (2014) were removed from the list because it was not found back in larger data samples. The time of observation differs about two weeks from M2025-U1 in solar longitude, and the ascending node and argument of perihelion differ about 20° compared to M2025-U1.

A review of past visual observations revealed a number of scattered radiants in the Pegasus region throughout the whole of October. Most of these are outside the date range parameters determined for this study.

A possible early sighting of M2025-U1 was by William Denning (Denning, 1899) where he recorded a radiant at R.A. 011° and Dec. +8° from 19–21 October, 1871. Denning assigned this the name epsilon-Piscids. Further detections were made during the first half of the 1890's by W. Denning, H. Corder and W. Doberek (Denning, 1899).

The next potential sighting of M2025-U1 was by Cuno Hofmeister from 20–21 October, 1909 with a radiant at R.A. 350° and Dec. +7° (Hoffmeister, 1948).

In more recent times M2025-U1 has potentially been detected on several occasions during the period 1978–1998 by WAMS/NAPOMS observers. A mean radiant position from nine radiants derived from meteor plots using gnomic projection charts was R.A. 004° and Dec. +07°. The meteors were characterized as having a slow speed. Rates varied from year to year. On some occasions no meteors were recorded whereas in other years rates reached as high as 2–3 meteors per hour. The observed meteor shower appeared to be active from 10 October to 23 October with a broad maximum from 16–21 October.

6 Conclusions

The discovery of a new meteor shower with a radiant in the constellation of Pegasus based on 124 meteors during 2025 October 19 – 27 has been confirmed by using two independent meteor shower search methods. The resulting mean orbits for both search methods are in good agreement. All meteors appeared during the solar-longitude interval 206° – 210° with a constant activity level without any peak. Orbits of this meteor shower were detected in previous years, but the activity level in past years remained well below the detection threshold. Future observations should confirm if this activity is annual or episodic.

The new meteor shower has been listed in the IAU MDC Working List of Meteor Showers under the temporary name-designation: M2025-U1[14].

Acknowledgments

This report is based on the data of the Global Meteor Network (Vida et al., 2020a; 2020b; 2021) which is released under the CC BY 4.0 license[15]. We thank all 825 participants in the Global Meteor Network project for their contribution and perseverance. A list with the names of the volunteers who contribute to GMN has been published in the 2024 annual report (Roggemans et al., 2025).

The following 348 cameras recorded one or more meteors that were identified as members of this new meteor shower: AU000D, AU000T, AU000V, AU000W, AU000X, AU000Y, AU0010, AU001A, AU001B, AU001E, AU001F, AU001P, AU001Q, AU001R, AU001S, AU002E, AU0030, AU003G, AU0046, AU0048, AU004J, BA0001, BA0003, BA0004, BA0005, BE0009, BE000G, BE000W, BE0010, BG0003, BG0004, BG0009, BG000B, BG000G, BR000F, BR000G, BR001H, BR001R, CA000E, CA000R, CA0032, CA0035, CH0002, CH0003, CL0002, CL0003, CZ0009, CZ000C, CZ000E, CZ000K, CZ000L, CZ000M, CZ000Q, CZ000R, DE0001, DE000B, DE000K, DE000Q, DE000W, DE000X, DK0007, DK0009, DK000A, DK000D, ES000C, ES001A, ES001D, FR000Y, FR0016, GR0009, HR0025, HR002T, HU0003, HU0004, HU0005, HU0006, HU0008, HU000B, KR0002, KR0004, KR000E, KR000F, KR000K, KR000P, KR000R, KR000S, KR0010, KR0016, KR001C, KR001D, KR001H, KR001J, KR001Y, KR0021, KR0023, KR0024, KR0027, KR0028, KR002A, KR002D, KR002R, KR0036, KR003G, KR003Q, NL000B, NL000S, NL000W, NL000Z, NL0011, NL0013, NL0014, NZ0004, NZ0008, NZ000W, NZ000Y, NZ0013, NZ0018, NZ001P, NZ001S, NZ001X, NZ002F, NZ002G, NZ002N, NZ002Q, NZ002S, NZ002T, NZ002U, NZ002V, NZ002Y, NZ002Z, NZ0032, NZ0035, NZ003C, NZ003G, NZ003K, NZ003N, NZ003Q, NZ003Y, NZ0040, NZ0042, NZ0045, NZ004B, NZ004E, NZ004L, NZ004N, NZ004U, NZ004V, NZ005B, NZ005G, NZ005H, NZ0061, NZ0063, NZ0065, NZ0066, PL000A, PL000B, PL000E, PL000F, PT0002, RO0001, RO0002, RU0008, RU0017, SK0005, SK0006, UA0001, UA0002, UK0001, UK0004, UK0006, UK0009, UK000F, UK000H, UK000S, UK001K, UK001L, UK0022, UK0025, UK0026, UK002D, UK002F, UK002J, UK002K, UK002L, UK002Q, UK003N,

[14] https://www.ta3.sk/IAUC22DB/MDC2022/Roje/pojedynczy_obiekt.php?lporz=02194&kodstrumienia=01240

[15] https://creativecommons.org/licenses/by/4.0/

UK003T, UK003W, UK003Z, UK004B, UK004E, UK004F, UK004G, UK004H, UK0051, UK0057, UK005C, UK005G, UK005H, UK005M, UK005N, UK0061, UK006C, UK006G, UK006H, UK006J, UK006P, UK0078, UK0079, UK007G, UK007H, UK007J, UK007P, UK007R, UK007U, UK007Y, UK0081, UK0084, UK008C, UK008D, UK008F, UK008G, UK008K, UK008Q, UK008S, UK008T, UK008U, UK008V, UK008X, UK008Z, UK0092, UK0098, UK0099, UK009C, UK009F, UK009G, UK009K, UK009M, UK009V, UK009W, UK009X, UK00A0, UK00A3, UK00A4, UK00A5, UK00A6, UK00AB, UK00AF, UK00AG, UK00AK, UK00AL, UK00AM, UK00AN, UK00AP, UK00AQ, UK00B1, UK00B2, UK00B5, UK00BA, UK00BJ, UK00BW, UK00C0, UK00C2, UK00C6, UK00C7, UK00CE, UK00D6, UK00D7, UK00DF, UK00DG, UK00DH, US0001, US0003, US0004, US0005, US0006, US0007, US0008, US0009, US000C, US000D, US000G, US000H, US000J, US000K, US000L, US000N, US000P, US000R, US000S, US000U, US000V, US001Q, US001R, US001U, US001V, US0020, US002A, US002R, US002X, US002Z, US0035, US0036, US0038, US0039, US003G, US003N, US003T, US0044, US0046, US0047, US004A, US004D, US004N, US0051, US005A, US005G, US005H, US005J, US005P, US005W, US005X, US005Y, US005Z, US0062, US0066, US0068, US006A, USL00G, USL00K, USL00L, USL00M, USL00N, USL00P, USL00Q, USL013, USL014, USL017, USL018, USL01B, USL01C, USL01D, USL01E, USN001, USN003, USN004, USN009, USV001.

References

Denning W.F. (1899). “General Catalogue of Radiant Points and Meteoric Showers and of Fireballs and of Shooting Stars observed at more than one station”. *Memoirs of the Royal Astronomical Society*, **53**, 203–292.

Drummond J. D. (1981). “A test of comet and meteor shower associations”. *Icarus*, **45**, 545–553.

Greaves J. (2025). Personal communications.

Hoffmeister C. (1948). “Meteorstrome”. Leipzig, J. A. Barth.

Jopek T. J. (1993). “Remarks on the meteor orbital similarity D-criterion”. *Icarus*, **106**, 603–607.

Jopek T. J., Rudawska R. and Pretka-Ziomek H. (2006). “Calculation of the mean orbit of a meteoroid stream”. *Monthly Notices of the Royal Astronomical Society*, **371**, 1367–1372.

Moorhead A. V., Clements T. D., Vida D. (2020). “Realistic gravitational focusing of meteoroid streams”. *Monthly Notices of the Royal Astronomical Society*, **494**, 2982–2994.

Roggemans P., Johannink C. and Campbell-Burns P. (2019). “October Ursae Majorids (OCU#333)”. *eMetN Meteor Journal*, **4**, 55–64.

Roggemans P., Campbell-Burns P., Kalina M., McIntyre M., Scott J. M., Šegon D., Vida D. (2025). “Global Meteor Network report 2024”. *eMetN Meteor Journal*, **10**, 67–101.

Rudawska R., Jenniskens P. (2014). “New meteor showers identifed in the CAMS and SonotaCo meteoroid orbit surveys”. In, T.J. Jopek, F.J.M. Rietmeijer, J. Watanabe, I.P. Williams, A.M., editors, *Meteoroids 2013*, Proceedings of the Astronomical Conference held at A.M. University, Poznań, Poland, Aug. 26-30, 2013. University Press, pages 217–224.

Southworth R. B. and Hawkins G. S. (1963). “Statistics of meteor streams”. *Smithsonian Contributions to Astrophysics*, **7**, 261–285.

Vida D., Gural P., Brown P., Campbell-Brown M., Wiegert P. (2020a). “Estimating trajectories of meteors: an observational Monte Carlo approach - I. Theory”. *Monthly Notices of the Royal Astronomical Society*, **491**, 2688–2705.

Vida D., Gural P., Brown P., Campbell-Brown M., Wiegert P. (2020b). “Estimating trajectories of meteors: an observational Monte Carlo approach - II. Results”. *Monthly Notices of the Royal Astronomical Society*, **491**, 3996–4011.

Vida D., Šegon D., Gural P. S., Brown P. G., McIntyre M. J. M., Dijkema T. J., Pavletić L., Kukić P., Mazur M. J., Eschman P., Roggemans P., Merlak A., Zubrović D. (2021). “The Global Meteor Network – Methodology and first results”. *Monthly Notices of the Royal Astronomical Society*, **506**, 5046–5074.

New meteor shower in Monoceros (M2025-V1)

Damir Šegon[1,2], Denis Vida[3,4], Paul Roggemans[5], James M. Scott[6], Jeff Wood[7]

[1] **Astronomical Society Istra Pula, Park Monte Zaro 2, 52100 Pula, Croatia**

[2] **Višnjan Observatory, Istarska 5, 52463 Višnjan, Croatia**

[3] **Department of Physics and Astronomy, University of Western Ontario, Richmond Street, London, N6A 3K7, Ontario, Canada**

[4] **Institute for Earth and Space Exploration, University of Western Ontario, Perth Drive, London, N6A 5B8, Ontario, Canada**
denis.vida@gmail.com

[5] **Pijnboomstraat 25, 2800 Mechelen, Belgium**

[6] **Department of Geoscience, Aarhus University, Høegh-Guldbergs Gade 2. DK-8000 Aarhus C, Denmark**
jscott@geo.au.dk

[7] **PO Box 162, Willetton, Western Australia 6955, Australia**

A meteor shower on a Long-Period Comet type orbit (T_J = –0.16) was detected during October 28 – November 4, 2025, by the Global Meteor Network. 57 meteors belonging to the new shower were observed between $215° < \lambda_\odot < 222°$ from a radiant at R.A. = 99.45° and Decl.= +6.95° in the constellation of Monoceros, with a geocentric velocity of 62.32 km/s. The new meteor shower has been listed in the IAU MDC Working List of Meteor Showers under the temporary name-designation: M2025-V1.

1 Introduction

The GMN radiant maps from October 28 until November 4, 2025 showed a clear concentration of related radiants in the constellation of Monoceros. The activity lasted one week with an almost constant level of activity with the radiant well visible on the radiant density maps see *Figure 1*. When the activity had ceased, 57 meteors of this new meteor shower had been registered by the Global Meteor Network[16] low-light video cameras. The shower was independently observed by 214 cameras in Australia, Bosnia and Herzegovina, Belgium, Bulgaria, Canada, Croatia, Czechia, Denmark, Germany, France, Greece, Hungary, the Netherlands, New Zealand, Poland, Romania, Russia, Slovakia, Slovenia, South Korea, Ukraine, United Kingdom and the United States.

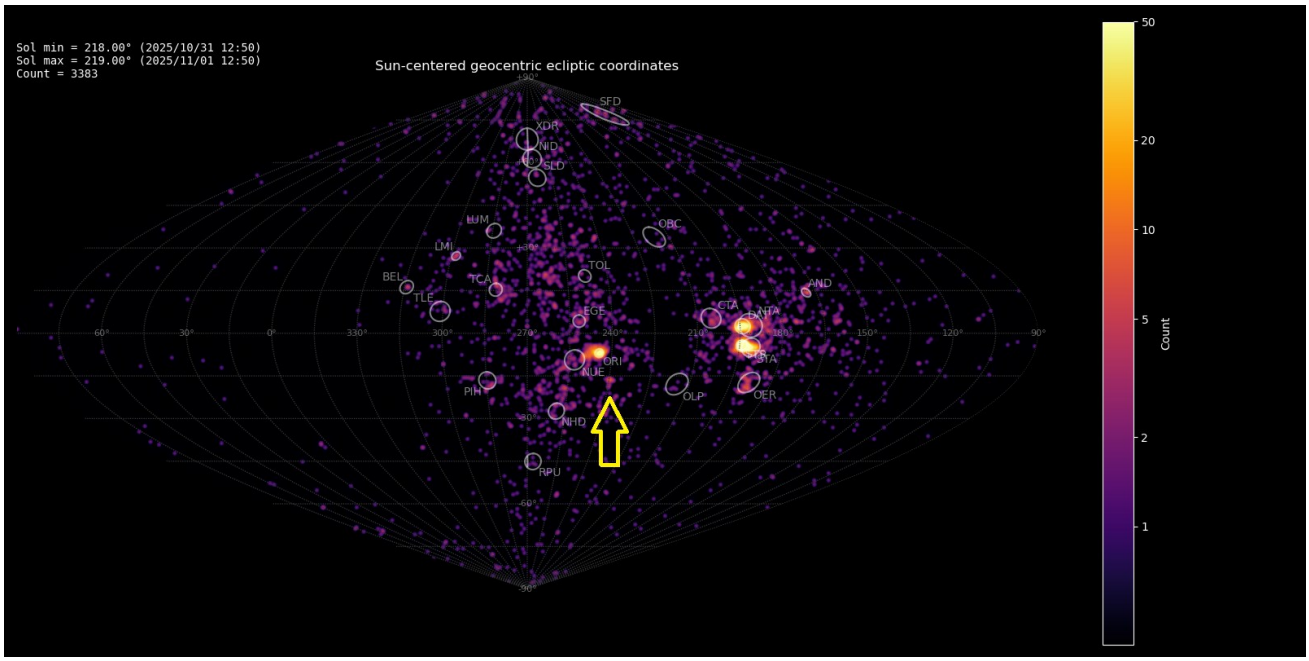

Figure 1 – Radiant density map in sinusoidal projection with 3383 radiants obtained by the Global Meteor Network during October 31 – November 1, 2025. A distinct concentration is visible in Sun-centered geocentric ecliptic coordinates which was identified as a new meteor shower with the temporary identification M2025-V1. Activity from this new source was detected during an entire week.

[16] https://globalmeteornetwork.org/data/

2 Shower classification based on radiants

The GMN shower association criteria assume that meteors within 1° in solar longitude, within 2.2° in radiant in this case, and within 10% in geocentric velocity of a shower reference location are members of that shower. Further details about the shower association are explained in Moorhead et al. (2020).

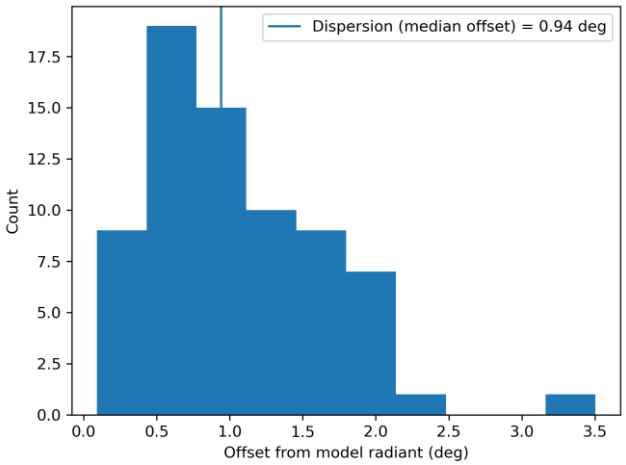

Figure 2 – Dispersion median offset on the radiant position.

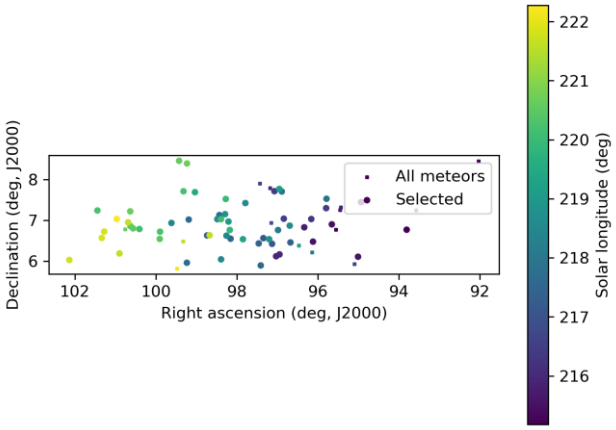

Figure 3 – The radiant distribution during the solar-longitude interval 215° – 222° in equatorial coordinates.

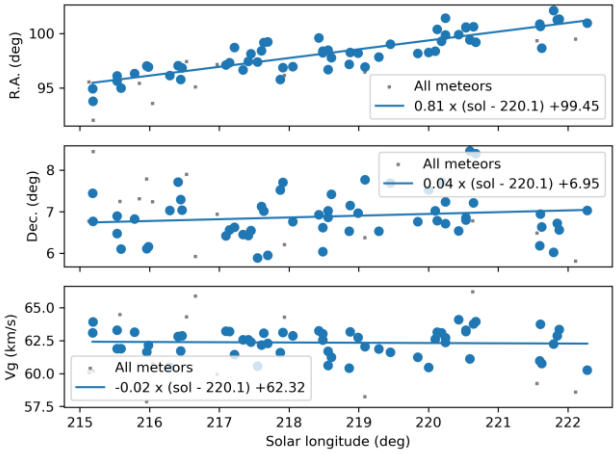

Figure 4 – The radiant drift.

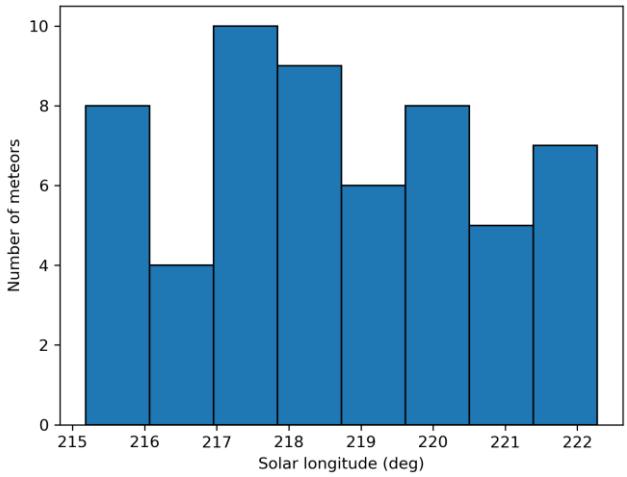

Figure 5 – The uncorrected number of shower meteors recorded per degree in solar longitude.

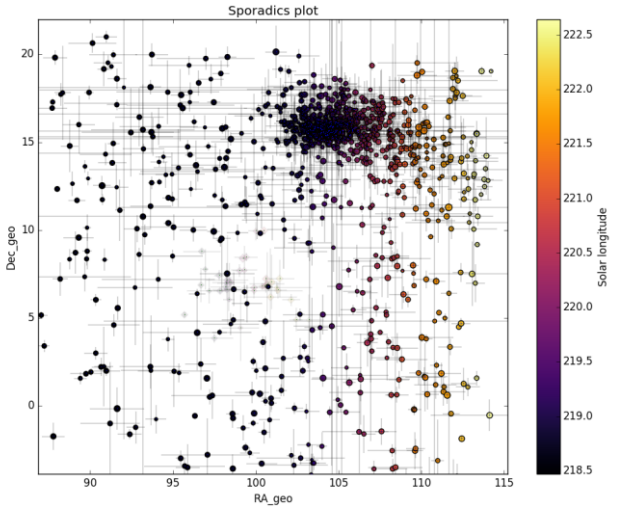

Figure 6 – All non-shower meteor radiants in geocentric equatorial coordinates during the shower activity. The pale diamonds represent the shower radiants plots, error bars represent two sigma values in both coordinates.

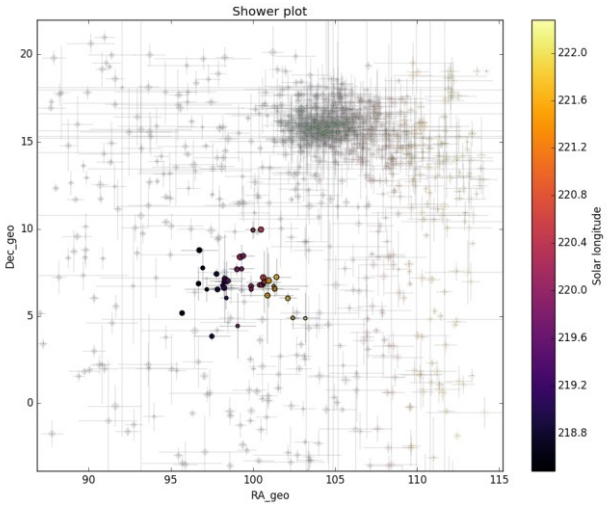

Figure 7 – The reverse of *Figure 6*, now the shower meteors are shown as circles and the non-shower meteors as grayed out diamonds.

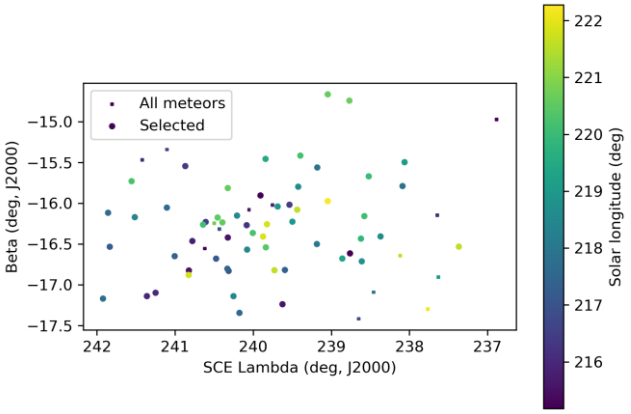

Figure 8 – The radiant distribution during the solar-longitude interval 215° – 222° in Sun centered geocentric ecliptic coordinates.

The shower had a median geocentric radiant with coordinates R.A. = 99.5°, Decl. = +7.0°, within a circle with a standard deviation of ±0.9° (equinox J2000.0). The radiant drift in R.A. is +0.81° on the sky per degree of solar longitude and +0.04° in Dec., both referenced to $\lambda_O = 220.1°$ (*Figures 3 and 4*). The uncorrected raw numbers of shower meteors per degree in solar longitude show a fluctuating activity level (*Figure 5*) since poor weather clouded out many cameras during some days of the shower activity. *Figures 6 and 7* show that the new activity source appeared on top of the sporadic background noise. The median Sun-centered ecliptic coordinates were $\lambda - \lambda_O = 239.7°$, $\beta = -16.2°$ (*Figure 8*). The geocentric velocity was 62.3 ± 0.2 km/s. The shower parameters as obtained by the GMN method are listed in *Table 1*.

3 Shower classification based on orbits

Meteor shower identification strongly depends on the methodology used to select candidate shower members. The sporadic background is everywhere present and risks contamination of the selections of shower candidates. In order to double check GMN meteor shower detections, another method, based on orbit similarity criteria is used. This approach serves to make sure that no spurious radiant concentrations are mistaken as new meteor showers.

A reference orbit is required to start an iterative procedure to approach a mean orbit, which is the most representative orbit for the meteor shower as a whole, removing outliers and sporadic orbits (Roggemans et al., 2019). Three different discrimination criteria are combined in order to have only those orbits which fit the different criteria thresholds. The D-criteria that we use are these of Southworth and Hawkins (1963), Drummond (1981) and Jopek (1993) combined. Instead of using a cutoff value for the thresholds of the D-criteria, these values are considered in different classes with different thresholds of similarity. Depending on the dispersion and the type of orbits, the most appropriate threshold of similarity is selected to locate the best fitting mean orbit as the result of an iterative procedure.

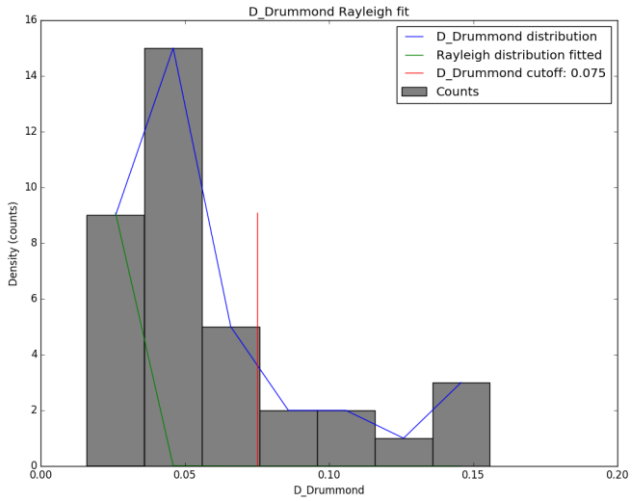

Figure 9 – Rayleigh distribution fit and Drummond D_D criterion cutoff.

The D-criteria cutoff has not been derived by Rayleigh statistics but manually and set to $D_D < 0.075$ (*Figure 9*). The use of D-criteria requires caution as the threshold values differ for different types of orbits. In this case, we distinguish seven classes of similarity:

- Poor: $D_{SH} < 0.2$ & $D_D < 0.08$ & $D_J < 0.2$.
- Very low: $D_{SH} < 0.15$ & $D_D < 0.06$ & $D_J < 0.15$.
- Low: $D_{SH} < 0.125$ & $D_D < 0.05$ & $D_J < 0.125$.
- Medium low: $D_{SH} < 0.1$ & $D_D < 0.04$ & $D_J < 0.1$.
- Medium high: $D_{SH} < 0.075$ & $D_D < 0.03$ & $D_J < 0.075$.
- High: $D_{SH} < 0.05$ & $D_D < 0.02$ & $D_J < 0.05$.
- Very high: $D_{SH} < 0.025$ & $D_D < 0.01$ & $D_J < 0.025$;

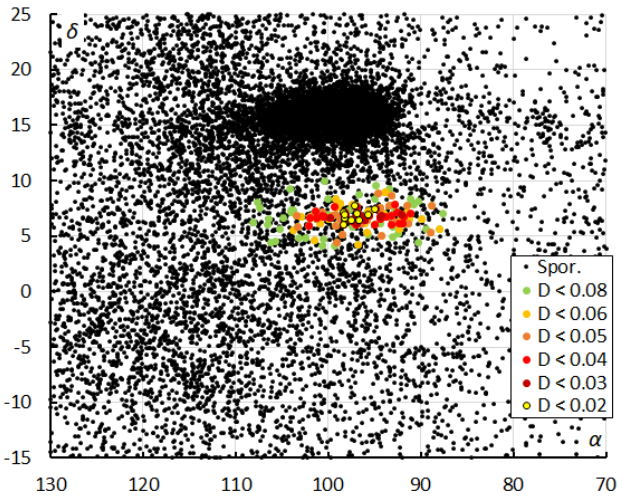

Figure 10 – The radiant distribution during the solar-longitude interval 208° – 229° in equatorial coordinates, color-coded for different threshold values of the D_D orbit similarity criteria.

This method resulted in a mean orbit with 143 related orbits that fit within the similarity threshold with $D_{SH} < 0.2$, $D_D < 0.08$ and $D_J < 0.2$, recorded between October 21 and November 11, 2025. This activity period is significantly longer than what has been detected based on the radiant association method. The plot of the radiant positions in equatorial coordinates, color-coded for different D-criteria thresholds, has its radiant at 97.0° in Right Ascension and

+6.8° in declination (*Figure 10*). The radiant positions appear as a long-stretched track caused by the radiant drift mainly in Right Ascension with $\Delta\alpha/\Delta\lambda_\odot = +0.89°$ and only $\Delta\delta/\Delta\lambda_\odot = -0.03°$ in declination. The dense radiant cloud 10° north of M2025-V1 are the annual major shower Orionids (ORI#8). Another less dense concentration around $\alpha = 115°$ and $\delta = -7°$ is caused by the November Hydrids (NHD#245), a shower that was removed from the MDC Working List because it was based on too few orbits (two). GMN observations proved that this shower exists but appears earlier in time than assumed in Jenniskens (2006). Around $\alpha = 77°$ and $\delta = +15°$ is another concentration which includes members of the alpha-Taurids (ATI#879) which were active between solar longitude 208° and 209°.

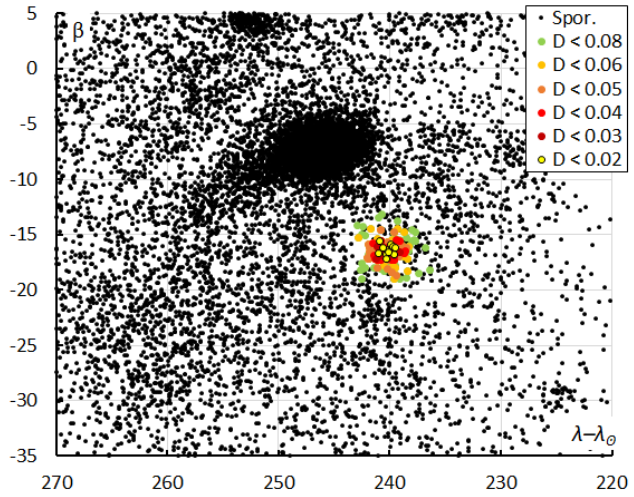

Figure 11 – The radiant distribution during the solar-longitude interval 208° – 229° in Sun-centered geocentric ecliptic coordinates, color-coded for different threshold values of the D_D orbit similarity criteria.

The radiant appears very compact in the plot in Sun-centered geocentric ecliptic coordinates (*Figure 11*) with an almost neglectable radiant drift. Radiants that fit the orbit similarity class with $D_{SH} < 0.2$ & $D_D < 0.08$ & $D_J < 0.2$ are all outliers which may be an indication that these thresholds are too tolerant. To avoid contamination with sporadic orbits only orbits that fit within the thresholds $D_{SH} < 0.125$ & $D_D < 0.05$ & $D_J < 0.125$ are taken into account for the solutions mentioned in *Table 1*.

Figure 11 shows some other interesting radiant concentrations, apart from the dense cloud with Orionids (ORI#8) and nu-Eridanids (NUE#337). At $\lambda–\lambda_\odot = 225°$ and $\beta = -30°$, we see the kappa-Orionids (KOR#833). At $\lambda–\lambda_\odot = 242°$ and $\beta = -22°$, we see the November Hydrids (NHD#245). At $\lambda–\lambda_\odot = 253°$ and $\beta = +5°$, we see the epsilon-Geminids (EGE#23) and at $\lambda–\lambda_\odot = 256°$ and $\beta = -3°$, we see the zeta-Cancrids (ZCN#243), another removed shower because it had no original reference. GMN obtained evidence for the existence of this minor shower.

If we look at the ratio shower meteors to non-shower meteors recorded by GMN (*Figure 12*) in 2.0°-time bins in solar longitude in steps of 0.25°, we see that the orbit classification method identified M2025-V1 before $\lambda_\odot = 214.0°$ and after $\lambda_\odot = 223.0°$, suggesting a longer activity period than what was covered by the radiant classification method. The fluctuations on the activity profile can be explained as due to small number statistics with 10 to 17 M2025-V1 meteors at best during each interval. Bad weather hampered many GMN cameras between $\lambda_\odot = 221.0° – 227°$.

Both methods identified 39 meteors in common. The radiant method associated 18 meteors not confirmed by the orbit identification method. The orbit shower identification had 32 meteors not found by the radiant association method, 30 of these recorded before or after the activity period obtained by the radiant association method.

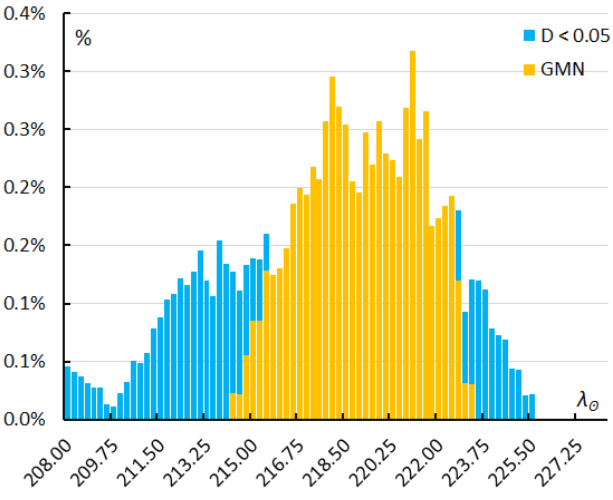

Figure 12 – The percentage of shower meteors relative to the total number of meteors recorded by GMN. Orange is the result for the GMN shower classification, blue for the orbit D-criteria method.

4 Orbit and parent body

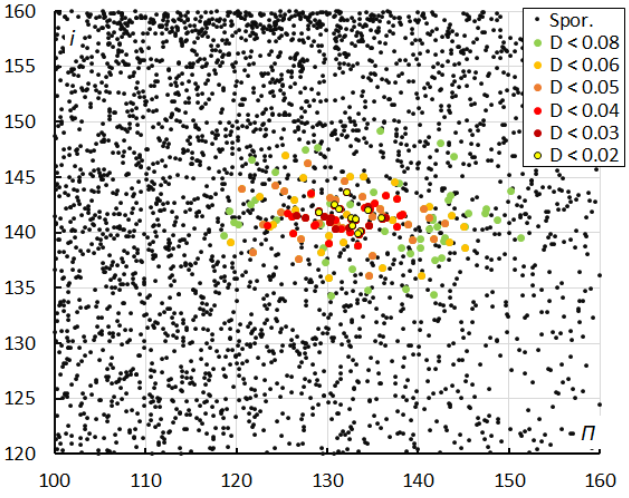

Figure 13 – The diagram of the inclination i versus the longitude of perihelion Π color-coded for different classes of D criteria thresholds, for $\lambda_\odot$ between 208° and 229°.

Looking at the diagram of inclination versus longitude of perihelion (*Figure 13*) there is a lot of scatter for the lower similarity classes which should be ignored. The dispersion in longitude of perihelion Π is due to the progression of the longitude of perihelion in function of time (expressed as

solar longitude in *Figure 14*). The inclination remains stable around 141°. The progression of the longitude of perihelion combined with the uncertainties on the eccentricity with $e = 0.970 \pm 0.029$ results in a lot of scatter in the diagram with Π versus e (*Figure 15*). The low similarity thresholds appear as outliers in this diagram too.

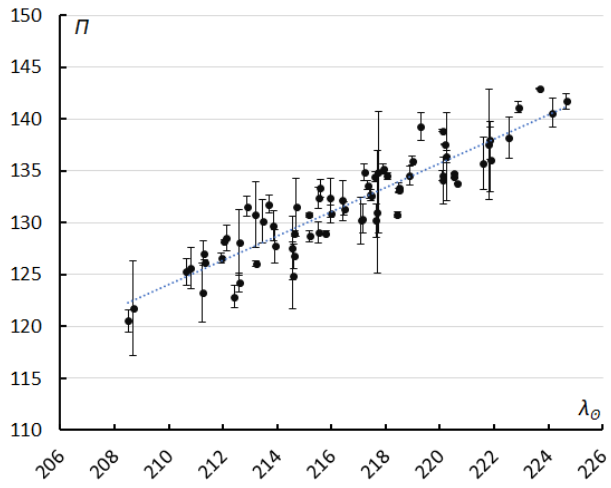

Figure 14 – The evolution of the longitude of perihelion Π in function of the solar longitude $\lambda_\odot$.

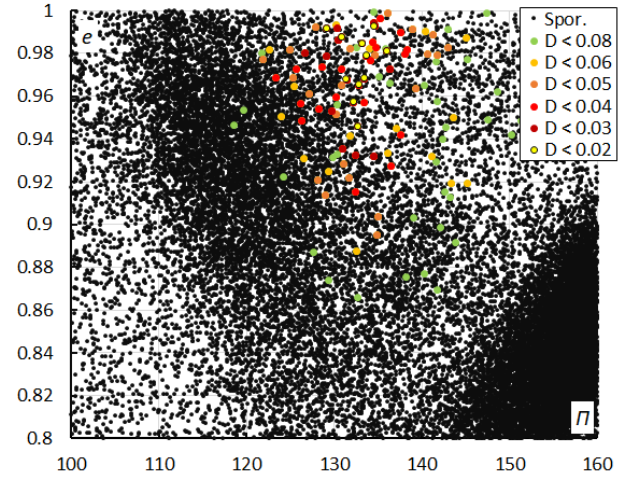

Figure 15 – The diagram of the eccentricity e versus the longitude of perihelion Π color-coded for different classes of D criteria threshold, for $\lambda_\odot$ between 208° and 229°.

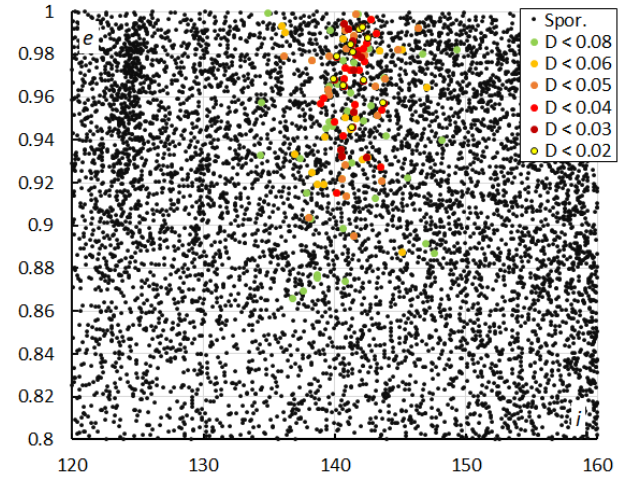

Figure 16 – The diagram of the eccentricity e versus the inclination i color-coded for different classes of D criteria threshold, for $\lambda_\odot$ between 208° and 229°.

The diagram of eccentricity versus inclination shows M2025-V1 dispersed in eccentricity but rather narrow in inclination. Two other such trails are visible at $i = 130°$ which is the kappa-Ursae Majorids (KUM#445), and at $i = 124°$, which is the Leonis Minorids (LMI#22), both dispersed in eccentricity. All these meteor showers have a high geocentric velocity of 60^+ km/s and the slightest velocity measurement uncertainty results in a large dispersion in eccentricity which is very sensitive to error margins on velocity.

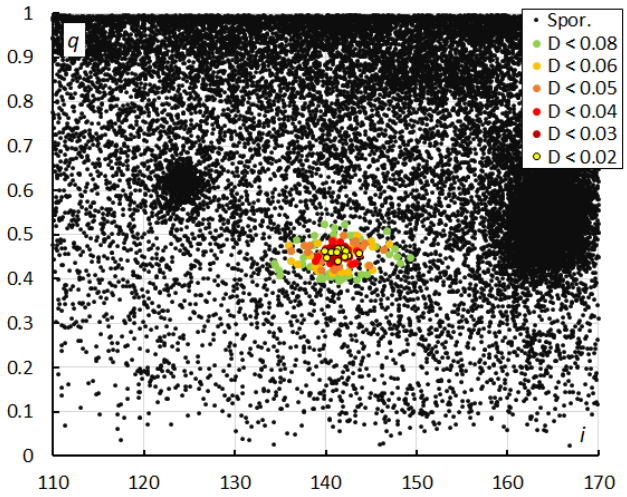

Figure 17 – The diagram of the perihelion distance q versus the inclination i color-coded for different classes of D criteria threshold, for $\lambda_\odot$ between 208° and 229°.

The M2025-V1 orbits appear very concentrated in perihelion distance q (*Figure 17*). The large concentration at right are the Orionids (ORI#8) and concentration at left are the Leonis Minorids (LMI#22).

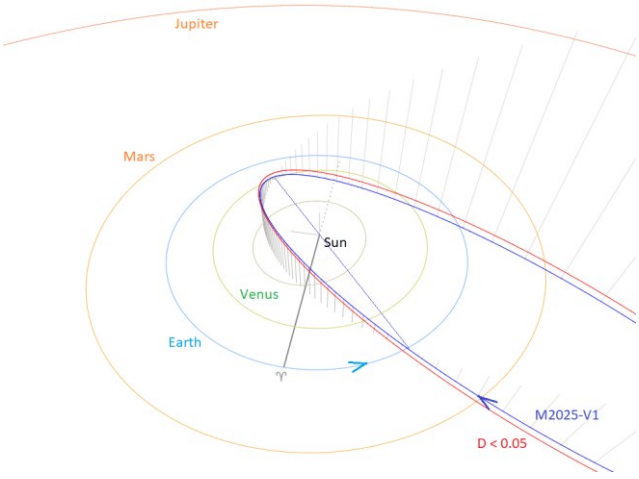

Figure 18 – Comparing the mean orbits for two solutions obtained by two methods, close-up at the inner Solar System. (Plotted with the Orbit visualization app provided by Pető Zsolt).

The Tisserand's parameter relative to Jupiter, T_j (= –0.16) identifies the orbit as of a Long-Period Comet type orbit. *Figure 18* compares two solutions as listed in *Table 1* obtained by two different methods. The meteoroid stream encounters the Earth from south of the ecliptic at its ascending node. *Figure 19* shows the orbits of the two

solutions as viewed from another perspective. The orbit shower association method selected M2025-V1 meteors almost a week sooner than the radiant association method, with a slightly higher geocentric velocity that results in a higher eccentricity and larger semi-major axis.

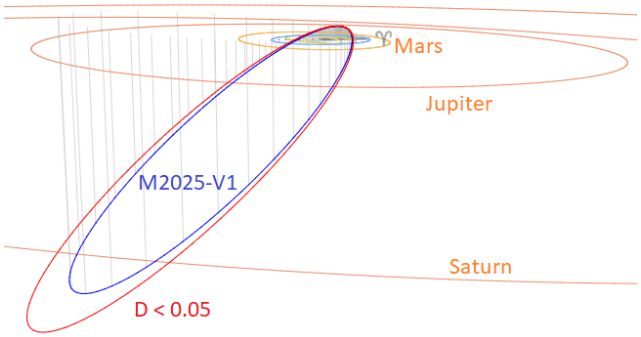

Figure 19 – Comparing the mean orbits for two solutions obtained by two methods. (Plotted with the Orbit visualization app provided by Pető Zsolt).

Table 1 – Comparing solutions derived by two different methods, GMN-method based on radiant positions and orbit association for $D_D < 0.05$ and $D_D < 0.04$.

	GMN	$D_D < 0.05$	$D_D < 0.04$
$\lambda_\odot$ (°)	220.1	217.1	216.5
$\lambda_{\odot b}$ (°)	215.0	208.4	210.8
$\lambda_{\odot e}$ (°)	222.3	224.7	222.5
α_g (°)	99.5	97.0	96.9
δ_g (°)	+7.0	+6.8	+6.8
$\Delta\alpha_g$ (°)	+0.81	+0.90	+0.94
$\Delta\delta_g$ (°)	+0.04	–0.03	+0.00
v_g (km/s)	62.3	62.8	62.8
H_b (km)	109.8	109.9	110.4
H_e (km)	95.8	95.1	95.4
H_p (km)	100.9	99.9	100.6
Mag_{Ap}	–0.8	–1.0	–1.0
λ_g (°)	99.77	97.2	97.2
$\lambda_g - \lambda_\odot$ (°)	239.37	240.3	240.3
β_g (°)	–16.16	–16.5	–16.5
a (A.U.)	10.855	15.2	15.5
q (A.U.)	0.442	0.459	0.458
e	0.959	0.970	0.971
i (°)	141.2	141.4	141.4
ω (°)	97.5	95.1	95.3
Ω (°)	38.6	36.6	36.5
Π (°)	136.1	131.7	131.8
T_j	–0.16	–0.31	–0.32
N	57	71	43

A top 10 parent-body search resulted in no candidates with a threshold for the Drummond D_D criterion value low enough to be a possible parent (*Table 2*). Orbit integrations are required to reconstruct the dynamical evolution to identify the parent body, if this has been discovered. M2025-V1 could be for instance an old dust trail somehow related to comet 1P/Halley which has been associated with several other meteor showers that were identified as components of the "Orionid Tail".

Table 2 – Top ten matches of a search for possible parent bodies with $D_D < 0.3$.

Name	D_D
C/1868 L1 (Winnecke)	0.186
1P/Halley	0.219
C/2000 W1 (Utsunomiya-Jones)	0.261
C/1845 L1 (Great June comet)	0.262
C/1914 J1 (Zlatinsky)	0.271
C/1902 R1 (Perrine)	0.279
C/1743 Q1	0.281
C/1596 N1	0.283
C/1808 M1 (Pons)	0.287
C/2025 A6 (Lemmon)	0.288

5 Past years' activity

Checking past GMN data on orbits that fit within the D-criteria threshold $D_{SH} < 0.125$ & $D_D < 0.05$ & $D_J < 0.125$, we found 45 orbits in 2024, 39 in 2023, 24 in 2022, 20 in 2021, 4 in 2020 and 3 in 2019. All orbits were recorded between 210° and 228° in $\lambda_\odot$, most of them between 217° and 225°. Among the 529076 SonotaCo orbits registered between 2007 and 2024, 47 orbits were found during these years. EDMOND had 33 orbits in its dataset recorded between 2009 and 2022. CAMS had 22 orbits of this shower recorded between 2010 and 2016. The shower has definitely an annual activity.

In personal communication Peter Jenniskens pointed attention that this shower had been identified late in the writing of his book (Jenniskens, 2023) and has been listed as the October epsilon-Monocerotids, although not yet reported or listed in the IAU-MDC Working List of Meteor Showers.

A review of past visual observations reveals visually derived radiants in the target region during late October and early November.

The earliest potential sighting of M2025-V1 appears to by Colonel G.L Tupman on 7 November 1869 (Gruber, 1879) who recorded a radiant position of R.A. 103° and Decl. +07° Tupman described this as "an active and well-defined shower". Doctor L. Gruber then combined his personal 1877 observations with Tupman's to determine a shower profile for the probable M2025-V1. He describes the shower as active from 2–14 November with a maximum on 10 November. The radiant position is given as R.A. 103° and Decl. +03°.

William Denning (1899) surprisingly does not seem to have seen M2025-V1 except for potentially in 1877 when he records a radiant at R.A. 107° and Decl. +11° with activity ranging from 10–13 November.

Cuno Hoffmeister (1948) recorded three possible radiants for M2025-V1 from 1935-37 as follows:

- Number 2539 (1935) $\lambda_\odot$ = 218.6°, R.A. 096° and Decl. +05°.
- Number 4394 (1937) $\lambda_\odot$ = 217.2°, R.A. 103° and Decl. +11°.
- Number 4409 (1937) $\lambda_\odot$ = 219.2°, R.A. 100° and Decl. +10°.

In more recent times M2025-V1 has potentially been recorded by Darryl Skelsey in NSW on 2 November 1972 (Buhagiar, 1982). Skelsey's radiant position was given as R.A. 102° and Decl. +06° In Western Australia, Maurice Clark and Michael Buhagiar (Buhagiar, 1982) appear to have recorded M2025-V1 on six occasions during the 1970's. Buhagiar described his shower as active between 24 October and 11 November with a maximum ZHR of 2 on 5 November. The mean radiant position was R.A. 105° and Decl. +06°.

During the period 1977–2002, WAMS/NAPOMS observers appear to have recorded M2025-V1. Potential activity was detected over the period 25 October to 8 November. Rates were generally low and varied from year to year. A broad maximum seems to occur between 31 October and 3 November. Six radiants were derived from meteor plots using gnomic projection maps. The mean position of these radiants was R.A. 101° and Decl. +09°.

6 Conclusions

A prominent source of meteor activity has been observed by the Global Meteor Network with a radiant in the constellation of Monoceros, first noted by Jenniskens (2023). The shower association method based on the orbit similarity criteria indicated a longer activity period starting at least five days earlier and lasting two days longer than found by the radiant association method. A search through past meteor orbit datasets revealed that this meteor shower produces a very weak but annual activity since meteor camera network data are available.

Acknowledgments

This report is based on the data of the Global Meteor Network (Vida et al., 2020a; 2020b; 2021) which is released under the CC BY 4.0 license[17]. We thank all 825 participants in the Global Meteor Network project for their contribution and perseverance. A list with the names of the volunteers who contribute to GMN has been published in the 2024 annual report (Roggemans et al., 2025).

The following 214 cameras recorded one or more meteors that were identified as members of this new meteor shower:

AU0002, AU000B, AU000C, AU000D, AU000R, AU000S, AU000U, AU001A, AU001B, AU001E, AU001Q, AU001S, AU001Y, AU001Z, AU0030, AU003E, AU003H, AU003H_2, AU0042, AU0043, BA0003, BE0002, BE0006, BE0008, BE000A, BE000G, BE000L, BE000P, BE000R, BE000U, BE000W, BE0016, BE0017, BE0018, BE001A, BG0003, BG000C, CA000R, CA001J, CA002N, CA0035, CZ0002, CZ0006, CZ000C, CZ000J, CZ000L, CZ000Q, CZ000R, CZ000U, CZ000X, DE0001, DE0004, DE000B, DE000C, DE000X, DE0011, DK0001, DK000C, FR0006, FR000A, FR000R, FR000X, FR000Z, GR0002, GR0003, HR0007, HR0025, HR0027, HR002G, HR002H, HR002J, HR002V, HR002W, HR002X, HU0002, HU0004, HU0005, HU000A, HU000B, HU000C, KR000B, KR000F, KR000J, KR000K, KR000P, KR000R, KR000S, KR001D, KR0023, KR002E, KR002J, KR002S, KR0036, KR003N, KR003T, KR003U, KR003W, NL0001, NL0006, NL0009, NL000C, NL000D, NL000K, NL000M, NL000R, NL000W, NL0010, NL0013, NL0014, NL0019, NZ0004, NZ000H, NZ0016, NZ001A, NZ001G, NZ0021, NZ0026, NZ0027, NZ002C, NZ002D, NZ002J, NZ002R, NZ002U, NZ002V, NZ002X, NZ002Y, NZ0030, NZ0037, NZ003B, NZ003E, NZ003Q, NZ003T, NZ003W, NZ004U, NZ004Z, NZ005G, NZ0063, PL0008, PL000F, PL000G, RO0001, RU000E, RU0017, SI0002, SI0004, SK0005, UA0003, UA0006, UK0008, UK001L, UK001S, UK001Z, UK003V, UK004E, UK004F, UK004J, UK005Y, UK006J, UK006V, UK0078, UK0079, UK007J, UK0080, UK008A, UK008F, UK009K, UK009Q, UK00A0, UK00AQ, UK00B0, UK00CD, UK00CS, UK00DE, US0005, US000D, US000G, US000J, US000R, US000U, US000V, US001R, US0020, US002A, US002Y, US003Q, US003T, US0044, US004C, US004P, US0055, US005A, US005D, US005E, US005G, US005J, US005Q, US005X, US005Y, USL00G, USL00K, USL00M, USL00P, USL00Q, USL016, USL017, USL018, USL019, USL01A, USL01B, USL01D, USL01E, USN001, USN002, USN003.

References

Buhagiar M. (1982). "Australian Visual Meteor Observations 1969-1982". A private unpublished paper.

Denning W.F. (1899). "General Catalogue of Radiant Points and Meteoric Showers and of Fireballs and of Shooting Stars observed at more than one station". *Memoirs of the Royal Astronomical Society*, **53**, 203–292.

Drummond J. D. (1981). "A test of comet and meteor shower associations". *Icarus*, **45**, 545–553.

Gruber L. (1879). "Grubers set of radiant points for November 1–18". *British Association for the Advancement of Science*, **49**, 122.

Hoffmeister C. (1948). "Meteorstrome". Leipzig, J.A. Barth.

[17] https://creativecommons.org/licenses/by/4.0/

Jenniskens P. (2006). Meteor Showers and their Parent Comets. Cambridge, UK: Cambridge University Press.

Jenniskens P. (2023). Atlas of Earth's Meteor Showers, Amsterdam: Elsevier, page 481.

Jopek T. J. (1993). "Remarks on the meteor orbital similarity D-criterion". *Icarus*, **106**, 603–607.

Jopek T. J., Rudawska R. and Pretka-Ziomek H. (2006). "Calculation of the mean orbit of a meteoroid stream". *Monthly Notices of the Royal Astronomical Society*, **371**, 1367–1372.

Moorhead A. V., Clements T. D., Vida D. (2020). "Realistic gravitational focusing of meteoroid streams". *Monthly Notices of the Royal Astronomical Society*, **494**, 2982–2994.

Roggemans P., Johannink C. and Campbell-Burns P. (2019). "October Ursae Majorids (OCU#333)". *eMetN Meteor Journal*, **4**, 55–64.

Roggemans P., Campbell-Burns P., Kalina M., McIntyre M., Scott J. M., Šegon D., Vida D. (2025). "Global Meteor Network report 2024". *eMetN Meteor Journal*, **10**, 67–101.

Southworth R. B. and Hawkins G. S. (1963). "Statistics of meteor streams". *Smithsonian Contributions to Astrophysics*, **7**, 261–285.

Vida D., Gural P., Brown P., Campbell-Brown M., Wiegert P. (2020a). "Estimating trajectories of meteors: an observational Monte Carlo approach - I. Theory". *Monthly Notices of the Royal Astronomical Society*, **491**, 2688–2705.

Vida D., Gural P., Brown P., Campbell-Brown M., Wiegert P. (2020b). "Estimating trajectories of meteors: an observational Monte Carlo approach - II. Results". *Monthly Notices of the Royal Astronomical Society*, **491**, 3996–4011.

Vida D., Šegon D., Gural P. S., Brown P. G., McIntyre M. J. M., Dijkema T. J., Pavletić L., Kukić P., Mazur M. J., Eschman P., Roggemans P., Merlak A., Zubrović D. (2021). "The Global Meteor Network – Methodology and first results". *Monthly Notices of the Royal Astronomical Society*, **506**, 5046–5074.

29-Piscids (PIS#1046) return in 2025

Paul Roggemans[1], **Denis Vida**[2,3], **Damir Šegon**[4,5], **James M. Scott**[6], **Jeff Wood**[7]

[1] **Pijnboomstraat 25, 2800 Mechelen, Belgium**

[2] **Department of Physics and Astronomy, University of Western Ontario, Richmond Street, London, N6A 3K7, Ontario, Canada**

[3] **Institute for Earth and Space Exploration, University of Western Ontario, Perth Drive, London, N6A 5B8, Ontario, Canada**
denis.vida@gmail.com

[4] **Astronomical Society Istra Pula, Park Monte Zaro 2, 52100 Pula, Croatia**

[5] **Višnjan Observatory, Istarska 5, 52463 Višnjan, Croatia**

[6] **Department of Geoscience, Aarhus University, Høegh-Guldbergs Gade 2. DK-8000 Aarhus C, Denmark**
jscott@geo.au.dk

[7] **PO Box 162, Willetton, Western Australia 6955, Australia**

The Global Meteor Network recorded enhanced activity from the 29-Piscids (PIS#1046) during November 2–9, 2025. In total, 50 meteors belonging to this meteor shower were observed between $218.0° < \lambda_\odot < 228.0°$ from a radiant at R.A. = 7.4° and Decl.= –5.3°, with a geocentric velocity of 11.8 km/s. In 2019 and 2024, the shower also displayed enhanced activity. Mean orbit solutions are presented for these years. This case study confirms the existence of the 29-Piscids and new solutions were added to the IAU-MDC Working List of Meteor Showers.

1 Introduction

Between the 2nd and 9th of November 2025 an episodic meteor shower known as the 29-Piscids[18] appeared on the radiant density maps of the GMN (*Figure 1*). This shower was first reported by Jenniskens in 2020. In 2019, a first activity was observed between solar longitude 202.3° to 205.0° with a maximum on $\lambda_\odot = 204.0°$ (October 17–18, 2019). One month later, during November 11–18, 2019. Activity stretched between solar longitude 228.3° and 234.9° and peaked at $\lambda_\odot = 231.4°$. Given the similar eccentricity and longitude of perihelion of the orbit both activities were assumed to be related to the same parent body and added to the MDC shower list as one single meteor shower (PIS#1046) (Jenniskens, 2020).

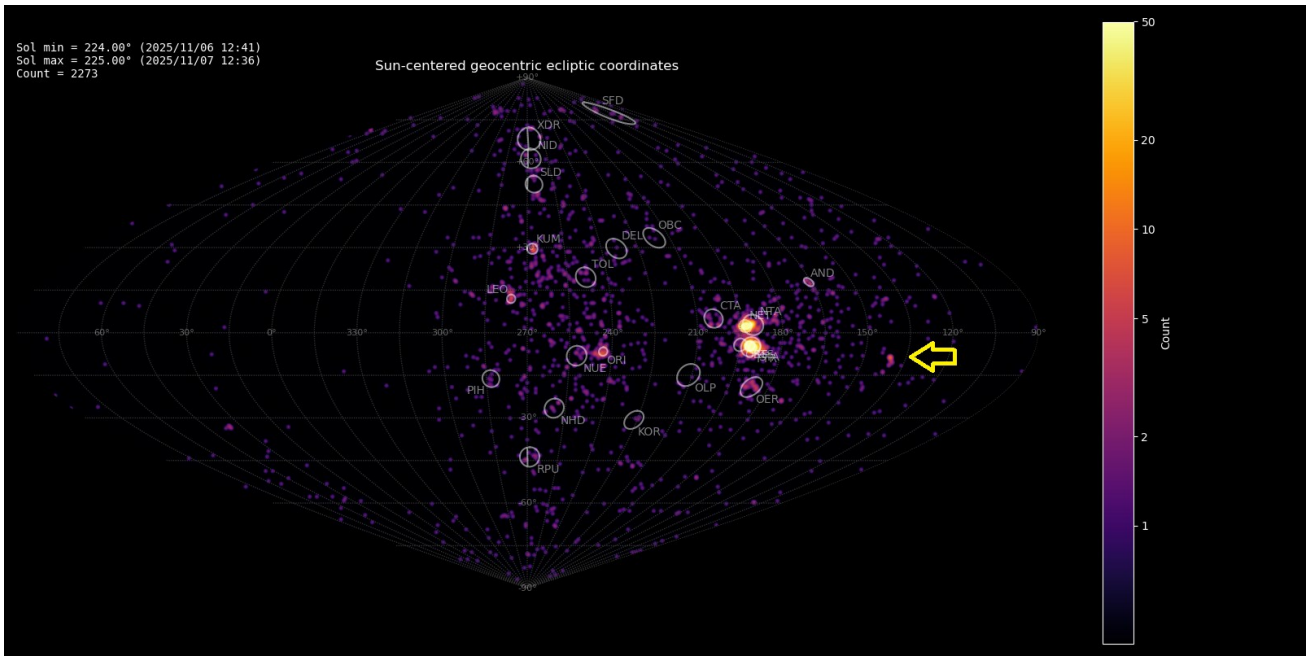

Figure 1 – Radiant density map (sinusoidal projection) with 2273 radiants obtained by the Global Meteor Network during 6–7 November, 2025. The position of the 29-Piscids in Sun-centered geocentric ecliptic coordinates is marked with a yellow arrow.

[18] https://www.ta3.sk/IAUC22DB/MDC2022/Roje/pojedynczy_obiekt.php?lporz=01993&kodstrumienia=01046

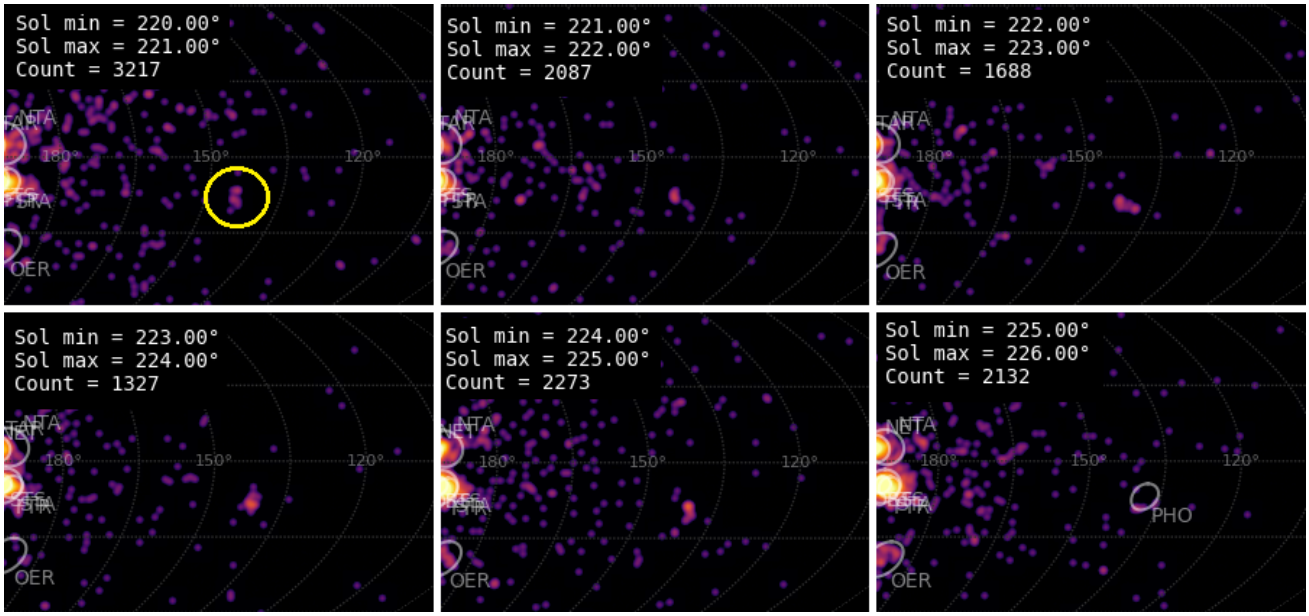

Figure 2 – The appearance of the 29-Piscids radiant between November 2–8, 2025 ($220.0° < \lambda_\odot < 226.0°$).

2 Shower classification based on radiants

The GMN shower association criteria assume that meteors within 1° in solar longitude, within 1.8° in radiant in this case, and within 10% in geocentric velocity of a shower reference location are members of that shower. Further details about the shower association are explained in Moorhead et al. (2020). Using these meteor shower selection criteria, 50 orbits have been identified as 29-Piscids.

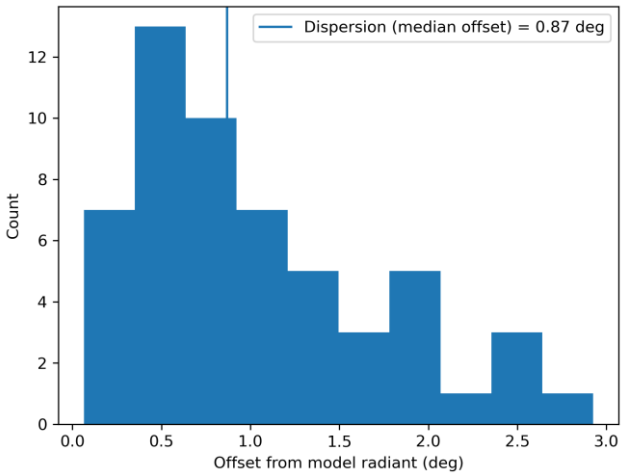

Figure 3 – Dispersion median offset on the radiant position.

The shower was independently observed in 2025 by 127 cameras in Australia, Bosnia and Herzegovina, Belgium, Brazil, Croatia, Czechia, Germany, Netherlands, New Zealand and South Africa, South Korea, Ukraine, United Kingdom and United States. The shower had a median geocentric radiant with coordinates R.A. = 7.37°, Decl. = –5.29°, within a circle with a standard deviation of ±0.9° (equinox J2000.0) (*Figure 3*). The radiant drift in R.A. is +0.13° on the sky per degree of solar longitude and –0.33° in Dec., both referenced to $\lambda_\odot = 221.0°$ (*Figures 4 and 5*). The median Sun-centered ecliptic coordinates were $\lambda - \lambda_\odot = 143.66°$, $\beta = -7.79°$ (*Figure 9*) with a strong drift in Sun-centered ecliptic coordinates $\Delta(\lambda-\lambda_\odot)/\Delta\lambda_\odot = -1.01°$ and $\Delta\beta/\Delta\lambda_\odot = -0.35°$. This means that one or more orbital elements changed during the transit of the Earth through the meteoroid stream. The geocentric velocity was 11.82 ± 0.09 km/s.

Figure 2 shows how the 29-Piscids radiant changed per degree in solar longitude, merging into the Phoenicids radiant (PHO#254)[19] after $\lambda_\odot = 225.0°$. 2019 observations showed that the Phoenicids were observed between solar longitude 230.4° and 233.7°, based on SonotaCo Network data (Shiba, 2022). The shower parameters as obtained by the GMN method are listed in *Table 1*.

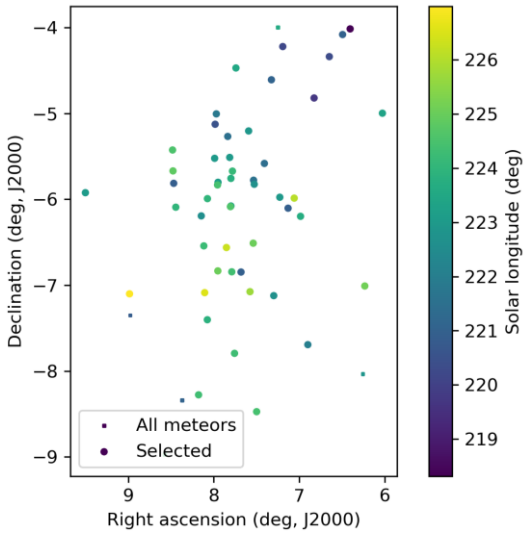

Figure 4 – The radiant distribution during the solar-longitude interval 218° – 227° in equatorial coordinates.

[19] https://www.ta3.sk/IAUC22DB/MDC2022/Roje/pojedynczy_obiekt.php?lporz=00710&kodstrumienia=00254

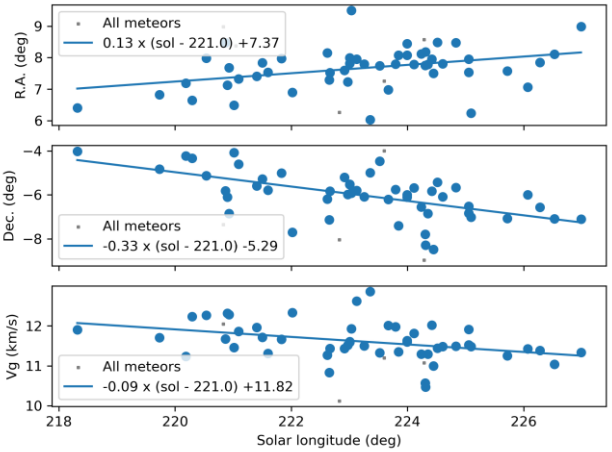

Figure 5 – The radiant drift.

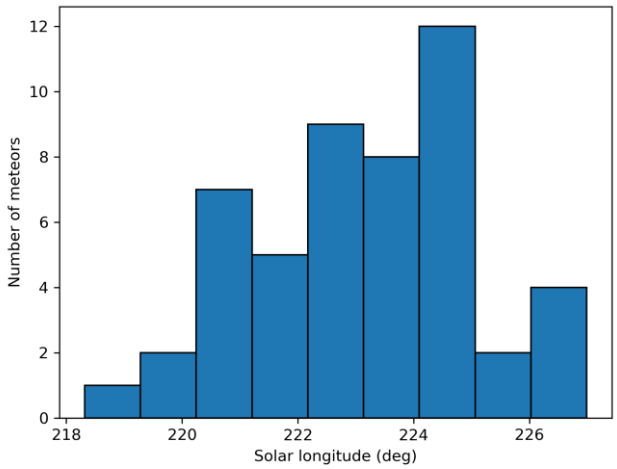

Figure 6 – The uncorrected number of shower meteors recorded per degree in solar longitude.

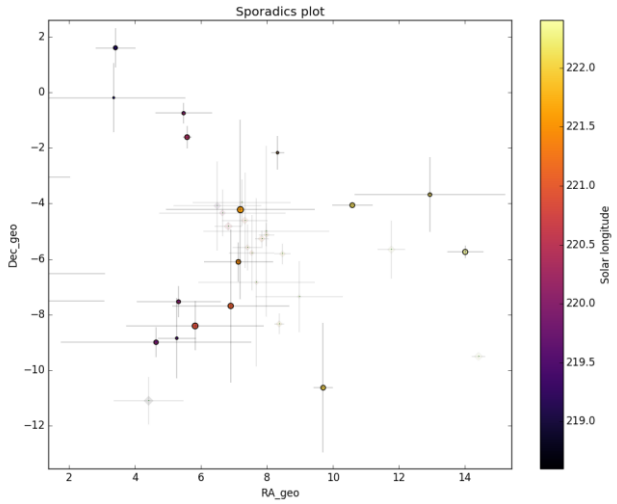

Figure 7 – All non-shower meteor radiants in geocentric equatorial coordinates during the shower activity. The pale diamonds represent the shower radiants plots, error bars represent two sigma values in both coordinates.

The uncorrected raw numbers of shower meteors per degree in solar longitude shows strong fluctuations that are due to the fact that a large number of GMN cameras were hampered by unfavorable weather circumstances during the considered time interval (*Figure 6*). *Figures 7 and 8* show that the 29-Piscids activity appeared on top of the sporadic background noise.

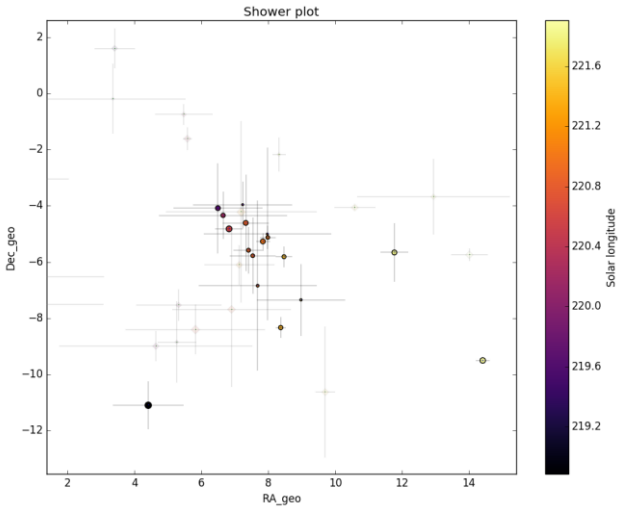

Figure 8 – The reverse of *Figure 7*, now the shower meteors are shown as circles and the non shower meteors as grayed out diamonds.

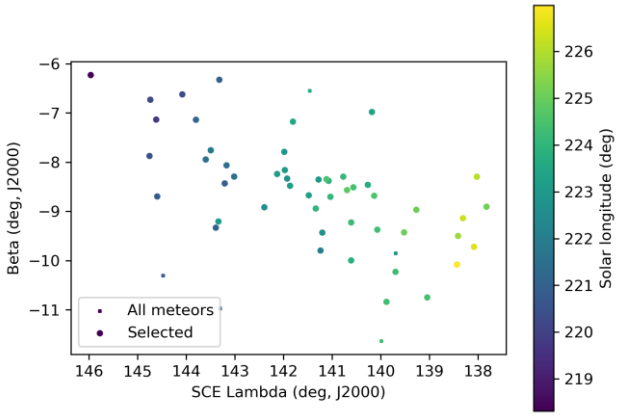

Figure 9 – The radiant distribution during the solar-longitude interval 218° – 227° in Sun centered geocentric ecliptic coordinates.

3 Shower classification based on orbits

Meteor shower identification strongly depends upon the methodology used to select candidate shower members. The sporadic background is almost everywhere present and risks contamination of selections of shower candidates. In order to double check GMN meteor shower detections, another method based on orbit similarity criteria is used. This procedure serves to make sure that no spurious radiant concentrations are mistaken as meteor showers.

A reference orbit is required to start an iterative procedure to approach a mean orbit, which is the most representative orbit for the meteor shower as a whole, removing outliers and sporadic orbits (Roggemans et al., 2019). The mean orbits are computed with the method described by Jopek et al. (2006). Three different discrimination criteria are combined in order to have only those orbits which fit the different criteria thresholds. The D-criteria that we use are these of Southworth and Hawkins (1963), Drummond (1981) and Jopek (1993) combined. Instead of using a single cutoff value for the threshold of the D-criteria, these values are considered in different classes with different thresholds of similarity. Depending upon the dispersion and the type of orbits, the most appropriate threshold of

similarity is selected to locate the best fitting mean orbit as the result of an iterative procedure.

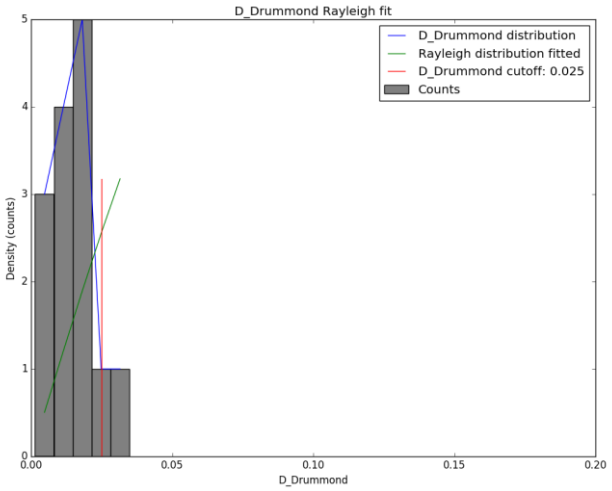

Figure 10 – Rayleigh distribution fit and Drummond D_D criterion cutoff.

The Rayleigh distribution fit indicates that a very small cutoff value is required with $D_D < 0.025$ (*Figure 10*). The use of D-criteria requires caution as the threshold values differ for different types of orbits. Because of the very small cutoff of the threshold values of the D-criteria, only four classes were plotted:

- Medium low: $D_{SH} < 0.1$ & $D_D < 0.04$ & $D_J < 0.1$;
- Medium: $D_{SH} < 0.075$ & $D_D < 0.03$ & $D_J < 0.075$.
- High: $D_{SH} < 0.05$ & $D_D < 0.02$ & $D_J < 0.05$.
- Very high: $D_{SH} < 0.025$ & $D_D < 0.01$ & $D_J < 0.025$.

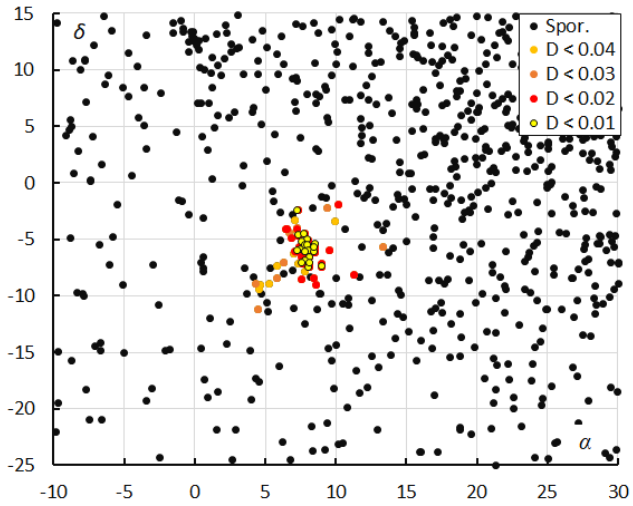

Figure 11 – The radiant distribution during the solar-longitude interval 217° – 228° in equatorial coordinates in 2025, color-coded for different threshold values of the D_D orbit similarity criterion.

This method resulted in a mean orbit with 53 related orbits that fit within the similarity thresholds with $D_{SH} < 0.075$, $D_D < 0.03$ and $D_J < 0.075$, recorded October 31 – November 9, 2025. The plot of the radiant positions in equatorial coordinates, color-coded for different D-criteria thresholds, has its radiant at 7.8° in Right Ascension and –5.9° in declination (*Figure 11*). A slightly more tolerant threshold of the D-criteria with $D_{SH} < 0.10$, $D_D < 0.04$ and $D_J < 0.1$ results in 65 orbits that fit these threshold values, but with a risk of including contamination with sporadics. Both solutions are mentioned in *Table 1*.

Looking at the Sun-centered geocentric ecliptic coordinates (*Figure 12*), the radiant appears stretched in Sun-centered longitude due to the strong drift in Sun-centered longitude.

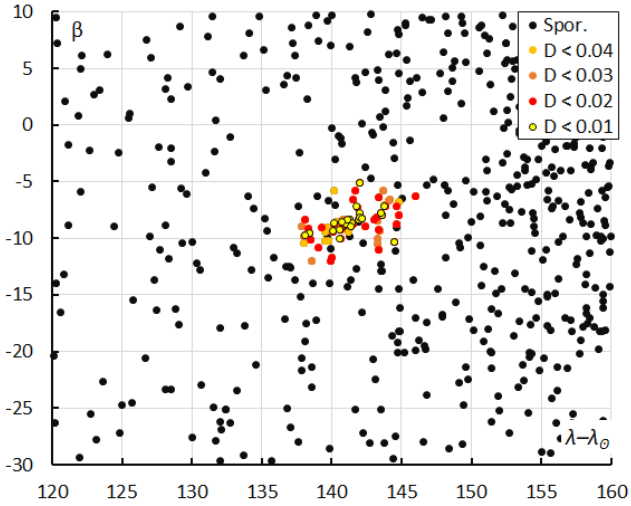

Figure 12 – The radiant distribution during the solar-longitude interval 217° – 228° in Sun-centered geocentric ecliptic coordinates, color-coded for different threshold values of the D_D orbit similarity criterion.

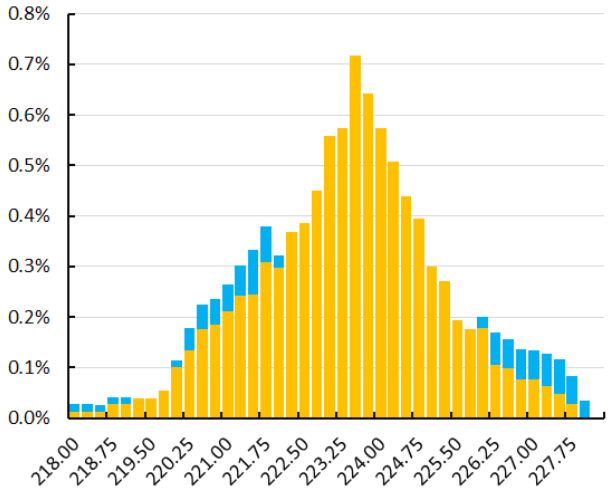

Figure 13 – The percentage of PIS-meteors relative to the total number of meteors recorded by cameras. Orange is the result for the GMN shower classification, blue for the D-criteria threshold method.

The uncorrected number of shower meteors recorded per degree in solar longitude in *Figure 6* was affected by weather circumstances. Considering the ratio of 29-Piscids meteors to the total number of meteors in 2°-time bins in solar longitude in steps of 0.25° the weather affected fluctuations are largely compensated (*Figure 13*). The best relative activity rates seem to have occurred at $\lambda_\odot = 223.5°$.

The results obtained from both shower association methods are in good agreement although both methods identified 40 meteors in common with different additional meteors in each sample. Ten 29-Piscids-meteors were identified based

on the radiant method but not selected by the orbit method with $D_{SH} < 0.075$ & $D_D < 0.03$ & $D_J < 0.075$. 13 orbits were identified as 29-Piscids-orbits but not identified by the radiant based method. Both methods agree on the activity duration.

4 Orbit and parent body

Looking at the diagram of inclination versus longitude of perihelion, we can see a dense concentration (*Figure 14*). At the same position as the 29-Piscids we find also some meteors classified as Phoenicids but this shower is actually a mis-classification in the IAU-MDC shower list based upon the common parent body of both showers.

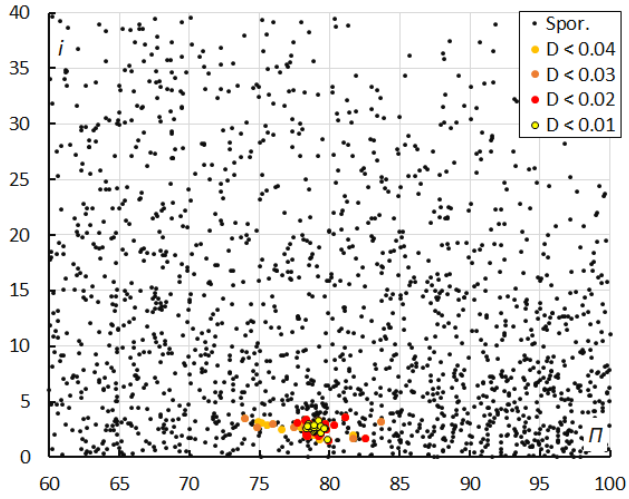

Figure 14 – The diagram of the inclination i versus the longitude of perihelion Π color-coded for different classes of D criteria thresholds, for $\lambda_\odot$ between 217° and 228°.

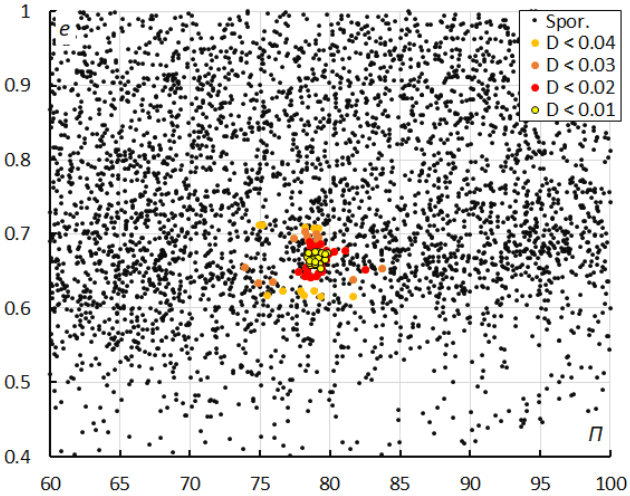

Figure 15 – The diagram of the eccentricity e versus the longitude of perihelion Π color-coded for different classes of D criteria thresholds, for $\lambda_\odot$ between 217° and 228°.

The eccentricity against the longitude of perihelion shows a dense concentration of 29-Piscids (*Figure 15*). The eccentricity appears also very concentrated against the inclination (*Figure 16*). This diagram displays some other striking concentrations. The dense cloud visible within $0° < i < 10°$ and $0.8 < e < 0.9$ is the Taurids complex with many delta-Arietids (DAT#631), Southern and Northern Taurids and several other minor showers of the Taurid complex. The concentration within $15° < i < 22°$ and $0.88 < e < 0.91$ is the established shower omicron-Eridanids (OER#338).

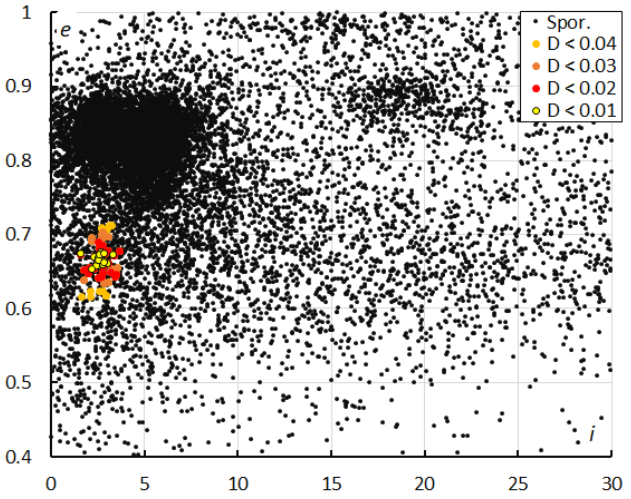

Figure 16 – The diagram of the eccentricity e versus the inclination i color-coded for different classes of D criteria thresholds, for $\lambda_\odot$ between 217° and 228°.

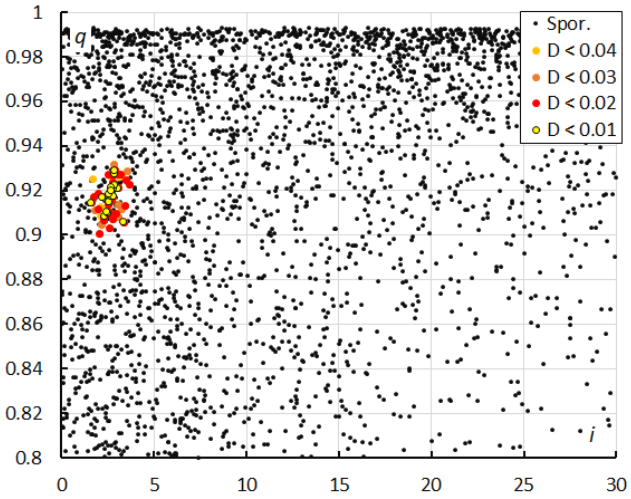

Figure 17 – The diagram of the perihelion distance q versus the inclination i color-coded for different classes of D criteria threshold, for $\lambda_\odot$ between 217° and 228°.

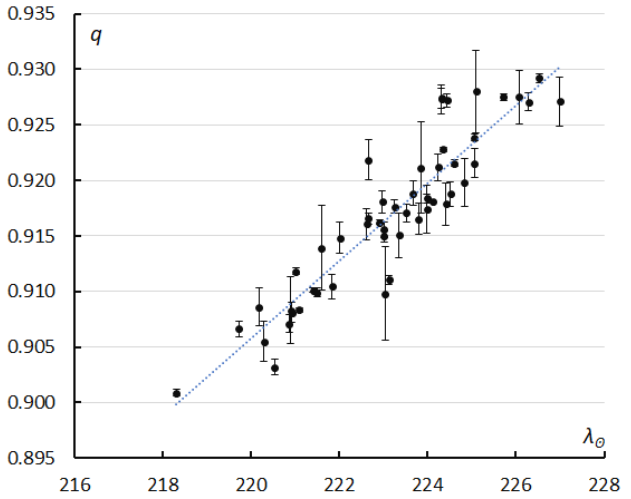

Figure 18 – The evolution of the perihelion distance q in function of the solar longitude $\lambda_\odot$ for the 2025 data.

Perihelion distance q versus inclination i appears stretched in perihelion distance (*Figure 17*). There is a clear trend in perihelion distance in function of time (*Figure 18*). Applying a simple linear regression this drift referenced to $\lambda_\odot = 221.0°$can be described as:

$$q = 0.0035\ (\lambda_\odot - 221.0°) + 0.9092$$

Jenniskens found a similar but slightly different trend of q versus the Node Ω to link the occurrence of the shower activity observed in October 2019 with the activity observed one month later (Jenniskens, 2020).

There is also a trend in the geocentric velocity which decreases with time (*Figure 19*) which can be approached with a linear regression as:

$$v_g = -0.0943\ (\lambda_\odot - 221.0°) + 11.817$$

The increase in perihelion distance q and decrease in geocentric velocity v_g has been visualized in *Figure 20*. If we extrapolate this trend to $\lambda_\odot = 232.2°$, we get $q = 0.948$ AU and $v_g = 10.8$ km/s, which matches the actually observed values within the uncertainty margins for the data listed under PHO in *Table 1*. Using $\lambda_\odot = 204.0°$ for the October activity reported by CAMS we find $q = 0.849$ AU and $v_g = 13.4$ km/s, which is slightly different from the observed values but could be explained by the uncertainty on the linear regression extrapolated over two weeks of time.

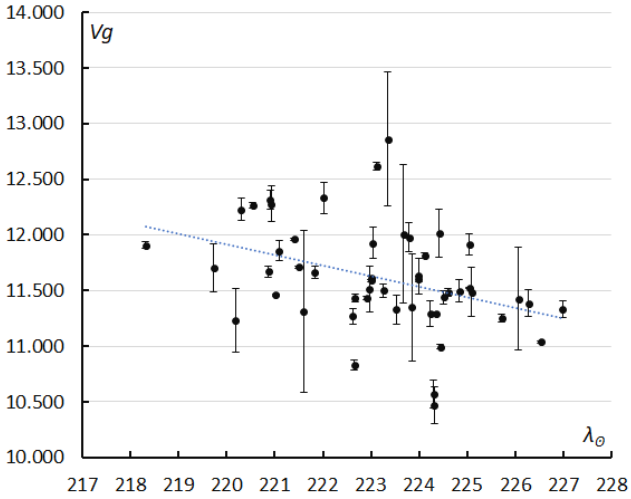

Figure 19 – The evolution of the geocentric velocity v_g in function of the solar longitude $\lambda_\odot$ for the 2025 data.

Table 1 – Comparing solutions derived by two different methods, GMN-method based on radiant positions and the orbit association method for $D_D < 0.04$, $D_D < 0.03$ and $D_D < 0.02$ in 2025, CAMS in 2019 (Jennislens, 2023) and the Phoenicids observed by SonotaCo Net (Shiba, 2022).

	2025				2019		
	GMN	$D_D < 0.04$	$D_D < 0.03$	$D_D < 0.02$	CAMS-Oct	CAMS-Nov.	PHO
$\lambda_\odot$ (°)	221.0	223.3	223.3	223.5	204.0	232.0	232.2
$\lambda_{\odot b}$ (°)	218.0	218.3	218.3	218.3	202.3	228.3	230.47
$\lambda_{\odot e}$ (°)	228.0	227.3	227.3	227.3	205.0	235.0	233.7
α_g (°)	7.4	7.8	7.8	7.8	4.3	6.8	6.7
δ_g (°)	–5.3	–6.0	–5.9	–5.9	–2.7	–7.6	–7.7
$\Delta\alpha_g$ (°)	+0.13	+0.34	+0.33	+0.20	+0.29	+0.07	+0.08
$\Delta\delta_g$ (°)	–0.33	–0.01	–0.04	–0.18	+0.21	–0.34	–0.54
v_g (km/s)	11.8	11.5	11.5	11.5	15.4	10.5	10.9
H_b (km)	89.6	89.4	89.5	89.6	–	–	88.0
H_e (km)	77.7	77.7	77.7	77.7	–	–	72.8
H_p (km)	82.4	82.2	82.2	82.2	–	–	–
Mag_{Ap}	0.5	0.5	0.5	0.4	–	–	–1.6
λ_g (°)	4.66	4.7	4.9	4.9	2.9	3.4	3.07
$\lambda_g - \lambda_\odot$ (°)	143.66	141.3	141.8	141.65	159.2	131.5	130.87
β_g (°)	–7.79	–8.7	–8.6	–8.6	–4.3	–9.5	–9.73
a (A.U.)	2.805	2.74	2.75	2.74	2.71	2.87	3.243
q (A.U.)	0.917	0.918	0.917	0.917	0.817	0.943	0.946
e	0.673	0.665	0.667	0.665	0.697	0.671	0.708
i (°)	2.6	2.6	2.65	2.6	1.89	2.69	2.7
ω (°)	35.4	35.4	35.6	35.6	55.3	27.0	26.6
Ω (°)	43.3	43.3	43.3	43.5	23.9	52.0	52.2
Π (°)	78.7	78.7	78.9	79.1	79.2	78.8	78.8
T_j	2.94	2.98	2.97	2.98	3.00	2.92	2.72
N	50	65	53	41	40	107	9

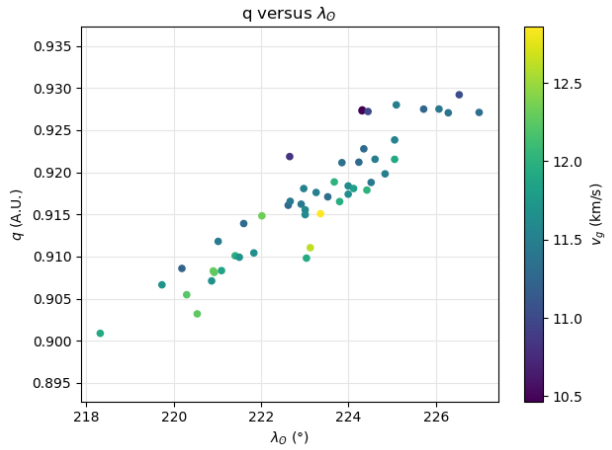

Figure 20 – The diagram of the perihelion distance q against the solar longitude $\lambda_\odot$, color-coded in function of the geocentric velocity v_g for the 2025 data.

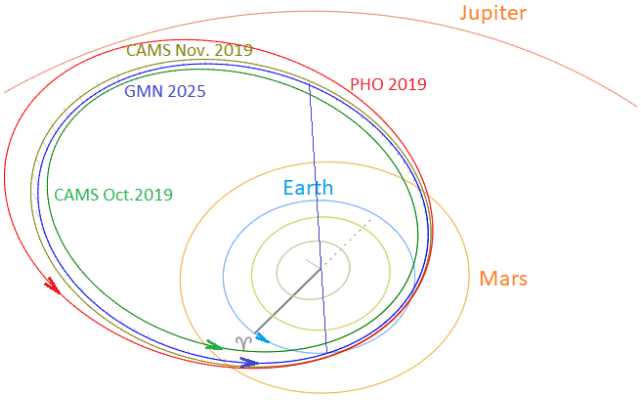

Figure 21 – Comparing the GMN solution for the 29-Piscids (blue), the solutions obtained by CAMS October 2019 and November 2019 and the solution for the Phoenicids 2019 by SonotaCo Net, close-up at the inner Solar System. (Plotted with the Orbit visualization app provided by Pető Zsolt).

The Tisserand's parameter relative to Jupiter, T_j (= 2.94), identifies the orbit as of a Jupiter Family Comet type orbit. *Figure 21* compares the orbits obtained in 2025 by GMN with those obtained by CAMS and SonotaCo Net in 2019. The meteoroid stream encounters the Earth at its descending node. The orbits are parallel and caused by dust trails from a common origin.

A parent-body search of the top 10 results in candidates with a threshold for the Drummond D_D criterion value lower than 0.035 (*Table 2*). Asteroid 2022 UX_{20} with $D_D < 0.006$ looks like the most plausible candidate but orbit integrations are required to assess if there is a relationship. However, the most likely parent maybe 289P/Blanpain, a lost comet supposed to have disintegrated into multiple fragments and dust.

Minor planet 2003 WY_{25} turned out to be in an orbit very similar to that of the lost comet D/1819 W1 (Blanpain) integrated forward in time and might be a remnant of comet D/1819 W1 (Blanpain). This comet was discovered on 1819 November 28, when it was unusually close to Earth. About 13 observations were made at Paris, Bologna, and Milan from 1819 December 14 to 1820 January 15, but the comet was then lost. Esko Lyytinen integrated the orbit of $2003WY_{25}$ back to 1819 and again forward for a range of orbits to confirm that the dust encountered Earth in December 1956 when the Phoenicids outburst was observed. Other years with possible activity caused by debris from D/Blanpain were predicted for 2019, 2034, 2039 and 2044, but not 2025 (Jenniskens and Lyytinen, 2005).

$2003WY_{25}$ does not appear within the top ten matches, but 289P/Blanpain does. The other objects are all very faint and discovered after $2003WY_{25}$, with very similar orbits and may be remnants of 289P/Blanpain just like $2003WY_{25}$.

Table 2 – Top ten matches of a search for possible parent bodies with $D_D < 0.035$

Name	D_D
2022 UX_{20}	0.006
2021 VQ_6	0.02
2019 VD	0.024
2024 VE	0.028
2024 TX_4	0.028
2022 CG_2	0.03
289P/Blanpain	0.032
2014 UA_8	0.032
2022 BR_1	0.033
2021 AY_2	0.033

5 Past years' activity

A detailed overview of past Phoenicid activity has been published in Roggemans et al. (2020) and Jenniskens and Lyytinen (2005).

Checking past years' meteor orbit data in the GMN orbit datasets, the 29-Piscids turned out to have produced better activity in 2024 than in 2025 when less cameras recorded these meteors. Most meteors were identified as PHO#254 in 2024 but the shower got no specific attention (*Figure 25*). 100 orbits were recorded that fit the D-criteria thresholds with $D_{SH} < 0.075$ & $D_D < 0.03$ & $D_J < 0.075$ in 2024. Each previous year a number of orbits fitted these criteria, indicating an annual activity although very weak. A search in previous years yield 25 orbits in 2023, 17 in 2022, 20 in 2021, 7 in 2020 and 28 in 2019 (*Figure 26*).

For other networks the orbit datasets were searched with slightly more tolerant D-criteria thresholds $D_{SH} < 0.1$ & $D_D < 0.04$ & $D_J < 0.1$ which surely risk to include some sporadic contamination. Using these criteria CAMS had the following numbers per year: 2010 (3), 2011 (6), 2012 (1), 2013 (14), 2014 (15), 2015 (13) and 2016 (17). SonotaCo Net had: 2008 (1), 2009 (2), 2010 (1), 2011 (0), 2012 (0), 2013 (4), 2014 (0), 2015 (2), 2016 (1), 2017 (1), 2018 (3), 2019 (7), 2020 (2), 2021 (7), 2022 (8), 2023 (2), 2024 (9). EDMOND had: 2007 (1), 2008 (1), 2009 (0), 2010 (2), 2011 (4), 2012 (3), 2013 (3), 2014 (3), 2015 (3), 2016 (6), 2017

(1), 2018 (3), 2019 (7), 2020 (4), 2021 (1), 2022 (1), 2023 (1).

Table 3 – Comparing solutions for 2024 and 2019 derived by two different methods, GMN-method based on radiant positions and orbit association for $D_D < 0.03$.

	2024		2019	
	GMN	$D_D < 0.03$	GMN	$D_D < 0.03$
$\lambda_\odot$ (°)	226.0	226.7	231.0	231.3
$\lambda_{\odot b}$ (°)	212.0	212.3	219.0	219.2
$\lambda_{\odot e}$ (°)	238.0	237.8	238.0	238.3
α_g (°)	6.5	6.5	6.5	6.6
δ_g (°)	–5.7	–5.7	–7.7	–7.7
$\Delta\alpha_g$ (°)	+0.07	+0.06	+0.16	+0.18
$\Delta\delta_g$ (°)	–0.10	–0.10	–0.27	–0.07
v_g (km/s)	10.8	10.96	10.3	10.3
H_b (km)	88.9	89.2	89.6	89.6
H_e (km)	77.1	78.0	78.7	78.4
H_p (km)	81.6	82.3	82.8	82.4
Mag_{Ap}	+0.8	+0.7	+1.1	+1.0
λ_g (°)	3.74	3.9	2.86	3.2
$\lambda_g - \lambda_\odot$ (°)	137.74	137.2	131.86	131.8
β_g (°)	–7.8	–7.7	–9.62	–9.5
a (A.U.)	2.674	2.77	2.768	2.79
q (A.U.)	0.930	0.926	0.946	0.945
e	0.652	0.665	0.658	0.661
i (°)	2.2	2.25	2.6	2.55
ω (°)	32.0	32.7	26.7	27.3
Ω (°)	46.4	45.8	51.7	51.4
Π (°)	78.4	78.5	78.5	78.7
T_j	3.03	2.97	2.98	2.96
N	104	91	29	25

Applying the iterative procedure to derive the best fitting mean orbit nine of the hundred orbits of 2024 were filtered out as outliers, for 2019 three of the 28 orbits were rejected as outliers. The resulting mean orbit parameters have been summarized in *Table 3* compared with the GMN radiant classification method.

Figure 22 shows the trend of the increasing perihelion distance q in function of time, using the data of 2019, 2024 and 2025 combined based on orbit classification. The trend for q and v_g in 2024 referenced to $\lambda_\odot$ = 226.7°can be described by the following equations:

$$q = 0.0031\ (\lambda_\odot - 226.7°) + 0.9298$$

$$v_g = -0.1162\ (\lambda_\odot - 226.7°) + 10.989$$

Figure 23 shows the trend of the decreasing geocentric velocity. In 2024 the shower activity lasted longer than in 2025 and in 2019 the shower displayed its activity a bit later than in 2025. Combining all 29-Piscids identified with the GMN radiant association method, the trend in increasing perihelion distance and decreasing velocity is very clear in *Figure 24*. It is obvious that the recorded orbits in 2019, 2024 and 2025 all belong to the same meteoroid stream 29-Piscids and should be identified as PIS#1046 because of the very different radiant position obtained for the Phoenicids outburst observed in 1956 and identified as PHO#254.

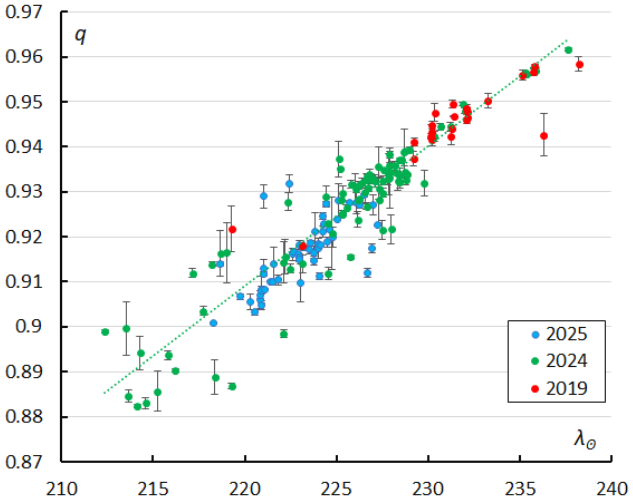

Figure 22 – The evolution of the perihelion distance q in function of the solar longitude $\lambda_\odot$.

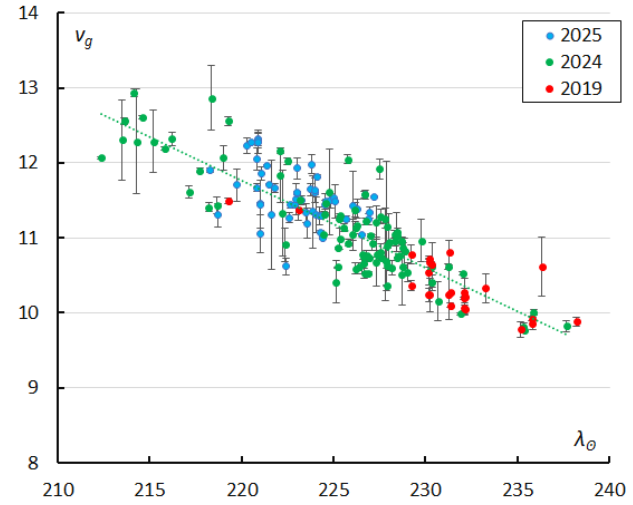

Figure 23 – The evolution of the geocentric velocity v_g in function of the solar longitude $\lambda_\odot$.

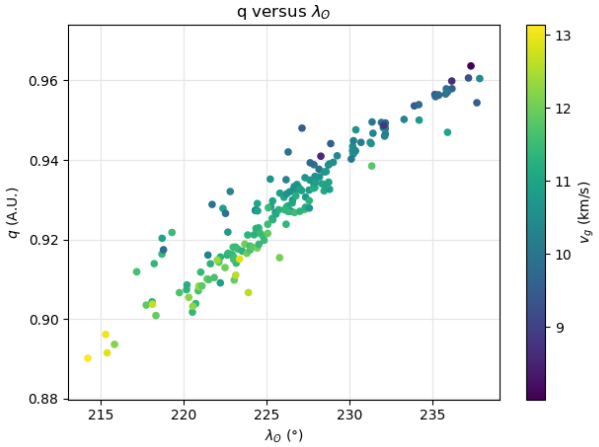

Figure 24 – The diagram of the perihelion distance q against the solar longitude $\lambda_\odot$, color-coded in function of the geocentric velocity v_g for the 2019, 2024 and 2025 data combined.

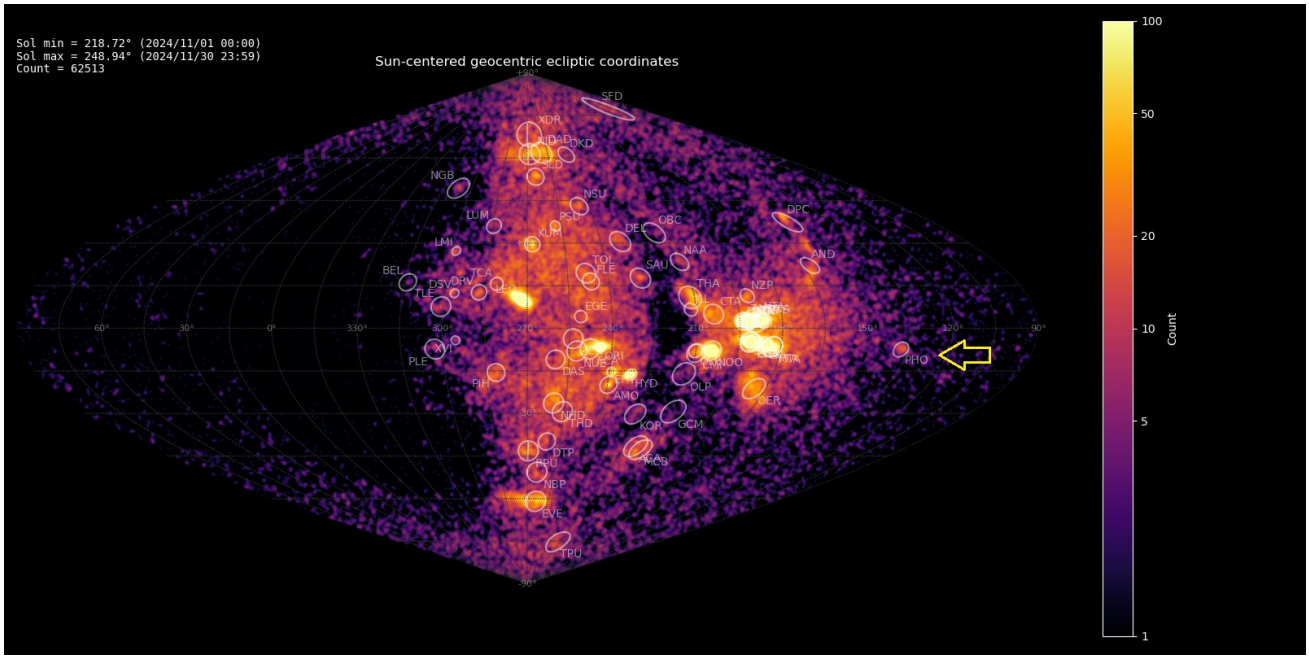

Figure 25 – Radiant density map (sinusoidal projection) with 62513 radiants obtained by the Global Meteor Network during November, 2024. The position of the 29-Piscids in Sun-centered geocentric ecliptic coordinates is marked with a yellow arrow.

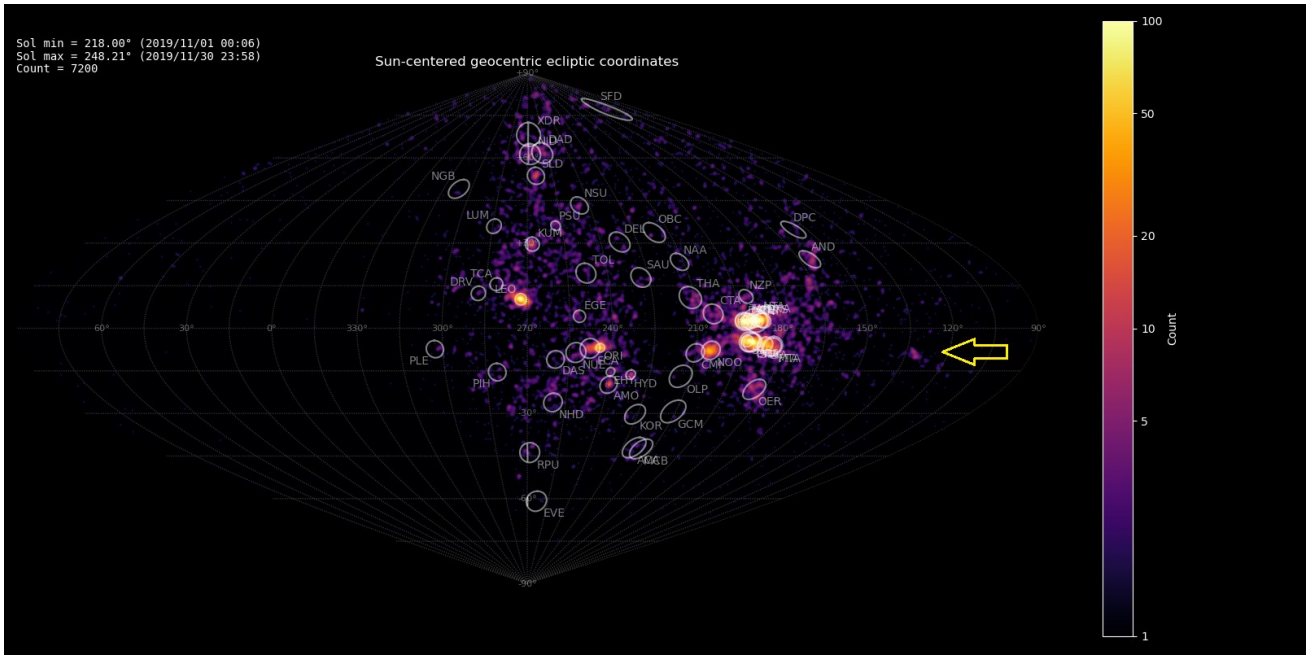

Figure 26 – Radiant density map (sinusoidal projection) with 7200 radiants obtained by the Global Meteor Network during November, 2019. The position of the 29-Piscids in Sun-centered geocentric ecliptic coordinates is marked with a yellow arrow.

6 Conclusion

The observed enhanced activity of the 29-Piscids in 2025 confirms the existence of this shower. More evidence has been found in the GMN dataset as this shower displayed enhanced activity in 2024 and 2019 too. Most of the orbits recorded in 2024 were classified as Phoenicids (PHO#254) although these matches perfectly with the 29-Piscids. The confusion arises from the erroneous inclusion of a 2019 entry in the IAU-MDC Working List of Meteor Showers listed under the Phoenicids, which originally concerned only the 1956 outburst with a radiant in the constellation Phoenix. The 2019 entry listed under Phoenicids is another solution for the activity listed under 29-Piscids and should be moved under this shower entity. Both showers likely have the same parent body, the disintegrated comet 289P/Blanpain. Some of the matching candidate parent bodies may actually be remnants of the broken-up comet. Esko Lyytinen computed that planetary perturbations with Jupiter caused the orbital node to shift to smaller values, as a result of which the annual shower now peaks earlier than the 1956 Phoenicid outburst (Jenniskens and Lyytinen, 2025). Mikiya Sato and Jun-ichi Watanabe found that the orbit of some dust trails released by 289P/Blanpain changed a lot by perturbations, so that the Earth approached the dust at the beginning of November, almost one month earlier than in 1956. In 2008 a theoretical radiant was calculated as R.A. = 7.0° and Decl. = –5.5° far north of the position of

the Phoenicids in 1956. (Sato and Watanabe, 2010). This position as well as the time predicted for the best activity (8 November) fit with the 29-Piscids radiant as observed in recent years. Sato and Watanabe (2014) confirmed activity recorded by SonotaCo Net in 2008 but no details about radiant or velocity were mentioned. They identified this activity as Phoenicids although the radiant position is far away from the 1956 position. The 2019 activity had been predicted but the time and radiant position differed from the actually observed outburst. Nothing was expected for 2024–2025 with enhanced activity of this episodic shower, other years showed only some weak annual activity.

Future studies and observations may help to unravel the remnants of the broken-up comet 289P/Blanpain with its dust trails and possible larger fragments such as minor planet 2003 WY_{25}, which is probably not the only surviving large piece. The actual 2019, 2024–2025 observations of the 29-Piscids may help stream modelers to adjust the model to fit the observed results.

Acknowledgments

This report is based on the data of the Global Meteor Network (Vida et al., 2020a; 2020b; 2021) which is released under the CC BY 4.0 license[20]. We thank all 825 participants in the Global Meteor Network project for their contribution and perseverance. A list with the names of the volunteers who contribute to GMN has been published in the 2024 annual report (Roggemans et al., 2025). The following 360 cameras recorded 29 Piscid meteors used for the 2019, 2024 and 2025 meteor shower data: AT0002, AT0004, AU0002, AU000A, AU000C, AU000D, AU000F, AU000S, AU000T, AU000V, AU000W, AU000X, AU000Y, AU0010, AU001A, AU001B, AU001E, AU001F, AU001K, AU001L, AU001P, AU001R, AU001S, AU001U, AU001V, AU001W, AU001X, AU001Y, AU001Z, AU0029, AU002A, AU0030, AU003E, AU003G, AU003J, AU0041, AU0047, AU0048, AU004B, AU004J, AU004K, BA0003, BA0005, BE0005, BE0007, BE000K, BE000P, BE000Q, BG0001, BG0002, BG0003, BG000B, BG000D, BG000K, BR000F, BR000S, BR000T, BR0015, BR001G, BR001W, BR002A, CA0005, CA000R, CA0012, CA001N, CA001R, CA0022, CA0023, CA002R, CA0031, CA0032, CH0002, CH0003, CZ0004, CZ000C, CZ000E, CZ000K, CZ000L, CZ000M, DE0001, DE0002, DE0004, DE000B, DE000K, DE000Q, DE000W, DE000X, DE0013, ES0001, ES000H, FR000A, FR000Y, FR000Z, FR0016, GR0002, GR0004, GR0005, GR0006, GR0009, HR0006, HR0008, HR000D, HR000K, HR000P, HR000Q, HR000R, HR000S, HR000W, HR0015, HR001J, HR001R, HR001X, HR001Z, HR0024, HR002D, HR002E, HR002F, HR002X, HR002Y, HU0001, HU0002, HU0003, KR0002, KR0009, KR000A, KR000B, KR000D, KR000H, KR000J, KR000P, KR0019, KR001S, KR0021, KR0023, KR0024, KR0027, KR0028, KR002C, KR002F, KR002G, KR002S, KR003A, KR003H, KR003J, KR003K, KR003L, KR003Q, KR003R, KR003S, KR003W, NL000C, NL000P, NL000Q, NL000T, NL000U, NL0010, NZ0001, NZ0003, NZ0004, NZ0007, NZ0009, NZ000B, NZ000D, NZ000G, NZ000N, NZ000R, NZ000V, NZ000X, NZ000Z, NZ0017, NZ0018, NZ0019, NZ001C, NZ001G, NZ001P, NZ001R, NZ001Z, NZ0022, NZ0023, NZ0026, NZ0027, NZ0029, NZ002C, NZ002D, NZ002E, NZ002G, NZ002K, NZ002L, NZ002N, NZ002P, NZ002Q, NZ002R, NZ002S, NZ002T, NZ002V, NZ002W, NZ002X, NZ002Y, NZ002Z, NZ0030, NZ0032, NZ0033, NZ0034, NZ0035, NZ0036, NZ0037, NZ003A, NZ003B, NZ003C, NZ003E, NZ003H, NZ003K, NZ003N, NZ003Q, NZ003S, NZ003T, NZ003U, NZ003W, NZ003Y, NZ0042, NZ0046, NZ0049, NZ004A, NZ004B, NZ004C, NZ004D, NZ004E, NZ004H, NZ004J, NZ004L, NZ004N, NZ004R, NZ0051, NZ0059, NZ005A, NZ005C, NZ005D, NZ005G, NZ005H, NZ005L, NZ005Y, NZ005Z, RO0001, RO0002, SI0002, SI0006, SK0006, UA0001, UA0002, UK0004, UK0006, UK000D, UK000F, UK001Z, UK0031, UK0055, UK005J, UK0061, UK0066, UK006P, UK0080, UK0092, UK0096, UK009D, UK009Q, UK009X, UK00A4, UK00A5, UK00AD, UK00B0, UK00B1, UK00B7, UK00BA, UK00BK, UK00BN, UK00BW, UK00CA, UK00CC, UK00CS, UK00CT, UK00D6, US0001, US0002, US0003, US0004, US0005, US0006, US0007, US0008, US0009, US000A, US000C, US000D, US000E, US000G, US000H, US000J, US000K, US000L, US000M, US000P, US000R, US000S, US000U, US001E, US001L, US001P, US001V, US0020, US0021, US0023, US002P, US002R, US002W, US0035, US0038, US003M, US003N, US003R, US003T, US0046, US004B, US004C, US004J, US004P, US004Q, US0051, US005D, US005E, US005F, US005J, US005X, US005Y, US005Z, USL004, USL007, USL009, USL00A, USL00B, USL00F, USL00J, USL00L, USL00M, USL00N, USL00Q, USL012, USL014, USL018, USL01E, USN001, USV001, USV002, USV003, ZA0001, ZA0006, ZA0007, ZA0008, ZA0009, ZA000C.

References

Drummond J. D. (1981). “A test of comet and meteor shower associations”. *Icarus*, **45**, 545–553.

Jenniskens P. and Lyytinen E. (2005). “Meteor showers from the debris of broken comets: D/1819 W1 (Blanpain), 2003 WY_{25}, and the Phoenicids”. *The Astronomical Journal*, **130**, 1286–1290.

Jenniskens P. (2020). “29 Piscids (PIS#1046) meteor shower 2019”. *eMetN Meteor Journal*, **5**, 370–371.

Jenniskens P. (2023). Atlas of Earth’s meteor showers. Elsevier, Cambridge, United states. ISBN 978-0-443-23577-1. Page 477.

Jopek T. J. (1993). “Remarks on the meteor orbital similarity D-criterion”. *Icarus*, **106**, 603–607.

Jopek T. J., Rudawska R. and Pretka-Ziomek H. (2006). “Calculation of the mean orbit of a meteoroid

[20] https://creativecommons.org/licenses/by/4.0/

stream". *Monthly Notices of the Royal Astronomical Society*, **371**, 1367–1372.

Moorhead A. V., Clements T. D., Vida D. (2020). "Realistic gravitational focusing of meteoroid streams". *Monthly Notices of the Royal Astronomical Society*, **494**, 2982–2994.

Roggemans P., Johannink C. and Campbell-Burns P. (2019). "October Ursae Majorids (OCU#333)". *eMetN Meteor Journal*, **4**, 55–64.

Roggemans P., Johannink C. and Martin P. (2020). "Phoenicids (PHO#254) activity in 2019". *eMetN Meteor Journal*, **5**, 4–10.

Roggemans P., Campbell-Burns P., Kalina M., McIntyre M., Scott J. M., Šegon D., Vida D. (2025). "Global Meteor Network report 2024". *eMetN Meteor Journal*, **10**, 67–101.

Sato M., Watanabe J. (2010). "Forecast for Phoenicids in 2008, 2014, and 2019". *Publications of the Astronomical Society of Japan*, **62**, 509–513.

Sato M., Watanabe J. (2014). "Correction effect to the radiant dispersion in case of low velocity meteor showers". In Jopek T. J., Rietmeijer F. J. M., Watanabe J., Williams I. P., editors, *Proceedings of the Meteoroids 2013 Conference*, Poznań, Poland, Aug. 26-30, 2013. A.M. University, pages 329–333.

Shiba Y. (2022). "Jupiter Family Meteor Showers by SonotaCo Network Observations". *WGN, Journal of the International Meteor Organization*, **50**, 38–61.

Southworth R. B. and Hawkins G. S. (1963). "Statistics of meteor streams". *Smithsonian Contributions to Astrophysics*, **7**, 261–285.

Vida D., Gural P., Brown P., Campbell-Brown M., Wiegert P. (2020a). "Estimating trajectories of meteors: an observational Monte Carlo approach - I. Theory". *Monthly Notices of the Royal Astronomical Society*, **491**, 2688–2705.

Vida D., Gural P., Brown P., Campbell-Brown M., Wiegert P. (2020b). "Estimating trajectories of meteors: an observational Monte Carlo approach - II. Results". *Monthly Notices of the Royal Astronomical Society*, **491**, 3996–4011.

Vida D., Šegon D., Gural P. S., Brown P. G., McIntyre M. J. M., Dijkema T. J., Pavletić L., Kukić P., Mazur M. J., Eschman P., Roggemans P., Merlak A., Zubrović D. (2021). "The Global Meteor Network – Methodology and first results". *Monthly Notices of the Royal Astronomical Society*, **506**, 5046–5074.

M2024-H1 activity confirmed in 2025

Paul Roggemans[1], **Denis Vida**[2,3], **Damir Šegon**[4,5], **James M. Scott**[6], **Jeff Wood**[7]

[1] **Pijnboomstraat 25, 2800 Mechelen, Belgium**

[2] **Department of Physics and Astronomy, University of Western Ontario, Richmond Street, London, N6A 3K7, Ontario, Canada**

[3] **Institute for Earth and Space Exploration, University of Western Ontario, Perth Drive, London, N6A 5B8, Ontario, Canada**
denis.vida@gmail.com

[4] **Astronomical Society Istra Pula, Park Monte Zaro 2, 52100 Pula, Croatia**

[5] **Višnjan Observatory, Istarska 5, 52463 Višnjan, Croatia**

[6] **Department of Geoscience, Aarhus University, Høegh-Guldbergs Gade 2. DK-8000 Aarhus C, Denmark**
jscott@geo.au.dk

[7] **PO Box 162, Willetton, Western Australia 6955, Australia**

A new meteor shower in Hercules that was discovered in 2024 by GMN and registered by the IAU-MDC as M2024-H1 reoccurred in 2025, from a radiant at R.A. = 261.5°, Decl. = +47.7°. The radiant position and activity period match perfectly with the 2024 observations but the activity was less intense in 2025 and the recorded meteors had a slightly slower geocentric velocity than in 2024. No relevant activity from this shower has been found in previous year's meteor orbit datasets.

1 Introduction

On 27 April 2024 the Global Meteor Network recorded 32 meteors in a short time interval between 20^h00^m–23^h40^m UTC (37.70° to 37.85° in solar longitude) from a radiant in the constellation of Hercules. This short outburst has been registered in the IAU-MDC Working List of Meteor Showers as M2024-H1[21] (Vida and Šegon, 2024).

This activity source has been detected again in 2025 although only sixteen M2024-H1 meteors were recorded, half of the total number recorded in 2024. The shower was independently observed in 2025 by 58 cameras in Australia, Belgium, Canada, Croatia, Czechia, Germany, Hungary, Italy, Netherlands, Portugal, Spain, United Kingdom and United States.

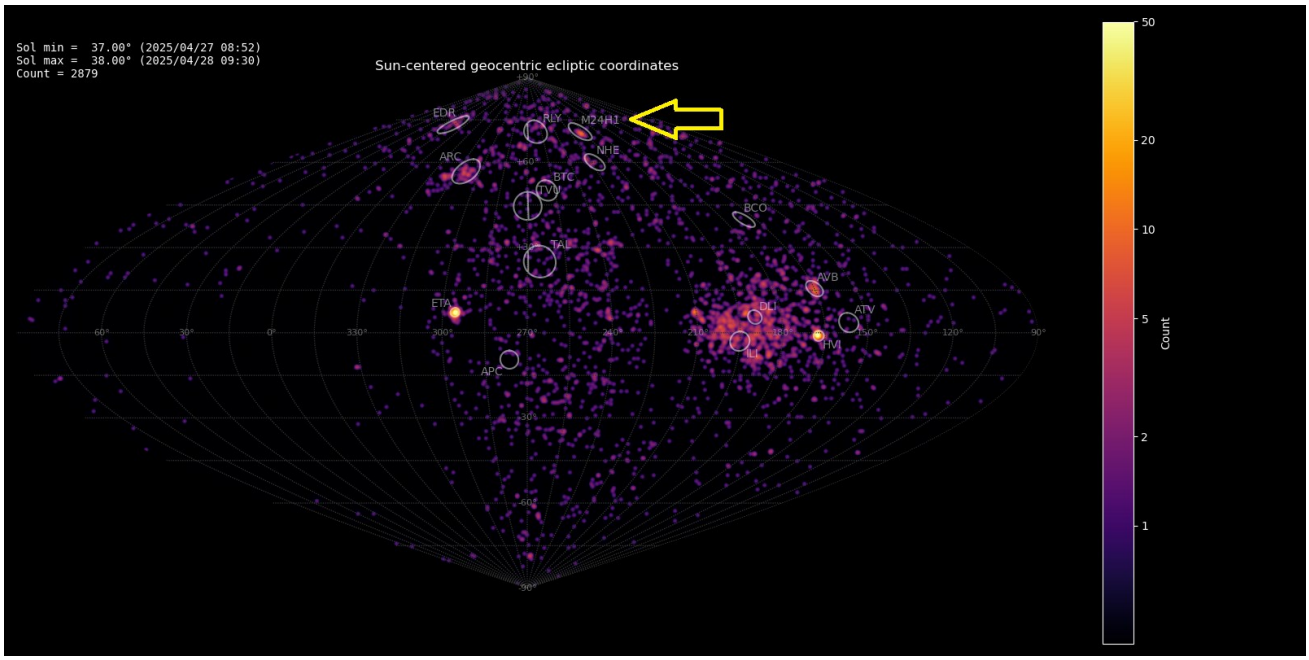

Figure 1 – Radiant density map (sinusoidal projection) with 2879 radiants obtained by the Global Meteor Network during 27–28 April, 2025. The position of the M2024-H1 radiant in Sun-centered geocentric ecliptic coordinates is marked with a yellow arrow.

[21] https://www.ta3.sk/IAUC22DB/MDC2022/Roje/pojedynczy_obiekt.php?lporz=02175&kodstrumienia=01224

2 Shower classification based on radiants

The GMN shower association criteria assume that meteors within 1° in solar longitude, within 1.2° in radiant in this case, and within 10% in geocentric velocity of a shower reference location are members of that shower. Further details about the shower association are explained in Moorhead et al. (2020). Using these meteor shower selection criteria, 16 orbits have been identified as M2024-H1 meteors.

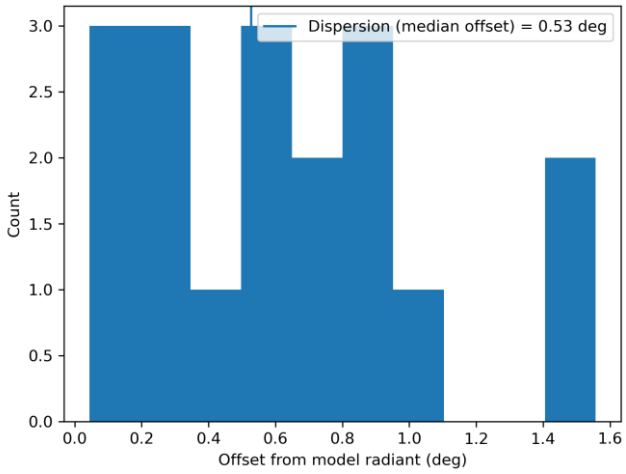

Figure 2 – Dispersion median offset on the radiant position.

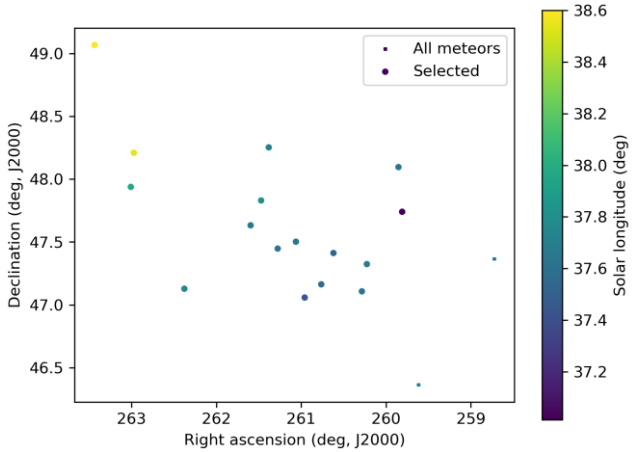

Figure 3 – The radiant distribution during the solar-longitude interval 37.0° – 38.6° in equatorial coordinates.

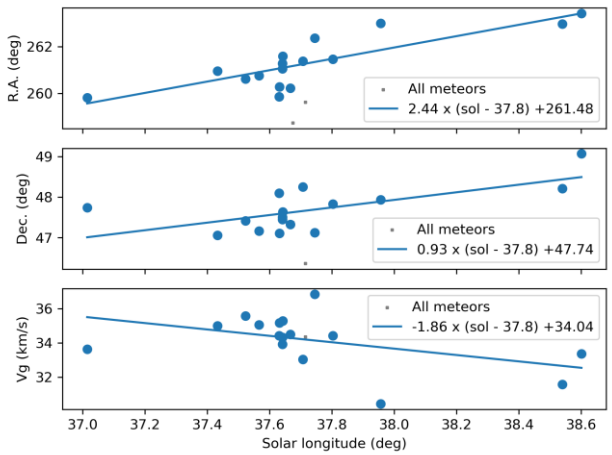

Figure 4 – The radiant drift.

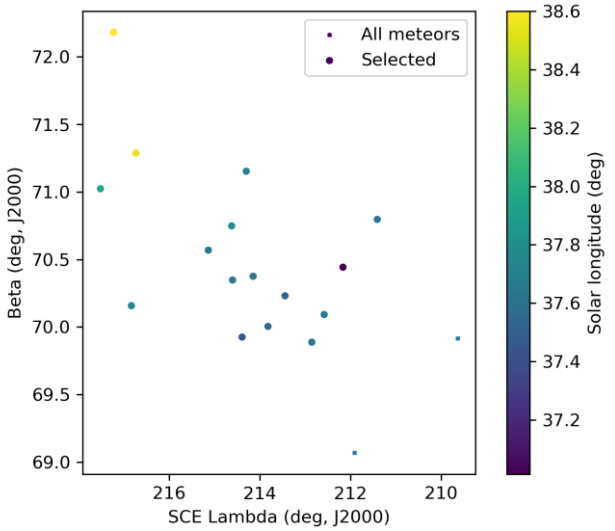

Figure 5 – The radiant distribution during the solar-longitude interval 37.0° – 38.6° in Sun centered geocentric ecliptic coordinates.

Table 1 – Comparing solutions for 2025 and 2024 derived by two different methods, GMN-method based on radiant positions and orbit association for $D_D < 0.04$.

	2025		2024	
	GMN	$D_D < 0.04$	GMN	$D_D < 0.04$
$\lambda_\odot$ (°)	37.8	37.6	37.78	37.81
$\lambda_{\odot b}$ (°)	37.0	36.6	37.71	37.71
$\lambda_{\odot e}$ (°)	39.0	38.8	37.85	37.86
α_g (°)	261.5	260.0	261.0	260.9
δ_g (°)	+47.7	+47.3	+47.5	+47.4
$\Delta\alpha_g$ (°)	+2.44	–	–	–
$\Delta\delta_g$ (°)	+0.93	–	–	–
v_g (km/s)	34.0	34.4	35.5	35.6
H_b (km)	103.6	103.2	104.3	105.1
H_e (km)	93.5	90.8	92.3	91.2
H_p (km)	100.0	98.5	99.1	98.7
Mag_{Ap}	–0.2	–0.3	–0.5	–0.7
λ_g (°)	252.52	249.9	251.7	251.3
$\lambda_g - \lambda_\odot$ (°)	214.72	212.4	213.9	213.6
β_g (°)	+70.66	+70.0	+70.3	+70.2
a (A.U.)	8.344	10.9	32.2	29.3
q (A.U.)	0.954	0.948	0.963	0.953
e	0.886	0.913	0.9701	0.968
i (°)	54.30	53.7	55.6	55.8
ω (°)	207.1	208.2	206.7	206.9
Ω (°)	37. 7	37.6	37.8	37.8
Π (°)	244.8	245.8	244.5	244.7
T_j	1.31	1.40	0.84	0.85
N	16	20	32	24

3 Shower classification based on orbits

Another method applied to classify meteor showers has been explained in Roggemans et al. (2019; 2026). Three different discrimination criteria are combined in order to have only those orbits which fit the different criteria thresholds. The D-criteria that we use are these of Southworth and Hawkins (1963), Drummond (1981) and Jopek (1993) combined. The mean orbits are computed with the method described by Jopek et al. (2006). The Rayleigh distribution fit of 2024 indicated that a cutoff value is required with $D_D < 0.04$ as D-criterion threshold.

The results obtained by the two methods for both years are listed in *Table 1*.

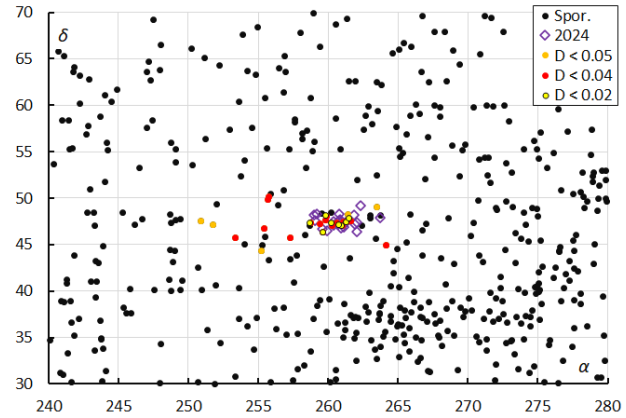

Figure 6 – The radiant distribution during the solar-longitude interval 36° – 39° in equatorial coordinates, color-coded for different threshold values of the D_D orbit similarity criterion.

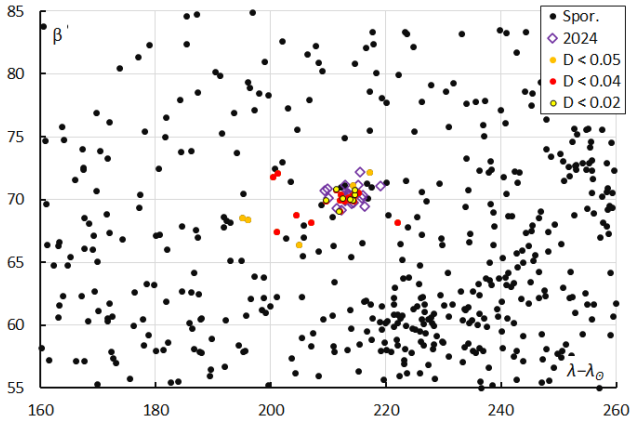

Figure 7 – The radiant distribution during the solar-longitude interval 36° – 39° in Sun-centered geocentric ecliptic coordinates, color-coded for different threshold values of the D_D orbit similarity criterion.

Comparing the radiant positions obtained in 2024 and 2025, we see that the radiant was very compact in 2024 and more dispersed in 2025. For 2025, three different D-criteria thresholds are shown, but for 2024 only the class with $D_{SH} < 0.1$ & $D_D < 0.04$ & $D_J < 0.1$ has been plotted. In equatorial coordinates (*Figure 6*) the radiant appears elongated due to the radiant drift in Right Ascension. *Figure 7* shows the radiant in Sun-centered ecliptic coordinates where the radiant drift due to the Earth's own motion is compensated, but also here some more scattered radiant points appear for 2025.

4 Orbit and parent body

Looking at the diagram of inclination versus longitude of perihelion, we can see a dense concentration for 2024 at slighter higher inclination than in 2025 when the points appear more dispersed (*Figure 8*). The diagram of eccentricity versus longitude of perihelion shows a remarkable offset in eccentricity between the data points of 2024 and 2025 (*Figure 9*). The inclination appears also slightly lower and more dispersed in 2025 compared to 2024, the perihelion distance remained stable (*Figure 10*).

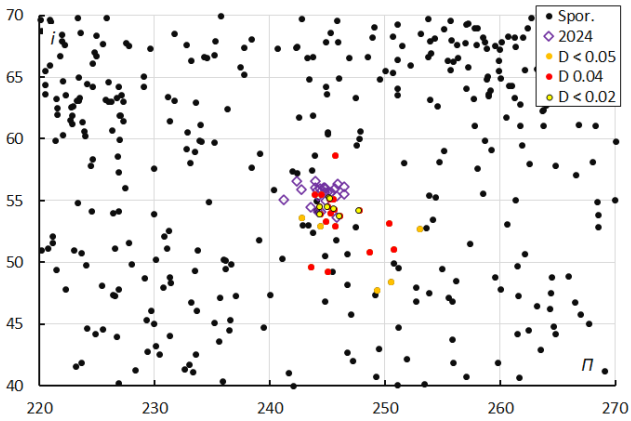

Figure 8 – The diagram of the inclination i versus the longitude of perihelion Π color-coded for different classes of D criteria thresholds, for $\lambda_\odot$ between 36° and 39°.

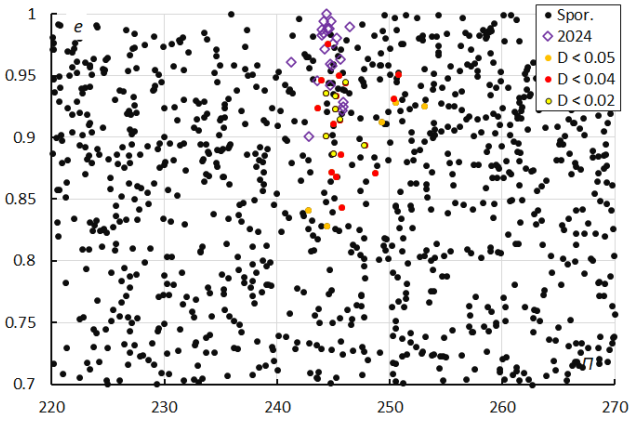

Figure 9 – The diagram of the eccentricity e versus the longitude of perihelion Π color-coded for different classes of D criteria thresholds, for $\lambda_\odot$ between 36° and 39°.

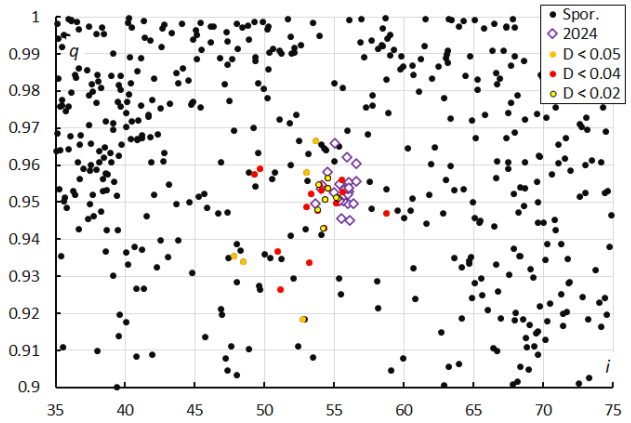

Figure 10 – The diagram of the perihelion distance q versus the inclination i color-coded for different classes of D criteria threshold, for $\lambda_\odot$ between 36° and 39°.

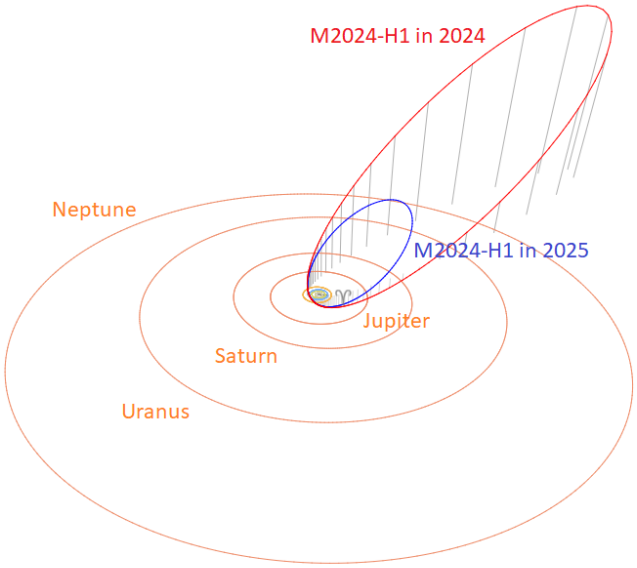

Figure 11 – Comparing the GMN solution for M2024-H1 in 2025 (blue) and in 2024 (red). (Plotted with the Orbit visualization app provided by Pető Zsolt).

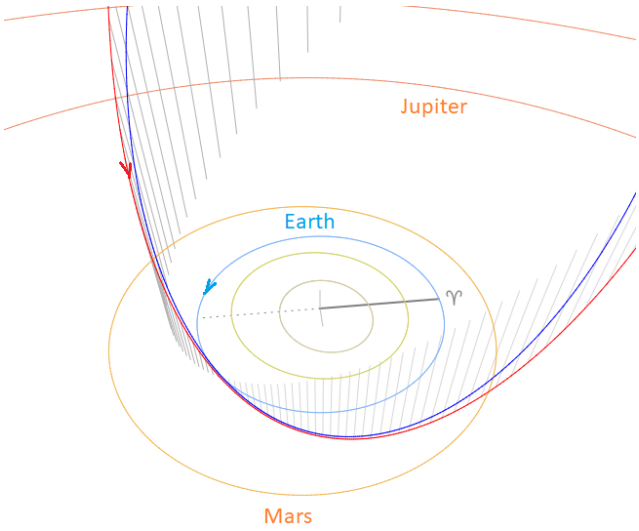

Figure 12 – Comparing the GMN solution for M2024-H1 in 2025 (blue) and in 2024 (red), close-up at the inner Solar System. (Plotted with the Orbit visualization app provided by Pető Zsolt).

The M2024-H1 meteoroids recorded in 2025 appeared less concentrated and with a slower geocentric velocity than in 2024 (see *Table 1*). The difference in velocity affects the orbital elements that are most sensitive for differences in velocity like the semi-major axis a, the eccentricity e and to less extend the inclination i. The radiant positions agree very well for both years, but the mean orbits in the solar system differ. There is no clear explanation for this and it looks like the dust encountered in 2025 was situated far inside the 2024 orbit. *Figure 11* shows the significant difference in semi-major axis. *Figure 12* visualizes the M2024-H1 orbit in the inner solar system. The meteoroid stream encounters the Earth orbit at its descending node from far above the ecliptic plane.

The Tisserand's parameter relative to Jupiter differs a lot between 2024 and 2025 as this parameter depends mainly upon the semi-major axis. Both values, $T_j = 0.84$ in 2024 and $T_j = 1.31$ in 2025, identify the orbit as of a Mellish type comet orbit. A parent body search did not return any known object with a similar orbit.

5 Past observations

A search was made through the meteor orbit datasets to check for activity of this shower using the orbit identification criteria with $D_{SH} < 0.1$ & $D_D < 0.04$ & $D_J < 0.1$. GMN data had only one candidate in 2023, 6 in 2022, 1 in 2021, 1 in 2020 and none in 2019. SonotaCo Net had nine for the entire dataset covering 2007–2024: 2 in 2023, 1 in 2019, 4 in 2017 and 2 in 2007. EDMOND had five candidates for the period 2002–2023: 3 in 2014, 1 in 2013 and 1 in 2012. CAMS had only one candidate in 2016 for the period 2011–2016.

6 Conclusion

The activity of M2024-H1 has been confirmed in 2025 with a radiant at the same position as in 2024 but with a slightly lower geocentric velocity. Most M2024-H1 meteors in 2025 were recorded during the same short duration interval as in 2024 but the level of activity was only half compared to 2024.

The short duration of this meteor shower, the very compactness of the radiant and orbits in 2024 indicates there was an outburst in 2024 while the activity recorded in 2025 appeared more dispersed inside the 2024 orbit. The number of candidate meteors in earlier years is statistically too small to confirm any past activity. Most likely this is an episodic meteor shower which is absent in most years. A very short duration of activity like observed in 2024 makes such shower vulnerable to weather circumstances so that earlier occurrences may have been clouded out or appeared during daylight. The activity level, even during an outburst, is too low to be detected by most observing techniques except for low light camera network with a dense global coverage. Future observations are required to determine the periodicity if the shower proves to be episodic.

Acknowledgments

This report is based on the data of the Global Meteor Network (Vida et al., 2020a; 2020b; 2021) which is released under the CC BY 4.0 license[22]. We thank all 825 participants in the Global Meteor Network project for their contribution and perseverance. A list with the names of the volunteers who contribute to GMN has been published in the 2024 annual report (Roggemans et al., 2025). The following 80 cameras detected M2024-H1 in 2024–2025 : AU0045, AU004B, BE0002, BE0006, BE0015, CA002J, CA002R, CZ0003, CZ0007, CZ0008, CZ000C, CZ000R, DE0001, DE0004, DE000Q, DE000S, DE000W, DE0013, DE0016, ES000U, ES0016, ES001F, HR002F, HR002J, HR002K, HU0003, IT0001, IT0004, NL0006, NL000G, NL000K, NL000M, NL000N, NL000S, NL000U, NL0011, NL0013, NL0014, NL0019, PT0002, SI0002, UK002F,

[22] https://creativecommons.org/licenses/by/4.0/

UK002K, UK0034, UK0035, UK003U, UK0041, UK0042, UK004M, UK005E, UK005G, UK005M, UK006D, UK006P, UK0079, UK007H, UK007Y, UK008C, UK008F, UK008T, UK0098, UK0099, UK009U, UK00A0, UK00A4, UK00AJ, UK00AN, UK00AT, UK00BJ, UK00CC, UK00CJ, US001P, US003N, US003T, US005B, US005P, USL00B, USL00K, USL014.

References

Drummond J. D. (1981). "A test of comet and meteor shower associations". *Icarus*, **45**, 545–553.

Jopek T. J. (1993). "Remarks on the meteor orbital similarity D-criterion". *Icarus*, **106**, 603–607.

Jopek T. J., Rudawska R. and Pretka-Ziomek H. (2006). "Calculation of the mean orbit of a meteoroid stream". *Monthly Notices of the Royal Astronomical Society*, **371**, 1367–1372.

Moorhead A. V., Clements T. D., Vida D. (2020). "Realistic gravitational focusing of meteoroid streams". *Monthly Notices of the Royal Astronomical Society*, **494**, 2982–2994.

Roggemans P., Johannink C. and Campbell-Burns P. (2019). "October Ursae Majorids (OCU#333)". *eMetN Meteor Journal*, **4**, 55–64.

Roggemans P., Campbell-Burns P., Kalina M., McIntyre M., Scott J. M., Šegon D., Vida D. (2025). "Global Meteor Network report 2024". *eMetN Meteor Journal*, **10**, 67–101.

Roggemans P., Vida D., Šegon D., Scott J.M., Wood J. (2026). "29-Piscids (PIS#1046) return in 2025". *eMetN Meteor Journal*, **11**, 31–41.

Southworth R. B. and Hawkins G. S. (1963). "Statistics of meteor streams". *Smithsonian Contributions to Astrophysics*, **7**, 261–285.

Vida D., Gural P., Brown P., Campbell-Brown M., Wiegert P. (2020a). "Estimating trajectories of meteors: an observational Monte Carlo approach - I. Theory". *Monthly Notices of the Royal Astronomical Society*, **491**, 2688–2705.

Vida D., Gural P., Brown P., Campbell-Brown M., Wiegert P. (2020b). "Estimating trajectories of meteors: an observational Monte Carlo approach - II. Results". *Monthly Notices of the Royal Astronomical Society*, **491**, 3996–4011.

Vida D., Šegon D., Gural P. S., Brown P. G., McIntyre M. J. M., Dijkema T. J., Pavletić L., Kukić P., Mazur M. J., Eschman P., Roggemans P., Merlak A., Zubrović D. (2021). "The Global Meteor Network – Methodology and first results". *Monthly Notices of the Royal Astronomical Society*, **506**, 5046–5074.

Vida D., Šegon D. (2024). "New shower in Hercules". *eMetN Meteor Journal*, **9**, 161–164.

M2024-N1 activity confirmed in 2025

Paul Roggemans[1], **Denis Vida**[2,3], **Damir Šegon**[4,5], **James M. Scott**[6], **Jeff Wood**[7]

[1] **Pijnboomstraat 25, 2800 Mechelen, Belgium**

[2] **Department of Physics and Astronomy, University of Western Ontario, Richmond Street, London, N6A 3K7, Ontario, Canada**

[3] **Institute for Earth and Space Exploration, University of Western Ontario, Perth Drive, London, N6A 5B8, Ontario, Canada**
denis.vida@gmail.com

[4] **Astronomical Society Istra Pula, Park Monte Zaro 2, 52100 Pula, Croatia**

[5] **Višnjan Observatory, Istarska 5, 52463 Višnjan, Croatia**

[6] **Department of Geoscience, Aarhus University, Høegh-Guldbergs Gade 2. DK-8000 Aarhus C, Denmark**
jscott@geo.au.dk

[7] **PO Box 162, Willetton, Western Australia 6955, Australia**

A new meteor shower in Fornax discovered in 2024 by GMN, registered by the IAU-MDC as M2024-N1 reoccurred in 2025, from a radiant at R.A. = 44.2°, Decl. = –38.2° between 30 June and 5 July. The radiant position and activity period match perfectly with the 2024 observations but the activity was less intense in 2025. The main component of this meteoroid stream consists of long period orbit but includes also a significant number of shorter period orbits.

1 Introduction

Between the 1st and 5th July 2024, the Global Meteor Network recorded 51 meteors from a radiant in the constellation of Fornax. This activity has been registered in the IAU-MDC Working List of Meteor Showers as M2024-N1[23] (Šegon et al., 2024). This activity had also been recorded by the CAMS network (Jenniskens, 2024). When the shower is officially confirmed by at least two independent networks, it may be nominated to be listed as an established shower.

This activity source has been detected again in 2025 with 38 M2024-N1 meteors recorded. The shower was independently observed in 2025 by 86 cameras in Australia, Brazil, Chile, New Zealand and South Africa.

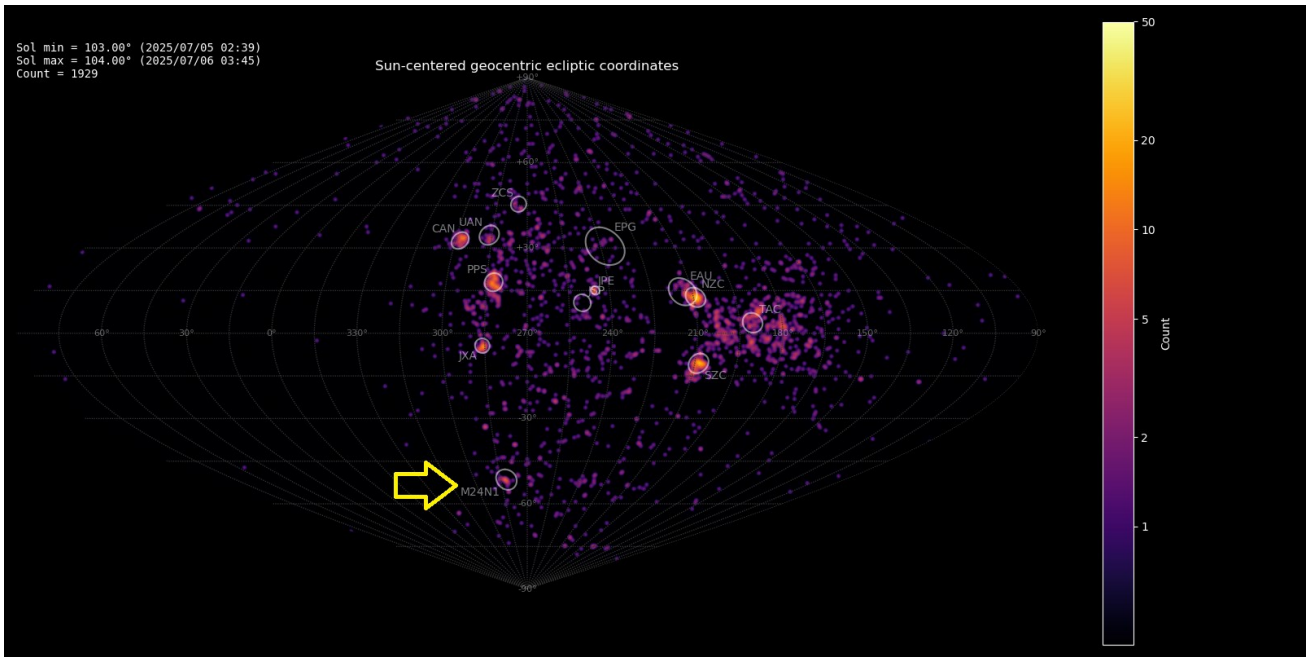

Figure 1 – Radiant density map (sinusoidal projection) with 1929 radiants obtained by the Global Meteor Network during 5–6 July, 2025. The position of the M2024-N1 radiant in Sun-centered geocentric ecliptic coordinates is marked with a yellow arrow.

[23] https://www.ta3.sk/IAUC22DB/MDC2022/Roje/pojedynczy_obiekt.php?lporz=02180&kodstrumienia=01225

2 Shower classification based on radiants

The GMN shower association criteria assume that meteors within 1° in solar longitude, within 3.5° in radiant in this case, and within 10% in geocentric velocity of a shower reference location are members of that shower. Further details about the shower association are explained in Moorhead et al. (2020). Using these meteor shower selection criteria, 38 orbits have been identified as M2024-N1 meteors in 2025.

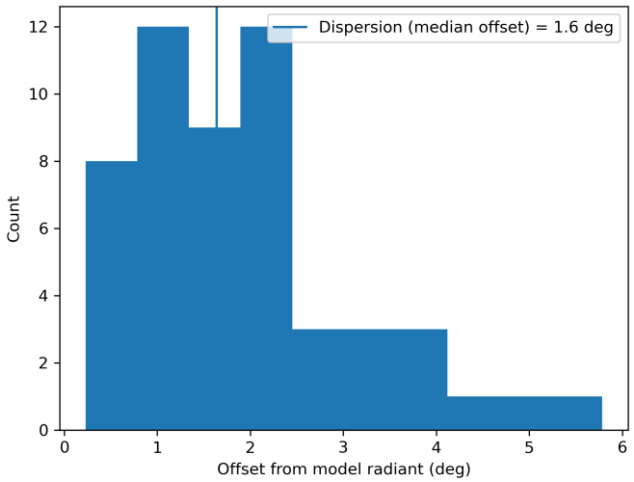

Figure 2 – Dispersion median offset on the radiant position.

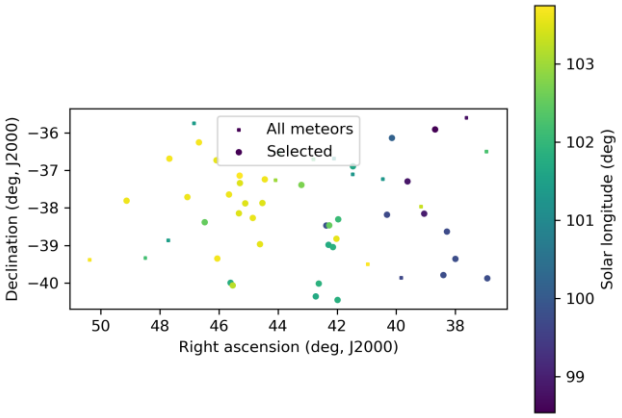

Figure 3 – The radiant distribution during the solar-longitude interval 99.0° – 104° in equatorial coordinates in 2025.

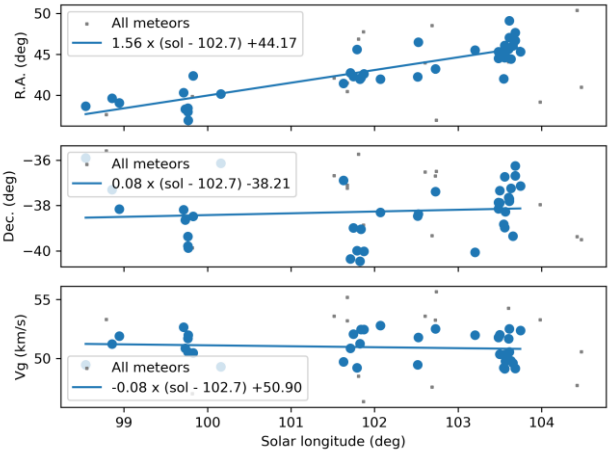

Figure 4 – The radiant drift.

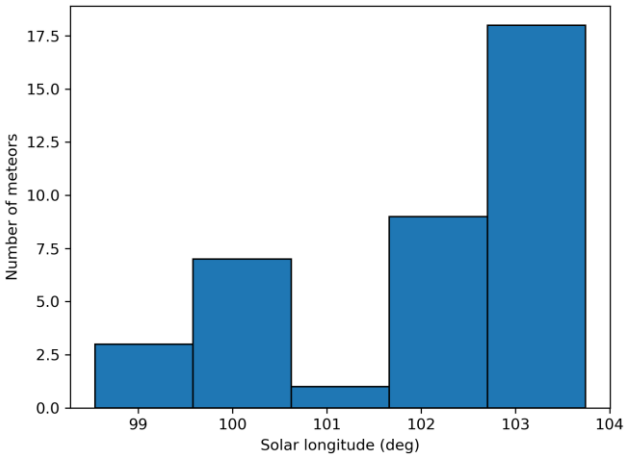

Figure 5 – The uncorrected number of M2024-N1 meteors per degree in solar longitude recorded in 2025.

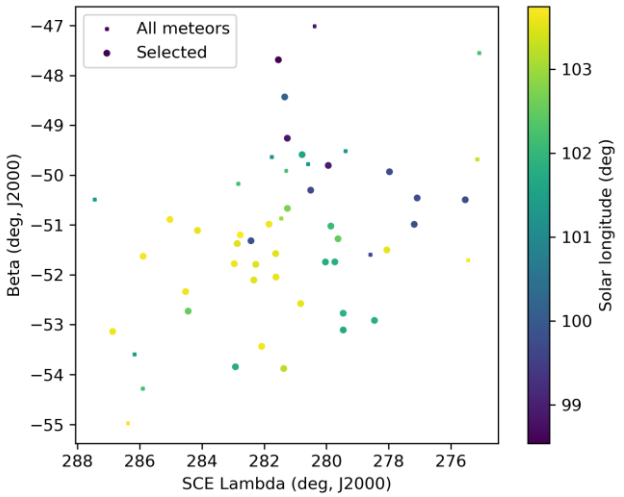

Figure 6 – The radiant distribution during the solar-longitude interval 99° – 104° in Sun centered geocentric ecliptic coordinates.

3 Shower classification based on orbits

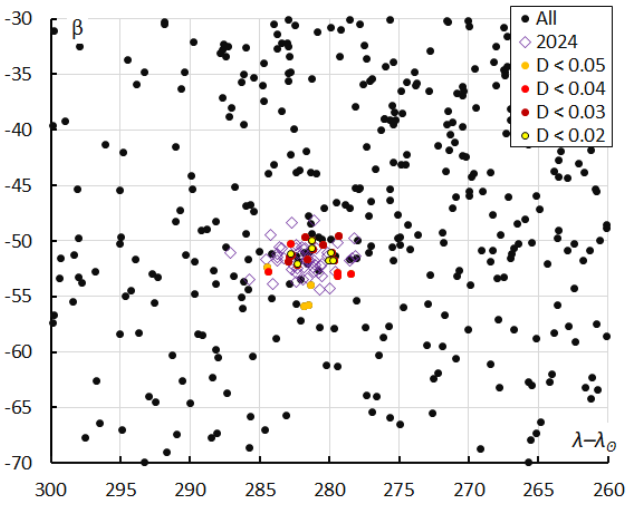

Figure 7 – The radiant distribution during the solar-longitude interval 99° – 104° in Sun centered geocentric ecliptic coordinates. Comparing the 2024 and 2025 results based on orbit identification.

Another method applied to classify meteor showers has been explained in Roggemans et al. (2019; 2026). Three different discrimination criteria are combined in order to have only those orbits which fit the different criteria

thresholds. The D-criteria that we use are these of Southworth and Hawkins (1963), Drummond (1981) and Jopek (1993) combined. The mean orbits are computed with the method described by Jopek et al. (2006). In 2024, a cutoff value with $D_D < 0.06$ as D-criterion threshold. In 2025, this cutoff value was reduced to $D_D < 0.05$ since last year's cutoff proved to be too tolerant.

The results obtained by the two methods for both years are listed in *Table 1*.

Table 1 – Comparing solutions for 2025 and 2024 derived by two different methods, GMN-method based on radiant positions and orbit association for $D_D < 0.05$ in 2025, $D_D < 0.06$ in 2024.

	2025		2024
	GMN	$D_D < 0.05$	$D_D < 0.06$
$\lambda_\odot$ (°)	102.5	102.7	102.78
$\lambda_{\odot b}$ (°)	98.5	99.7	100.02
$\lambda_{\odot e}$ (°)	103.8	103.8	103.98
α_g (°)	44.2 ± 0.3	46.6 ± 2.1	44.04 ± 1.6
δ_g (°)	–38.2 ± 0.2	–38.2 ± 1.5	–38.3 ± 1.3
$\Delta\alpha_g$ (°)	+1.56 ± 0.15	+1.80	+0.63
$\Delta\delta_g$ (°)	+0.08 ± 0.12	–0.02	+0.47
v_g (km/s)	50.9 ± 0.2	52.2 ± 1.0	51.7 ± 1.0
H_b (km)	107.4 ± 4.2	109.2 ± 3.4	109.0 ± 2.8
H_e (km)	96.7 ± 5.9	92.9 ± 6.1	94.3 ± 4.8
H_p (km)	101.1 ± 5.6	101.6 ± 5.2	101.2 ± 4.3
Mag_{Ap}	–0.7	–1.5	–0.9
λ_g (°)	24.5 ± 0.4	24.3 ± 1.4	24.24 ± 2.0
$\lambda_g - \lambda_\odot$ (°)	281.8 ± 0.4	281.5 ± 1.6	281.64 ± 1.8
β_g (°)	–51.7 ± 0.2	–51.7 ± 1.7	–51.72 ± 1.3
a (A.U.)	7.6 ± 0.08	44.5	18.3
q (A.U.)	0.988 ± 0.011	0.991 ± 0.007	0.988 ± 0.009
e	0.871 ± 0.113	0.978 ± 0.037	0.946 ± 0.056
i (°)	92.7 ± 1.8	93.1 ± 2.5	92.7 ± 2.0
ω (°)	341.1 ± 4.3	342.3 ± 2.5	340.73 ± 3.0
Ω (°)	282.1 ± 1.7	282.6 ± 1.0	282.86 ± 0.8
Π (°)	263.1 ± 4.3	264.9 ± 2.3	263.9 ± 3.1
T_j	0.63 ± 0.60	0.05	0.23
N	38	22	51

The shower classification and the orbit classification methods agree on the radiant position but differ in eccentricity. The iterations to locate the best fitting mean orbit for the concentration of orbits converge on a selection of orbits with slightly faster geocentric velocity v_g, which drastically affects the eccentricity e and semi-major axis a. The uncertainty on the eccentricity derived from the radiant classification method is unusually large. Sorting the dataset on the heliocentric velocity v_h shows that 21 of the 38 meteors selected by the radiant classification method had $v_h < 41$ km/s. All these orbits failed to fit the threshold of the similarity criteria and were rejected as outliers by the orbit selection method. The orbit classification method selected only meteors with $v_h > 41$ km/s with a larger spread in radiant position than permitted for the radiant classification method but with a small uncertainty on the eccentricity.

Methods for distinguishing shower meteors always risks some contamination with sporadic meteors that share the same radiant position. In this particular case, it seems that there is a source with a slightly slower velocity and shorter period orbits that fits the radiant classification method but fails to fit with the orbit classification criteria. Therefore, the result of the orbit classification method has here been chosen as the solution for M2024-N1 for 2025.

4 Orbit and parent body

Comparing the diagrams of inclination and eccentricity versus longitude of perihelion in 2024 and in 2025 (*Figures 8 and 9*), it is evident that a large dispersion in eccentricity appeared for 2024 when a threshold cutoff of $D_D < 0.06$ was used. This value appears to have been too tolerant.

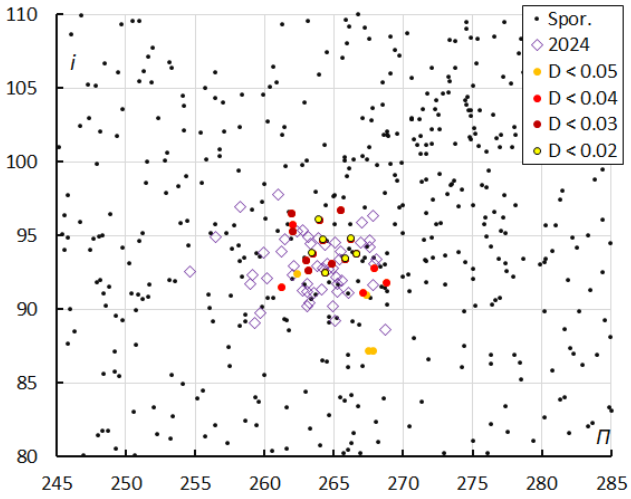

Figure 8 – The diagram of the inclination i versus the longitude of perihelion Π color-coded for different classes of D criteria thresholds, for $\lambda_\odot$ between 99° and 104°.

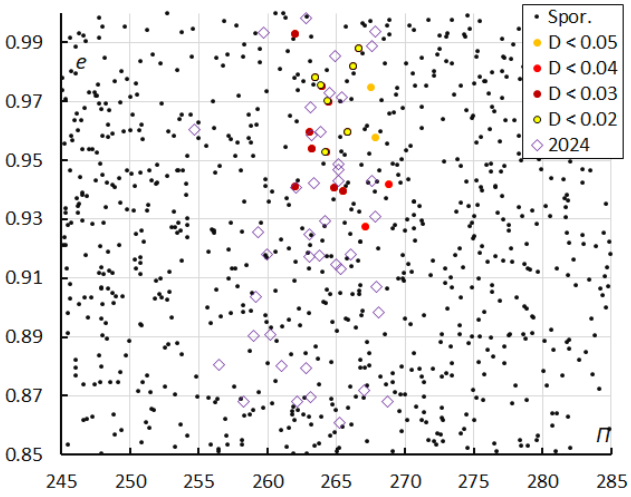

Figure 9 – The diagram of the eccentricity e versus the longitude of perihelion Π color-coded for different classes of D criteria thresholds, for $\lambda_\odot$ between 99° and 104°.

The Tisserand's parameter relative to Jupiter depends

mainly upon the semi-major axis. Both values, T_j = 0.23 in 2024 and T_j = 0.05 in 2025, identify the orbit as of a Long Period Comet type orbit. The result of the radiant classification method with T_j = 0.63 also suggests a Long Period Comet type orbit, despite the presence of the many short period orbits. A parent body search did not return any known object with a similar orbit.

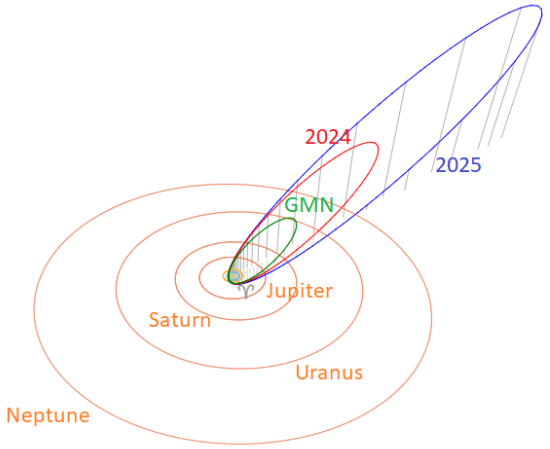

Figure 10 – Comparing the solutions for M2024-N1 in 2025 (blue), in 2024 (red) and the radiant classification method in 2025 (green). (Plotted with the Orbit visualization app provided by Pető Zsolt).

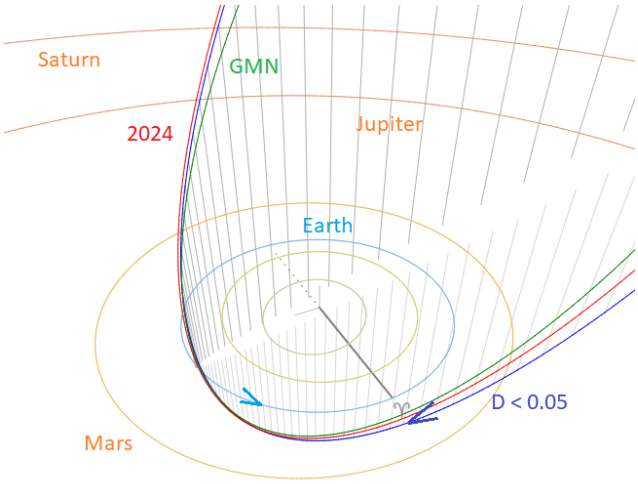

Figure 11 – Comparing the solutions for M2024-N1 in 2025 (blue), in 2024 (red) and the radiant classification solution in 2025 (green), close-up at the inner Solar System. (Plotted with the Orbit visualization app provided by Pető Zsolt).

The M2024-N1 meteor shower consists mainly of very long period orbits with a substantial number of shorter period orbits dispersed inside the main long period component. *Figure 10* shows the large difference in aphelia. An error margin of ±0.02 on eccentricities with $e > 0.95$ results in large uncertainties on semi-major axis a and aphelion distance Q as:

$$a = q/(1-e)$$

$$Q = a(1+e)$$

Where q is the perihelion distance. This explains why the aphelion distance Q is not a relevant parameter in this case.

The iterative procedure to locate the most representative mean orbit converged at a very long period orbit in 2025 (blue in *Figures 10 and 11*) with as similarity thresholds $D_{SH} < 0.125$ & $D_D < 0.05$ & $D_J < 0.125$. In 2024 the analysis was done with $D_{SH} < 0.15$ & $D_D < 0.06$ & $D_J < 0.15$, which resulted in shorter period orbits. No radiant classification method has been applied in 2024. In 2025 the radiant classification method identifies all long and short period orbits that fit the radiant and velocity selection criteria, resulting in a very large spread on the mean eccentricity. The orbit classification method only looks at the orbit similarity and results in a larger spread in the radiant position. The occurrence of many short period orbits within the main component of long period orbits may indicate an old dust population in which particles gradually loose energy due to different physical processes forcing the dust onto shorter period orbits towards the Sun.

Question is how do we define a meteoroid stream by its radiant and orbit with such a large dispersion in eccentricity? A solution here could be to use the heliocentric velocity instead of the geocentric velocity to filter away outliers that cause the large spread on the eccentricity. In that case we ignore the dust that evolved onto the shorter period orbits inside the main component. Another solution would be to add the error margins on the orbital parameters to indicate the degree of dispersion of the meteor shower.

Zooming in at the orbits in the inner Solar System we see that the three solutions look almost identical, longitude of perihelion, perihelion distance, node and inclination all agree very well (*Figure 11*). The M2024-N1 meteoroid stream encounters the Earth at its ascending node on a steep retrograde orbit, almost perpendicular to the ecliptic plane.

5 Conclusion

Global Meteor Network cameras confirmed activity from the M2024-N1 meteor shower radiant in Fornax in 2025. As this meteor shower had been independently published by the CAMS network in 2024 (Jenniskens, 2024), reporting of the CAMS solution for this activity to the IAU-MDC would qualify this shower to be listed as a candidate established shower. We trust it is only a matter of time before this M2024-N1 will be confirmed by an independent network.

Acknowledgments

This report is based on the data of the Global Meteor Network (Vida et al., 2020a; 2020b; 2021) which is released under the CC BY 4.0 license[24]. We thank all 825 participants in the Global Meteor Network project for their contribution and perseverance. A list with the names of the volunteers who contribute to GMN has been published in the 2024 annual report (Roggemans et al., 2025). The

[24] https://creativecommons.org/licenses/by/4.0/

following 175 cameras contributed to the M2024-N1 discovery in 2024–2025 : AU0002, AU0003, AU000A, AU000B, AU000C, AU000D, AU000F, AU000Q, AU000R, AU000S, AU000V, AU000W, AU000X, AU000Y, AU001A, AU001B, AU001C, AU001E, AU001F, AU001P, AU001Q, AU001R, AU001S, AU001V, AU001W, AU001X, AU001Y, AU001Z, AU0029, AU002A, AU0030, AU0031, AU0035, AU0038, AU003A, AU003F, AU003H, AU003K, AU0040, AU0042, AU0046, AU0047, AU004L, AU004M, BR0001, BR000G, BR000W, BR001F, BR001M, CL0002, CL0003, NZ0003, NZ0004, NZ0007, NZ0008, NZ000B, NZ000D, NZ000F, NZ000G, NZ000N, NZ000Q, NZ000T, NZ000V, NZ000X, NZ000Y, NZ000Z, NZ0010, NZ0012, NZ0013, NZ0014, NZ0015, NZ0016, NZ0017, NZ0018, NZ0019, NZ001A, NZ001B, NZ001C, NZ001F, NZ001G, NZ001H, NZ001J, NZ001L, NZ001N, NZ001P, NZ001Q, NZ001R, NZ001S, NZ001W, NZ001X, NZ001Y, NZ001Z, NZ0020, NZ0022, NZ0023, NZ0024, NZ0026, NZ0027, NZ0028, NZ0029, NZ002B, NZ002C, NZ002E, NZ002F, NZ002G, NZ002H, NZ002K, NZ002L, NZ002N, NZ002P, NZ002Q, NZ002R, NZ002S, NZ002T, NZ002V, NZ002W, NZ002X, NZ002Y, NZ002Z, NZ0030, NZ0032, NZ0033, NZ0034, NZ0036, NZ0037, NZ0038, NZ0039, NZ003A, NZ003C, NZ003E, NZ003F, NZ003G, NZ003H, NZ003K, NZ003N, NZ003R, NZ003S, NZ003T, NZ003U, NZ003V, NZ003W, NZ003X, NZ003Y, NZ003Z, NZ0040, NZ0041, NZ0042, NZ0044, NZ0045, NZ0046, NZ0049, NZ004A, NZ004B, NZ004C, NZ004D, NZ004E, NZ004J, NZ004L, NZ004M, NZ004N, NZ004R, NZ004S, NZ004T, NZ004U, NZ004V, NZ004X, NZ0051, NZ0059, NZ005D, NZ005Y, NZ005Z, ZA0002, ZA0007, ZA0008 and ZA000C.

References

Drummond J. D. (1981). “A test of comet and meteor shower associations”. *Icarus*, **45**, 545–553.

Jenniskens P. (2024). “Psi-Fornacid meteors 2024”. CBET 5415, 2024 July 15, editor D.W.E. Green.

Jopek T. J. (1993). “Remarks on the meteor orbital similarity D-criterion”. *Icarus*, **106**, 603–607.

Jopek T. J., Rudawska R. and Pretka-Ziomek H. (2006). “Calculation of the mean orbit of a meteoroid stream”. *Monthly Notices of the Royal Astronomical Society*, **371**, 1367–1372.

Moorhead A. V., Clements T. D., Vida D. (2020). “Realistic gravitational focusing of meteoroid streams”. *Monthly Notices of the Royal Astronomical Society*, **494**, 2982–2994.

Roggemans P., Johannink C. and Campbell-Burns P. (2019). “October Ursae Majorids (OCU#333)”. *eMetN Meteor Journal*, **4**, 55–64.

Roggemans P., Campbell-Burns P., Kalina M., McIntyre M., Scott J. M., Šegon D., Vida D. (2025). “Global Meteor Network report 2024”. *eMetN Meteor Journal*, **10**, 67–101.

Šegon D., Vida D., Roggemans P. (2024a). “Psi-Fornacid meteors 2024 = M2024-N1”. CBET 5416; 2024 July 16, editor D. W. E. Green.

Šegon D., Vida D., Roggemans P., Rollinson D., Scott J.M. (2024b). “New meteor shower in Fornax”. *eMetN Meteor Journal*, **9**, 279–285.

Southworth R. B. and Hawkins G. S. (1963). “Statistics of meteor streams”. *Smithsonian Contributions to Astrophysics*, **7**, 261–285.

Vida D., Gural P., Brown P., Campbell-Brown M., Wiegert P. (2020a). “Estimating trajectories of meteors: an observational Monte Carlo approach - I. Theory”. *Monthly Notices of the Royal Astronomical Society*, **491**, 2688–2705.

Vida D., Gural P., Brown P., Campbell-Brown M., Wiegert P. (2020b). “Estimating trajectories of meteors: an observational Monte Carlo approach - II. Results”. *Monthly Notices of the Royal Astronomical Society*, **491**, 3996–4011.

Vida D., Šegon D., Gural P. S., Brown P. G., McIntyre M. J. M., Dijkema T. J., Pavletić L., Kukić P., Mazur M. J., Eschman P., Roggemans P., Merlak A., Zubrović D. (2021). “The Global Meteor Network – Methodology and first results”. *Monthly Notices of the Royal Astronomical Society*, **506**, 5046–5074.

Possible new meteor shower in Draco (M2025-Y1)

Yury Harachka

Minsk, Belarus
astronominsk@gmail.com

A possible new meteor shower has been discovered during the night of December 12–13, 2025 (at $\lambda_\odot = 260.9°$) by Belarusian and Ukrainian video meteor networks. The radiant is situated in the constellation Draco at $\alpha = 212.4°$ and $\delta = +66.1°$, the meteors had a geocentric velocity v_g of 40.9 ± 0.8 km/s. The new meteor shower has been listed in the IAU MDC Working List of Meteor Showers under the temporary name-designation: M2025-Y1.

1 Observations

During the night of 12–13 December 2025, the Belarusian and the Ukrainian meteor networks recorded activity from an unidentified radiant in the constellation Draco. 10 multi-station meteors within a concentration of radiants were captured. *Figure 1* shows images of four meteors from this activity, which had a medium angular velocity and absolute magnitudes in the range –1.4m to +0.5m.

Figure 2 shows the locations of the camera stations and the projection of recorded meteors onto the Earth's surface.

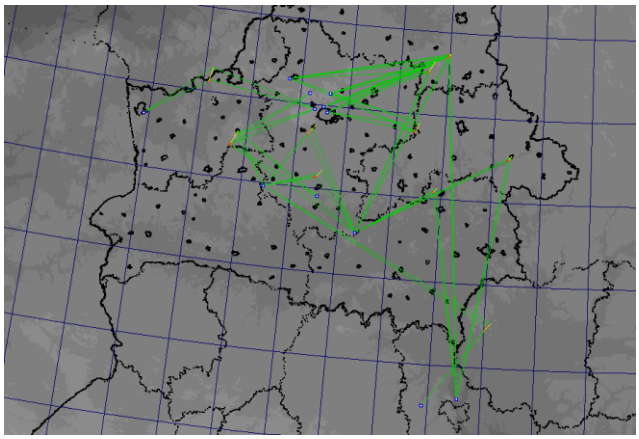

Figure 2 – Meteor trajectories from this unknown meteor shower projected on the Earth's surface.

Figure 2 shows the locations of the camera stations and the projection of recorded meteors onto the Earth's surface.

2 Results

The data were processed using UFOOrbit[25] (SonotaCo). *Table 1* shows the calculated individual parameters for each meteor on the night of December 12th to 13th, 2025.

The radiant parameters and orbital elements averaged for the ten meteors are as follows:

- $\lambda_\odot = 260.8995° \pm 0.1082°$
- $\alpha_g = 212.36° \pm 1.63°$
- $\delta_g = 66.07° \pm 0.71°$
- $v_g = 40.9 \pm 0.8$ km/s
- $a = 8.15 \pm 1.95$ AU
- $q = 0.971 \pm 0.002$ AU
- $e = 0.873 \pm 0.039$
- $\omega = 193.813° \pm 1.177°$
- $\Omega = 260.899°$
- $i = 67.88° \pm 1.18°$
- $T_j = 1.10$

Figure 3 shows the distribution of the radiants at the celestial sphere in the constellation Draco. A concentrated group of radiants is located within a circle with a diameter of 3 degrees on the celestial sphere. There are three more radiants to the south-west and one to the north-east of the main group. They may also belong to the unknown shower. However, due to their separation from the main group, it was decided not to take these meteors into account.

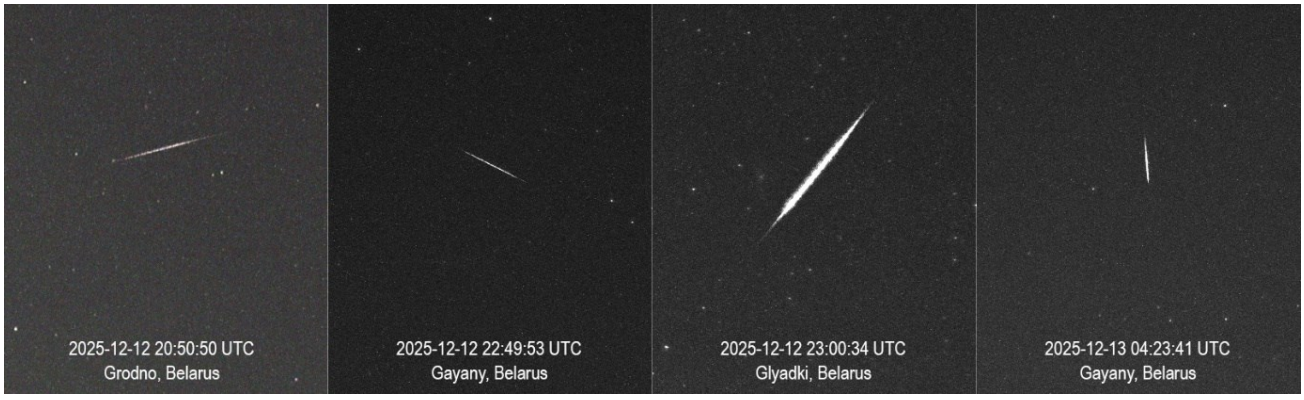

Figure 1 – Four meteors from the possible new meteor shower recorded during the night of 12–13 December 2025.

[25] http://www.sonotaco.com/

Table 1 – The orbital parameters of the ten meteors recorded from the possible new meteor shower M2025-Y1.

#	$\lambda_\odot$ (°)	α_g (°)	δ_g (°)	v_g (km/s)	a (A.U.)	q (A.U.)	e	ω (°)	Ω (°)	i (°)	Abs Mag	Dur (sec)	H_b (km)	H_e (km)
1	260.73	213.60	67.15	40.50	9.397	0.970	0.8967	194.22	260.73	66.72	+0.1	0.488	106.2	94.7
2	260.78	212.04	65.15	42.00	11.218	0.974	0.9132	192.34	260.78	69.55	–0.2	0.376	106.8	97.1
3	260.81	210.38	65.78	41.74	9.324	0.970	0.8960	194.47	260.81	69.27	+0.5	0.511	108.4	93.8
4	260.82	214.36	67.09	39.99	7.553	0.971	0.8714	193.92	260.82	66.11	–1.2	0.643	105.6	89.0
5	260.92	212.78	66.13	41.14	9.551	0.972	0.8983	193.43	260.92	68.03	–0.3	0.354	103.9	92.2
6	260.96	213.98	65.73	40.60	7.229	0.974	0.8653	192.34	260.96	67.49	+0.3	0.448	107.2	91.7
7	260.96	211.60	65.81	39.70	4.440	0.970	0.7814	194.73	260.96	67.01	–0.4	0.284	105.1	95.4
8	260.97	209.14	65.99	41.67	8.427	0.967	0.8853	195.82	260.97	69.30	+0.2	0.233	101.9	93.3
9	261.01	212.62	66.69	40.68	8.351	0.970	0.8839	194.48	261.01	67.29	–1.4	0.407	105.3	89.8
10	261.05	213.05	65.16	40.62	5.982	0.974	0.8372	192.38	261.05	67.98	–1.0	0.269	103.8	93.2

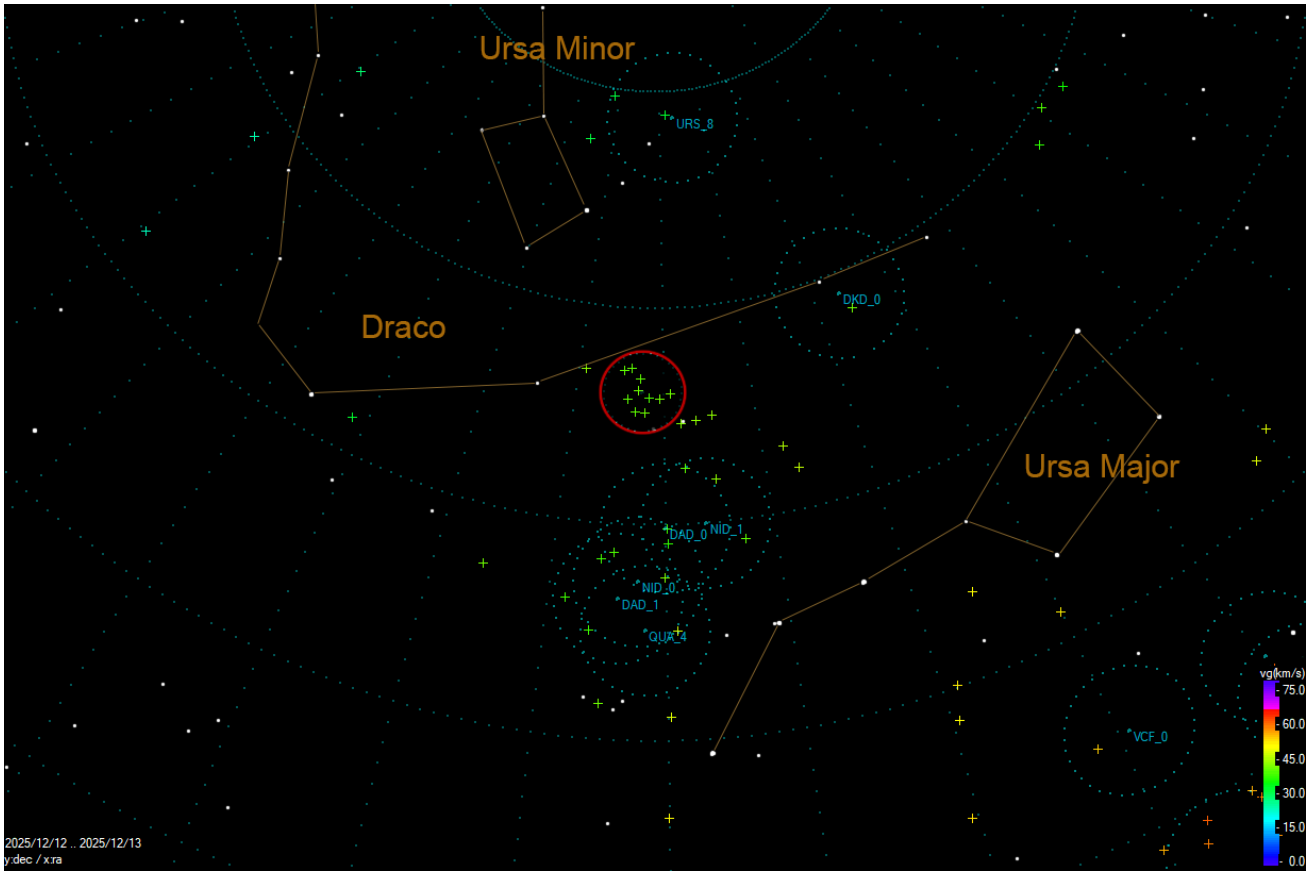

Figure 3 – Distribution of the radiants at the celestial sphere. The red circle indicates the radiant area of the possible new meteor shower. The blue circles show the established meteor showers according to the IAU-MDC[26].

Approximately 5 degrees south are the radiants of the established meteor showers December alpha-Draconids (DAD, #00334, peak activity on 8 December), the November i-Draconids (NID, #00392, peak activity on 24 November) and the Quadrantids (QUA, #00010, peak activity on 2 January). To the west is the radiant of the December kappa-Draconids (DKD, #00336, peak activity on 4 December). The discovered unidentified concentration of radiants is located too far from known meteor showers, which display their peak activity either much earlier (DAD, NID, DKD) or much later (QUA). All this may indicate that the detected activity may belong to a new meteor shower, which, however, may be dynamically related to already known showers. *Figure 4* shows the orbits in space which belong to the Mellish-type showers.

3 Spectrum

One of the cameras, equipped with a diffraction grating, captured the spectrum of a meteor (#4 in *Table 1*) from an

[26] https://www.ta3.sk/IAUC22DB/MDC2022/Roje/roje_lista.php?corobic_roje=0&sort_roje=0

unidentified shower with a magnitude of –0.3m. Due to the insufficient brightness of the meteor, the spectrum image turned out to be dim and slightly noisy, but the main peaks were clearly visible. This allowed us to determine the spectral type of the meteor based on the methodology suggested by Borovička et al. (2005). After calibrating the spectrum and taking into account the spectral sensitivity of the equipment, the intensities of the MgI – 2, FeI – 15, and NaI – 1 multiplets were measured. The spectrum and ternary diagram are shown in *Figure 5*. The position of the spectrum on the ternary diagram (relative intensities are MgI: 34.3%, FeI: 19.2%, NaI: 46.5%) indicates that this spectrum belongs to the Fe-poor type. Meteoroids of this type are rich in magnesium and have a normal sodium content, but their iron content is significantly depleted. This indicates the cometary origin and it is typical for meteoroids with Halley-type orbits.

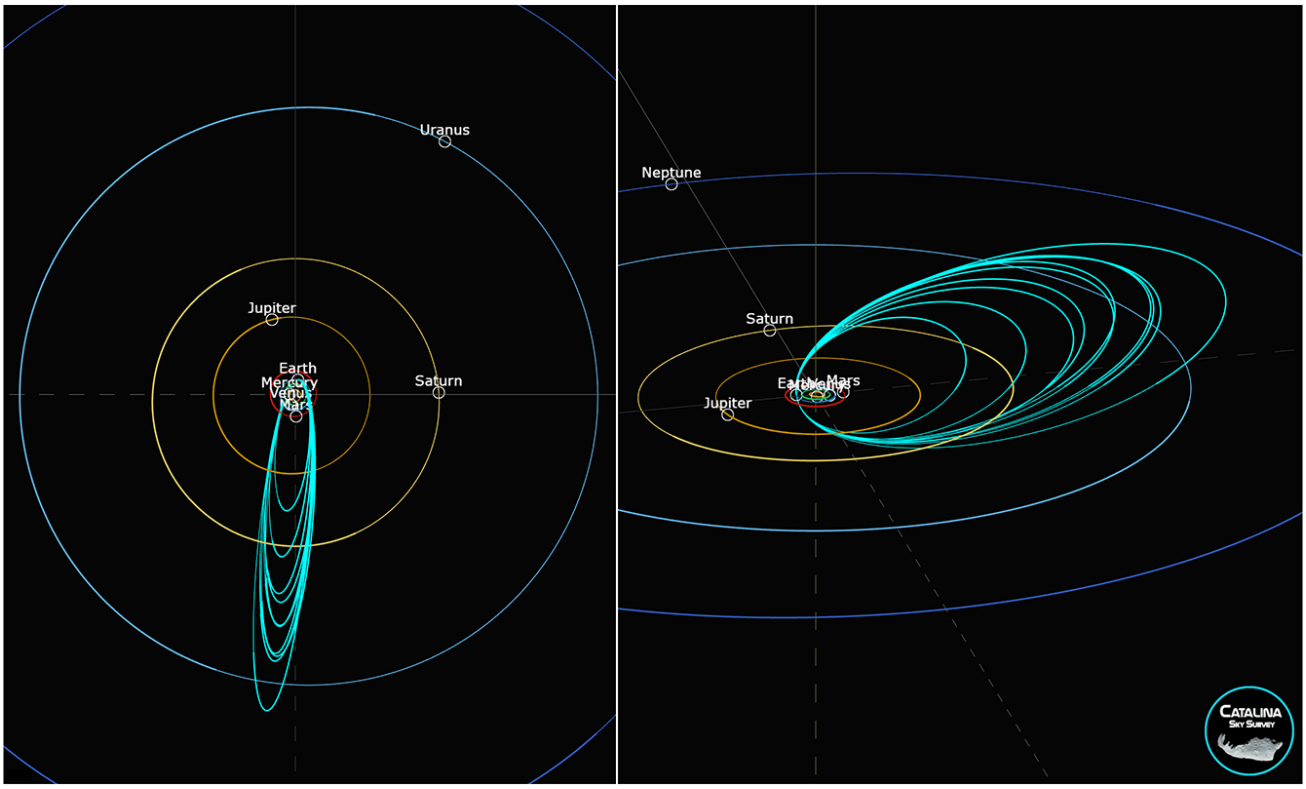

Figure 4 – The plotting of the orbits was made using the CSS Orbit View[27] application.

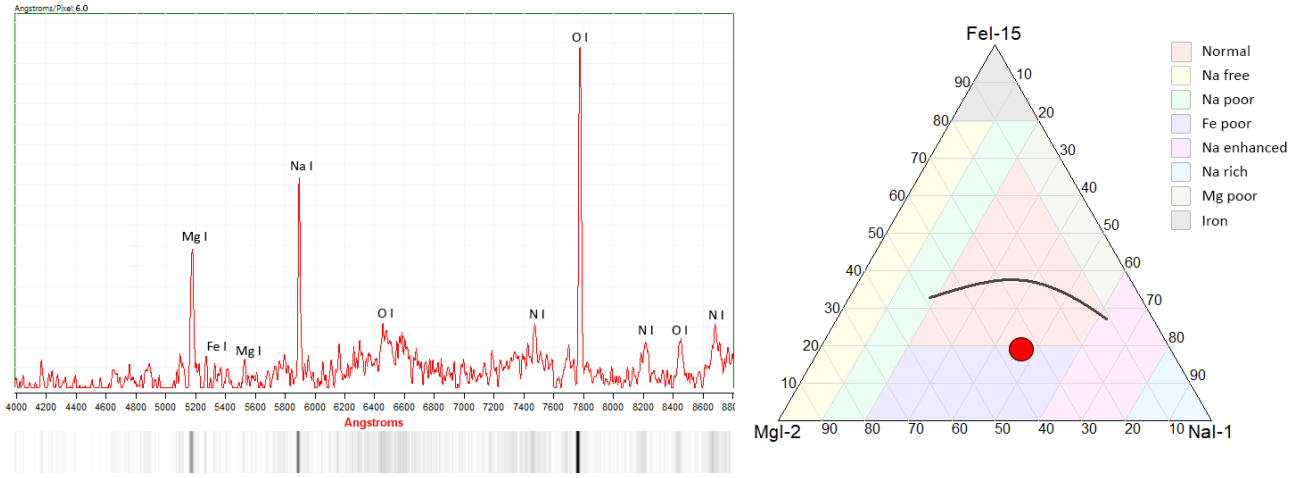

Figure 5 – Meteor spectrum from an unidentified shower on the left side and ternary diagram on the right side, showing the measured relative intensities of the MgI – 2, FeI – 15, and NaI – 1 multiplets in this meteor spectrum. The black curve on the ternary diagram shows the typical position of meteor spectra for chondritic composition. The red circle shows the position of the meteor spectrum from an unidentified shower.

[27] https://neofixer.arizona.edu/css-orbit-view

Acknowledgment

The author would like to thank all operators and people involved in the Belarusian and Ukrainian meteor networks. We would especially like to thank our Ukrainian colleagues who continue to be involved in meteor astronomy even despite constant blackouts during this difficult time for Ukraine. The author would also like to thank *Paul Roggemans* for his help in writing this report.

- Belarusian meteor network: *Alexander Mikulich, Andrey Prokopovich, Andrey Shohan, Ivan Sergei, Konstantin Morozov, Mikhail Abgarian* and *Ruslan Zavadich.*
- Ukrainian meteor network: *Alexander Aitov.*

References

Borovička J., Koten P., Spurný P., Boček J., Štork R. (2005). "A survey of meteor spectra and orbits: evidence for three populations of Na-free meteoroids". *Icarus*, **174**, 15–30.

The Eccentrids of the Mars family in the minor bodies system

Alexandra Terentjeva and Elena Bakanas

Institute of Astronomy of the Russian Academy of Sciences, Moscow, Russia
ater@inasan.ru; oterma@yandex.ru

A group of 39 Eccentrid asteroids ($e \geq 0.4$) belonging to the Mars family has been identified. Of the 670 orbits of meteoroid streams in several catalogues, only one Librid meteoroid stream, No. 50, has been found (Terentjeva, 1966), which also belongs to the Eccentrids of the Mars family. Among the 39 asteroids, 15 groupings have been discovered, comprising 33 asteroids, i.e. 84.6% of the asteroids in the system of the Eccentrids of the Mars family represent 'organized' matter. The distribution of asteroids by longitude of perihelion has been studied, and some features of this unique system of bodies are discussed.

Accepted for publication 15 November 2025.

1 Introduction

The Eccentrids as a system of meteoroid bodies were discovered by A. K. Terentjeva (Galibina and Terentjeva, 1981), although she had recorded meteoroid streams of the Eccentrids much earlier, in 1967–1968, when identifying minor meteor streams (Terentjeva, 1967). In our work (Terentjeva and Barabanov, 2016), we define the Eccentrids as a special group of meteoroid bodies, the orbits of which fall within the limits of $a < 1$ AU, $e \geq 0.4$, $Q \leq 1.1$ AU. In this work, 52 asteroids were found among 11673 near-Earth objects (NEOs), and some features of this system of bodies were studied. Eight asteroid streams of the Eccentrids were found. Together with the Eccentrid meteoroid system, the Eccentrid asteroid system forms a single population of minor bodies of the Solar System.

But are there in fact Eccentrids of the Mars family, i.e. minor bodies with orbits of high eccentricity belonging to the Mars family? This is the question we set in this work.

2 Research results

The work of M. Bielicki (1972) provides the limit values of the perturbation region for the planets of the Solar System. The limiting distances for planetary families (AU):

- Mercury 0.002
- Venus 0.010
- Earth 0.014
- Mars 0.010
- Jupiter 0.50
- Saturn 0.62
- Uranus 0.67
- Neptune 1.11
- Pluto 0.55

These data show that the radius of the sphere of influence of Mars on the perturbed body is very small. Our selection criteria for the orbits of the Eccentrids of the Mars family were: $e \geq 0.4$ and $1.51 \leq Q \leq 1.53$ AU. From the NASA JPL catalogue[28], which contained 1448137 asteroids as of 11 May 2025, 39 asteroid orbits of the Eccentrids of the Mars family were selected (*Table 1*).

Table 1 – The Eccentrid asteroids of the Mars family. Equinox J2000.0. *H* is the absolute magnitude of the asteroid, *D* is the diameter of the asteroid.

No	Full name	Epoch	*a* (AU)	*e*	*q* (AU)	*Q* (AU)	Ω (°)	ω (°)	*i* (°)	π (°)	*H*	*D* km	Period years
1	2021 UA1	05-05-2025	1.086	0.405	0.646	1.525	125.93	163.25	0.01	289.18	31.84	–	1.131
2	2016 CD31	05/05/2025	1.044	0.454	0.570	1.519	240.49	12.71	0.46	253.20	26.90		1.067
3	2008 JC	05/05/2025	1.045	0.463	0.561	1.529	47.86	58.17	2.50	106.03	26.50		1.069
4	2013 SL20	05/05/2025	1.080	0.403	0.645	1.516	8.49	115.65	4.29	124.14	24.62		1.123
5	2013 AH76	01/17/2013	0.985	0.547	0.447	1.523	347.19	353.77	4.55	340.96	22.88		0.978
6	2014 JN2	05/03/2014	0.894	0.692	0.276	1.512	219.84	148.81	6.32	8.64	24.27		0.845
7	2002 JD9	05/05/2025	1.056	0.440	0.591	1.521	208.16	139.08	6.61	347.24	23.20		1.085
8	2018 VD	05/05/2025	1.068	0.419	0.620	1.516	38.78	252.38	7.61	291.17	27.10		1.103

[28] https://ssd.jpl.nasa.gov/

No	Full name	Epoch	a (AU)	e	q AU	Q AU	Ω (◦)	ω (◦)	i (◦)	π (◦)	H	D km	Period years
9	2022 DY1	05/05/2025	1.050	0.448	0.579	1.520	156.05	249.83	7.85	45.89	27.92	–	1.076
10	2018 BB5	05/05/2025	0.956	0.593	0.389	1.523	128.84	136.24	7.96	265.08	24.40		0.935
11	2018 KL2	05/05/2025	1.051	0.437	0.591	1.510	212.55	170.89	8.66	23.44	21.70		1.077
12	2019 EO	05/05/2025	0.994	0.532	0.465	1.523	130.26	255.55	9.35	25.80	23.18		0.991
13	2010 LJ61	05/05/2025	1.046	0.460	0.565	1.526	70.83	48.35	9.80	119.18	20.95	0.192	1.069
14	2021 VP6	05/05/2025	1.030	0.483	0.533	1.527	16.55	181.06	10.28	197.61	21.57	–	1.045
15	4034 Vishnu 1986 PA	05/05/2025	1.059	0.444	0.589	1.530	157.87	296.69	11.17	94.56	18.48	0.420	1.090
16	2021 TJ57	05/05/2025	1.008	0.507	0.497	1.519	4.68	180.12	11.63	184.80	21.46	–	1.012
17	2007 US	05/05/2025	0.962	0.583	0.402	1.523	24.02	203.06	12.40	227.08	22.74		0.944
18	516155 2016 DP	05/05/2025	1.022	0.477	0.535	1.510	54.36	254.00	13.33	308.36	20.11		1.034
19	152742 1998 XE12	05/05/2025	0.878	0.739	0.229	1.527	280.02	353.16	13.44	273.18	19.10	0.413	0.823
20	512234 2015 VO66	05/05/2025	0.952	0.600	0.381	1.523	64.46	219.31	14.02	283.77	20.62		0.929
21	2016 GG216	05/05/2025	1.008	0.515	0.489	1.528	171.94	157.16	14.71	329.10	23.15		1.013
22	2019 SM2	09/21/2019	0.980	0.550	0.440	1.519	174.65	51.02	15.08	225.67	26.10	–	0.969
23	2020 KK5	05/05/2025	0.932	0.634	0.341	1.523	83.25	325.07	15.15	48.32	21.93	–	0.900
24	88213 2001 AF2	05/05/2025	0.954	0.595	0.386	1.522	114.25	194.99	17.81	309.24	19.48	0.912	0.932
25	2014 MS67	05/05/2025	1.021	0.496	0.514	1.527	253.71	217.37	18.80	111.07	21.20		1.031
26	481127 2005 UJ6	05/05/2025	1.068	0.416	0.624	1.513	42.36	131.41	19.00	173.77	21.50		1.104
27	2025 DU2	05/05/2025	1.043	0.452	0.572	1.514	345.23	291.59	19.07	276.82	24.25	–	1.065
28	2022 FV	05/05/2025	1.062	0.428	0.607	1.516	3.90	300.62	19.34	304.53	24.15	–	1.094
29	3753 Cruithne 1986 TO	05/05/2025	0.998	0.515	0.484	1.511	126.19	43.88	19.80	170.07	15.44	2.071	0.997
30	234341 2001 FZ57	05/05/2025	0.944	0.604	0.374	1.515	22.09	339.98	20.67	2.07	18.93	0.344	0.918
31	2012 VN6	05/05/2025	1.043	0.461	0.563	1.524	216.94	26.24	21.03	243.19	21.38		1.065
32	141531 2002 GB	05/05/2025	0.992	0.529	0.467	1.517	40.81	8.32	22.55	49.13	19.15	0.303	0.988
33	2008 LC2	06/03/2008	1.012	0.499	0.507	1.518	78.92	303.73	23.65	22.65	24.25		1.018
34	2011 FP29	04/01/2011	1.055	0.447	0.584	1.526	9.08	332.76	24.79	341.84	21.95		1.083
35	2016 VU2	05/05/2025	0.987	0.548	0.446	1.527	235.37	18.54	26.79	253.91	22.00		0.980
36	2020 UF3	05/05/2025	0.967	0.574	0.412	1.522	29.65	127.45	27.49	157.09	28.38	–	0.951
37	2015 KB57	05/05/2025	0.945	0.607	0.371	1.518	239.61	208.83	29.67	88.44	22.30		0.918
38	250458 2004 BO41	05/05/2025	1.019	0.493	0.517	1.521	337.74	254.46	35.55	232.19	18.00	0.630	1.028
39	2023 VT10	11/16/2023	0.903	0.694	0.277	1.529	232.52	326.71	39.27	199.23	22.21	–	0.858

Table 2 – Orbital elements and other parameters of the Librid meteoroid stream (J1950.0)[1]. The source for both is No 50 in Terentjeva (1966).

Date (UT)	α_g (°)	δ_g (°)	v_∞ km/s	a AU	e	q AU	Q AU	ω (°)	Ω (°)	i (°)	π (°)
1954 IV 7.30	206	–11	18.8	1.04	0.48	0.55	1.5	294	17	0	311
1953 IV 11.40	212	–10	18.1	1.02	0.46	0.55	1.5	296	21	2	317

([1]) Over 50 years, the difference due to precession is less than 1°, which is not significant.

Now let us consider meteoroid streams. We reviewed the most significant known catalogues of orbits of meteoroid and fireball streams (Cook, Lindblad, Terentjeva, Halliday et al., Rudawska, Jenniskens), totalling 670 orbits of streams. It turned out that among them there is only one meteoroid stream of the Librids, No. 50 from the catalogue by A. Terentjeva (1966), which meets the selected criteria and is an Eccentrid of the Mars family. The elements of its orbit and other parameters are given in *Table 2*. Thus, the Eccentrids of the Mars family constitute 0.0027% of asteroids and 0.15% of meteoroid streams, i.e. two orders of magnitude more.

Let us analyze the data for 39 asteroids of the Eccentrids of the Mars family (*Table 1*). Of the 39 asteroids, 8 asteroids, i.e. 20%, enter at perihelion inside the orbit of Mercury. These are asteroids with absolute magnitudes of 19–24 and diameters ranging from 344 m to 912 m (according to three estimates). The remaining 31 asteroids out of 39 enter at perihelion inside the orbit of Venus. These data indicate the role of these planets in gravitational influence. Let us consider the distribution of 39 asteroids by longitude of perihelion, π (*Figure 1*). Two maxima are clearly visible in the intervals $0° < \pi < 30°$ and $270° < \pi < 300°$ (12.8% of asteroids in each). It is also worth noting a slightly smaller third maximum (10.3% of asteroids) in the interval $90° < \pi < 120°$, on either side of which there is a deficit of longitudes of perihelion in the intervals from $\pi = 60°$ to $\pi = 90°$ and from $\pi = 120°$ to $\pi = 150°$.

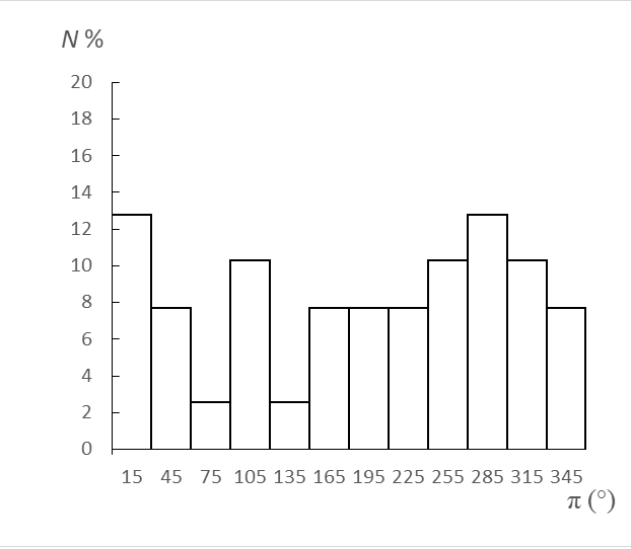

Figure 1 – Distribution of the longitudes of perihelion π of the Eccentrid asteroids of the Mars family.

I. I. Putilin (1953), studying the distribution of longitudes of perihelion of asteroids in the Main Belt, found a clear maximum in the interval $0° < \pi < 20°$. This is now well known and is explained by the action of secular perturbations from large planets, mainly Jupiter ($\pi = 15°.4$). This maximum of the Main Belt lies within the slightly wider first maximum of the Eccentrids of the Mars family in the interval $0° < \pi < 30°$ (*Figure 1*). None of the nine known planets falls within the region of the second maximum of the Eccentrids of the Mars family in the interval from $\pi = 270°$ to $\pi = 300°$. However, directly opposite the second maximum is the third maximum, with an interval from $\pi = 90°$ to $\pi = 120°$. Interestingly, Earth ($\pi = 102°.8$) is located in this interval and appears to be involved in its formation.

As for the two deficits in longitudes of perihelion in the intervals $60° < \pi < 90°$ and $120° < \pi < 150°$ (*Figure 1*), Mercury falls into the first one ($\pi = 77°.5$), and Venus into the second one ($\pi = 131°.7$). Both planets have a very small radius of influence on the perturbed body, 0.002 AU for Mercury and 0.010 for Venus (see above).

I. I. Putilin discovered a dependence of the distribution of the longitude of perihelion on eccentricity. '*The greater the eccentricity of the orbit, the more pronounced the tendency of perihelia to group around a certain longitude*', he wrote (Terentjeva and Barabanov, 2016). In the work mentioned, this dependence is confirmed on the system of the Eccentrid asteroids of the Earth group ($Q \leq 1.1$ AU). In our case with the Eccentrids of the Mars family, this dependence is even more pronounced (*Figure 1*). Among the population of 39 Eccentrid asteroids of the Mars family, orbits with $e = 0.5$ account for 44%, and those with $e = 0.6$–0.7 account for 26%. Apparently, on average, e of the Eccentrids of the Mars family is higher than that of the Eccentrids of the Earth group.

Similar to meteoroid bodies and asteroids of the system of the Eccentrids of the Earth group, the Eccentrid asteroids of the Mars family tend to make groupings. Among 39 asteroids (*Table 1*), we identified 15 groupings, of which 13 groupings have 2 orbits, one grouping has 3 orbits, and one has 4 orbits. These data are shown in *Table 3*.

Thus, 15 groupings include 33 orbits (out of 39). This means that 84.6% of the asteroid orbits in the system of the Eccentrids of the Mars family represent 'organized' matter.

Table 3 – Groupings of the Eccentrids of the Mars family.

Number, No. in *Table 1*	Number, No. in *Table 1*
1, 8	12, 33
2, 31	13, 25
3, 13, 15, 25	14, 16
4, 13	16, 29
7, 34	17, 22
1, 8, 28	18, 28
10, 35	31, 38
11, 34	

3 Conclusion

Mars, as we can see, is weak enough to create its own large family of minor bodies, since the radius of its gravitational influence is very small. Nevertheless, a group of 39 Eccentrid asteroids of the Mars family has been found, which together with the Eccentrids of the Earth group (Terentjeva and Barabanov, 2016) form a single exotic

population of minor bodies in the inner region of the Solar System.

Acknowledgments

This paper was translated into English by *I. Kurenya*.

The authors thank *Paul Roggemans* for his efforts enabling the preparation and publication of this paper.

References

Bielicki M. (1972). “A new orbital classification for periodic comets”. In, Gleb Aleksandrovich Chebotarev, E. I. Kazimirchak-Polonskaia, and B. G. Marsden, editors, Proceedings from IAU Symposium no. 45, *The Motion, Evolution of Orbits, and Origin of Comets*, held in Leningrad, U.S.S.R., August 4–11, 1970. International Astronomical Union, Dordrecht, Reidel, pages 370–372.

Galibina I. V. and Terentjeva A. K. (1981). “Evolution of meteoroid orbits under the influence of secular perturbations”. *Solar System Research*, **15**, No. 3, pages 132–137.

Putilin I. I. (1953). “Malye planety (Minor Planets)”. Moscow. Izd. Tekhn. Teoret. Lit. (In Russian).

Terentjeva A. K. (1966). “Minor meteor streams”. Results of researches of international geophysical projects: Meteor Investigations. No. 1. Publishing House “Nauka”, Moscow, pages 62–132. (In Russian). See also *eMetN* (2017), **2**, Issue 3, 95.

Terentjeva A. K. (1967). “Orbits of minor meteor streams”. *Astron. Tsirk. AN SSSR*, No. 415, 1–7. (In Russian).

Terentjeva A. K. and Barabanov S. I. (2016). “Asteroids in the Eccentrid meteor system”. *Solar System Research*, **50**, No. 5, pages 337–343.

Eccentrids in the GMN orbit dataset

Paul Roggemans

Pijnboomstraat 25, 2800 Mechelen, Belgium
paul.roggemans@gmail.com

A search was made to select all short period meteor orbits in the GMN meteor orbit dataset. The dataset was tested for the presence of the Eccentrid meteors and the presence of similar orbits for all 39 asteroids listed by Terentjeva and Bakanas (2026). A distribution of the longitude of perihelion was made for 304 meteor orbits that fit the definition for the Eccentrids of the Mars family.

1 Introduction

The article of Terentjeva and Bakanas (2026) describes a specific population of minor bodies with very short period orbits which are rare in meteor orbit datasets. How many such short period orbits can be found in the GMN meteor orbit dataset? A search was made on 2.7 million meteor orbits obtained in the period December 2018 to November 2025, using the following query: $a < 1.25$ AU and $e > 0.4$ and $Q < 1.6$ AU and $i < 40°$. This first selection yields 6986 meteor orbits or 0.26% of the total sample.

The upper limits for a and Q were set higher than $a < 1$ AU and $Q < 1.1$ AU as defined by Terentjeva and Bakanas (2026), in order to take the uncertainty margin on these parameters into account. Contrary to asteroid orbits which are often based on many observations and measurements, meteor orbits suffer larger uncertainties, especially on the semi-major axis a and aphelion Q. If we apply these limits strictly, 979 meteor orbits or 0.036 % of the total remain. This proves that this type of orbits is extremely rare. Applying the same selection criteria on the meteor orbit data for the orbits of the Eccentrids of the Mars family defined by Terentjeva and Bakanas (2026) with: $e \geq 0.4$ and $1.51 \leq Q \leq 1.53$ AU results in 304 orbits or 0.011% of the GMN dataset.

2 Librid meteoroid stream

The 6986 eccentrids were searched for meteors with $\alpha = 206 \pm 3°$, $\delta = -11 \pm 3°$ and $v_\infty = 18.8 \pm 1.9$ km/s and with $\alpha = 212 \pm 3°$, $\delta = -10 \pm 3°$ and $v_\infty = 18.1 \pm 1.8$ km/s and did not yield any matching meteors. Using the D-criteria with both orbits as reference, four meteors for the first orbit and two for the second were found, too few to define a meteor shower. No activity from this radiant seems to have been observed in recent years.

3 Other known meteor showers among the Eccentrids?

Four known meteor showers were found within the selection of 6986 Eccentrids:

- October Leporids (OLP#384), 166 meteors were associated with this shower by GMN. The orbital parameters differ significantly from the IAU-MDC[29] record since the Eccentrid orbits were selected for $i < 40°$, covering this shower only partially. The $T_J = 6.89$ indicates an asteroidal shower.
- Epsilon-Pegasids (EPG#326), 110 meteors were associated with this shower by GMN. These orbital parameters differ significantly from the IAU-MDC[30] since the orbit selection covers this shower only partially. The $T_J = 7.09$ indicates an asteroidal shower.
- 62-Andromedids (SAN#924), 77 meteors were associated with this shower by GMN. The orbital parameters fit perfectly with those listed in the IAU-MDC[31]. The $T_J = 6.99$ indicates an asteroidal shower.
- November theta-Aurigids (THA#390), 5 meteors were associated with this shower by GMN. These orbital parameters differ significantly from the IAU-MDC[32] since the orbit selection covers this shower only partially and five meteors are too few to be statistically relevant. The $T_J = 6.53$ indicates an asteroidal shower.

The mean orbits were computed using the method of Jopek et al. (2006) using the preliminary shower classification by GMN based on the radiant position and velocity (*Table 1*). Only orbits fitting the criteria for Eccentric meteor orbits were used. Therefore, these results are not representative for these meteoroid streams as a whole since shower members that did not fit the definition of Eccentrids were excluded.

[29] https://www.ta3.sk/IAUC22DB/MDC2022/Roje/pojedynczy_obiekt.php?lporz=00967&kodstrumienia=00384
[30] https://www.ta3.sk/IAUC22DB/MDC2022/Roje/pojedynczy_obiekt.php?lporz=00826&kodstrumienia=00326
[31] https://www.ta3.sk/IAUC22DB/MDC2022/Roje/pojedynczy_obiekt.php?lporz=01868&kodstrumienia=00924
[32] https://www.ta3.sk/IAUC22DB/MDC2022/Roje/pojedynczy_obiekt.php?lporz=00979&kodstrumienia=00390

The 979 orbits with $a < 1$ A.U. and $Q < 1.1$ A.U. do not include a single known shower meteor.

The 6986 meteor orbits were tested against the 39 asteroid orbits using the D-criteria thresholds with $D_{SH} < 0.125$ & $D_D < 0.05$ & $D_J < 0.125$. Only two have a relevant number of matching orbits. 2013 SL20 and 2014 JN2.

- 2014 JN2 has 11 meteors with $\alpha = 250.2°$, $\delta = -28.1°$, $v_g = 21.7$ km/s, $a = 0.86$ A.U., $q = 0.276$ A.U., $e = 0.680$, $i = 7.1°$, $\Omega = 225.1°$, $\omega = 142.5°$ and $\Pi = 7.5°$.
- 2013 SL20 has 12 meteors with $\alpha = 28.8°$, $\delta = +3.7°$, $v_g = 12.2$ km/s, $a = 1.08$ A.U., $q = 0.635$ A.U., $e = 0.410$, $i = 3.0°$, $\Omega = 17.9°$, $\omega = 106.4°$ and $\Pi = 124.3°$.

All orbits have been visualized in the inner Solar System in *Figure 1*.

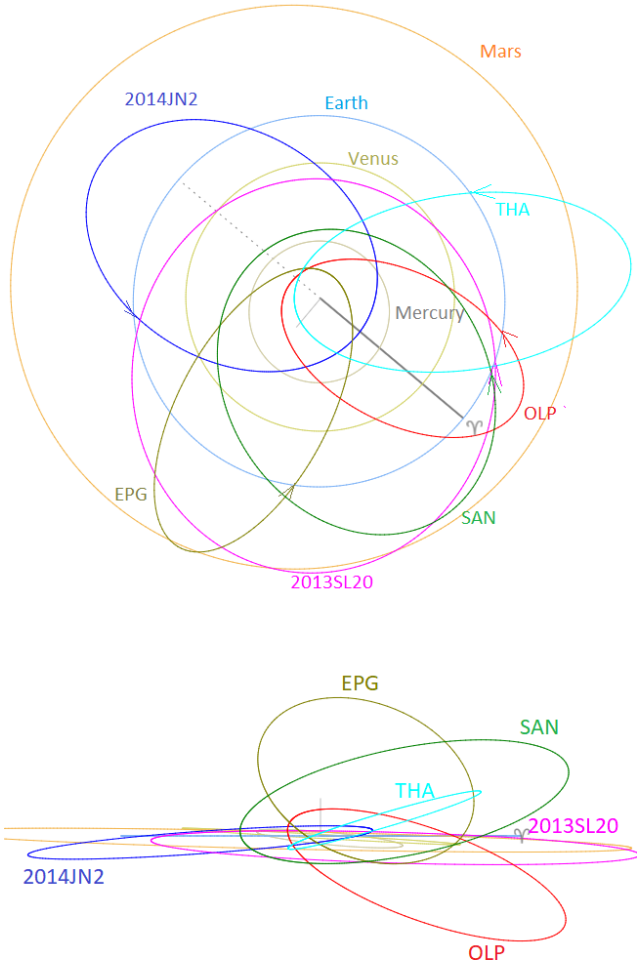

Figure 1 – Plot of the mean orbits found for 2014 JN2 and 2013SL20 related meteors and the four showers in *Table 1*. Top: projection of the orbits in the ecliptic plane, bottom: view in the direction of the ecliptic plane. (Plotted with the Orbit visualization app provided by Pető Zsolt).

For most meteoroid streams the orbital elements show a drift during Earth's transit. This is also the case for the aphelia Q that appear to increase during the passage of Earth for some showers. Only the 62-Andromedids (SAN#924) show no increase in Q. *Figure 2* shows the drift for the epsilon-Pegasids (EPG#326) as example.

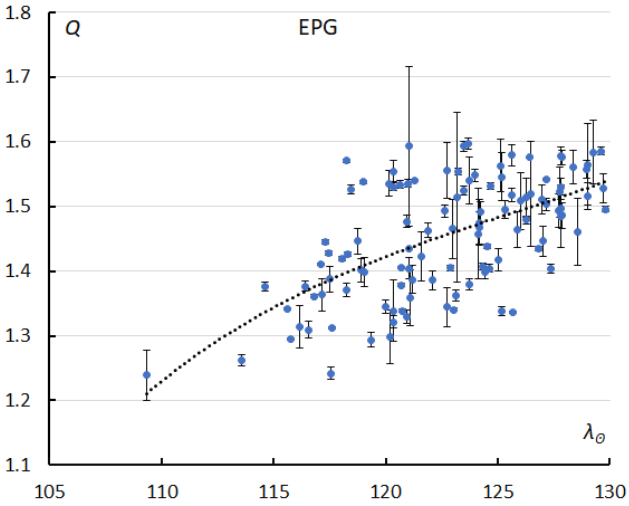

Figure 2 – The change in aphelion distance Q in function of time ($\lambda_\odot$) for the epsilon-Pegasids.

Table 1 – The mean orbits valid for the shower meteors found within the selection of Eccentrid orbits, limited by the selection with $e > 0.4$ and $Q < 1.6$ AU and $i < 40°$.

	OLP #384	EPG #326	SAN #924	THA #390
$\lambda_\odot$ (°)	210.8	123.1	197.0	254.5
$\lambda_{\odot b}$ (°)	197.0	109.0	193.0	251.0
$\lambda_{\odot e}$ (°)	223.0	130.0	199.0	262.0
α_g (°)	71.3	338.4	38.0	112.8
δ_g (°)	+1.5	+9.7	+46.4	+31.9
$\Delta\alpha_g$ (°)	+0.66	+0.65	+1.03	–
$\Delta\delta_g$ (°)	+0.36	–0.21	+0.67	–
v_g (km/s)	27.4	27.3	17.0	27.7
H_b (km)	92.9	91.6	87.0	93.7
H_e (km)	83.3	84.3	72.3	88.3
H_p (km)	86.8	87.9	78.6	91.4
Mag_{Ap}	+0.8	+0.9	+0.6	+1.6
λ_g (°)	69.7	343.6	51.4	109.4
$\lambda_g - \lambda_\odot$ (°)	218.2	220.1	214.5	215.0
β_g (°)	–20.6	+17.7	+29.6	+10.0
a (A.U.)	0.80	0.77	0.82	0.85
q (A.U.)	0.182	0.143	0.394	0.144
e	0.773	0.816	0.518	0.830
i (°)	34.6	34.0	21.3	18.8
ω (°)	150.0	335.3	320.5	331.6
Ω (°)	30.3	122.7	196.7	255.4
Π (°)	180.4	98.0	157.3	227.0
Q (A.U.)	1.42	1.41	1.24	1.56
T_j	6.89	7.09	6.99	6.53
N	166	110	77	5

The meteoroids appear to be solid particles as these penetrate deep into the atmosphere. The 979 selected orbits with $a < 1.0$ A.U. and $e > 0.4$ and $Q < 1.1$ A.U. have an average beginning height of 86.8±5.8 km and 79.1±6.3 km as ending height. This can be explained by the asteroidal origin of this meteoroid population or by the frequent perihelion passages with an average perihelion distance of $q = 0.24±0.11$ A.U., which is very close to the Sun, within the orbit of planet Mercury where no fragile particles survive.

4 Eccentrids of the Mars family

The article by Terentjeva and Bakanas (2026) includes a plot with the distribution of the longitude of perihelion Π, based upon asteroids. The same plot has been made based upon the 304 meteor orbits that fit the criteria of Eccentrids of the Mars family. A strong peak is visible at $\Pi = 105±15°$ (*Figure 3*). The distribution is slightly different between the result for meteor orbits and the asteroid orbits which can be explained by the different mass size. Smaller particles suffer a lot of planetary perturbations and solar radiation and rapidly disperse in the inner solar system.

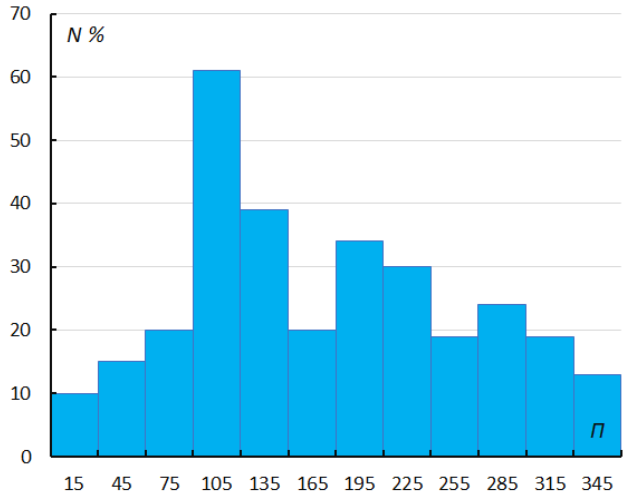

Figure 3 – Distribution of the longitudes of perihelion Π of the 304 Eccentrid meteor orbits of the Mars family.

Two of the above-mentioned meteor showers, Epsilon-Pegasids (10 meteors) and October Leporids (18 meteors), have orbits that fulfil the definition of Eccentrids of the Mars family with $e \geq 0.4$ and $1.51 \leq Q \leq 1.53$ AU. However, as shown above only a part of the stream orbits fit these criteria as the aphelia distances change during the transit of the Earth.

All these meteors have common properties, with a Tisserand parameter relative to Jupiter $T_J = 6.51±0.34$ indicating asteroidal origin and particles that ablate deep in the atmosphere at 91.1±5.9 km with an average terminal height of 81.9±7.0 km.

Acknowledgments

This report is based on the data of the Global Meteor Network (Vida et al., 2020a; 2020b; 2021) which is released under the CC BY 4.0 license[33]. We thank all 825 participants in the Global Meteor Network project for their contribution and perseverance. A list with the names of the volunteers who contribute to GMN has been published in the 2024 annual report (Roggemans et al., 2025). The author also thanks *Alexandra Terentjeva* and *Elena Bakanas* for drawing attention to this specific dust population.

References

Drummond J. D. (1981). "A test of comet and meteor shower associations". *Icarus*, **45**, 545–553.

Jopek T. J. (1993). "Remarks on the meteor orbital similarity D-criterion". *Icarus*, **106**, 603–607.

Jopek T. J., Rudawska R. and Pretka-Ziomek H. (2006). "Calculation of the mean orbit of a meteoroid stream". *Monthly Notices of the Royal Astronomical Society*, **371**, 1367–1372.

Roggemans P., Campbell-Burns P., Kalina M., McIntyre M., Scott J. M., Šegon D., Vida D. (2025). "Global Meteor Network report 2024". *eMetN Meteor Journal*, **10**, 67–101.

Southworth R. B. and Hawkins G. S. (1963). "Statistics of meteor streams". *Smithsonian Contributions to Astrophysics*, **7**, 261–285.

Terentjeva A., Bakanas E. (2026). "The Eccentrids of the Mars family in the minor bodies system". *eMetN Meteor Journal*, **11**, 56–59.

Vida D., Gural P., Brown P., Campbell-Brown M., Wiegert P. (2020a). "Estimating trajectories of meteors: an observational Monte Carlo approach - I. Theory". *Monthly Notices of the Royal Astronomical Society*, **491**, 2688–2705.

Vida D., Gural P., Brown P., Campbell-Brown M., Wiegert P. (2020b). "Estimating trajectories of meteors: an observational Monte Carlo approach - II. Results". *Monthly Notices of the Royal Astronomical Society*, **491**, 3996–4011.

Vida D., Šegon D., Gural P. S., Brown P. G., McIntyre M. J. M., Dijkema T. J., Pavletić L., Kukić P., Mazur M. J., Eschman P., Roggemans P., Merlak A., Zubrović D. (2021). "The Global Meteor Network – Methodology and first results". *Monthly Notices of the Royal Astronomical Society*, **506**, 5046–5074.

[33] https://creativecommons.org/licenses/by/4.0/

On the candidate meteor shower M2022-Q2

John Greaves

Shower M2022-Q2 of the International Astronomical Union's Meteor Data Centre. Problems with a recent suggestion for formally naming M2022-Q2 upon confirmation.

1 Introduction

Greaves (2022) published a notification of a potential summer meteor shower based preliminarily on searches within UKMON data (see said paper and references therein). Jenniskens[34] suggests a name for this shower, which includes a month name greatly inconsistent with the shower's Solar Longitude.

Whatever the situation, the current International Astronomical Union F1 Working Group Meteor Shower Nomenclature (MSN-WG)[35] has the final say on any proposed terminology.

2 Discussion

Jenniskens proposes in his table a name prefixed with the month Feb, yet the table also includes the Solar Longitude value from Greaves (2022) of 113.7 degrees which lies within the month of July. Greaves (2022) is entitled "A potential new summer shower in Lacerta", although the paper is not referenced by Jenniskens.

At the time the current author offered any potential naming rights upon confirmation of M2022-Q2 as being valid to the UKMON as part of their data was involved in the original noting of the potentiality of a shower. There was no response on this matter and accordingly after some time the current author emailed the IAU-MDC to propose the name 15 Lacertids due to the shower radiant's proximity thereto along with the code FTL, decided upon after fully checking that such had never been used before in the IAU-MDC list for any earlier shower still within the working list of showers or even subsequently removed and/or lost from the working list of showers.

Under the current wording of the rules, given this recent occurrence and the potential for the current author being deceased before any firm confirmation, if any, of M2022-Q2 as a shower occurs, the current author being also the same author of Greaves (2022) hereby formally renominates M2022-Q2's formal shower name as the 15 Lacertids with code FTL.

3 Conclusion

The name 15 Lacertids with acronym FTL, both currently unused in the IAU MDC lists, were and are suggested for any formal name should the candidate meteor shower M2022-Q2 ever be confirmed and updated in the IAU-MDC, subject to the IAU working group F1 Meteor Shower Nomenclature (WG-MSN) approval or modification. Reasons are given for this, and, reasons for rejecting the name suggested by Jenniskens are given, not least of which said name includes a reference to the month of February when the shower is clearly stated to be a summer shower of Solar Longitude 113.7 degrees in Greaves (2022).

References

Greaves J. (2022). "A potential new summer shower in Lacerta". *eMetN Meteor Journal*, **7**, 195–198.

[34] https://www.emeteornews.net/2025/11/25/provisional-meteor-shower-names-2022-2025/

[35] https://iau.org/WG276/WG276/Structure.aspx?code=276

Possible dark flight parameters of the Okulovka meteorite

Kővágó Gábor

fotospentax@gmail.com

Different solutions were tested to estimate the most likely main remaining mass for the fireball that appeared on 27 October 2025 over the Novgorod region of Russia from which a meteorite has been found on the ground.

1 Introduction

On October 27, 2025 at 6^h32^m local time, a spectacular fireball passed over the Novgorod region of Russia. The meteorite from the fall – currently the only one – was found in early November, crashing into a roof structure. I participated in the prediction of the strewn field with my program – Metlab[36] (2024). Below, I will try to determine the possible limits of certain parameters of the dark flight using the computer model, taking into account the position of the only known meteorite.

2 Details

This is the second year that I have been trying to help the Polish Skytinel network (2025), and since then we have been modeling the strewn field of all possible meteorite falls with Mateusz Zmija. Since we wrote different programs for the calculation and used different sources for the upper atmosphere winds, if our results are largely the same, it probably means something good. This was the case in the Okulovka fall.

I received the calculated data of the trajectory on October 30, when we made the first strewn field maps starting from different heights. The end of the trajectory was recorded by a camera with relatively poor resolution and from a big distance, so we could not be sure that the real end of the trajectory could be seen. The last definitely measured position was at an altitude of 30 km, so we made strewn fields for altitudes of 30–25–20 km by extrapolating the trajectory.

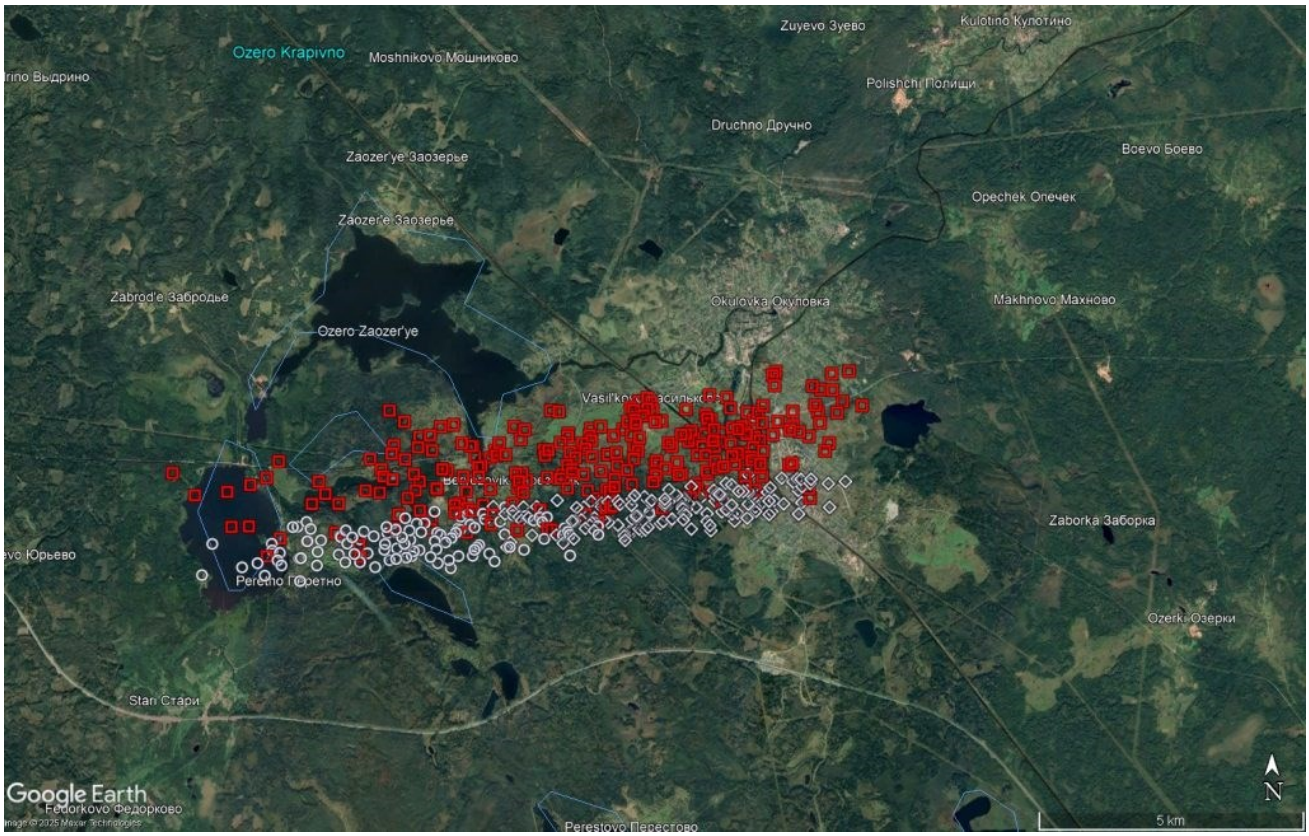

Figure 1 – Strewn field of 5 kg main mass from height 24.5 km and fragmentation below 7 km of 450 – 500 g.

[36] https://www.emeteornews.net/2024/10/11/the-metlab-software/

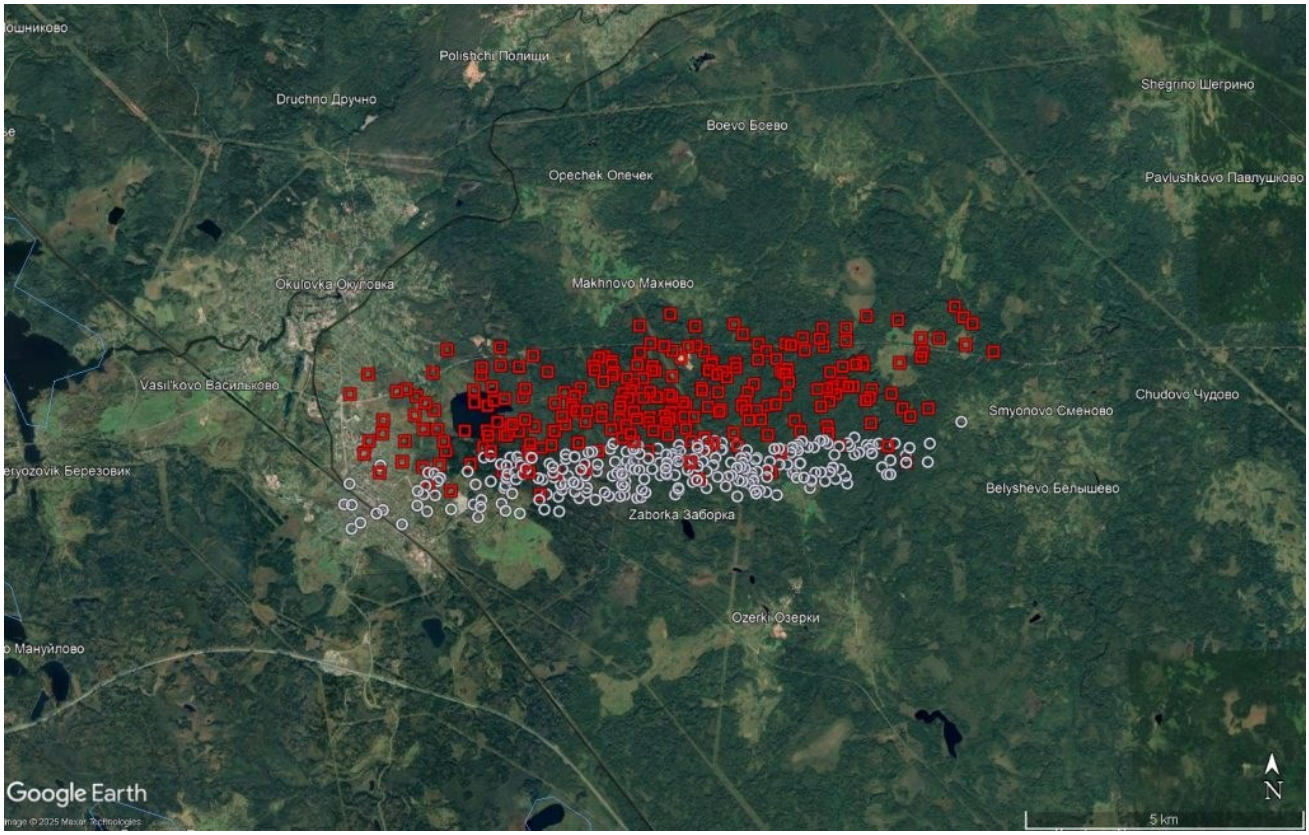

Figure 2 – Strewn field of 5 kg main mass from height 26.3 km and fragmentation below 8 km of 450 – 500 g.

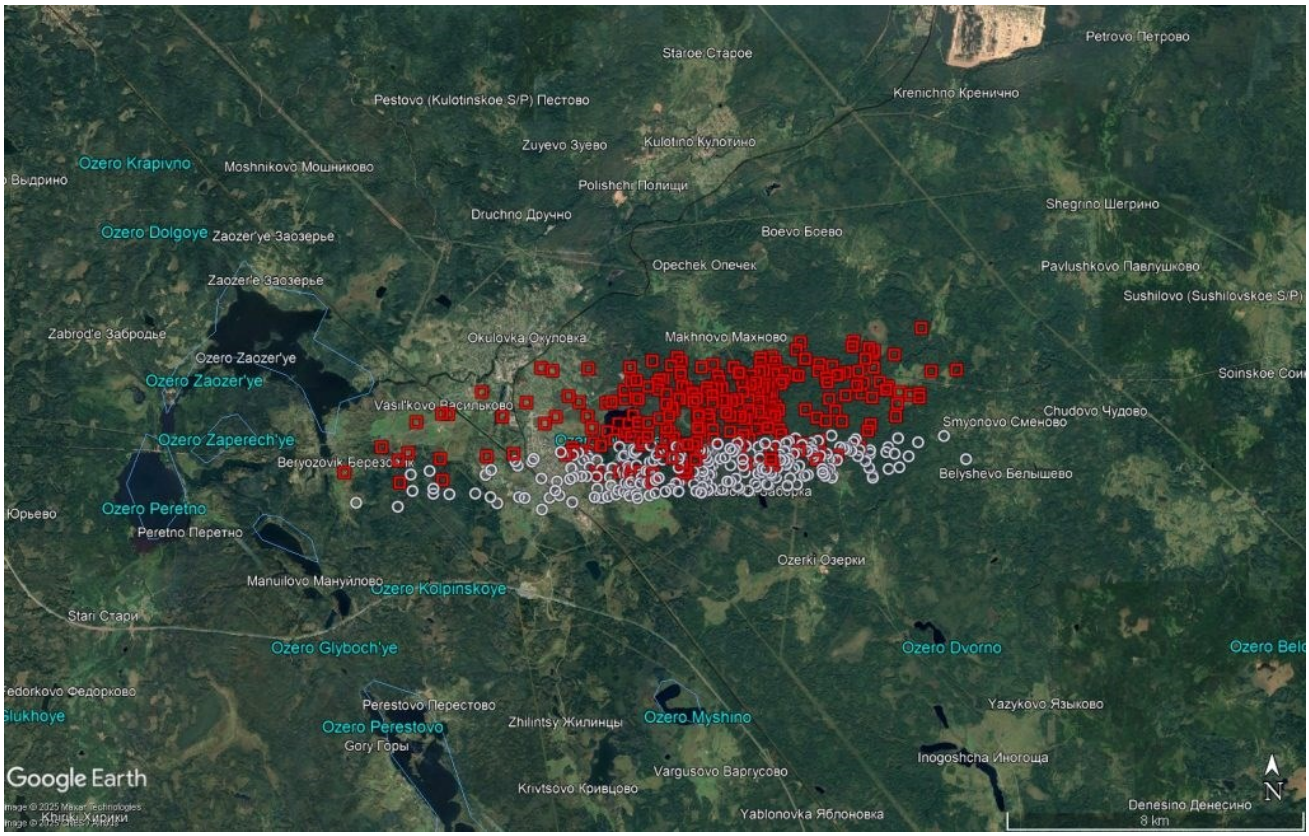

Figure 3 – Strewn Strewn field of 15 kg main mass from height 27.4 km and fragmentation below 5 km of 450 – 500 g.

We learned about the found meteorite and its position at the beginning of November, as the finder requested that the exact location be kept secret, so it will not be included in this article. The dynamic mass calculation gave a result of 5 – 15 kg for the final pieces. My goal was to find an optimal solution for which the extrapolation of the trajectory is the shortest in the given mass range. It seems certain that the approx. 410 g found was a part detached from a larger piece during dark flight, which may have originally been of greater (~500g) mass. Unfortunately, as long as only one meteorite is found in the strewn field, neither the size of this

larger piece nor the height of its separation can be determined precisely.

Legend to the images:

- blue – pieces that have switched to dark flight higher along the trajectory;
- white – pieces starting from the end of the trajectory;
- red – pieces detached during the dark flight;
- square symbol – the shape of the meteorite is more square;
- round symbol – the shape of the meteorite is more rounded;
- The number of points displayed does not reflect the probability of the pieces there.

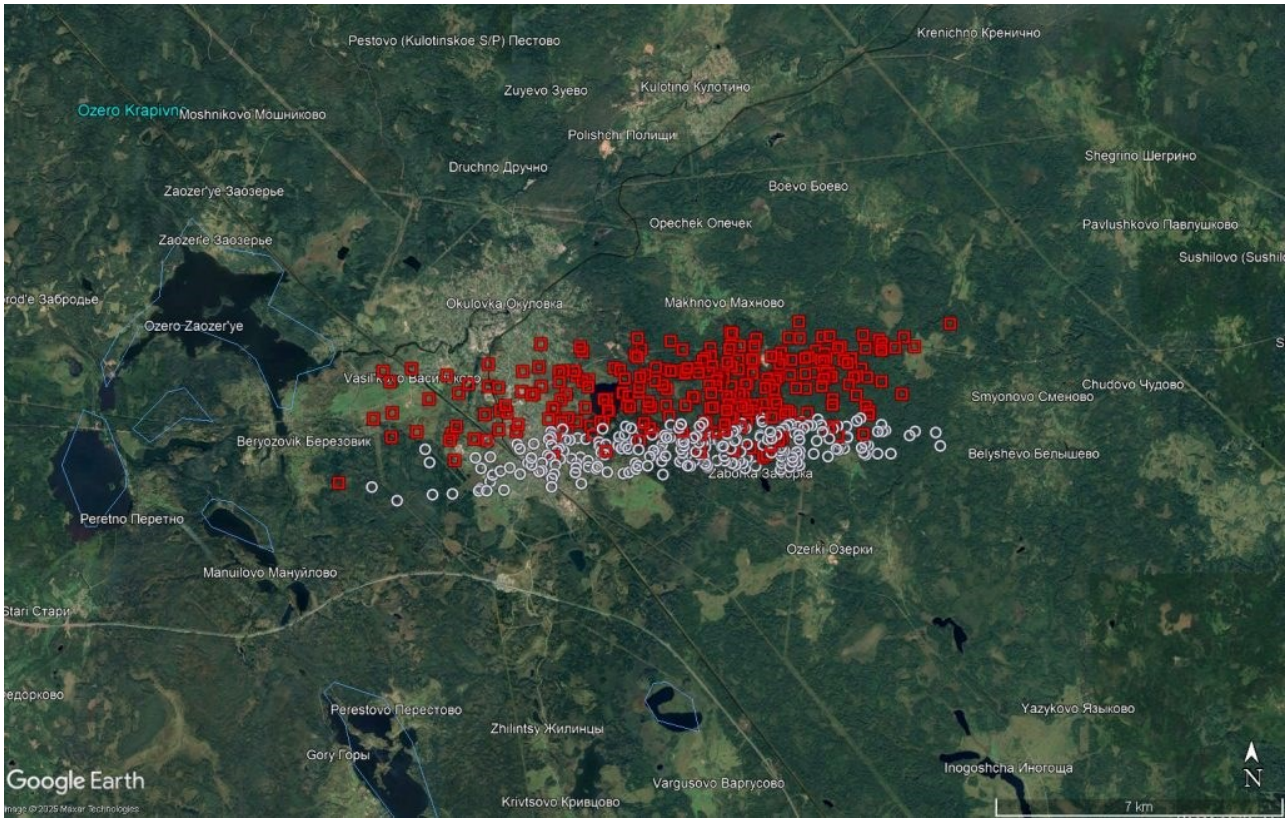

Figure 4 – Strewn field of 10 kg main mass from height 26.8 km and fragmentation below 5 km of 450 – 500 g.

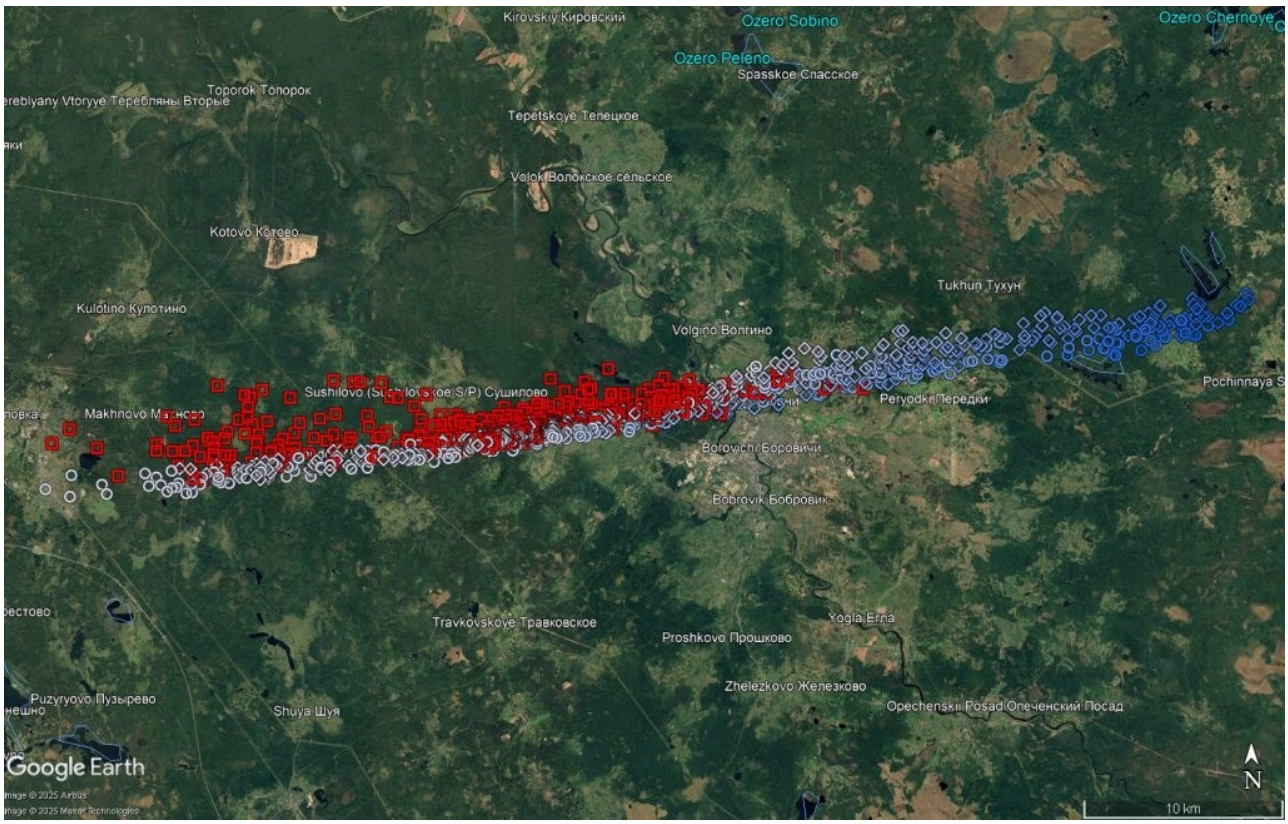

Figure 5 – The whole strewn field from 3 g – 10 kg, end height 26.8 km, fragmentation below 5 km of 50 – 500 g.

3 Conclusion

The results obtained show that the trajectory must be extrapolated at least 4 kilometers further if the main mass was 5 kg. In the case of a 15 kg mass, only a 2.5 km extension is sufficient. In addition, in the case of a smaller main mass, the height region for separation during the dark flight is also 3 km narrower. Based on these, it is more likely that the main mass is more like 10 kg. Of course, each mass can be answered using the model, this is just a more likely case out of all possible events. How could be possible that the trajectory is 2–3 km longer than the measurement from the footage? As I mentioned earlier, the only footage was taken from a long distance (>300km) of the end of the fall, and also with low resolution and low FPS. This in itself is enough to explain, however, the fall occurred at dawn on the site, almost in a blue sky, which could also have suppressed the fading end of the trajectory.

Acknowledgments

We would like to thank *Stanisław Korotkij* and *Yevgeny Trofimov* for providing the recordings and data that allowed us to conduct analyses of the event.

References

Kővágó G. (2024). "The MetLab software". *eMetN Meteor Journal*, **9**, 410–414.

Skytinel Team, Mateusz Zmija (2025). "Moscow fireball and meteorite fall in Novgorod Oblast". https://skytinel.com/moskiewski-bolid-i-spadek-meteorytow-w-obwodzie-nowogrodzkim/

October 2025 CARMELO report

Mariasole Maglione[1], **Lorenzo Barbieri**[2]

[1] **GAV, Gruppo Astrofili Vicentini, Italy**
mariasole@astrofilivicentini.it

[2] **CARMELO network and AAB: Associazione Astrofili Bolognesi, Italy**
carmelometeor@gmail.com

The CARMELO network (Cheap Amateur Radio Meteor Echoes LOgger) is a collaboration of SDR radio receivers aimed at detecting meteor echoes. This report presents the data for October 2025.

1 Introduction

October is the month of the Orionids (ORI). The CARMELO network recorded a moderate increase in meteor activity between October 21 and 22, and a further increase between October 26 and 27.

2 Methods

The CARMELO network consists of SDR radio receivers. In them, a microprocessor (Raspberry) performs three functions simultaneously:

- By driving a dongle, it tunes the frequency on which the transmitter transmits and tunes like a radio, samples the radio signal and through the FFT (Fast Fourier Transform) measures frequency and received power.
- By analyzing the received data for each packet, it detects meteor echoes and discards false positives and interference.
- It compiles a file containing the event log and sends it to a server.

The data are all generated by the same standard, and are therefore homogeneous and comparable. A single receiver can be assembled with a few devices whose total current cost is about 210 euros.

To participate in the network read the instructions on this page[37].

3 October data

In the plots that follow, all available at this page[38], the abscissae represent time, which is expressed in UT (Universal Time) or in solar longitude (Solar Long), and the ordinates represent the hourly rate, calculated as the total number of events recorded by the network in an hour divided by the number of operating receivers.

In *Figure 1*, the trend of signals detected by the receivers for the month of October.

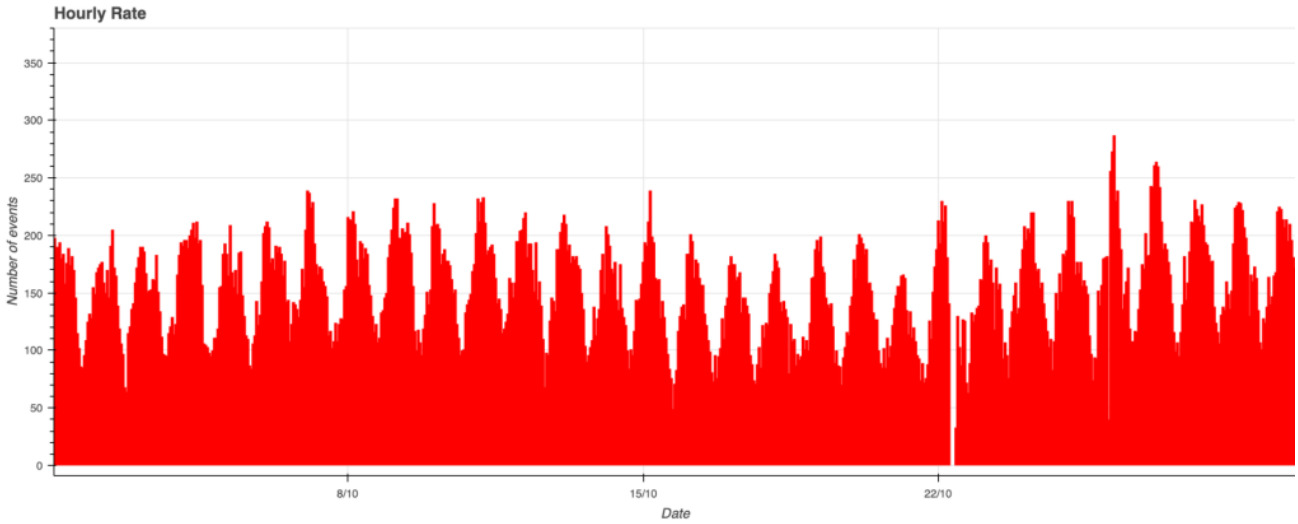

Figure 1 – October 2025 data trend.

[37] http://www.astrofiliabologna.it/about_carmelo

[38] http://www.astrofiliabologna.it/graficocarmelohr

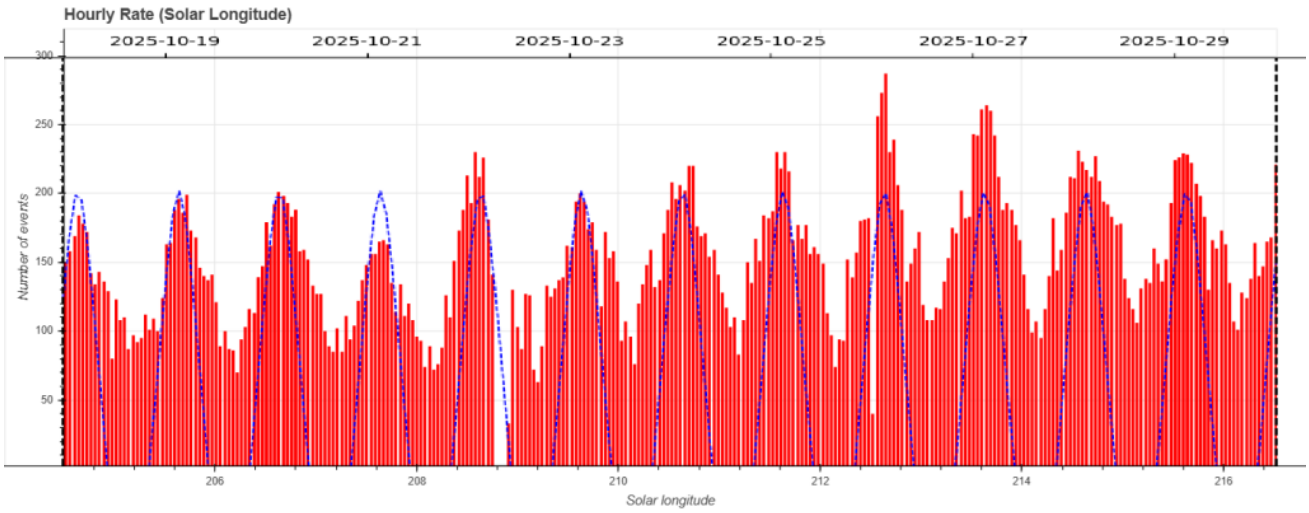

Figure 2 – Hourly rate of events recorded between October 17 and 29 versus on solar longitude.

4 Orionids

The Orionids (ORI,#8) are an annual meteor shower originating from Comet 1P/Halley. Every year, the Earth encounters the stream of particles left by the comet along its orbit, giving rise to the shower, which is active between early October and the first days of November. The peak of activity is usually around October 22, with a ZHR that can reach about 25 meteors per hour under favorable conditions. These meteors are quite fast: they enter the Earth's atmosphere at about 67.5 km/s, producing rapid and thin trails, sometimes with particularly bright meteors.

The Orionids have also shown episodes of sudden increases in activity (outbursts) in the past. In particular, in 1993, an unexpected outburst was recorded on the nights between October 16 and 18, a few days before the expected peak. During those nights, very bright meteors were also observed at solar longitudes around 202°–205°. The phenomenon did not repeat itself the following year (Jenniskens, 2006).

The radiant of the Orionids is located in the constellation Orion, near the star Betelgeuse. This means that the meteors appear to come from this area of the sky. For observers in the northern hemisphere, such as the CARMELO network, the radiant rises late in the evening and reaches its maximum elevation in the hours just before dawn. In *Figure 2*, the hourly rate of signals received on days when an increase in the number of meteors was recorded, consistent with Orionid activity, is overlaid with a blue line indicating the elevation of the radiant.

This year, the CARMELO network detected a noticeable increase in the hourly rate of events detected between solar longitudes 208° and 209°, i.e., between October 21 and 22. However, just as the Earth was expected to pass through the peak of the Orionid meteor shower on October 22, the Graves radar was turned off for about 4 hours.

We also noticed a further increase between solar longitudes 212° and 214°, i.e. between October 26 and 27 (see *Figure 2*).

5 The CARMELO network

The network currently consists of 14 receivers, 12 of which are operational, located in Italy, the UK, Croatia and the USA. The European receivers are tuned to the Graves radar station frequency in France, which is 143.050 MHz. Participating in the network are:

- Lorenzo Barbieri, Budrio (BO) ITA;
- Associazione Astrofili Bolognesi, Bologna ITA;
- Associazione Astrofili Bolognesi, Medelana (BO) ITA;
- Paolo Fontana, Castenaso (BO) ITA;
- Paolo Fontana, Belluno (BL) ITA;
- Associazione Astrofili Pisani, Orciatico (PI) ITA;
- Gruppo Astrofili Persicetani, San Giovanni in Persiceto (BO) ITA;
- Roberto Nesci, Foligno (PG) ITA;
- MarSEC, Marana di Crespadoro (VI) ITA;
- Gruppo Astrofili Vicentini, Arcugnano (VI) ITA;
- Associazione Ravennate Astrofili Theyta, Ravenna (RA) ITA;
- Mike German a Hayfield, Derbyshire UK;
- Mike Otte, Pearl City, Illinois USA.

The authors' hope is that the network can expand both quantitatively and geographically, thus allowing the production of better-quality data.

References

Jenniskens P. (2006). "Meteor showers and their parent comets". Cambridge University Press, p. 301–302.

November 2025 CARMELO report

Mariasole Maglione[1], **Lorenzo Barbieri**[2]

[1] **GAV, Gruppo Astrofili Vicentini, Italy**
mariasole@astrofilivicentini.it

[2] **CARMELO network and AAB: Associazione Astrofili Bolognesi, Italy**
carmelometeor@gmail.com

The CARMELO network (Cheap Amateur Radio Meteor Echoes LOgger) is a collaboration of SDR radio receivers aimed at detecting meteor echoes. This report presents the data for November 2025.

1 Introduction

November is the month of the Leonids (LEO), but this year the CARMELO network did not record particularly intense activity around the predicted peak of the shower.

2 Methods

The CARMELO network consists of SDR radio receivers. In them, a microprocessor (Raspberry) performs three functions simultaneously:

- By driving a dongle, it tunes the frequency on which the transmitter transmits and tunes like a radio, samples the radio signal and through the FFT (Fast Fourier Transform) measures frequency and received power.
- By analyzing the received data for each packet, it detects meteor echoes and discards false positives and interference.
- It compiles a file containing the event log and sends it to a server.

The data are all generated by the same standard, and are therefore homogeneous and comparable. A single receiver can be assembled with a few devices whose total current cost is about 210 euros.

To participate in the network read the instructions on this page[39].

3 November data

In the plots that follow, all available at this page[40], the abscissae represent time, which is expressed in UT (Universal Time) or in solar longitude (Solar Long), and the ordinates represent the hourly rate, calculated as the total number of events recorded by the network in an hour divided by the number of operating receivers.

In *Figure 1*, the trend of signals detected by the receivers for the month of November.

4 Leonids

In November, the sky once again hosts the Leonid (LEO) meteor shower, associated with the periodic comet 55P/Tempel–Tuttle and linked to its orbital cycle of about 33 years. Each time the comet passes perihelion, it releases a new trail of debris responsible for the spectacular meteor "storms" observed in years like 1966 or, more recently, 2001.

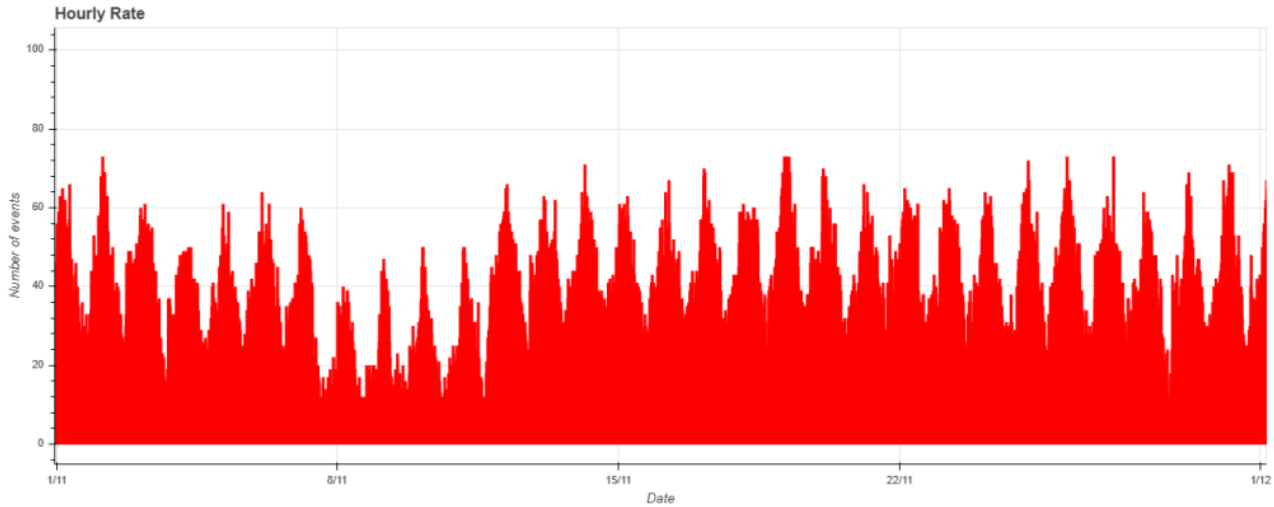

Figure 1 – November 2025 data trend.

[39] http://www.astrofiliabologna.it/about_carmelo

[40] http://www.astrofiliabologna.it/graficocarmelohr

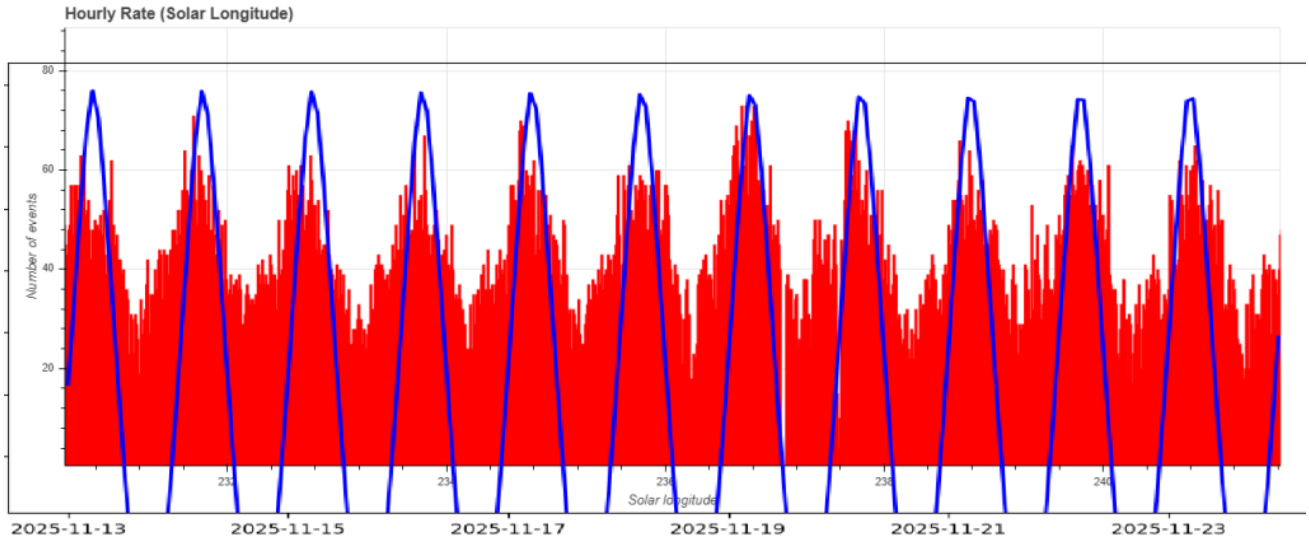

Figure 2 – Hourly rate of events recorded between November 13 and 23, based on solar longitude.

In recent years, however, the reservoir of dust encountered by Earth in mid-November has gradually become depleted. Until the comet's next return, expected in 2031, the shower will continue to exhibit increasingly modest activity. According to estimates from the International Meteor Organization (IMO), this year Earth crossed two segments of the 1699 trail on the evening of November 17, with a predicted rate of about 15–20 meteors per hour (Rendtel, 2025). However, the radiant, located in the constellation Leo, rose only around 23^h30^m in Italy, right at the time of the expected peak, preventing the detection of a high number of events.

Models also indicated possible encounters with older trails: the 1167 trail (forecast for November 9), the 1633 trail (November 15), and an initial passage through the 1699 trail. Yet, as often happens with the Leonids during this material-poor phase, the predictions came with a wide margin of uncertainty.

The activity recorded this year by the CARMELO network confirms the overall weakness of the shower. Even visual observations, such as those reported by the Global Meteor Network[41], showed a very low ZHR, with no significant variations at the expected peak times.

The only slightly more noticeable increase in CARMELO detections appears on the morning of November 19, around solar longitude 236.8° (see *Figure 2*, where the radiant-height graph is shown in blue).

Given the high speed of the Leonids, about 72 km/s, one would normally expect to detect radio echoes featuring strong head echoes and clear Doppler shifts, which are characteristic signatures of the fastest meteors. Even in this respect, however, the network's data indicate a very low presence of events attributable to high-velocity meteors.

5 The CARMELO network

The network currently consists of 14 receivers, 12 of which are operational, located in Italy, the UK, Croatia and the USA. The European receivers are tuned to the Graves radar station frequency in France, which is 143.050 MHz. Participating in the network are:

- Lorenzo Barbieri, Budrio (BO) ITA;
- Associazione Astrofili Bolognesi, Bologna ITA;
- Associazione Astrofili Bolognesi, Medelana (BO) ITA;
- Paolo Fontana, Castenaso (BO) ITA;
- Paolo Fontana, Belluno (BL) ITA;
- Associazione Astrofili Pisani, Orciatico (PI) ITA;
- Gruppo Astrofili Persicetani, San Giovanni in Persiceto (BO) ITA;
- Roberto Nesci, Foligno (PG) ITA;
- MarSEC, Marana di Crespadoro (VI) ITA;
- Gruppo Astrofili Vicentini, Arcugnano (VI) ITA;
- Associazione Ravennate Astrofili Theyta, Ravenna (RA) ITA;
- Mike German a Hayfield, Derbyshire UK;
- Mike Otte, Pearl City, Illinois USA.

The authors' hope is that the network can expand both quantitatively and geographically, thus allowing the production of better-quality data.

References

Rendtel J. (2025). 2025 Meteor shower calendar. IMO. Page 17.

[41] https://globalmeteornetwork.org/flux/plots/flux_LEO_sol%3D224.00-245.00_year_2025.png

Radio meteors October 2025

Felix Verbelen

Vereniging voor Sterrenkunde & Volkssterrenwacht MIRA, Grimbergen, Belgium
felix.verbelen@gmail.com

An overview of the radio observations during October is given.

1 Introduction

The graphs show both the daily totals (*Figure 1 and 2*) and the hourly numbers (*Figure 3 and 4*) of "all" reflections counted automatically, and of manually counted "overdense" reflections, overdense reflections longer than 10 seconds and longer than 1 minute, as observed here at Kampenhout (BE) on the frequency of our VVS-beacon (49.99 MHz) during the month of October 2025.

The hourly numbers, for echoes shorter than 1 minute, are weighted averages derived from:

$$N(h) = \frac{n(h-1)}{4} + \frac{n(h)}{2} + \frac{n(h+1)}{4}$$

Local interference and unidentified noise remained very limited and quite weak lightning activity was only registered on the 20th. However, there were fairly strong solar flares almost daily, mostly of type III.

This month, several showers were active, with the Orionids especially standing out with an increase in long-duration reflections which peaked on October 22nd. Also on October 10th, there was a clear surge of overdense reflections between 15h and 18h UT when the Draco radiant was near the local zenith. Further analysis of the registrations shows several other smaller showers.

During this month 17 reflections with a duration of more than 1 minute were observed. A selection of some notable or strong reflections is shown in *Figures 5 to 22*. Many more are available upon request.

In addition to the usual graphs, you will also find the raw counts in cvs-format[42] from which the graphs are derived. The table contains the following columns: day of the month, hour of the day, day + decimals, solar longitude (epoch J2000), counts of "all" reflections, overdense reflections, reflections longer than 10 seconds and reflections longer than 1 minute, the numbers being the observed reflections of the past hour.

[42] https://www.emeteornews.net/wp-content/uploads/2025/11/202510_49990_FV_rawcounts.csv

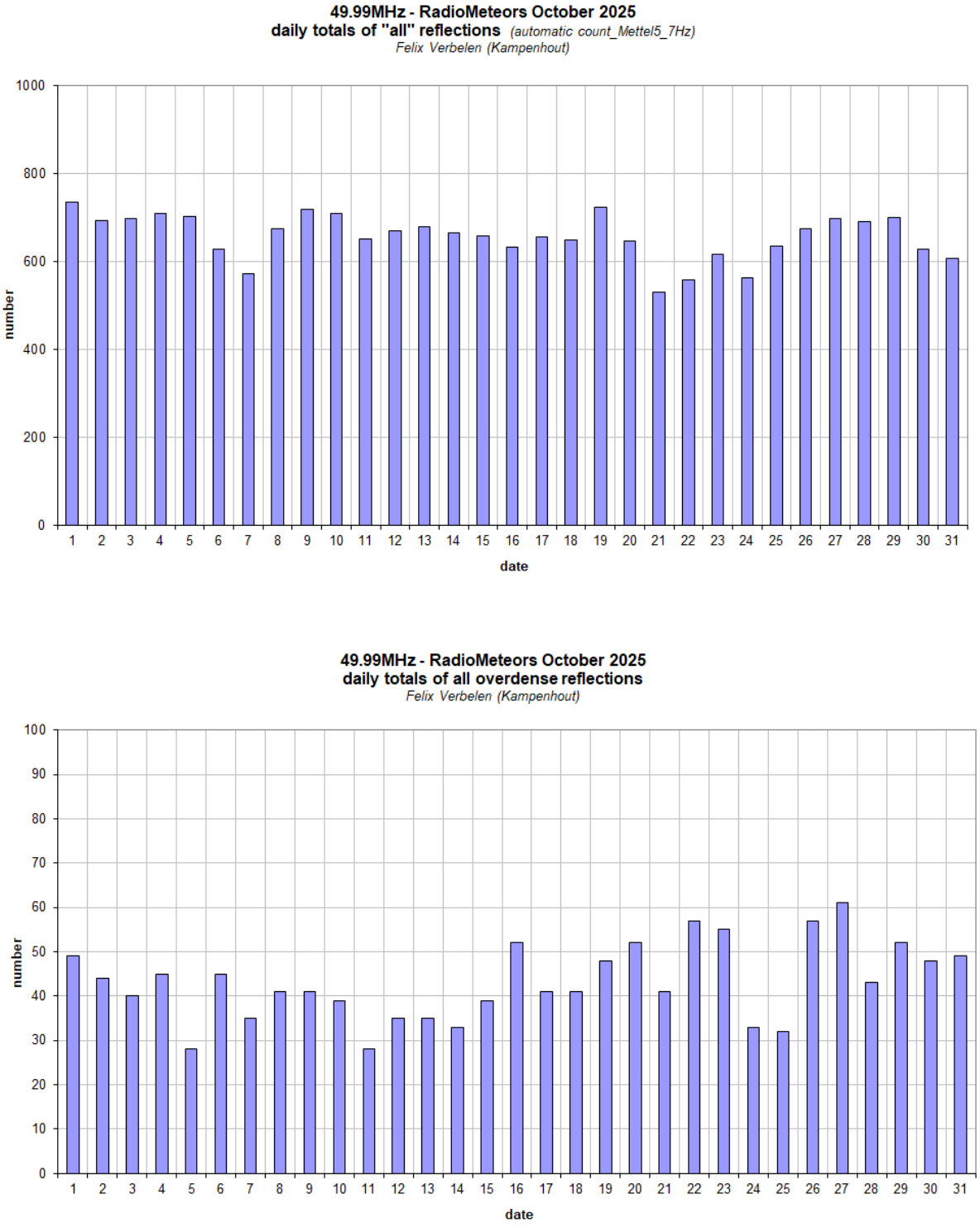

Figure 1 – The daily totals of "all" reflections counted automatically, and of manually counted "overdense" reflections, as observed here at Kampenhout (BE) on the frequency of our VVS-beacon (49.99 MHz) during October 2025.

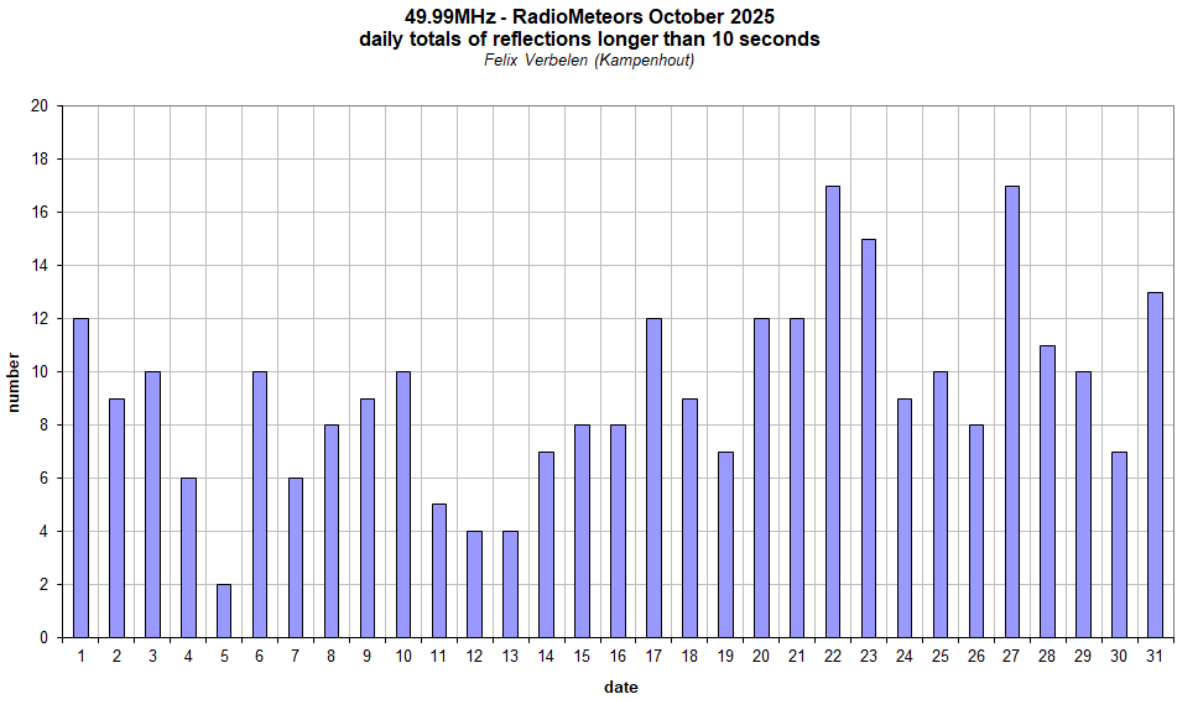

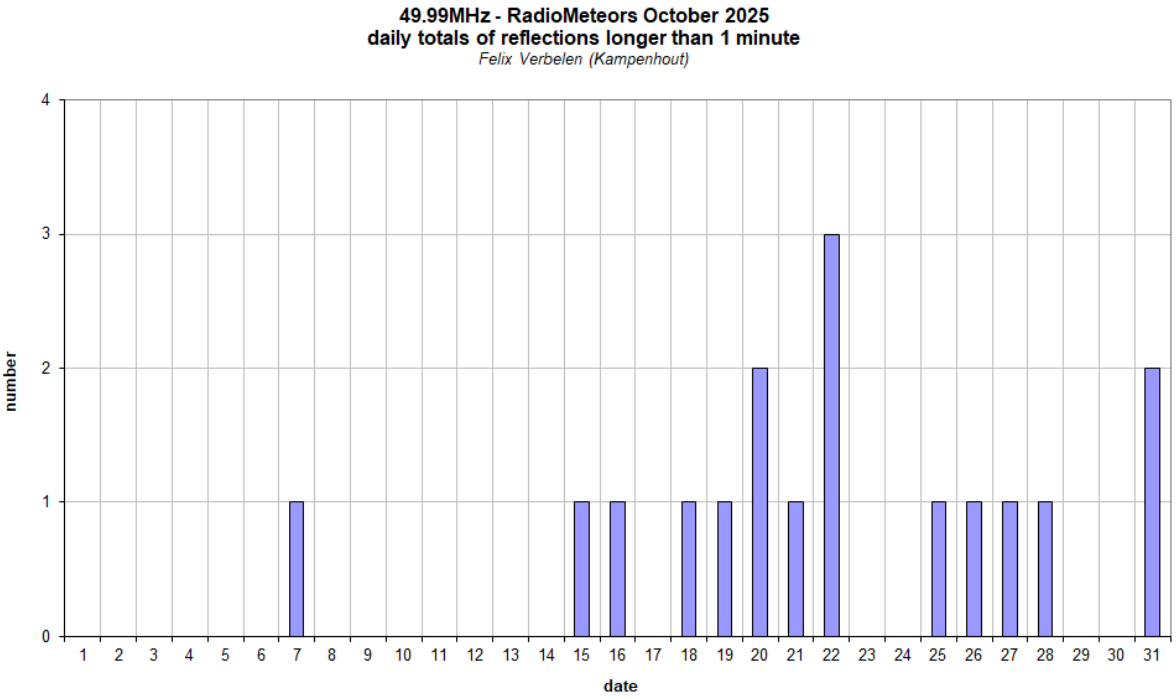

Figure 2 – The daily totals of overdense reflections longer than 10 seconds and longer than 1 minute, as observed here at Kampenhout (BE) on the frequency of our VVS-beacon (49.99 MHz) during October 2025.

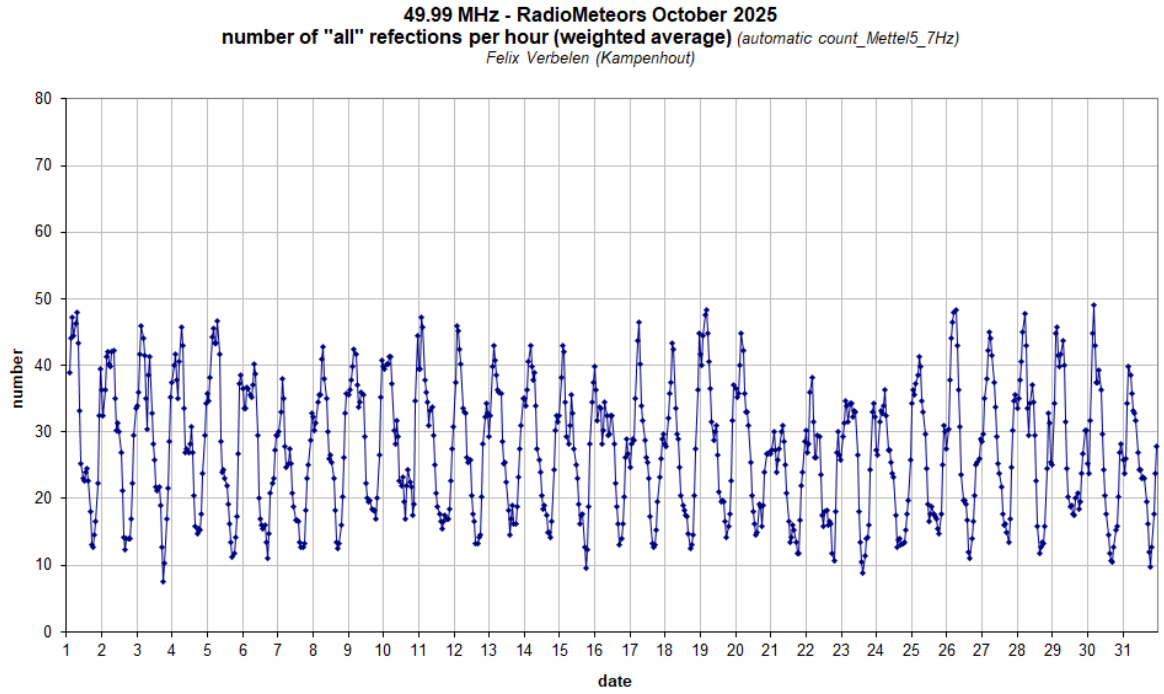

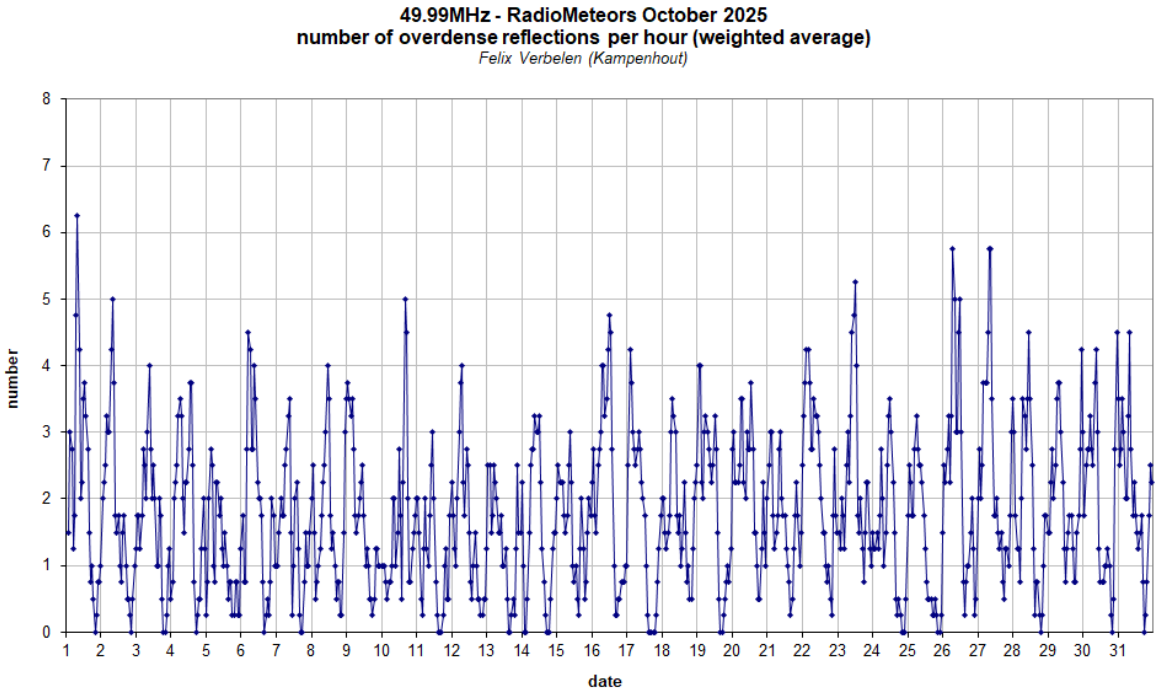

Figure 3 – The hourly numbers of "all" reflections counted automatically, and of manually counted "overdense" reflections, as observed here at Kampenhout (BE) on the frequency of our VVS-beacon (49.99 MHz) during October 2025.

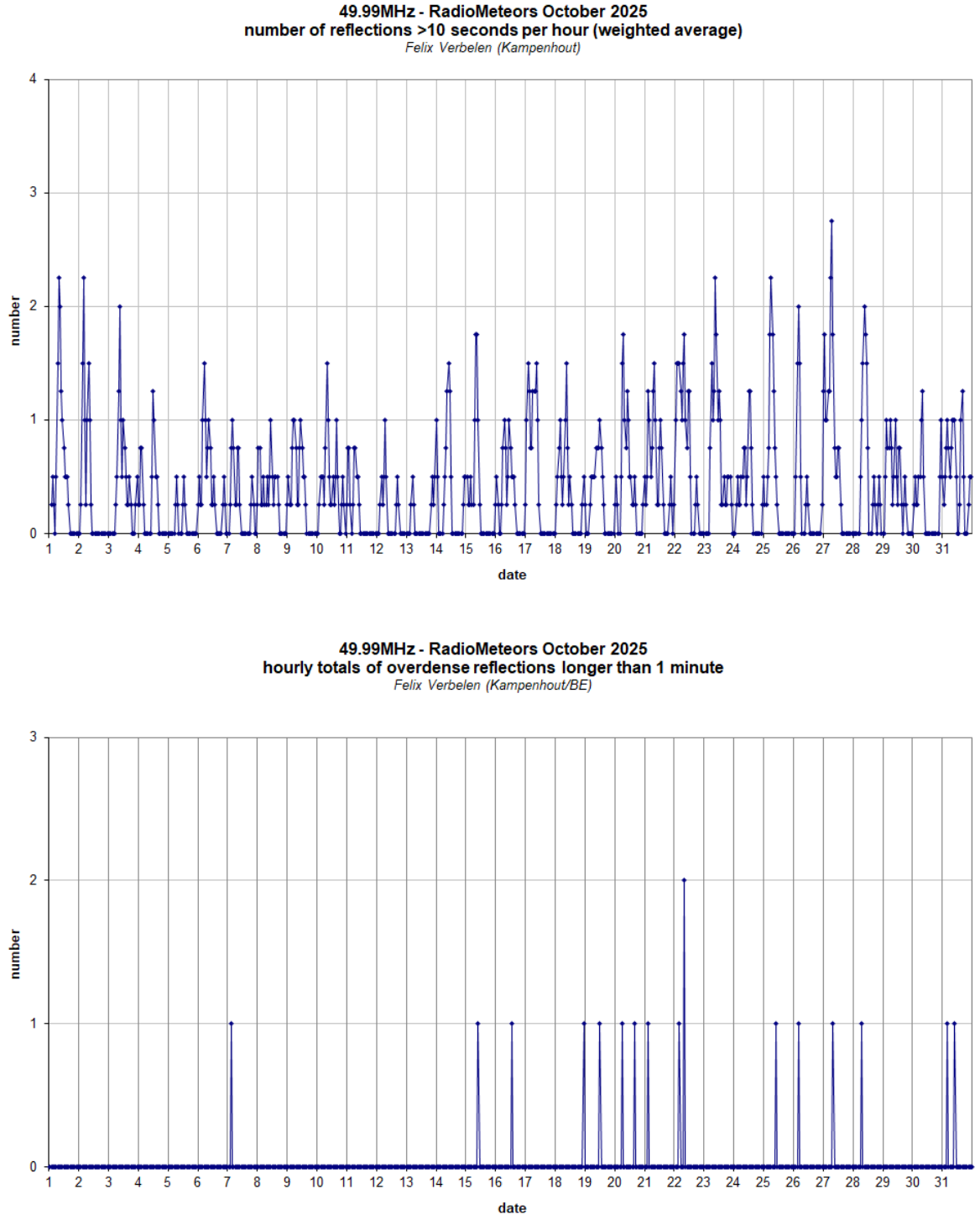

Figure 4 – The hourly numbers of overdense reflections longer than 10 seconds and longer than 1 minute, as observed here at Kampenhout (BE) on the frequency of our VVS-beacon (49.99 MHz) during October 2025.

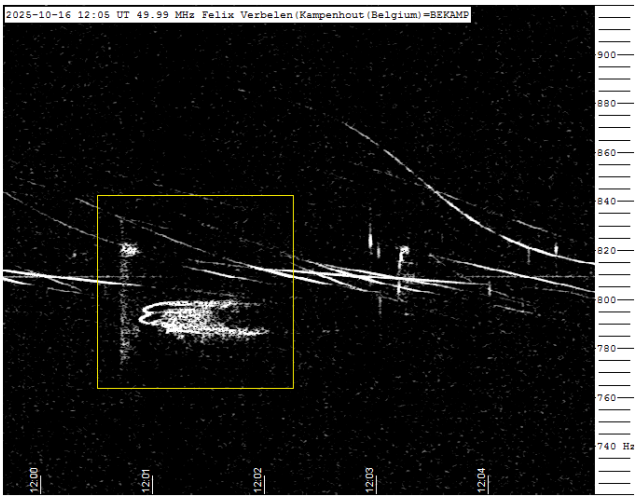

Figure 5 – Meteor echoes October 16, 12^{h}05^{m} UT.

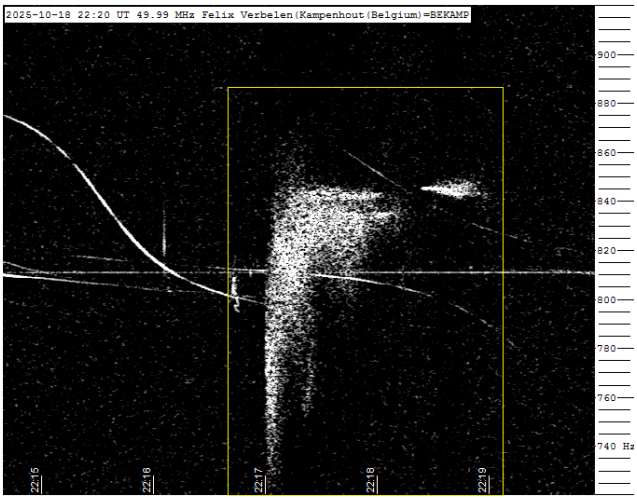

Figure 6 – Meteor echoes October 18, 22^{h}20^{m} UT.

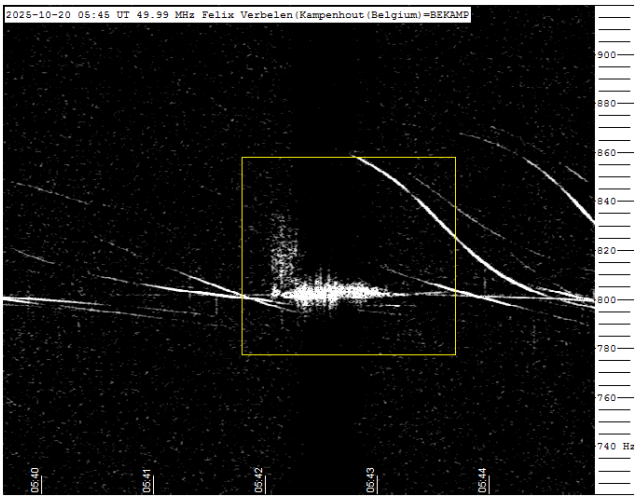

Figure 7 – Meteor echoes October 20, 05^{h}45^{m} UT.

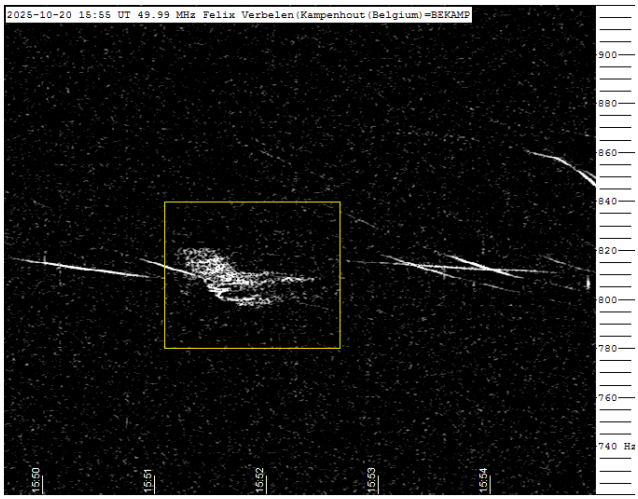

Figure 8 – Meteor echoes October 20, 15^{h}55^{m} UT.

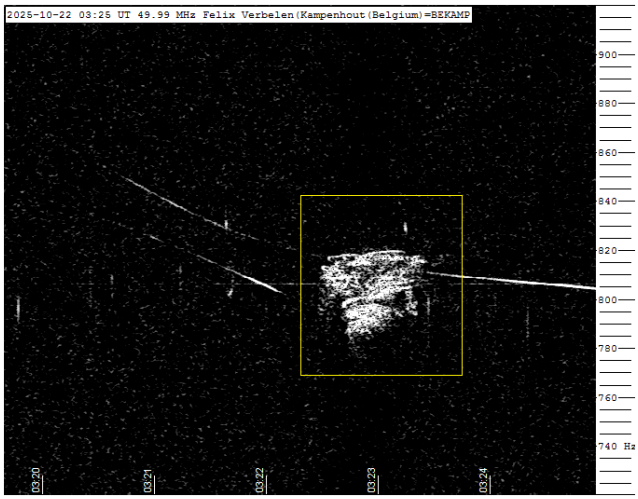

Figure 9 – Meteor echoes October 22, 03^{h}25^{m} UT.

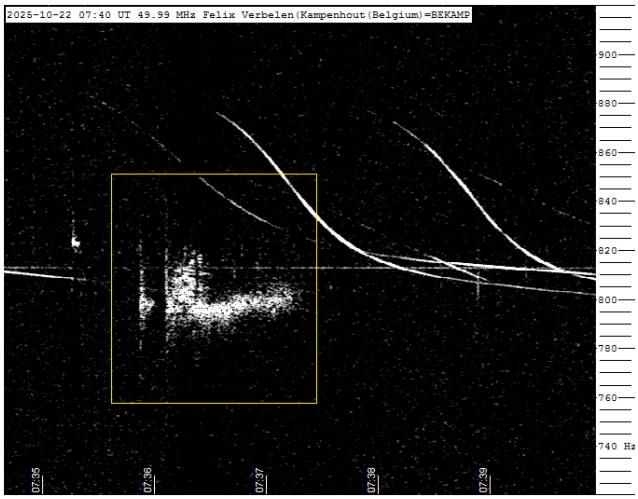

Figure 10 – Meteor echoes October 22, 07^{h}40^{m} UT.

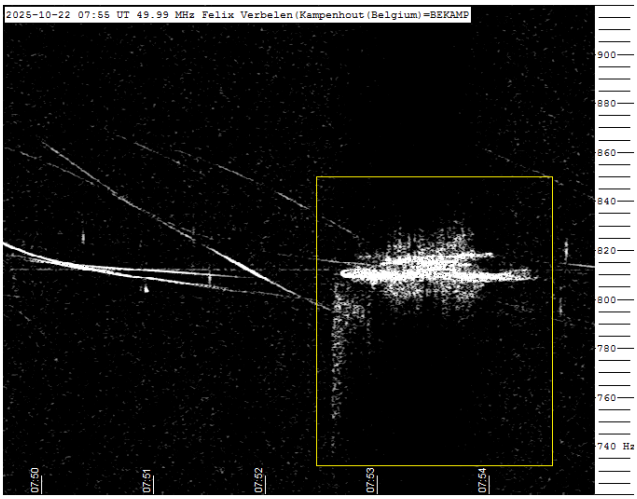

Figure 11 – Meteor echoes October 22, 07^{h}55^{m} UT.

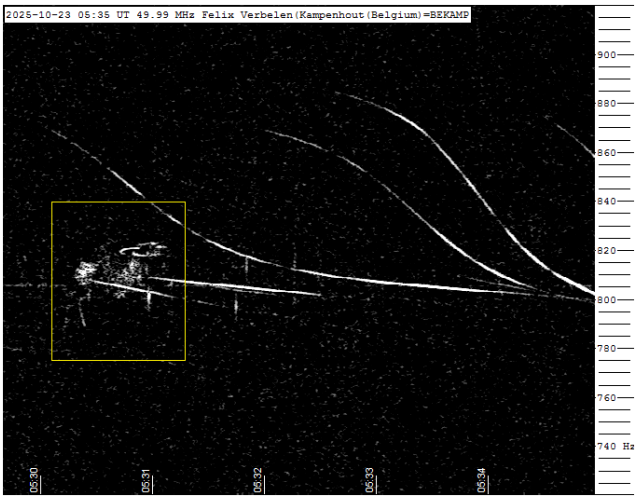

Figure 12 – Meteor echoes October 23, 05^{h}35^{m} UT.

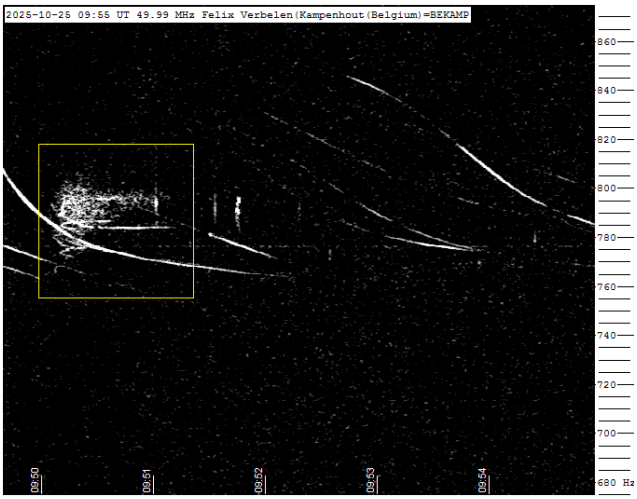

Figure 13 – Meteor echoes October 25, 09^{h}55^{m} UT.

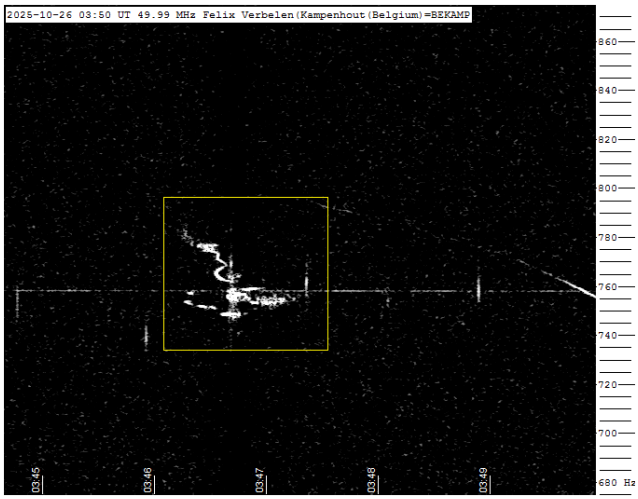

Figure 14 – Meteor echoes October 26, 03^{h}50^{m} UT.

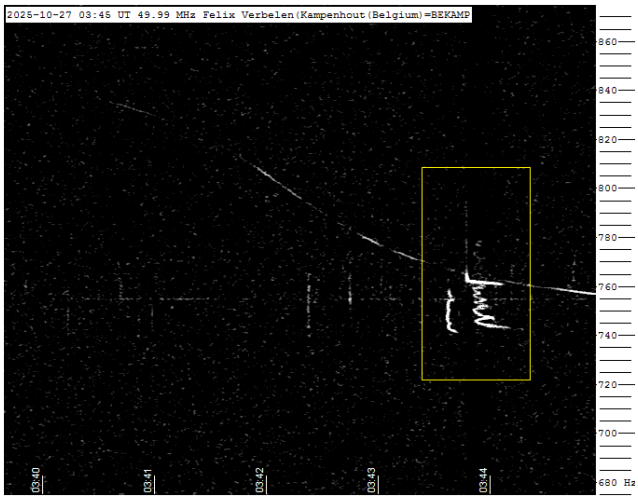

Figure 15 – Meteor echoes October 27, 03^{h}45^{m} UT.

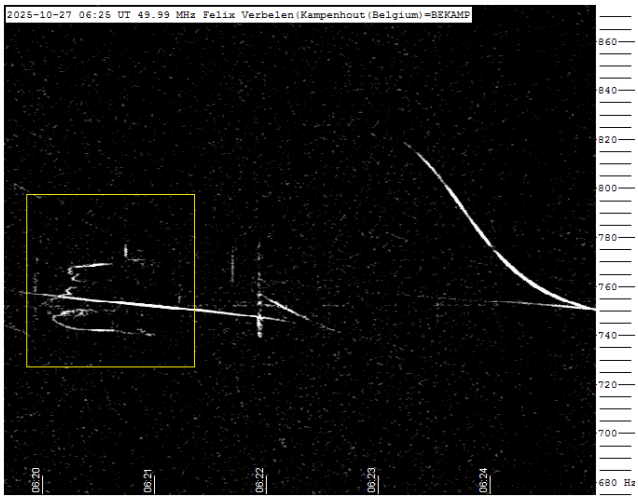

Figure 16 – Meteor echoes October 27, 06^{h}25^{m} UT.

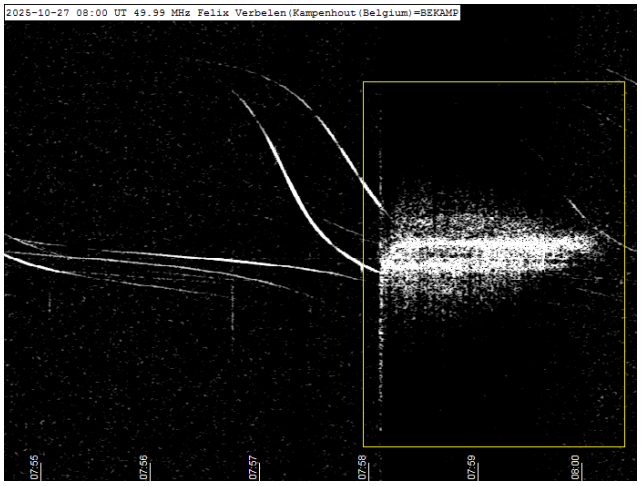

Figure 17 – Meteor echoes October 27, 08^{h}00^{m} UT.

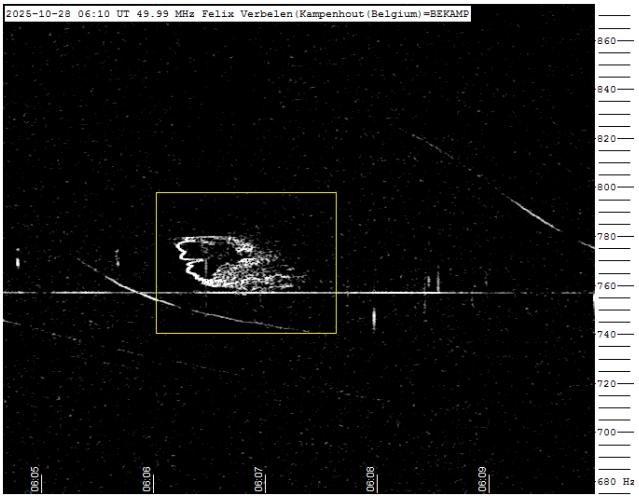

Figure 18 – Meteor echoes October 28, 06^{h}10^{m} UT.

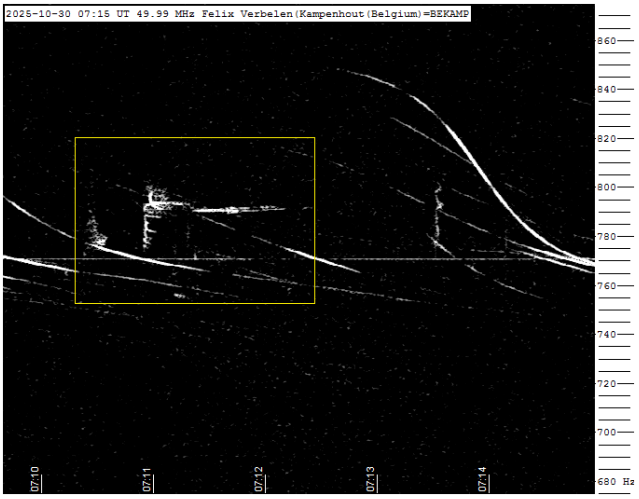

Figure 19 – Meteor echoes October 30, 07^{h}15^{m} UT.

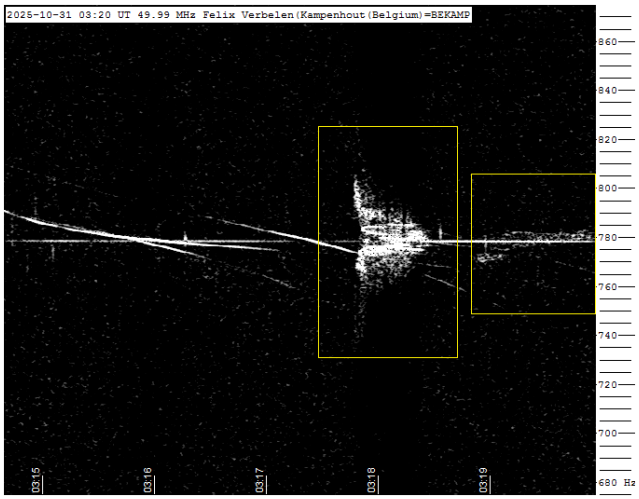

Figure 20 – Meteor echoes October 31, 03^{h}20^{m} UT.

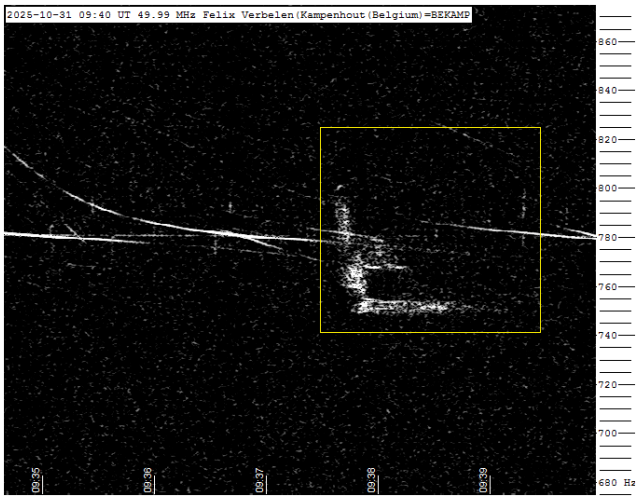

Figure 21 – Meteor echoes October 31, 09^{h}40^{m} UT.

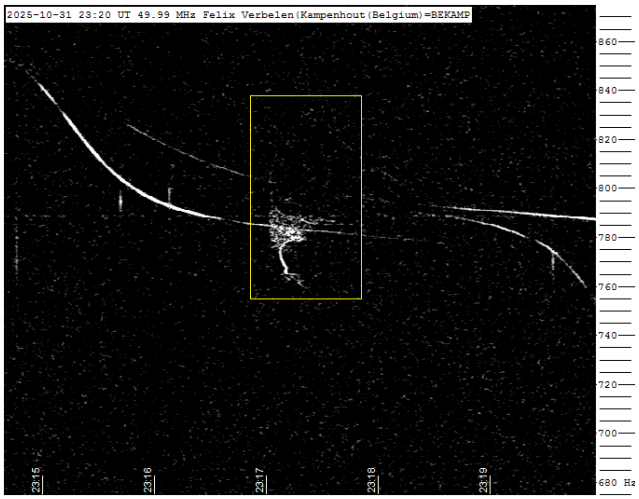

Figure 22 – Meteor echoes October 31, 23^{h}20^{m} UT.

Radio meteors November 2025

Felix Verbelen

Vereniging voor Sterrenkunde & Volkssterrenwacht MIRA, Grimbergen, Belgium
felix.verbelen@gmail.com

An overview of the radio observations during November is given.

1 Introduction

The graphs show both the daily totals (*Figure 1 and 2*) and the hourly numbers (*Figure 3 and 4*) of "all" reflections counted automatically, and of manually counted "overdense" reflections, overdense reflections longer than 10 seconds and longer than 1 minute, as observed here at Kampenhout (BE) on the frequency of our VVS-beacon (49.99 MHz) during the month of November 2025.

The hourly numbers, for echoes shorter than 1 minute, are weighted averages derived from:

$$N(h) = \frac{n(h-1)}{4} + \frac{n(h)}{2} + \frac{n(h+1)}{4}$$

Local interference and unidentified noise remained weak, and no significant lightning activity was recorded.

The general meteor activity remained quite limited, though there was an increase at the beginning of the month and a few short bursts, notably on 8–9, 15–16, and 30 November.

This month, 12 reflections longer than 1 minute were observed here. A selection, along with a few other interesting reflections is shown in *Figures 5 to 20*. Many more are available upon request.

In addition to the usual graphs, you will also find the raw counts in cvs-format[43] from which the graphs are derived. The table contains the following columns: day of the month, hour of the day, day + decimals, solar longitude (epoch J2000), counts of "all" reflections, overdense reflections, reflections longer than 10 seconds and reflections longer than 1 minute, the numbers being the observed reflections of the past hour.

[43] https://www.emeteornews.net/wp-content/uploads/2025/12/202511_49990_FV_rawcounts.csv

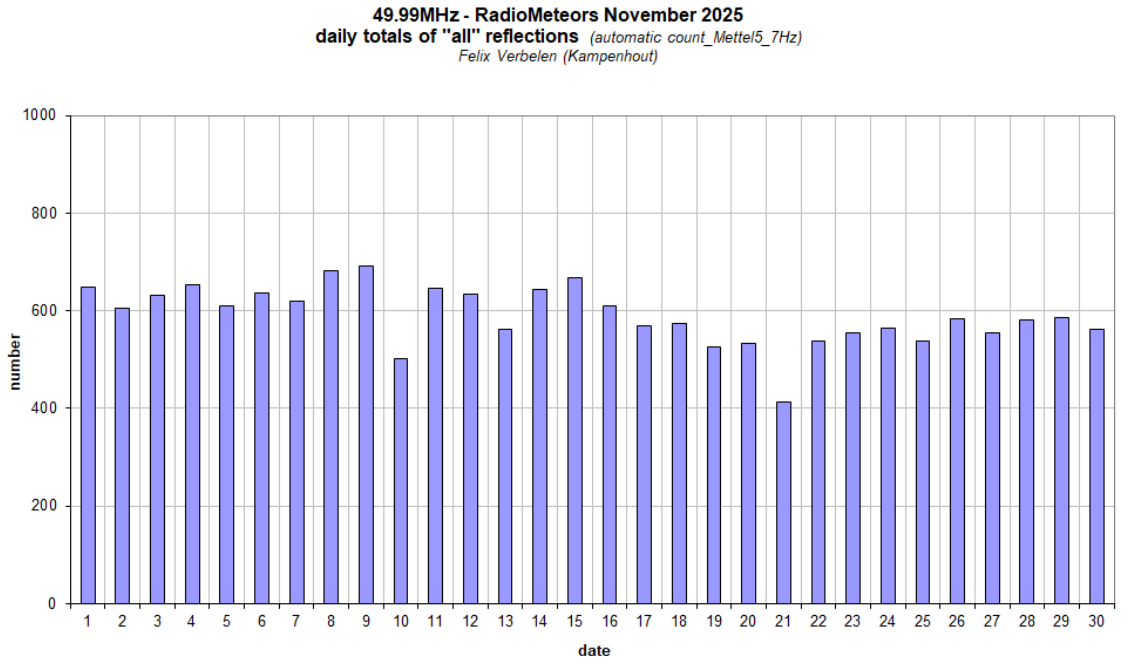

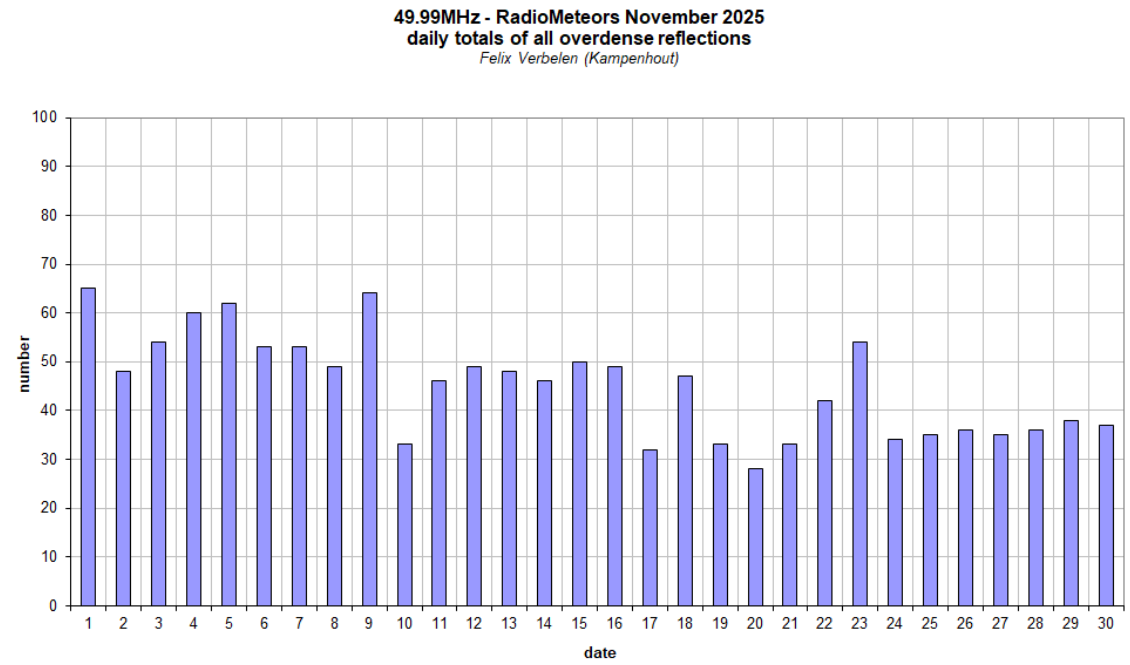

Figure 1 – The daily totals of "all" reflections counted automatically, and of manually counted "overdense" reflections, as observed here at Kampenhout (BE) on the frequency of our VVS-beacon (49.99 MHz) during November 2025.

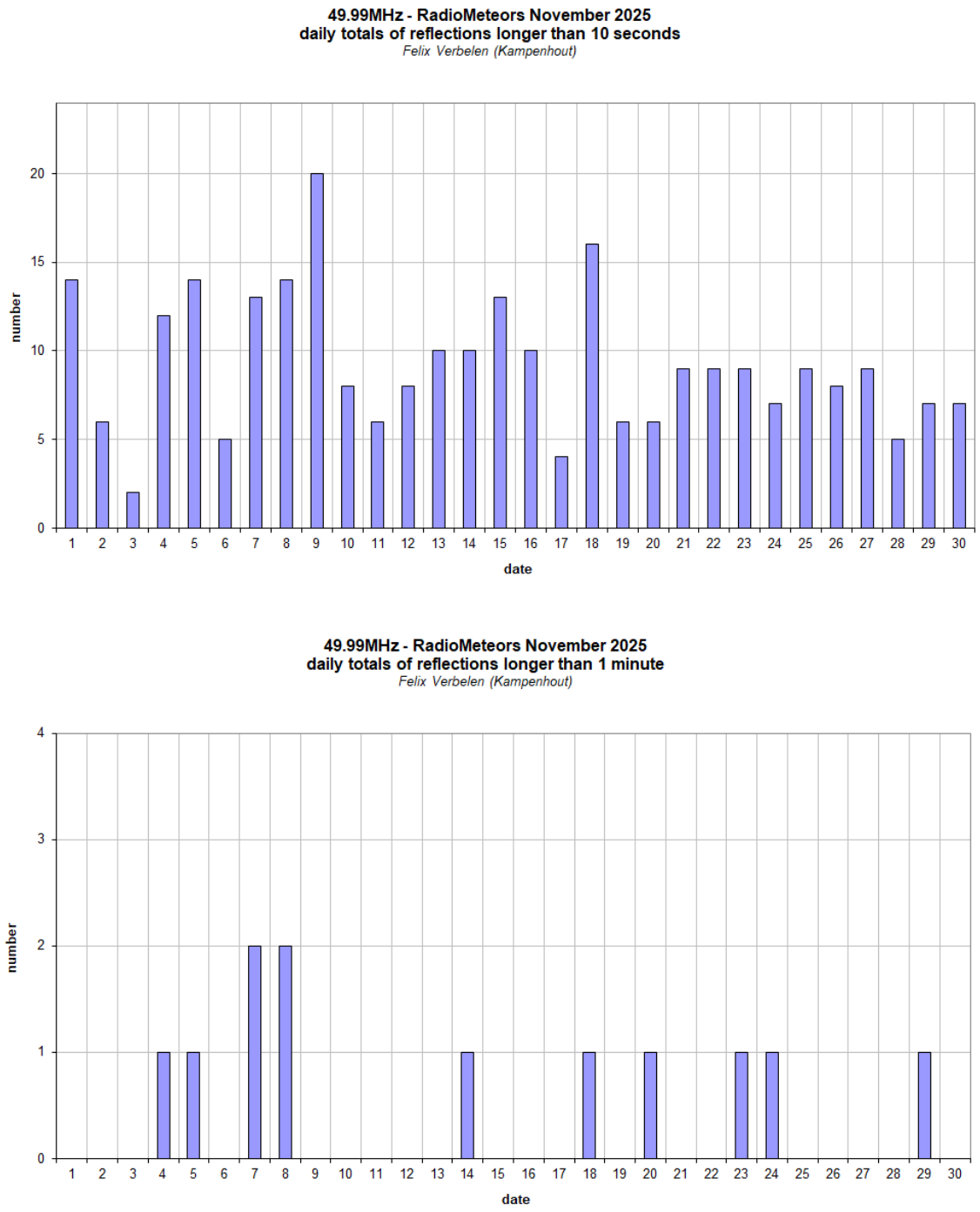

Figure 2 – The daily totals of overdense reflections longer than 10 seconds and longer than 1 minute, as observed here at Kampenhout (BE) on the frequency of our VVS-beacon (49.99 MHz) during November 2025.

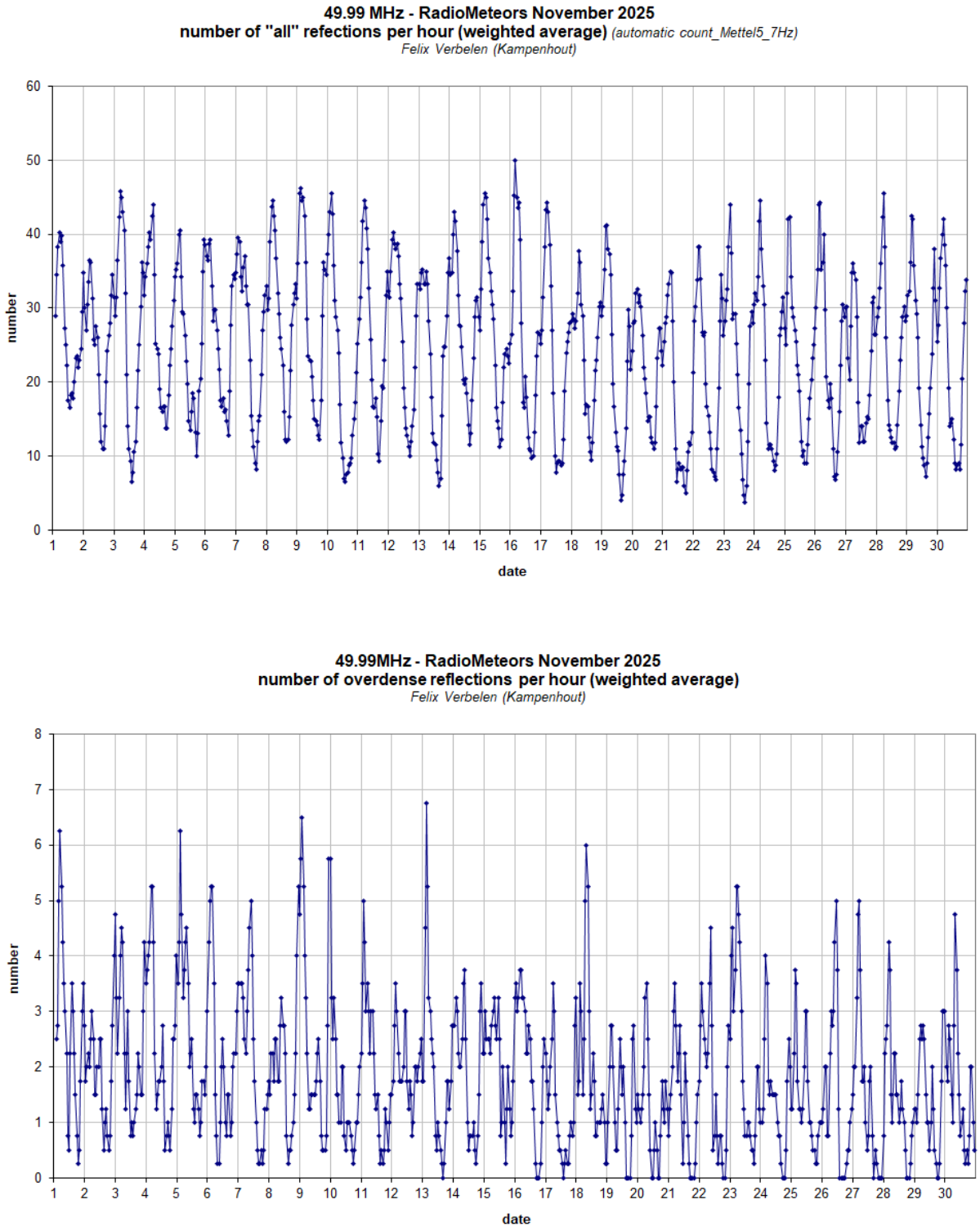

Figure 3 – The hourly numbers of "all" reflections counted automatically, and of manually counted "overdense" reflections, as observed here at Kampenhout (BE) on the frequency of our VVS-beacon (49.99 MHz) during November 2025.

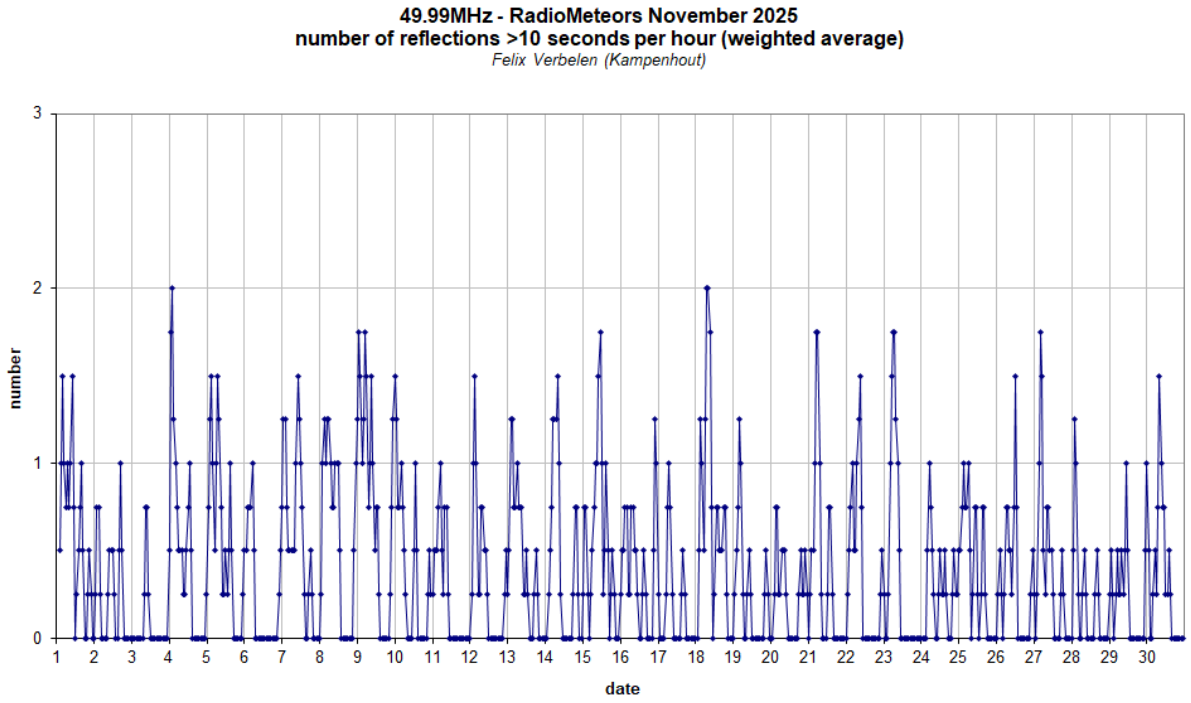

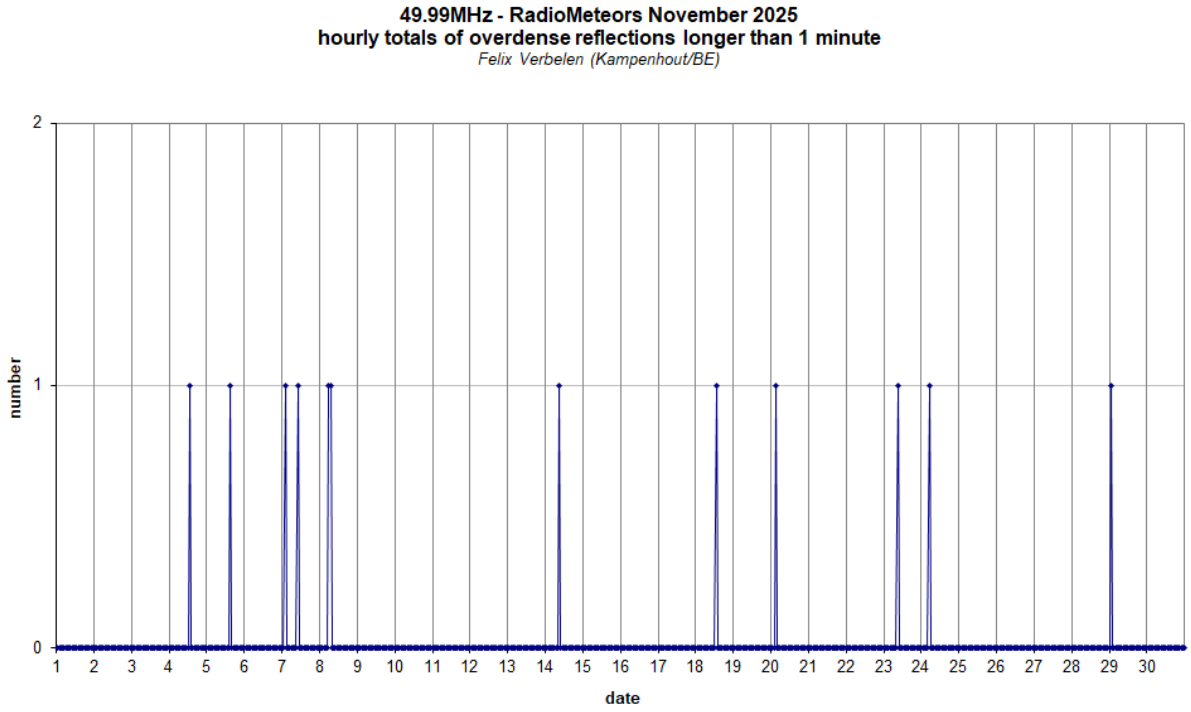

Figure 4 – The hourly numbers of overdense reflections longer than 10 seconds and longer than 1 minute, as observed here at Kampenhout (BE) on the frequency of our VVS-beacon (49.99 MHz) during November 2025.

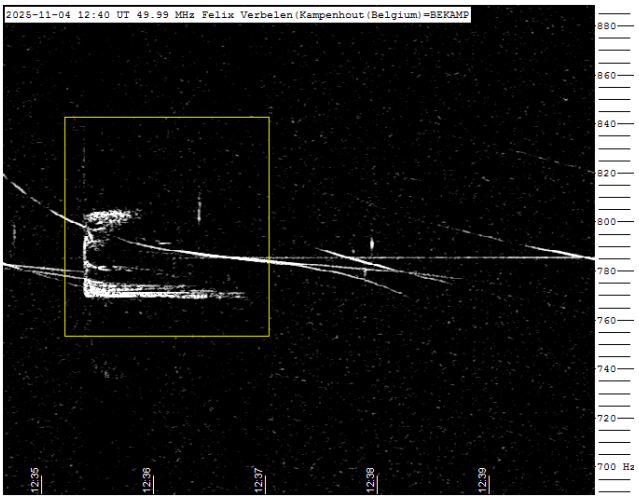

Figure 5 – Meteor echoes November 4, 12^h40^m UT.

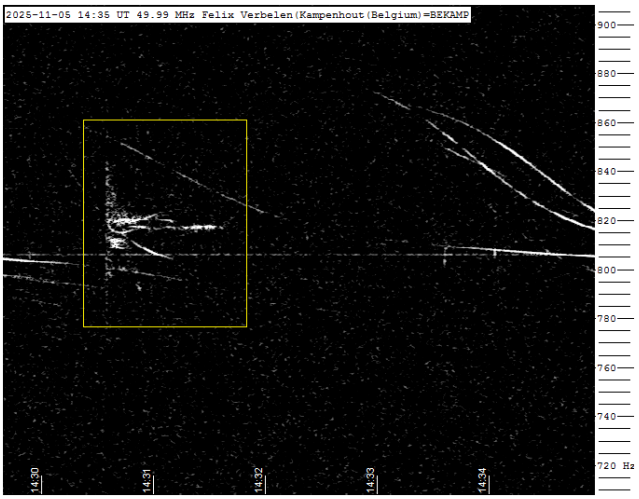

Figure 6 – Meteor echoes November 5, 14^h35^m UT.

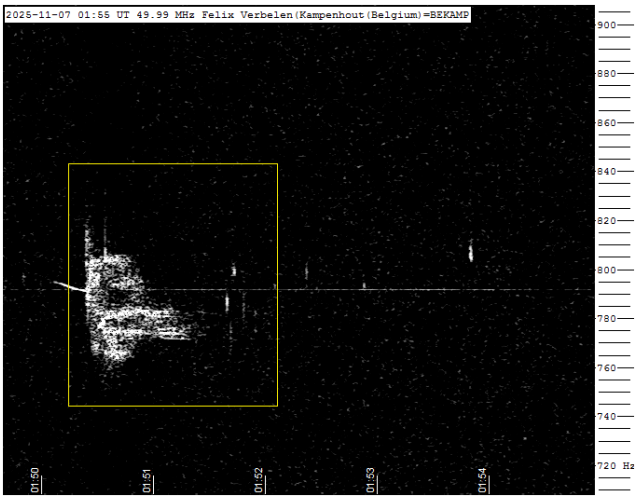

Figure 7 – Meteor echoes November 7, 1^h55^m UT.

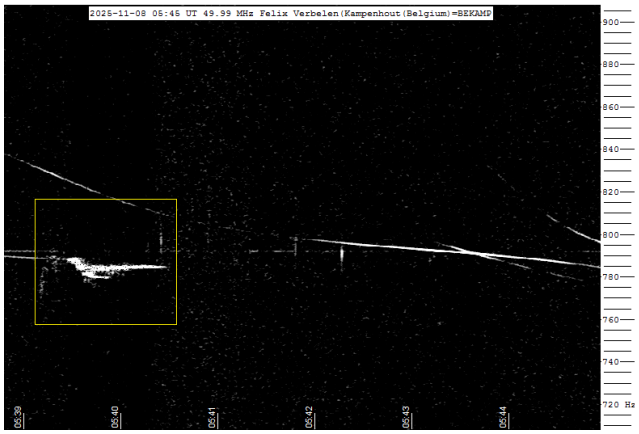

Figure 8 – Meteor echoes November 8, 5^h45^m UT.

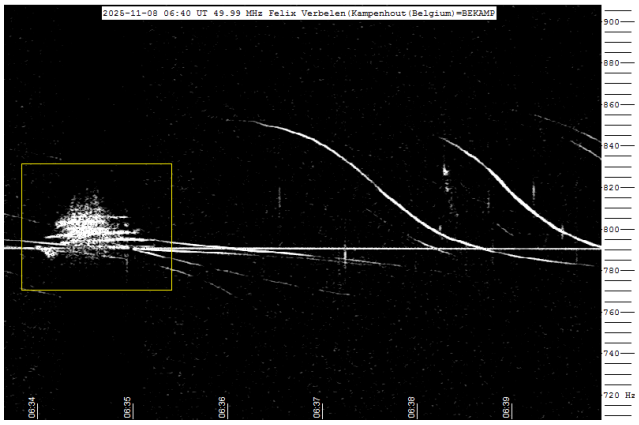

Figure 9 – Meteor echoes November 8, 6^h40^m UT.

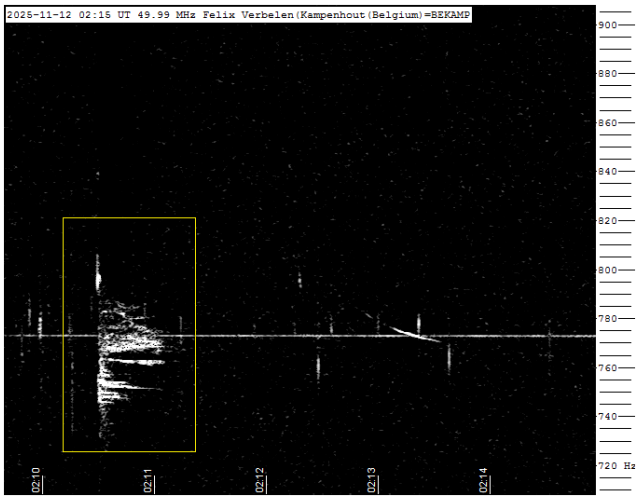

Figure 10 – Meteor echoes November 12, 2^h15^m UT.

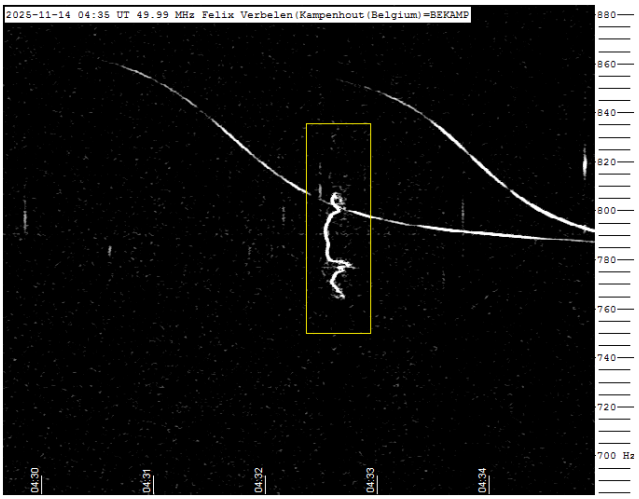

Figure 11 – Meteor echoes November 14, 4^{h}35^{m} UT.

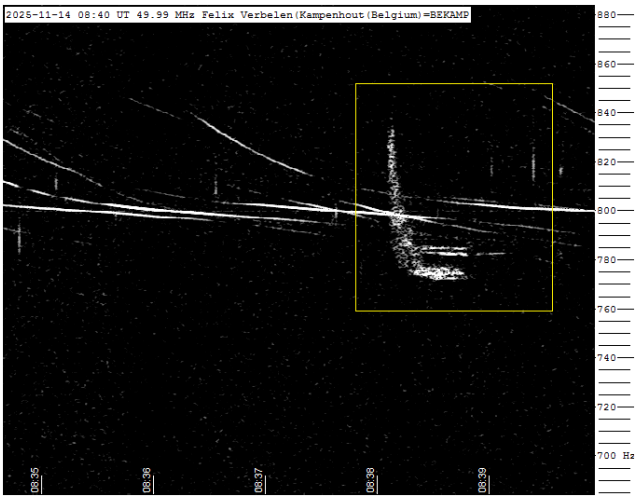

Figure 12 – Meteor echoes November 14, 8^{h}40^{m} UT.

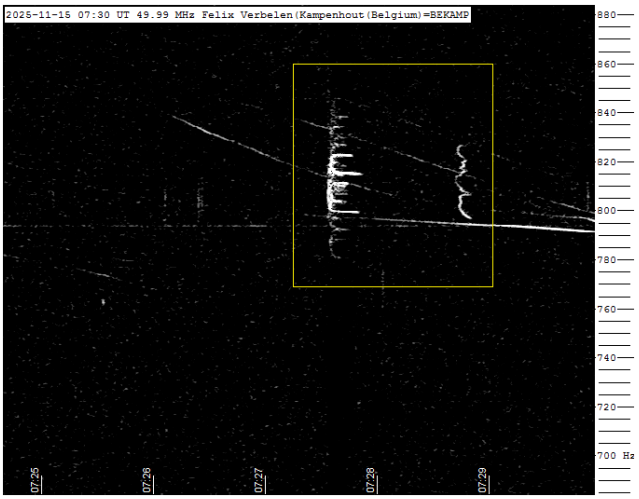

Figure 13 – Meteor echoes November 15, 7^{h}30^{m} UT.

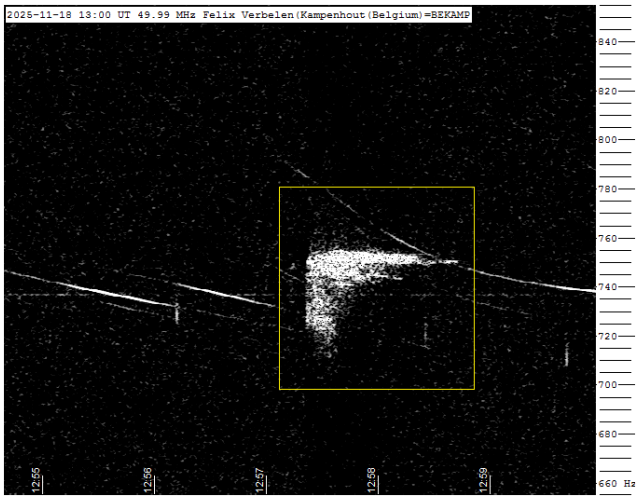

Figure 14 – Meteor echoes November 18, 13^{h}00^{m} UT.

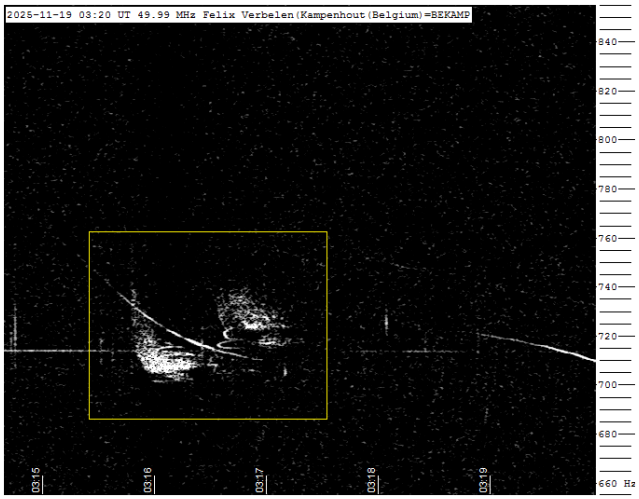

Figure 15 – Meteor echoes November 19, 3^{h}20^{m} UT.

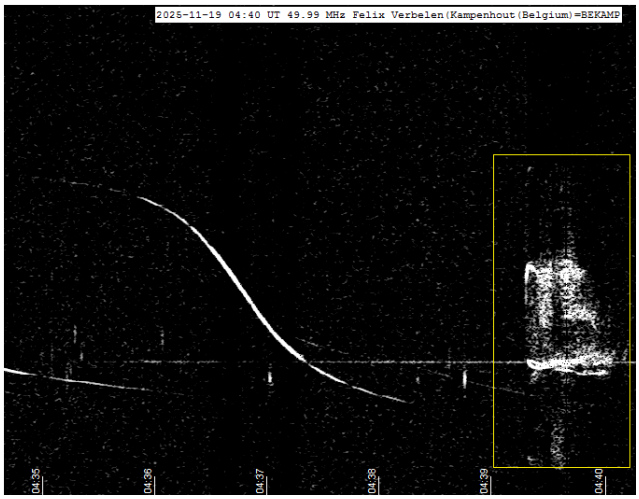

Figure 16 – Meteor echoes November 19, 4^{h}40^{m} UT.

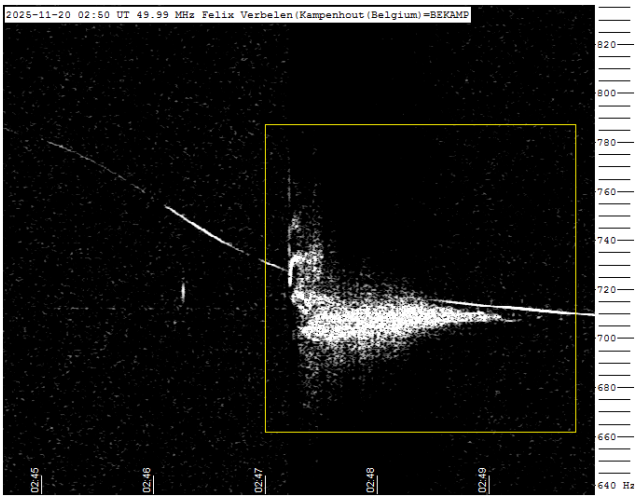

Figure 17 – Meteor echoes November 20, 2^h50^m UT.

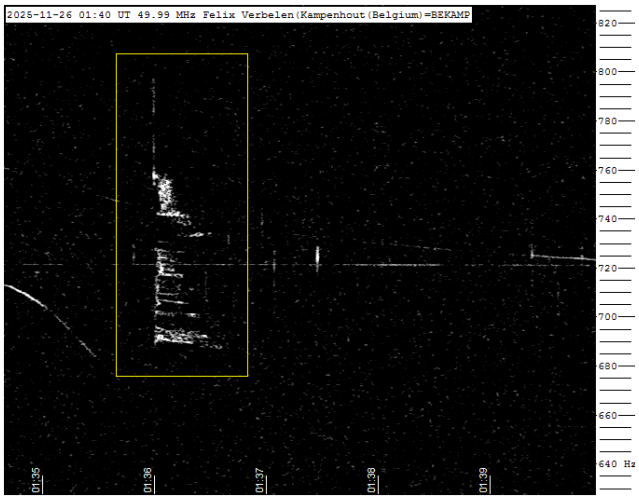

Figure 19 – Meteor echoes November 26, 1^h40^m UT.

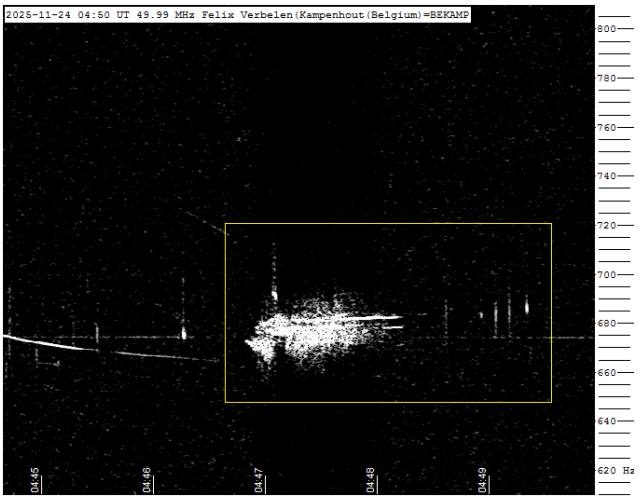

Figure 18 – Meteor echoes November 24, 4^h50^m UT.

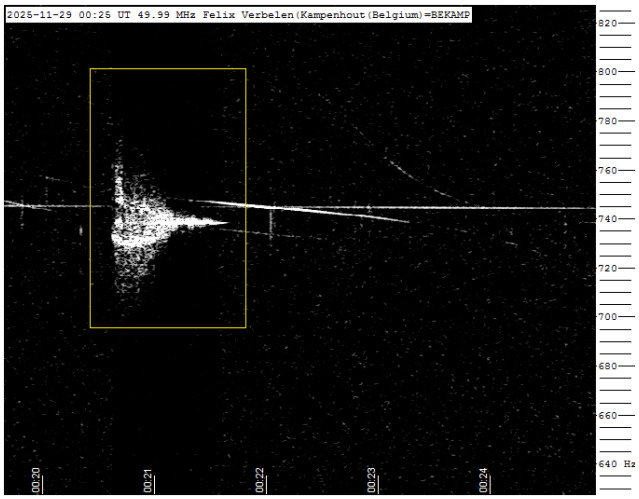

Figure 20 – Meteor echoes November 29, 0^h25^m UT.

eMetN METEOR JOURNAL

Since 2016 the mission of eMetN Meteor Journal is to offer meteor news to a global audience and to provide a swift exchange of information in all fields of active amateur meteor work. eMetN Meteor Journal is freely available without any fees. eMetN Meteor Journal is independent from any country, society, observatory or institute. Articles are abstracted and archived with ADS Abstract Service: https://ui.adsabs.harvard.edu/search/q=eMetN

You are welcome to contribute to eMetN Meteor Journal on a regular or casual basis, if you wish to. Anyone can become an author or editor, for more info read: https://www.emeteornews.net/writing-content-for-emeteornews/

Articles for eMetN Meteor Journal should be submitted to: paul.roggemans@gmail.com

Contact: info@emeteornews.net

Contributors:

- Bakanas E.
- Barbieri L.
- Campbell-Burns P.
- Greaves J.
- Harachka Y.
- Kővágó G.
- Maglione M.
- Merlak A.
- Roggemans P.
- Scott J.M.
- Šegon D.
- Terentjeva A.
- Verbelen F.
- Vida D.
- Wood J.

Online publication https://www.emeteornews.net and https://www.emetn.net
ISSN 3041-4261, publisher: Paul Roggemans, Pijnboomstraat 25, 2800 Mechelen, Belgium